

Volume IV

Supporting
Analyses

March 1976

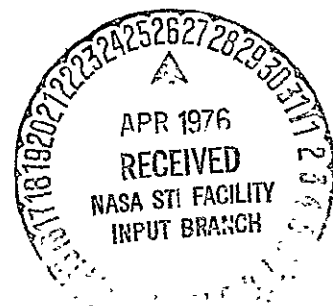
Space Tug Docking Study

(NASA-CR-144242) SPACE TUG DOCKING STUDY.
VOLUME 4: SUPPORTING ANALYSES Final Report
(Martin Marietta Corp.) · 262 p HC \$9.00

N76-21248

CSCL 22B

Unclas
25165



MARTIN MARIETTA

MCR-76-3
Contract NAS8-31542
Data Procurement Document No. 510
Data Requirement No. MA-03

Volume IV

Supporting
Analyses

March 1976

**SPACE TUG
DOCKING STUDY**

Approved By



G. J. Dickman
Program Manager

MARTIN MARIETTA CORPORATION
P. O. Box 179
Denver, Colorado 80201

FOREWORD

This study was performed under Contract NAS8-31542 for the George C. Marshall Space Flight Center of the National Aeronautics and Space Administration under the direction of Mr. James I. Newcomb and Mr. Paul T. Craighead, the Contracting Officer's Representatives. The final report consists of five volumes:

- Volume I - Executive Summary
- Volume II - Study of Results
- Volume III - Procedures and Plans
- Volume IV - Supporting Analyses
- Volume V - Cost Analysis

The study results were developed during the period from June 1975 to January 1976. Principal Martin Marietta contributors to the study were:

Glen Dickman	Study Manager
G. Dickman	Task A Leader, Requirements and Data Base Development
B. King	System Requirements and Operations Analyses
R. Zermuehlen	Subsystem Requirements
R. Schappell	Video Sensors
W. Kopp	Ranging Sensors
C. Park	Docking Dynamics Analysis
B. Dickman	Docking Simulation Program
F. Vandenberg	Rendezvous Simulation Program
M. Crissey, J. Hays, C. Lord	Docking Mechanics
R. Chamberlain	Payload Requirements
R. Zermuehlen	Task B Leader, Candidate System Definition
B. King	Task C Leader, Simulation Demonstration Test Program Definition
E. Cody	Task D Leader, Programmatic Definition

Volume IV - SUPPORTING ANALYSES

CONTENTS

	<u>Page</u>
List of Figures	iv
List of Tables	vi
Acronyms/Abbreviations	ix
 I. Dynamic Analyses and Tools	 I-1 thru I-42
 II. Program Dock Description	 II-1 thru II-42
 III. Sensor and Docking Mechanism Requirements Deri- vation	 III-1 thru III-66
 IV. Docking Mechanism Evaluation	 IV-1 thru IV-24
 V. Operations Analysis	 V-1 thru V-10
 VI. Supplemental Sensor Analysis	 IV-1 thru IV-68

<u>Figure</u>		<u>Page</u>
I-1	Ellipsoidal Tank Representation	I-16
I-2	Typical Body of the System	I-27
I-3	Tug/Spacecraft System Topology	I-32
I-4	Tug Coordinate System for Definition of Inertial Properties	I-35
I-5	SEOS Spacecraft Schematic	I-36
I-6	Mechanism Loads in Terms of Loads at Reference Point	I-37
I-7	Typical Docking Trajectory	I-40
II-1	RCS Engine Forces and Moments	II-5
II-2	PROGRAM DOCK Listing	II-25 thru II-37
II-3	Sample PROGRAM DOCK Input	II-38
II-4	Sample PROGRAM DOCK Output	II-39 thru II-42
III-1	Requirements - Ranging Sensor	III-19 thru III-21
III-2	Requirements - Video/Lighting	III-24 thru III-26
III-3	Requirements - Docking Mechanism	III-27
III-4	Requirements - Target Cues	III-31
III-5	Requirements - Control System/Man	III-32
III-6	Requirements - Ranging Sensor	III-33
III-7	Requirements - Video/Lighting	III-34
III-8	Requirements - Docking Mechanism	III-35 & III-36
III-9	Requirements - Spacecraft Cues	III-41
III-10	Requirements - Control System/Man	III-42 & III-43
III-11	Requirements - Ranging Sensor	III-44 thru III-46
III-12	Requirements - Video/Lighting	III-50
III-13	Requirements - Docking Mechanism	III-51
III-14	Requirements - Spacecraft Cues	III-54
III-15	Requirements - Control System/Man	III-55
III-16	Requirements - Ranging Sensor	III-56
III-17	Requirements - Docking Mechanism	III-57 & III-58
III-18	Requirements - Spacecraft Cues	III-59
III-19	Requirements - Control System/Man	III-60

LIST OF FIGURES (Cont'd)

<u>Figure</u>		<u>Page</u>
III-20	Requirements - Ranging Sensor	III-61
III-21	Requirements - Video/Lighting	III-62
III-22	Requirements - Docking Mechanism	III-63
III-23	Requirements - Spacecraft Cues	III-64
III-24	Requirements - Control/Man	III-65
IV-1	Docking Mechanism Concept Comparison	IV-24
V-1	Reference Spacecraft are Shadowed less than 28% of Orbital Period	V-10
VI-1	Close-in Signal-to-Noise Ratio	VI-6
VI-2	Radar Characteristics Summary - Modified Apollo/LM Radar	VI-8
VI-3	Radar Characteristics Summary - Modified Apollo/LM Radar for Tug	VI-14
VI-4	Shuttle Camera Characteristics	VI-34
VI-5	Area Calculations	VI-48
VI-6	Area Measurement Repeatability	VI-48

<u>Table</u>		<u>Page</u>
I-1	Summary of Topology	I-33
I-2	Summary of Fluid Geometry	I-34
I-3	Summary of Fluid Masses	I-34
I-4	Tug Inertial Properties	I-35
I-5	SEOS Spacecraft Properties	I-36
II-1	Program Dock Geometry	II-2
II-2	RCS Engine Geometry	II-3
II-3	Phase Plane Representation	II-9
II-4	Simplified PROGRAM DOCK Flow	II-11
II-5	PROGRAM DOCK Flow Diagram	II-17
		thru
		II-24
III-1	The Docking Budget Issue	III-2
III-2	Sensors Provide Intelligence	III-3
III-3	Mechanisms Complete the Docking	III-3
III-4	Angular Misalignment Geometry	III-5
III-5	Angular Misalignment Program	III-7
III-6	Lateral Displacement Geometry	III-9
III-7	Lateral Displacement Program	III-11
III-8	Lateral Velocity Geometry	III-13
III-9	Lateral Velocity Computer Program	III-14
III-10	Roll Angular Misalignment	III-15
III-11	Stem Articulation Angle (B)	III-16
III-12	Angular Misalignment vs Axial Docking	
	Velocity	III-22
III-13	Lateral Displacement vs Lateral Vehicle	
	Velocity	III-23
III-14	Angular Misalignment vs Lateral Vehicle	
	Velocity	III-28
III-15	Lateral Displacement vs Lateral Vehicle	
	Velocity	III-29
III-16	Lateral Velocity at Docking Interface vs	
	Lateral Velocity	III-30
III-17	Angular Misalignment vs Translation Deadband	III-37
III-18	Stem Lateral Displacements at Insertion . . .	III-38
III-19	Stem Articulation Angle vs Translation Limit	
	Cycle	III-39
III-20	Stem Articulation Rate vs Lateral Vehicle	
	Velocity	III-40
III-21	Angular Misalignment vs Lateral Vehicle	
	Velocity	III-47
III-22	Angular Misalignment vs Target Attitude	
	Uncertainty	III-48
III-23	Lateral Displacement vs Lateral Vehicle	
	Velocity	III-49
III-24	Lateral Displacement vs Lateral Vehicle	
	Velocity	III-52
III-25	Lateral Velocity at Docking Interface vs	
	Lateral Vehicle Velocity	III-53

LIST OF TABLES (Cont'd)

<u>Table</u>		<u>Page</u>
IV-1	Key Docking Mechanism Selection Issues . . .	IV-2
IV-2	Probe and Drogue Docking System	IV-4
IV-3	Cone and Ring Docking System	IV-4
IV-4	Gemini Docking System	IV-5
IV-5	Inflatable Probe Docking System	IV-5
IV-6(a,b&c)	Stem, Stem and Cable and Inflatable Tunnel .	IV-6
IV-7	Typical Phases of Docking	IV-9
IV-8	ASTP Docking Mechanism	IV-10
IV-9	MDAC Docking System	IV-12
IV-10	Square Frame Attachment Mechanism	IV-13
IV-11	MMSE Docking System	IV-14
IV-12	MMSE Structural Detail	IV-15
IV-13	Hybrid Soft Dock Concept	IV-16
IV-14	Extendible Boom Concepts	IV-18
IV-15	Capture Latch Concepts	IV-19
IV-16	Steering Mechanism Concepts	IV-20
IV-17	Selected Nonimpact Design Concept	IV-22
IV-18	Nonimpact System Design Detail	IV-22
V-1	Mission and Orbital Variations Impact System Design	V-1
V-2	Manual System Operations Scenerio	V-3
V-3	Autonomous System Operations Scenerio . . .	V-4
V-4	Hybrid System Operations Scenerio	V-5
V-5	Manual Docking System Maximizes Mission Operation Interfaces	V-6
V-6	Mission Control Handover Considerations . .	V-8
V-7	Time in Darkness is a Function of Orbital Parameters	V-9
VI-1	Modified Apollo/LM Rendezvous Radar Range "Bias" Error vs Range	VI-7
VI-2	Rendezvous Radar Block Diagram	VI-9
VI-3	ECCO Reflector Experimental Data	VI-16
VI-4	Passive RF Tracking Aids (Docking Mode) . .	VI-21
VI-5	Onboard Rendezvous and Docking System Configuration	VI-40
VI-6	Video Processor Block Diagram	VI-41
VI-7	Far-Steering Video Functions	VI-42
VI-8	Near-Steering and Stationkeeping	VI-43
VI-9	Laboratory Setup	VI-44
VI-10	Test Scene	VI-45
VI-11	Digitized Brightness Map; 0 = Dark; = Light	VI-46
VI-12	Thresholded Version	VI-47
VI-13	Object Center Test A	VI-49
VI-14	Object Center Test B	VI-49
VI-15	Center Test, Simulated Spacecraft 1	VI-51
VI-16	Center Test, Simulated Spacecraft 2	VI-51
VI-17	Orientation Test	VI-52

LIST OF TABLES (Cont'd)

<u>Table</u>		<u>Page.</u>
VI-18	Stereo Ranging Test (Left View)	VI-53
VI-19	Stereo Ranging Test (Right View)	VI-53
VI-20	Image Data Laboratory Setup	VI-59
VI-21	Image Data Compression, Transmission and Reconstruction Flow	VI-61
VI-22	Zero Order Predictor, Floating Aperture . . .	VI-62
VI-23	First Order Predictor	VI-63
VI-24	Zero Order Interpolator (Peak Error Criteria)	VI-63
VI-25	First Order Interpolator	VI-64
VI-26	System Block Diagram	VI-66

ACS	Attitude Control System
A/C	Analog to Digital
ASTP	Apollo Soyuz Test Project
ATP	Authority to Proceed
Avg.	Average
c.g.	center of gravity
cm	centimeter
Cmnd	command
C(S)M	Command (Service) Module
D/A	Digital to Analog
db	decibel
deg	degree
DOCKRB	MMC Docking Dynamics Program using Rigid Body Analysis
DOF	Degrees of Freedom
EREP	Earth Resources Experiment Package
FOV	Field of View
fps	feet per second
ft	feet
ICW	Interrupted Continuous Wave
IDM	International Docking Mechanism
I/F	Interface
IMPRES	MMC Dynamic Docking Program
IMU	Inertial Measuring Unit
in	inch
IUS	Interim Upper Stage
kg	kilogram
km	kilometer
LH ₂	Liquid Hydrogen
LM	Lunar Module
LO ₂	Liquid Oxygen
LOS	Line-of-Sight

ACRONYMS/ABBREVIATIONS (Cont'd)

m	meter
max.	maximum
MDAC	McDonnell Douglas Astronautics Company
MHz	Mega-hertz
MMC	Martin Marietta Corporation
MMSE	Multi-use Mission Support Equipment
ms or m/s	milli-second
MSFC	Marshall Space Flight Center
MTBF	Mean Time between Failures
NASA	National Aeronautics and Space Administration
n.mi.	nautical miles
PRF	Pulse Repetition Frequency
RCS	Reaction Control System
RF	Radio Frequency
RPM	Revolutions per Minute
RSS	Root Sum Square
S/C	Spacecraft
sec	second
SEOS	Synchronous Earth Observation Satellite
SGLS	Space Ground Link System
SIT	Silicon Intensified Target
SLR	Scanning Laser Radar
sq	square
S/N	Signal/Noise
SSPD	Space Shuttle Payload Descriptions
STDN	Space Tracking Data Network
STEM	Storable Extendible Member
STS	Shuttle Transportation System
TBD	To Be Determined
TDRS(S)	Tracking Data Relay Satellite (System)
TM	Telemetry
TV	Television
vel.	velocity
VDC	Volts - direct current
VP	Video Processor
w/r	with respect
ZOI	Zero Order Interpolator
ZOP	Zero Order Predictor

I. DYNAMIC ANALYSES AND TOOLS

Problems associated with spacecraft docking have received considerable attention in the past few years. This was primarily necessitated by the docking requirements of the Apollo, Skylab, and Apollo/Soyouz missions. In addition, missions of the future, in particular those associated with Space Shuttle and Space Tug operations, that require docking of space vehicles with satellites will necessitate extensive analyses. The docking maneuver and its associated responses will, no doubt, be of prime consideration in the design of these large, flexible structures. Other considerations that must be included in the design of docking attenuation mechanisms include definition of successful capture boundaries, definition of spacecraft attitude control requirements, propellant utilization studies, and man/machine interaction or the degree of automation.

Tests to simulate the docking maneuver are very expensive, and generally the results are not conclusive because of the differences between the test and space environment. Accurate and economical analytical formulations of the docking maneuver are imperative with respect to many aspects of vehicle and docking mechanism design.

This chapter summarizes the dynamics analyses tools that were developed (or extended from existing analyses) and implemented during the course of these investigations. Two digital codes were employed. The first considers the Tug/spacecraft/attenuation mechanism as a dynamical system of interconnected rigid bodies. An interface for inclusion of control logic is available. Large amplitude propellant motions are accounted for with a pendulum analog that assumes the fluid to move as a point mass on a spherical constraint surface. The second code is a modification of the Martin Marietta developed IMPRES program for detailed docking dynamics analysis. An interface for inclusion of control logic is available. Large amplitude propellant motions are accounted for through inclusion of an analog which assumes that the fluid moves as a point mass on an ellipsoidal constraint surface. This analog is an extension of the Martin Marietta developed approach which has been validated through comparison with experimental results.

The following references may be used to provide additional clarification of the analytical techniques:

- 1) Orbital Docking Dynamics, MCR-74-23, Martin Marietta Corporation, Denver, Colorado, April 1974 (Contract NAS8-26159)
- 2) Dynamic Analysis of a Flexible Spacecraft with Rotating Components, MCR-75-18, Martin Marietta Corporation, Denver, Colorado, August 1975 (Contract NAS8-30761)

A. IMPRES - DOCKING DYNAMICS ANALYSIS OF SPACECRAFT WITH EXPLICIT MECHANISM DEFINITION

The analysis of spacecraft docking requires an accurate mathematical description of the mechanical system and solution of the resulting differential equations. Generally speaking, impact problems involve the use of kinematical conditions of constraint, and except for very elementary or degenerate situations, the conditions of constraint are nonholonomic. A nonholonomic constraint can be mathematically expressed only in terms of differential displacements. The corresponding equation of constraint cannot, therefore, be used to eliminate one coordinate in terms of remaining coordinates. A given mechanical system might include various combinations of holonomic constraints, or it might include constraint conditions that are enforced at times and relaxed at others, depending on position or other functions of configuration state. The last mentioned circumstance would correspond, at best, to a piecewise holonomic constraint condition. This formulation of the equations of motion is general to the extent of including any type, or combination of types, of kinematical constraint conditions. To achieve this objective, we have employed Lagrange's method of undetermined multipliers. An extremely celebrated and useful feature inherent in the use of Lagrange's multipliers is that holonomic constraints can be dealt with in exactly the same way as nonholonomic constraints; if a mathematical expression of constraint can be written in terms of displacement coordinates, then it can also be written in terms of differential displacements, simply by differentiating the former equation. Thus, if Lagrange's multipliers are used to implement all constraint conditions, then it is unnecessary to distinguish between types of constraints.

1. Basic Approach - For an unconservative system with general type constraints, Lagrange's equations of motion are

$$\frac{d}{dt} \left(\frac{\partial T}{\partial \dot{q}_r} \right) - \frac{\partial T}{\partial q_r} + \frac{\partial V}{\partial q_r} = Q_r + \sum_s b_{rs} \lambda_s ; \quad \sum_r b_{sr} \dot{q}_r = b_{st}(t). \quad (I.A-1)$$

where the index (r) ranges from 1 through the number of generalized coordinates while the index (s) ranges from 1 through the number of constraint equations. The term on the right side of the second set of equations accounts for the possibility of rheonomic (moving) constraints. The first set represents a set of second-order ordinary differential equations, while the second represents a set of algebraic equations to be satisfied simultaneously with the motion equations.

We have employed a Hamiltonian approach to problem formulation. In this technique generalized accelerations are eliminated in favor of generalized momenta to replace n second-order equations with 2n first-order equations. The Hamiltonian function is defined as the sum of kinetic and potential energies

$$H = T+V \quad (I.A-2)$$

and the generalized momenta are

$$p_r = \frac{\partial T}{\partial \dot{q}_r} \quad (I.A-3)$$

The kinetic energy of a discretized scleronomic mechanical system is of positive-definite quadratic form in the generalized velocities,

$$T = 1/2 \sum_i \sum_j M_{ij} \dot{q}_i \dot{q}_j, \quad (I.A-4)$$

or, in matrix notation,

$$T = 1/2 \left\{ \dot{q} \right\}^T \left[M \right] \left\{ \dot{q} \right\} \quad (I.A-5)$$

From the definition (I.A-3), it follows that

$$\left\{ p \right\} = \left[M \right] \left\{ \dot{q} \right\} \quad (I.A-6)$$

and, as $\left[M \right]$ is positive-definite, an inverse exists and

$$\left\{ \dot{q} \right\} = \left[M \right]^{-1} \left\{ p \right\} \quad (I.A-7)$$

With reference to Equations (I.A-5) and (I.A-7), we have two ways to express kinetic energy:

$$T = 1/2 \left\{ \dot{q} \right\}^T \left\{ p \right\} \quad (I.A-8)$$

or

$$T = 1/2 \left\{ p \right\}^T \left[M \right]^{-1} \left\{ p \right\} . \quad (I.A-9)$$

Now, because the potential energy depends on position and not velocity, it is permissible to write the first of Equations (I.A-1) as

$$\frac{d}{dt} \left[\frac{\partial}{\partial \dot{q}_r} (T - V) \right] - \frac{\partial}{\partial q_r} (T - V) = Q_r + \sum_s b_{rs} \lambda_s \quad (I.A-10)$$

but from the definition Equation (I.A-2) it follows that

$$T - V = 2T - T - V = 2T - H, \quad (I.A-11)$$

and in terms of configuration coordinates (p and q) we write

$$T - V = \left\{ \dot{q} \right\}^T \left\{ p \right\} - 1/2 \left\{ p \right\}^T \left[M \right]^{-1} \left\{ p \right\} - V . \quad (I.A-12)$$

Now, substituting Equation (I.A-12) into Equation (I.A-10) yields

$$\begin{aligned} \dot{p}_r &= Q_r - \frac{\partial H}{\partial q_r} + \sum_s b_{rs} \lambda_s \\ \dot{q}_r &= \frac{\partial H}{\partial p_r} \end{aligned} \quad (I.A-13)$$

$$\sum_r b_{sr} \dot{q}_r = b_{st}(t)$$

These are Hamilton's equations of motion with constraints shown in an abstract form; however, they are general and all-encompassing.

2. Generalized Coordinates - Selection of generalized coordinates assumes that impact occurs only between two bodies, the Tug (chase vehicle) and a spacecraft (target vehicle). For each there is a set of generalized coordinates; attenuation mechanism coordinates are considered separately. As Tug, spacecraft and impact mechanism are independent except for the equations of constraint and the corresponding Lagrange multipliers, it is permissible to develop equations for each. Hence we have applied Equations (I.A-13) to the three mechanical subsystems and the total set of generalized coordinates is

$$\{q_1\} = \begin{pmatrix} x_{1T} \\ x_{2T} \\ x_{3T} \end{pmatrix} \quad \begin{array}{l} \text{Projections of the position vector from the origin of} \\ \text{the inertial reference frame to the spacecraft mass} \\ \text{center, onto the orthogonal inertial axes} \end{array}$$

$$\{q_2\} = \begin{pmatrix} \beta_{0T} \\ \beta_{1T} \\ \beta_{2T} \\ \beta_{3T} \end{pmatrix} \quad \begin{array}{l} \text{Euler parameters, used to describe the attitude of the} \\ \text{spacecraft body-fixed axis system with respect to the} \\ \text{inertial reference axis system} \end{array}$$

$$\{q_3\} = \begin{pmatrix} \xi_{1T} \\ \xi_{2T} \\ \cdot \\ \cdot \\ \cdot \\ \xi_{NT} \end{pmatrix} \quad \begin{array}{l} \text{Generalized modal displacements for spacecraft elastic} \\ \text{deflection} \end{array}$$

$$\{q_4\} = \begin{pmatrix} x_{1C} \\ x_{2C} \\ x_{3C} \end{pmatrix} \quad \begin{array}{l} \text{Projections of the position vector from the origin of} \\ \text{the inertial reference frame to the Tug mass center,} \\ \text{onto the orthogonal inertial axes} \end{array}$$

$$\{q_5\} = \begin{pmatrix} \beta_{0C} \\ \beta_{1C} \\ \beta_{2C} \\ \beta_{3C} \end{pmatrix} \quad \begin{array}{l} \text{Euler parameters, used to describe the attitude of the} \\ \text{Tug's body-fixed axis system with respect to the inertial} \\ \text{reference axis system} \end{array}$$

$$\{q_6\} = \begin{pmatrix} \xi_{1C} \\ \xi_{2C} \\ \cdot \\ \cdot \\ \cdot \\ \xi_{NC} \end{pmatrix} \quad \begin{array}{l} \text{Generalized modal displacements for Tug elastic deflec-} \\ \text{tion} \end{array}$$

$$\{\rho\} = \begin{pmatrix} \rho_1 \\ \rho_2 \\ \cdot \\ \cdot \\ \cdot \\ \rho_{N\rho} \end{pmatrix} \quad \begin{array}{l} \text{Generalized displacements of parts of the impact attenua-} \\ \text{tion mechanism} \end{array}$$

3. Motion Equations for An Elastic Vehicle - The kinetic energy of an elastic vehicle is

$$T = 1/2 m \left(\bar{v}_c \cdot \bar{v}_c \right) + 1/2 \bar{\omega} \cdot \bar{h} + 1/2 \sum_k \dot{\xi}_k^2 \quad (\text{I.A-14})$$

where

m is the mass,

\bar{v}_c is the absolute velocity of the mass center,

$\bar{\omega}$ is the angular velocity of the body-fixed axis system,

\bar{h} is the moment of momentum of the body (as if it were considered rigid) about an axis through the mass center,

$\dot{\xi}_k$ is the time rate of change of the elastic normal deflection in the k^{th} mode.

Equation (I.A-14) has no coupling terms between rigid velocities and elastic velocities as a consequence of neglecting the contribution of elastic tangential velocities due to the angular rotation rate.

The potential energy includes only strain energy due to elastic deflection and it follows that

$$V = 1/2 \sum_k \omega_k^2 \xi_k^2 \quad (I.A-15)$$

The Lagrangian function is

$$\begin{aligned} \Lambda &= T - V \\ &= 1/2 m \left(\dot{x}_1^2 + \dot{x}_2^2 + \dot{x}_3^2 \right) + 1/2 \left[\dot{\beta} \right] \left[\beta_\omega \right]^T \left[\tilde{I} \right] \left[\beta_\omega \right] \left\{ \dot{\beta} \right\} \\ &\quad + 1/2 \sum_k \dot{\xi}_k^2 - 1/2 \sum_k \omega_k^2 \xi_k^2 \end{aligned} \quad (I.A-16)$$

where

$$\left\{ \dot{\beta} \right\} = \begin{bmatrix} \dot{\beta}_0 \\ \dot{\beta}_1 \\ \dot{\beta}_2 \\ \dot{\beta}_3 \end{bmatrix} \quad (I.A-17)$$

$$\left[\tilde{I} \right] = \begin{bmatrix} 1 & 0 & 0 & 0 \\ 0 & I_{11} & -I_{12} & -I_{13} \\ 0 & -I_{12} & I_{22} & -I_{23} \\ 0 & -I_{13} & -I_{23} & I_{33} \end{bmatrix} \quad (I.A-18)$$

and

$$\begin{bmatrix} \beta_\omega \end{bmatrix} = 2 \begin{bmatrix} \beta_0 & \beta_1 & \beta_2 & \beta_3 \\ -\beta_1 & \beta_0 & \beta_3 & -\beta_2 \\ -\beta_2 & -\beta_3 & \beta_0 & \beta_1 \\ -\beta_3 & \beta_2 & -\beta_1 & \beta_0 \end{bmatrix} \quad (\text{I.A-19})$$

and it follows that the Hamiltonian function is

$$\begin{aligned} H = & 1/2 \left(p_{X_1}^2 + p_{X_2}^2 + p_{X_3}^2 \right) / m \\ & + 1/2 \begin{bmatrix} p_{\beta_0} & p_{\beta_1} & p_{\beta_2} & p_{\beta_3} \end{bmatrix} \begin{bmatrix} \beta_\omega \end{bmatrix}^{-1} \begin{bmatrix} \tilde{\Gamma} \end{bmatrix}^{-1} \begin{bmatrix} \beta_\omega \end{bmatrix}^{-1T} \begin{bmatrix} p_{\beta_0} \\ p_{\beta_1} \\ p_{\beta_2} \\ p_{\beta_3} \end{bmatrix} \\ & + 1/2 \sum_k p_{\xi_k}^2 + 1/2 \sum_k \omega_k^2 \xi_k^2. \end{aligned} \quad (\text{I.A-20})$$

Now with reference to Equation (I.A-13), the translational equations are

$$\dot{p}_{X_j} = Q_{X_j} + \sum_s b_{X_j s} \lambda_s \quad (\text{I.A-21})$$

$$\dot{X}_j = 1/m p_{X_j} \quad (\text{I.A-22})$$

and the rotational equations, which involve only the Euler parameters, are

$$\begin{aligned} \dot{p}_{\beta_k} = & Q_{\beta_k} + 1/2 [p_{\beta_0}, p_{\beta_1}, p_{\beta_2}, p_{\beta_3}] \frac{\partial}{\partial \beta_k} \left(\begin{bmatrix} \beta_\omega \end{bmatrix}^T \begin{bmatrix} \tilde{I} \end{bmatrix} \begin{bmatrix} \beta_\omega \end{bmatrix} \right)^{-1} \begin{bmatrix} p_{\beta_0} \\ p_{\beta_1} \\ p_{\beta_2} \\ p_{\beta_3} \end{bmatrix} \\ & + \sum_s b_{\beta_k s} \lambda_s \end{aligned} \quad (\text{I.A-23})$$

which, with some algebraic manipulations, become

$$\left\{ \dot{p}_\beta \right\} = \left\{ Q_\beta \right\} + \begin{bmatrix} p_\beta \end{bmatrix} \begin{bmatrix} \tilde{I} \end{bmatrix} \begin{bmatrix} \beta_\omega \end{bmatrix} \left\{ \dot{\beta} \right\} + \begin{bmatrix} b_{\lambda\beta} \end{bmatrix}^T \left\{ \lambda \right\} \quad (\text{I.A-24})$$

$$\left\{ \dot{\beta} \right\} = 1/16 \begin{bmatrix} \beta_\omega \end{bmatrix}^T \begin{bmatrix} \tilde{I} \end{bmatrix}^{-1} \begin{bmatrix} \beta_\omega \end{bmatrix} \left\{ p_\beta \right\} \quad (\text{I.A-25})$$

The equations corresponding to vehicle elastic deflections are

$$\dot{p}_{\xi_j} = Q_{\xi_j} - \omega_j^2 \xi_j + \sum_s b_{\xi_j s} \lambda_s \quad (\text{I.A-26})$$

$$\dot{\xi}_j = p_j \quad (\text{I.A-27})$$

4. Mechanism Equations - To accommodate a general impact attenuation device it is necessary to assume that large deformations occur between working parts of the mechanism. The contribution to potential energy from internal mechanism restoring forces is substantial, but because force-displacement characteristics are nonlinear, in general, it is extremely difficult to derive a potential energy function corresponding to mechanism displacements. Additional special treatment given to the mechanism includes the effects of restoring forces with those due to non-conservative (dissipative) internal forces in the mechanism generalized force vector $\{Q_\rho\}$. This circumvents expressing potential energy for the mechanism, and because mass of the mechanism is negligible, a Hamiltonian function is zero. The first of Hamilton's equations, (I.A-13) as applied to the mechanism yields.

$$\{Q_\rho\} + [b_{\lambda\rho}]^T \{\lambda\} = \{0\}, \quad (\text{I.A-28})$$

because

$$p_{\rho_j} = \dot{p}_{\rho_j} = 0.$$

5. System Equations - The previous developments applied to Tug, spacecraft and mechanism yield the motion and constraint equations:

$$\left\{ \dot{p}_1 \right\} = \left\{ Q_1 \right\} + \left[b_{\lambda 1} \right]^T \left\{ \lambda \right\} \quad (\text{I.A-29})$$

$$\left\{ \dot{p}_2 \right\} = \left\{ Q_2 \right\} + \left[p_{\beta 2} \right] \left[\tilde{I}_2 \right] \left[\beta_{\omega 2} \right] \left\{ \dot{q}_2 \right\} + \left[b_{\lambda 2} \right]^T \left\{ \lambda \right\} \quad (\text{I.A-30})$$

$$\left\{ \dot{p}_3 \right\} = \left\{ Q_3 \right\} - \left[\omega_3^2 \right] \left\{ q_3 \right\} + \left[b_{\lambda 3} \right]^T \left\{ \lambda \right\} \quad (\text{I.A-31})$$

$$\left\{ \dot{p}_4 \right\} = \left\{ Q_4 \right\} + \left[b_{\lambda 4} \right]^T \left\{ \lambda \right\} \quad (\text{I.A-32})$$

$$\left\{ \dot{p}_5 \right\} = \left\{ Q_5 \right\} + \left[p_{\beta 5} \right] \left[\tilde{I}_5 \right] \left[\beta_{\omega 5} \right] \left\{ \dot{q}_5 \right\} + \left[b_{\lambda 5} \right]^T \left\{ \lambda \right\} \quad (\text{I.A-33})$$

$$\left\{ \dot{p}_6 \right\} = \left\{ Q_6 \right\} - \left[\omega_6^2 \right] \left\{ q_6 \right\} + \left[b_{\lambda 6} \right]^T \left\{ \lambda \right\} \quad (\text{I.A-34})$$

$$\left\{ \dot{q}_1 \right\} = 1/m_1 \left\{ p_1 \right\} \quad (\text{I.A-35})$$

$$\left\{ \dot{q}_2 \right\} = 1/16 \left[\beta_{\omega 2} \right]^T \left[\tilde{I}_2 \right]^{-1} \left[\beta_{\omega 2} \right] \left\{ p_2 \right\} \quad (\text{I.A-36})$$

$$\left\{ \dot{q}_3 \right\} = \left\{ p_3 \right\} \quad (\text{I.A-37})$$

$$\left\{ \dot{q}_4 \right\} = 1/m_4 \left\{ p_4 \right\} \quad (\text{I.A-38})$$

$$\left\{ \dot{q}_5 \right\} = 1/16 \left[\beta_{\omega 5} \right]^T \left[\tilde{I}_5 \right]^{-1} \left[\beta_{\omega 5} \right] \left\{ p_5 \right\} \quad (\text{I.A-39})$$

$$\left\{ \dot{q}_6 \right\} = \left\{ p_6 \right\} \quad (\text{I.A-40})$$

$$\left\{ 0 \right\} = \left\{ Q_p \right\} + \left[b_{\lambda p} \right]^T \left\{ \lambda \right\} \quad (\text{I.A-41})$$

$$\begin{aligned} \left[b_{\lambda 1} \right] \left\{ \dot{q}_1 \right\} + \left[b_{\lambda 2} \right] \left\{ \dot{q}_2 \right\} + \left[b_{\lambda 3} \right] \left\{ \dot{q}_3 \right\} + \left[b_{\lambda 4} \right] \left\{ \dot{q}_4 \right\} \\ + \left[b_{\lambda 5} \right] \left\{ \dot{q}_5 \right\} + \left[b_{\lambda 6} \right] \left\{ \dot{q}_6 \right\} + \left[b_{\lambda p} \right] \left\{ \dot{p} \right\} = \left\{ 0 \right\} \end{aligned} \quad (\text{I.A-42})$$

where Equations (I.A-29, 30, 31, 35, 36 and 37) refer to the spacecraft, Equations (I.A-32, 33, 34, 38, 39, and 40) refer to the Tug, Equations (I.A-41) are for the mechanism and Equations (I.A-42) are the constraint equations.

As the final step in the basic development we have transformed the generalized momenta equations to ordinary momenta. Ordinary translational momenta are related to generalized translational momenta as

$$\left\{ h \right\} = \left[\gamma \right] \left\{ p \right\} \quad (\text{I.A-43})$$

where $\begin{bmatrix} \gamma \end{bmatrix}$ is a matrix of direction cosines relating body attitude to the inertial reference and ordinary angular momenta are related to generalized angular momenta as

$$\{h\} = \begin{bmatrix} T_\beta \end{bmatrix}^T \{p\} \quad (I.A-44)$$

where $\begin{bmatrix} T_\beta \end{bmatrix}$ relates Euler parameter derivatives to spin vector components.

Application of the above to both Tug and spacecraft yields

$$\{\dot{h}_1\} = \{G_1\} + \begin{bmatrix} \bar{b}_{\lambda 1} \end{bmatrix}^T \{\lambda\} + \begin{bmatrix} \Omega_2 \end{bmatrix} \{h_1\} \quad (I.A-45)$$

$$\{\dot{h}_4\} = \{G_4\} + \begin{bmatrix} \bar{b}_{\lambda 4} \end{bmatrix}^T \{\lambda\} + \begin{bmatrix} \Omega_5 \end{bmatrix} \{h_4\} \quad (I.A-46)$$

where

$$\{G_1\} = [\gamma_2] \{Q_1\}, \quad \{G_4\} = [\gamma_5] \{Q_4\},$$

$$\begin{bmatrix} \bar{b}_{\lambda 1} \end{bmatrix}^T = [\gamma_2] \begin{bmatrix} b_{\lambda 1} \end{bmatrix}^T, \quad \begin{bmatrix} \bar{b}_{\lambda 4} \end{bmatrix}^T = [\gamma_5] \begin{bmatrix} b_{\lambda 4} \end{bmatrix}^T$$

$$\begin{bmatrix} \Omega_2 \end{bmatrix} = \begin{bmatrix} 0 & \omega_{zT} & -\omega_{yT} \\ -\omega_{zT} & 0 & \omega_{xT} \\ \omega_{yT} & -\omega_{xT} & 0 \end{bmatrix}, \quad \begin{bmatrix} \Omega_5 \end{bmatrix} = \begin{bmatrix} 0 & \omega_{zC} & -\omega_{yC} \\ -\omega_{zC} & 0 & \omega_{xC} \\ \omega_{yC} & -\omega_{xC} & 0 \end{bmatrix}$$

for the translational momenta and

$$\{\dot{h}_2\} = \{G_2\} + \begin{bmatrix} \bar{b}_{\lambda 2} \end{bmatrix}^T \{\lambda\} + \begin{bmatrix} \Omega_2 \end{bmatrix} \{h_2\} \quad (I.A-47)$$

$$\{\dot{h}_5\} = \{G_5\} + \begin{bmatrix} \bar{b}_{\lambda 5} \end{bmatrix}^T \{\lambda\} + \begin{bmatrix} \Omega_5 \end{bmatrix} \{h_5\} \quad (I.A-48)$$

where

$$\{G_2\} = [T_{\beta 2}]^T \{Q_2\} , \quad \{G_5\} = [T_{\beta 5}]^T \{Q_5\} ,$$

$$[\bar{b}_{\lambda 2}]^T = [T_{\beta 2}]^T [b_{\lambda 2}] , \quad [\bar{b}_{\lambda 5}]^T = [T_{\beta 5}]^T [b_{\lambda 5}]$$

for the angular momenta.

The elastic deformation equations are unchanged and are summarized as

$$\{\dot{h}_3\} = \{G_3\} - \left[\omega_3^2 \right] \{q_3\} + [\bar{b}_{\lambda 3}]^T \{\lambda\} , \quad (I.A-49)$$

$$\{\dot{h}_6\} = \{G_6\} - \left[\omega_6^2 \right] \{q_6\} + [\bar{b}_{\lambda 6}]^T \{\lambda\} \quad (I.A-50)$$

where

$$\{\dot{h}_3\} = \{\dot{p}_3\} , \quad \{\dot{h}_6\} = \{\dot{p}_6\}$$

$$\{G_3\} = \{Q_3\} , \quad \{G_6\} = \{Q_6\} \quad \text{and}$$

$$[\bar{b}_{\lambda 3}] = [b_{\lambda 3}] , \quad [\bar{b}_{\lambda 6}] = [b_{\lambda 6}] .$$

With the new definitions of momenta, it follows that the auxiliary non-holonomic velocities are:

$$\left\{ \begin{matrix} U_1 \end{matrix} \right\} = \frac{1}{m_1} \left\{ \begin{matrix} h_1 \end{matrix} \right\}$$

$$\left\{ \begin{matrix} \omega_2 \end{matrix} \right\} = \left[\tilde{I}_2 \right]^{-1} \left\{ \begin{matrix} h_2 \end{matrix} \right\}$$

$$\left\{ \begin{matrix} U_4 \end{matrix} \right\} = \frac{1}{m_4} \left\{ \begin{matrix} h_4 \end{matrix} \right\}$$

$$\left\{ \begin{matrix} \omega_5 \end{matrix} \right\} = \left[\tilde{I}_5 \right]^{-1} \left\{ \begin{matrix} h_5 \end{matrix} \right\} .$$

(I.A-51)

Now the generalized velocities, expressed in terms of nonholonomic velocities, are

$$\begin{aligned} \begin{Bmatrix} \dot{q}_1 \end{Bmatrix} &= \begin{bmatrix} \gamma_2 \end{bmatrix}^T \begin{Bmatrix} U_1 \end{Bmatrix} \\ \begin{Bmatrix} \dot{q}_2 \end{Bmatrix} &= \begin{bmatrix} T_{\beta 2} \end{bmatrix} \begin{Bmatrix} \omega_2 \end{Bmatrix} \\ \begin{Bmatrix} \dot{q}_4 \end{Bmatrix} &= \begin{bmatrix} \gamma_4 \end{bmatrix}^T \begin{Bmatrix} U_4 \end{Bmatrix} \\ \begin{Bmatrix} \dot{q}_5 \end{Bmatrix} &= \begin{bmatrix} T_{\beta 5} \end{bmatrix} \begin{Bmatrix} \omega_5 \end{Bmatrix} \end{aligned} \quad (\text{I.A-52})$$

and the constraint equations become

$$\begin{aligned} \begin{bmatrix} \bar{b}_{\lambda 1} \end{bmatrix} \begin{Bmatrix} U_1 \end{Bmatrix} + \begin{bmatrix} \bar{b}_{\lambda 2} \end{bmatrix} \begin{Bmatrix} \omega_2 \end{Bmatrix} + \begin{bmatrix} \bar{b}_{\lambda 3} \end{bmatrix} \begin{Bmatrix} \dot{q}_3 \end{Bmatrix} \\ + \begin{bmatrix} \bar{b}_{\lambda 4} \end{bmatrix} \begin{Bmatrix} U_4 \end{Bmatrix} + \begin{bmatrix} \bar{b}_{\lambda 5} \end{bmatrix} \begin{Bmatrix} \omega_5 \end{Bmatrix} + \begin{bmatrix} \bar{b}_{\lambda 6} \end{bmatrix} \begin{Bmatrix} \dot{q}_6 \end{Bmatrix} \\ + \begin{bmatrix} \bar{b}_{\lambda \rho} \end{bmatrix} \begin{Bmatrix} \dot{\rho} \end{Bmatrix} = \begin{Bmatrix} 0 \end{Bmatrix}, \end{aligned} \quad (\text{I.A-53})$$

where $\begin{bmatrix} \bar{b}_{\lambda 3} \end{bmatrix} = \begin{bmatrix} b_{\lambda 3} \end{bmatrix}$ and $\begin{bmatrix} \bar{b}_{\lambda 6} \end{bmatrix} = \begin{bmatrix} b_{\lambda 6} \end{bmatrix}$.

6. The State Vector - The motion and constraint equations are expressed as a set of simultaneous first-order differential equations

$$\dot{V}_i = f(V_1, V_2, \dots, V_n, t) \quad (\text{I.A-54})$$

where

$$V = \left\{ q_1, \dots, q_6, \rho, h_1, \dots, h_6, \delta_{cs} \right\} \quad (\text{I.A-55})$$

and (q_1) thru (q_6) represents generalized coordinates for the elastic target and chase vehicles, (ρ) represents the generalized displacements of the impact attenuation mechanism, (h_1) thru (h_6) correspond to the momenta of the two elastic vehicles (there are no momenta corresponding to the (assumed) massless impact attenuation mechanism) and (δ_{cs}) represents pertinent control system parameters.

7. The Large Amplitude Fluid Motion Model* - Developments to this point have presented the system governing equations for the impact analysis of two orbiting vehicles without consideration of any propellant motions. In the case of the Space Tug an extension to consider these effects is warranted. Consider a vehicle with an (assumed) ellipsoidal tank as shown in Figure I-1.

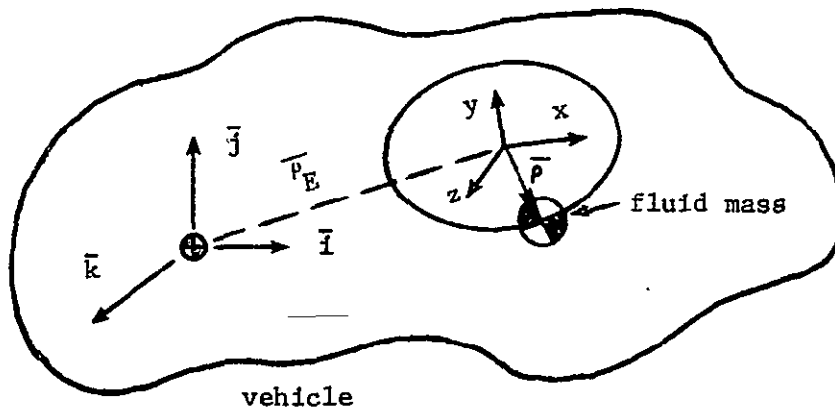


Figure I-1 Ellipsoidal Tank Representation

Using a spherical coordinate transformation in terms of the coordinates ρ, ϕ, θ yields

$$\begin{aligned} x &= \rho \cos \phi \\ y &= \rho \sin \phi \cos \theta \\ z &= \rho \sin \phi \sin \theta \end{aligned} \tag{I.A-56}$$

* This approach to fluid motion coupling was developed by Carl. S. Bodley, Martin Marietta Corporation, November 1975.

for the cartesian coordinates subject to the boundary constraint

$$\left(\frac{x}{a}\right)^2 + \left(\frac{y}{b}\right)^2 + \left(\frac{z}{c}\right)^2 = 1 \quad (\text{I.A-57})$$

where a, b, c define the shape of the ellipsoid. It follows that

$$\rho = \left[\left(\frac{\cos \phi}{a} \right)^2 + \left(\frac{\sin \phi \cos \theta}{b} \right)^2 + \left(\frac{\sin \phi \sin \theta}{c} \right)^2 \right]^{-\frac{1}{2}} \quad (\text{I.A-58})$$

and, therefore, the coordinates ϕ, θ are sufficient to describe the fluid motion on the ellipsoidal surface.

For the rigid Tug vehicle with two tanks define the vector of velocities

$$\{U\} = \begin{bmatrix} u_C \\ v_C \\ w_C \\ \omega_{xC} \\ \omega_{yC} \\ \omega_{zC} \\ \dot{x}_1 \\ \dot{y}_1 \\ \dot{z}_1 \\ \dot{x}_2 \\ \dot{y}_2 \\ \dot{z}_2 \end{bmatrix} \quad (\text{I.A-59})$$

where u_C , v_C and w_C represent the translational velocity of the Tug center of mass; ω_{xC} , ω_{yC} and ω_{zC} represent the angular velocity of the Tug center of mass; and \dot{x}_1 , \dot{y}_1 , \dot{z}_1 and \dot{x}_2 , \dot{y}_2 , \dot{z}_2 represent the inertial velocity of the LH_2 and LO_2 fluid masses, respectively. Now it follows that

$$\begin{Bmatrix} U \end{Bmatrix} = \begin{bmatrix} T \end{bmatrix} \begin{Bmatrix} v \end{Bmatrix} \quad (\text{I.A-60})$$

with $\begin{Bmatrix} v \end{Bmatrix} = \begin{bmatrix} u_C \\ v_C \\ w_C \\ \omega_{xC} \\ \omega_{yC} \\ \omega_{zC} \\ \dot{\phi}_1 \\ \dot{\theta}_1 \\ \dot{\phi}_2 \\ \dot{\theta}_2 \end{bmatrix}$

and $\begin{bmatrix} T \end{bmatrix} = \begin{bmatrix} I & & & \\ & I & & \\ & & \gamma^T & \\ & & & \gamma^T \end{bmatrix} \begin{bmatrix} B \end{bmatrix},$

$$\begin{bmatrix} B \end{bmatrix} = \begin{bmatrix} I & & & \\ & I & & \\ I & Sk_1 & A_1 & \\ I & Sk_2 & & A_2 \end{bmatrix}.$$

In the above definitions, note that

I = identity matrix,

γ = coordinate rotation to inertial frame from body reference frame,

$$Sk_i = \begin{bmatrix} \tilde{z}_i & -\tilde{y}_i \\ -\tilde{z}_i & \tilde{x}_i \\ \tilde{y}_i & -\tilde{x}_i \end{bmatrix} \quad (i = 1, 2) ,$$

$$A_i = \begin{bmatrix} A_i & D_i \\ B_i & E_i \\ C_i & F_i \end{bmatrix} \quad (i = 1, 2)$$

$$\text{and} \quad \begin{pmatrix} \tilde{x}_i \\ \tilde{y}_i \\ \tilde{z}_i \end{pmatrix} = \begin{pmatrix} x_{Ei} \\ y_{Ei} \\ z_{Ei} \end{pmatrix} + \begin{bmatrix} R_i^C \end{bmatrix} \begin{pmatrix} x_i \\ y_i \\ z_i \end{pmatrix}$$

The notation $\begin{bmatrix} R_i^C \end{bmatrix}$ denotes the coordinate rotation transformation to the Tug body-axis system from the i^{th} tank local reference frame.

We now make the assumption that the tanks are positioned such that the local x-axis is parallel to the Tug longitudinal axis and Equation (I.A-58) reduces to

$$\rho_i = \left[\left(\frac{\cos \phi_i}{a_i} \right)^2 + \left(\frac{\sin \phi_i}{b_i} \right)^2 \right]^{-\frac{1}{2}} \quad (\text{I.A-61})$$

$$\text{with} \quad \dot{\rho}_i = \rho^3 \dot{\phi}_i \sin \phi_i \cos \phi_i \left(\frac{1}{a_i^2} - \frac{1}{b_i^2} \right) \quad (\text{I.A-62})$$

and, therefore

$$A = -\rho \sin \phi + K \rho^3 \sin \phi \cos^2 \phi$$

$$B = \rho \cos \phi \cos \theta + K \rho^3 \sin^2 \phi \cos \phi \cos \theta$$

$$C = \rho \cos \phi \sin \theta + K \rho^3 \sin^2 \phi \cos \phi \sin \theta$$

$$D = 0 \quad (\text{I.A-63})$$

$$E = -\rho \sin \phi \sin \theta$$

$$F = \rho \sin \phi \cos \theta$$

$$\text{with } K = \left(\frac{1}{a^2} - \frac{1}{b^2} \right).$$

Also, we have

$$\begin{aligned} \dot{A} &= -\dot{\rho} \sin \phi - \rho \dot{\phi} \cos \phi + K \left[3 \rho^2 \dot{\rho} \sin \phi \cos^2 \phi \right. \\ &\quad \left. + \rho^3 \dot{\phi} (\cos^3 \phi - 2 \sin^2 \phi \cos \phi) \right] \\ \dot{B} &= \dot{\rho} \cos \phi \cos \theta - \rho \dot{\phi} \sin \phi \cos \theta - \rho \dot{\theta} \cos \phi \sin \theta \\ &\quad + K \left[3 \rho^2 \dot{\rho} \sin^2 \phi \cos \phi \cos \theta + \rho^3 \dot{\phi} (2 \sin \phi \cos^2 \phi \cos \theta \right. \\ &\quad \left. - \sin^3 \phi \cos \theta) - \rho^3 \dot{\theta} \sin^2 \phi \cos \phi \sin \theta \right] \end{aligned} \quad (\text{I.A-64})$$

$$\begin{aligned} \dot{C} &= \dot{\rho} \cos \phi \sin \theta - \rho \dot{\phi} \sin \phi \sin \theta + \rho \dot{\theta} \cos \phi \cos \theta \\ &\quad + K \left[3 \rho^2 \dot{\rho} \sin^2 \phi \cos \phi \sin \theta \right. \\ &\quad \left. + \rho^3 \dot{\phi} (2 \sin \phi \cos^2 \phi \sin \theta - \sin^3 \phi \sin \theta) \right. \\ &\quad \left. + \rho^3 \dot{\theta} \sin^2 \phi \cos \phi \cos \theta \right] \end{aligned}$$

$$\dot{D} = 0$$

$$\dot{E} = -\dot{\rho} \sin \phi \sin \theta - \rho \dot{\phi} \cos \phi \sin \theta - \rho \dot{\theta} \sin \phi \cos \theta$$

$$\dot{F} = \dot{\rho} \sin \phi \cos \theta + \rho \dot{\phi} \cos \phi \cos \theta - \rho \dot{\theta} \sin \phi \sin \theta$$

8. Inclusion of Fluid Motion Analog into Basic Approach - The ellipsoid tank representation developed previously has been incorporated into the basic equations of motion and constraint and the original IMPRES code was modified in a consistent fashion. This involved a redefinition of the equations of motion for the Tug vehicle only; the applicable spacecraft equations of motion and those pertinent to the attenuation mechanism required no modification.

For the Tug vehicle, the equations of motion as developed previously and extended to include fluid interactions can be written in a most concise form as

$$\left\{ \dot{h} \right\} = \left\{ G \right\} + \left[\Omega \right] \left\{ h \right\} + \left[b_F^T \right] \left\{ \lambda_F \right\} . \quad (\text{I.A-65})$$

If we now define

$$\left\{ \bar{h} \right\} = \left[T^T \right] \left\{ h \right\} \quad (\text{I.A-66})$$

where $\left[T \right]$ is as described previously, it follows that

$$\left\{ \dot{\bar{h}} \right\} = \left[T^T \right] \left\{ \dot{h} \right\} + \left[\dot{T}^T \right] \left\{ h \right\} \quad (\text{I.A-67})$$

defines the new momenta equations for the Tug vehicle.

9. Digital Code and Sample Program Data - The original IMPRES code was delivered to Marshall Space Flight Center under Contract NAS8-26159 and is not reproduced here; only those portions of the code that were added or modified during this study are included.

A note regarding the structure of program input data is indicated in that input requirements have been slightly extended. The original version requires user-supplied input to define the initial conditions. With reference to MCR-74-23 (Martin Marietta Corporation, April 1974), these initial conditions are defined by the array

$$\begin{array}{cccc} X_C & Y_C & Z_C & 0 \\ l & m & n & \emptyset \\ u_C & v_C & w_C & 0 \\ \omega_{xC} & \omega_{yC} & \omega_{zC} & 0 \end{array}$$

where

row 1 defines inertial coordinates of Tug mass center,
row 2 defines Tug inertial attitude
row 3 defines Tug translational velocity with respect to spacecraft
row 4 defines Tug angular velocity with respect to spacecraft

which must be augmented such that

row 5 = $\begin{bmatrix} \phi_1 & \theta_1 & \phi_2 & \theta_2 \end{bmatrix}$, the initial fluid orientations and
row 6 = $\begin{bmatrix} \dot{\phi}_1 & \dot{\theta}_1 & \dot{\phi}_2 & \dot{\theta}_2 \end{bmatrix}$, the initial fluid rates.

Also, the program code reads an array (FLUID) containing pertinent fluid and tank geometric data, viz

$$\text{FLUID} = \begin{bmatrix} m_1 & a_1 & b_1 & x_{E1} & y_{E1} & z_{E1} \\ m_2 & a_2 & b_2 & x_{E2} & y_{E2} & z_{E2} \end{bmatrix}$$

where m_i = fluid mass

a_i, b_i = tank coefficients

x_{Ei}, y_{Ei}, z_{Ei} = position of tank center with respect to Tug mass center

and two coordinates rotation transformations (TROT1 and TROT2) which orient the local tank coordinates frames with respect to the Tug body-fixed coordinate frame.

B. DOCKRB - DOCKING DYNAMICS ANALYSIS OF SPACECRAFT USING RIGID BODY ANALYSIS

The approach developed within this section differs markedly from that presented previously in that the Tug/spacecraft dynamical system is assumed to consist of a number of interconnected rigid bodies. The assembled system, or any portion thereof, may be spinning or nonspinning and members of the system may experience large relative excursions with respect to each other. The system is, by its inherent nature, a feedback system where inertial forces (e.g., arising from centrifugal or Coriolis acceleration) and restoring and damping forces are motion dependent.

The following subsections detail the basic analytical techniques and describe the application to the Tug/spacecraft docking simulation.

1. System Characterizing Equations - The state equations governing the dynamic response of the total system are summarized as

$$\left\{ \dot{U} \right\}_j = [m]_j^{-1} \left(\left\{ G \right\}_j + [b]_j^T \left\{ \lambda \right\} \right) \quad (\text{I.B-1})$$

$$\left\{ \dot{\beta} \right\} = \sum_j [B]_j \left\{ U \right\}_j \quad (\text{I.B-2})$$

$$\left\{ \dot{\delta} \right\} = f(\left\{ \beta \right\}, \left\{ \dot{\beta} \right\}, \left\{ \delta \right\}) \quad (\text{I.B-3})$$

subject to the constraint equations

$$\sum_j [b]_j \left\{ U \right\}_j = \left\{ \dot{\alpha} \right\} \quad (\text{I.B-4})$$

where the index j ranges over the number of bodies which comprise the system. The first three sets of equations represent n first order, nonlinear, ordinary differential equations while the last represents m additional conditions of kinematic constraint.

State variables of the configuration space include absolute velocities $\left\{ U \right\}$, position coordinates (both angular and cartesian position) $\left\{ \beta \right\}$, and additional variables $\left\{ \delta \right\}$ that are referred to as control variables.

Equations (I.B-1) represent dynamic equilibrium equations for the j th body. They state that a mass matrix $[m]_j$, postmultiplied by a vector of relative accelerations $(\ddot{U})_j$, produces a vector of inertial forces that is balanced by all other state and time dependent forces $(G)_j$ and interconnection constraint forces, $([b]_j^T \{\lambda\})$. The constraint forces $([b]_j^T \{\lambda\})$ are necessary in order that the kinematic constraint equations are satisfied; elements of the vector (λ) are actually Lagrange multipliers. Equations (I.B-2) represent a kinematical transformation, transforming nonholonomic velocities to time derivatives of position coordinates. Equations (I.B-3) are auxiliary differential equations used to implement control dynamics and other feedback effects.

Equations (I.B-4) are an active set of kinematic conditions and Equations (I.B-2) are a passive set. The active set is used to calculate m of the dependent elements of the $(U)_j$ vectors in terms of the remaining independent elements and the prescribed velocities $(\dot{\alpha})$, some of which may be zero and some user-defined functions of time. Thus, the constraint equations are of a general form because nonholonomic, rheonomic conditions may be so represented.

Lagrange multipliers are included for two reasons: (1) a monitor of the multipliers as a function of system motion gives the interconnection forces and torques, and (2) it is convenient to calculate and use the (λ) vector in Equation (I.B-1). The Lagrange multipliers are calculated by differentiating Equation (I.B-4) and combining the result with Equation (I.B-1) giving

$$\{\lambda\} = \left(\sum_j [b]_j [m]_j^{-1} [b]_j^T \right)^{-1} \left[\{\ddot{\alpha}\} - \sum_j \left([b]_j \{U\}_j + [b]_j [m]_j^{-1} \{G\}_j \right) \right] \quad (\text{I.B-5})$$

The differential equations of motion for the system are of the general form:

$$\dot{y}_i = f(y_1, y_2, \dots, y_{n-m}; t), \quad (\text{I.B-6})$$

where the state vector and its time derivative are

$$\{y\} = \begin{bmatrix} \{U\}_1 \\ \{U\}_2 \\ \vdots \\ \{U\}_{NB} \\ \beta_1 \\ \beta_2 \\ \vdots \\ \beta_{N\beta} \\ \delta_1 \\ \delta_2 \\ \vdots \\ \delta_{N\delta} \end{bmatrix} \quad \{\dot{y}\} = \begin{bmatrix} \{\dot{U}\}_1 \\ \{\dot{U}\}_2 \\ \vdots \\ \{\dot{U}\}_{NB} \\ \dot{\beta}_1 \\ \dot{\beta}_2 \\ \vdots \\ \dot{\beta}_{N\beta} \\ \dot{\delta}_1 \\ \dot{\delta}_2 \\ \vdots \\ \dot{\delta}_{N\delta} \end{bmatrix}$$

with NB the total number of bodies of the system, $N\beta$ the total number of position coordinates necessary to orient the system and $N\delta$ the total number of auxiliary (control) differential equations required.

2. Dynamic Equations for a Single Body - Lagrange's equations for a rigid body are

$$\frac{d}{dt} \left(\frac{\partial T}{\partial \dot{q}_j} \right) - \frac{\partial T}{\partial q_j} = Q_j + \sum_{i=1}^m a_{ji} \lambda_i \quad (\text{I.B-7})$$

and

$$\sum_{j=1}^n a_{ij} \dot{q}_j + a_{it} = 0$$

The generalized constraint forces $\left(\sum_i a_{ji} \lambda_i \right)$ augment the generalized forces Q_j (that arise due to the action of external factors) and are necessary in order that the additional conditions of constraint be satisfied. Equations (I.B-7) are complete and general, and the auxiliary constraint equations are in an all encompassing form, because holonomic conditions may be so represented. The coefficients (a_{ij}) may depend explicitly on the time (t), thus the constraint conditions as shown account for both rheonomic and scleronomic situations.

In the equations, n is the number of generalized coordinates involved in the representation and m is the number of auxiliary conditions of constraint. Note that, although the q_j are generalized coordinates (as they must be for the Lagrangian formulation) they are independent only in the isolated case when $m=0$, or when there are no auxiliary constraint conditions.

The generalized coordinates chosen to represent a typical body include three Euler angles to indicate attitude of the body fixed axis system relative to an inertial frame and three projections (components) of the position vector from the origin of the inertial frame to the origin of the body fixed reference system. Note that the origin of the body fixed axis system needn't necessarily coincide with the body's mass center. For the r^{th} body, the generalized coordinates are:

$$\{q_r\} = \begin{bmatrix} \psi \\ \theta \\ \phi \\ X \\ Y \\ Z \end{bmatrix}_r \quad \begin{array}{l} \text{Attitude} \\ \text{Euler Angles} \\ \\ \text{Body's reference} \\ \text{point position} \\ \text{coordinates} \end{array}$$

and, there exists a transformation that relates a set of nonholonomic velocities to the generalized velocities. This transformation is

$$\{U\} = [\beta] \{\dot{q}\}$$

(I.B-8)

where

$$\begin{bmatrix} \beta \end{bmatrix} = \begin{bmatrix} \pi & \\ & \gamma \end{bmatrix} \quad (\text{I.B-9})$$

and the elements of the transformation (γ) are direction cosines relating attitude of the body fixed axis system to the inertial frame. The transformation (π) is also a rotation transformation; however, it is not orthonormal because it relates vector components based on an orthogonal basis to those of a skew (non-orthogonal) basis; namely the axes about which Euler rotations are measured.

Kinetic energy for the typical body is

$$T = \frac{1}{2} \int_V (\bar{\mathbf{v}} \cdot \bar{\mathbf{v}}) \sigma dV \quad (\text{I.B-10})$$

where $\bar{\mathbf{v}}$ is the velocity field and, with reference to Figure I-2, can be expressed as

$$\bar{\mathbf{v}} = \bar{\mathbf{v}}_R + \bar{\boldsymbol{\omega}} \times \bar{\boldsymbol{\rho}}_O \quad (\text{I.B-11})$$

with $\bar{\mathbf{v}}_R = \frac{d\bar{\mathbf{x}}_R}{dt}$

Now, substituting Equation (I.B-11) into Equation (I.B-10) and performing the integration yields

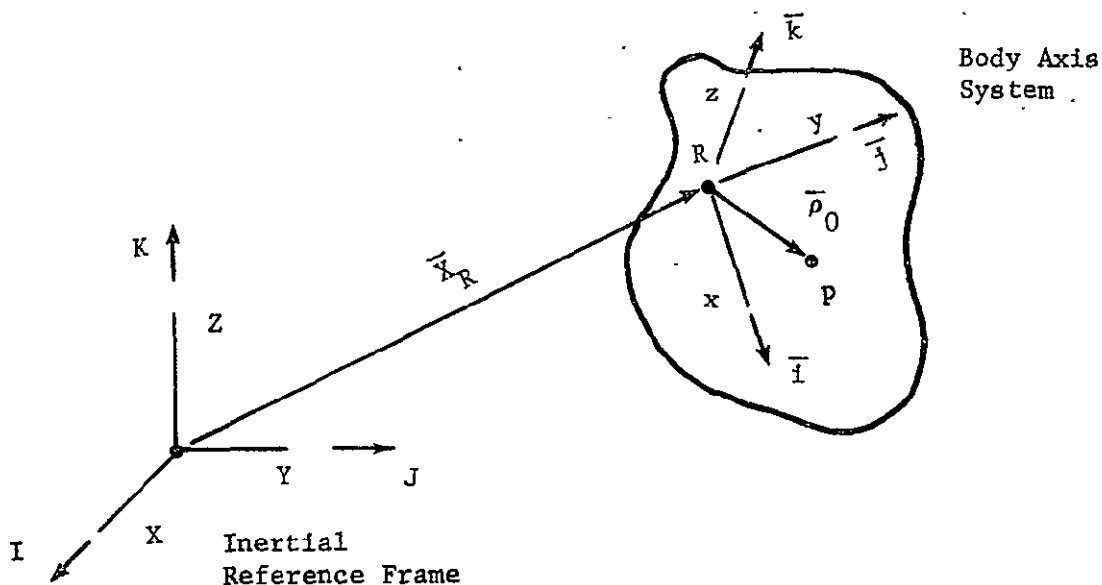


Figure I-2 Typical Body of the System

$$T = \frac{1}{2} m \begin{bmatrix} u & v & w \end{bmatrix} \begin{Bmatrix} u & v & w \end{Bmatrix} + \frac{1}{2} \begin{bmatrix} \omega_x & \omega_y & \omega_z \end{bmatrix} \begin{bmatrix} J_{xx} & -J_{xy} & -J_{xz} \\ -J_{yx} & J_{yy} & -J_{yz} \\ -J_{zx} & -J_{zy} & J_{zz} \end{bmatrix} \begin{Bmatrix} \omega_x \\ \omega_y \\ \omega_z \end{Bmatrix} \quad (\text{I.B-12})$$

where $m = \int_V \sigma dV$

$$J_{xx} = \int_V (y^2 + z^2) \sigma dV,$$

$$J_{xy} = \int_V x y \sigma dV,$$

$$S_x = \int_V x \sigma dV,$$

and all other quantities in Equation (I.B-12) are obtained by cyclic permutations of x , y and z . As kinetic energy is of quadratic form in $\{U\}$ we have

$$T = \frac{1}{2} \begin{bmatrix} U \end{bmatrix} \begin{bmatrix} m \end{bmatrix} \begin{Bmatrix} U \end{Bmatrix} \quad (\text{I.B-13})$$

with $\begin{bmatrix} m \end{bmatrix} = \begin{bmatrix} J_{xx} & -J_{xy} & -J_{xz} & -S_z & S_y \\ & J_{yy} & -J_{yz} & S_z & -S_x \\ & & J_{zz} & -S_y & S_x \\ \hline & \text{symmetric} & & m & \\ & & & & m \\ & & & & & m \end{bmatrix} \quad (\text{I.B-14})$

or, using Equations (I.B-14), (I.B-8) and (I.B-13), the kinetic energy becomes

$$T = \frac{1}{2} \left[\dot{q} \right] \left[\beta \right]^T \left[m \right] \left[\beta \right] \left\{ \dot{q} \right\} . \quad (\text{I.B-15})$$

Let us now refer back to Lagrange's Equations and re-express them in matrix format

$$\begin{aligned} \frac{d}{dt} \left(\left[\beta \right]^T \left[m \right] \left[\beta \right] \left\{ \dot{q} \right\} \right) = \\ + \left\{ Q \right\} + \frac{1}{2} \left\{ \left[\dot{q} \right] \left[\beta_{,j} \right]^T \left[m \right] \left[\beta \right] \left\{ \dot{q} \right\} \right\} \\ + \frac{1}{2} \left\{ \left[\dot{q} \right] \left[\beta \right]^T \left[m \right] \left[\beta_{,j} \right] \left\{ \dot{q} \right\} \right\} + \left[a \right]^T \left\{ \lambda \right\} \end{aligned} \quad (\text{I.B-16})$$

and

$$\left[a \right] \left\{ \dot{q} \right\} = - \left\{ a_t \right\} . \quad (\text{I.B-17})$$

Now define the ordinary momenta to be

$$\begin{aligned} \left\{ p \right\} &= \left[m \right] \left[\beta \right] \left\{ \dot{q} \right\} \\ &= \left[m \right] \left\{ U \right\} \end{aligned}$$

and, since $\left\{ U \right\} = \left[\beta \right] \left\{ \dot{q} \right\}$

it follows that $\left\{ \dot{q} \right\} = \left[\beta \right]^{-1} \left\{ U \right\}$. With this we have

$$\begin{aligned} \left\{ \dot{p} \right\} &= \left[\beta \right]^{-1T} \left\{ Q \right\} + \left[\beta \right]^{-1T} \left(\left\{ \left[\dot{q} \right] \left[\beta_{,j} \right]^T \left\{ p \right\} \right\} - \left[\dot{\beta} \right]^T \left\{ p \right\} \right) \\ &+ \left[\beta \right]^{-1T} \left[a \right]^T \left\{ \lambda \right\} , \end{aligned} \quad (\text{I.B-18})$$

and

$$\left[a \right] \left[\beta \right]^{-1} \left\{ U \right\} = \left\{ -a_t \right\} . \quad (\text{I.B-19})$$

Note now that $\begin{bmatrix} \beta \end{bmatrix}^{-1T}$ transforms the generalized forces $\{Q\}$ to forces "acting in the quasi-coordinates",

$$\{G_{ex}\} = \begin{bmatrix} \beta \end{bmatrix}^{-1T} \{Q\} ;$$

thus $\{G_{ex}\}$ contains ordinary forces and moments due to external sources and corresponds to time derivatives of the ordinary momenta.

Because the transformation $\begin{bmatrix} \beta \end{bmatrix}$ depends only on the Euler angles, it follows that only the first six elements of the column

$$\begin{bmatrix} \beta \end{bmatrix}^{-1T} \left(\begin{bmatrix} \dot{q} \end{bmatrix} \begin{bmatrix} \beta_{,j} \end{bmatrix} \{p\} - \begin{bmatrix} \dot{\beta} \end{bmatrix}^T \{p\} \right)$$

are non-zero, and one finds after considerable algebraic manipulation that this column may be reexpressed as

$$\begin{bmatrix} \tilde{\Omega} \end{bmatrix} \{p\} = \begin{bmatrix} \omega_z & -\omega_y & w & -v \\ -\omega_z & \omega_x & -w & u \\ \omega_y & -\omega_x & v & -u \\ \hline & & \omega_z & -\omega_y \\ & & -\omega_z & \omega_x \\ & & \omega_y & -\omega_x \end{bmatrix} \begin{bmatrix} p(\omega_x) \\ p(\omega_y) \\ p(\omega_z) \\ p(u) \\ p(v) \\ p(w) \end{bmatrix} \quad (I.B-20)$$

so that equations (I.B-18) and (I.B-19) can finally be expressed as

$$\{\dot{p}\} = \{G_{ex}\} + \begin{bmatrix} \tilde{\Omega} \end{bmatrix} \{p\} + \begin{bmatrix} b \end{bmatrix}^T \{\lambda\} \quad (I.B-21)$$

$$\begin{bmatrix} b \end{bmatrix} \{U\} = \{\dot{a}\} \quad (I.B-22)$$

where $\begin{bmatrix} b \end{bmatrix} = \begin{bmatrix} a \end{bmatrix} \begin{bmatrix} \beta \end{bmatrix}^{-1}$

and $\{\dot{a}\} = -\{a_t\}$.

The constraint equations are now expressed in terms of the nonholonomic velocities $\{U\}$; the coefficients $[b]$ are obtained directly from relatively simple, vectorial expressions of kinematic constraint. The same $[b]$ coefficients are transposed and used to multiply $\{\lambda\}$, producing constraint forces/torques corresponding to the ordinary momenta.

If we now define $\{G\}$ to be

$$\{G\} = \{G_{ex}\} + [\tilde{\Omega}][m]\{U\} \quad (I.B-23)$$

it follows that the dynamic equilibrium equations for the r^{th} body are

$$\{\dot{U}\}_r = [m]_r^{-1} \{G\}_r + [b]_r^T \{\lambda\} \quad (I.B-24)$$

to be used in conjunction with system kinematic constraint equations

$$\sum_r [b]_r \{U\}_r = \{\dot{\alpha}\} \quad (I.B-25)$$

This is the same form as that given by Equations (I.B-1) and (I.B-4).

3. Application to Tug Docking - The rigid body developments discussed previously were applied to the analysis of the Space Tug/spacecraft docking maneuver. This was accomplished by considering the total system to consist of six bodies as shown in Figure 1-3 .

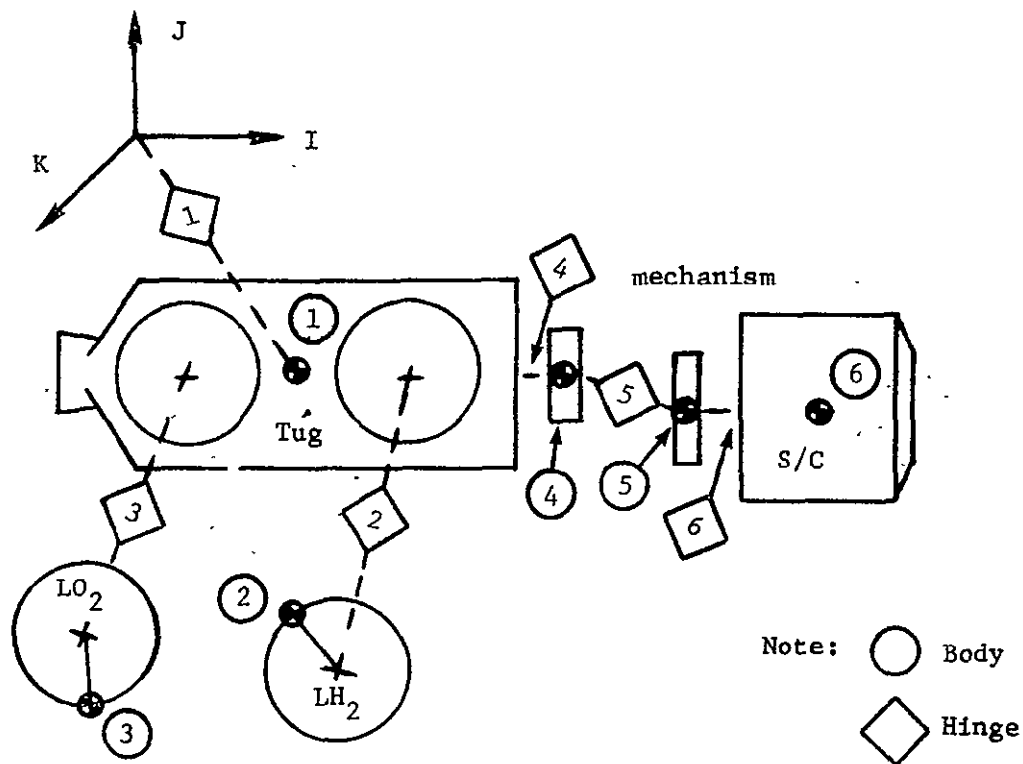


Figure I-3 Tug/Spacecraft System Topology

With reference to the figure, Body 1 (Tug structure) is positioned with respect to an inertial reference through definition of Hinge 1*. Bodies 2 and 3 (LH_2 and LO_2 fluid mass) are positioned with respect to Body 1 via Hinges 2 and 3 respectively while Body 4 (Tug attenuation mechanism) is positioned with respect to Body 1 via Hinge 4. Hinge 5 defines the position of Body 5 (spacecraft attenuation mechanism) with respect to Body 4 and Body 6 (spacecraft structure) is

* A hinge is defined to be a pair of structural hard points with a point situated on each of two contiguous bodies.

positioned with respect to Body 5 via Hinge 6.

At each hinge or connection point there are six possible degrees of freedom. The topology of the complete system is defined by fixing any or all of the relative degrees of freedom (fixed constraint) or by prescribing the relative motion corresponding to the degrees of freedom (rheonomic constraint). Table I-1 summarizes the total system topology.

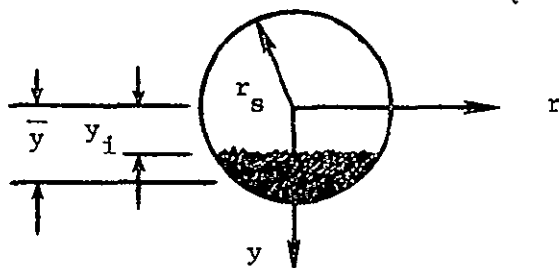
Table I-1 Summary of Topology

<u>Body</u>	
1	Tug structure + engine
2	LH ₂ fluid mass
3	LO ₂ fluid mass
4	Tug attenuation mechanism
5	S/C attenuation mechanism
6	S/C structure
<u>Hinge</u>	
1	Body 1 to inertia - no constraints, 6 DOF
2	Body 2 to Body 1 - constrain translation, 3 DOF
3	Body 3 to Body 1 - constrain translation, 3 DOF
4	Body 4 to Body 1 - user option, 0-6 DOF
5	Body 5 to Body 4 - user prescribed, 6 DOF (rheonomic)
6	Body 5 to Body 6 - user option, 0-6 DOF

4. The Large Amplitude Fluid Motion Model - The large amplitude fluid motion model assumes that the liquid is constrained to move as a point mass on a spherical surface as indicated in Figure I.B-2. This assumption is not considered to be unduly restrictive in view of the known Tug tank geometry.

From MSFC 68M00039-2 we have that the volumes of the LH₂ and LO₂ tanks are 1748 ft³ and 640 ft³, respectively so that, for a spherical approximation, the equivalent tank radii are 7.47 ft and 5.34 ft, respectively. Now it can be shown that an expression for the ratio of propellant volume to tank volume is given by

$$\alpha = V_p/V_t = 1/2 + 3\beta/4 + \beta^3/4 \quad (\text{I.B-26})$$



where V_p = volume of propellant
 V_t = volume of tank
 $\beta = y_i/r_s$
 y_i = fluid level in tank
 r_s = equivalent spherical radius

and an expression for the ratio of propellant centroid location to equivalent spherical radius is given by

$$\gamma = \bar{y}/r_s = 3(1 - 2\beta^2 + \beta^4)/16\alpha \quad . \quad (I.B-27)$$

Table I-2 summarizes results for three burn ratios where r_e denotes the equivalent radius arm for the LH₂ and LO₂ fluid masses.

Table I-2 Summary of Fluid Geometry

% burn	% fill	y_i/r_s	\bar{y}/r_s	r_e (in.)	
				LH ₂	LO ₂
70	30	.28	.531	47.61	34.06
50	50	.0	.375	33.63	24.06
30	70	-.28	.227	20.36	14.56

The appropriate fluid masses are noted in Table I-3 where densities of 4.4 and 71 lb/ft³ for LH₂ and LO₂ are assumed.

Table I-3 Summary of Fluid Masses

% burn	LH ₂ (lbs)	LO ₂ (lbs)	burn ratio
70	2138	12802	5.987
50	3564	21336	5.987
30	4989	29870	5.987

5. Vehicle Inertial Characteristics - The inertial properties of the Tug were taken from MSFC 68M00039-2. With reference to the coordinate system indicated in Figure I-4, we have the properties listed in Table I-4 .

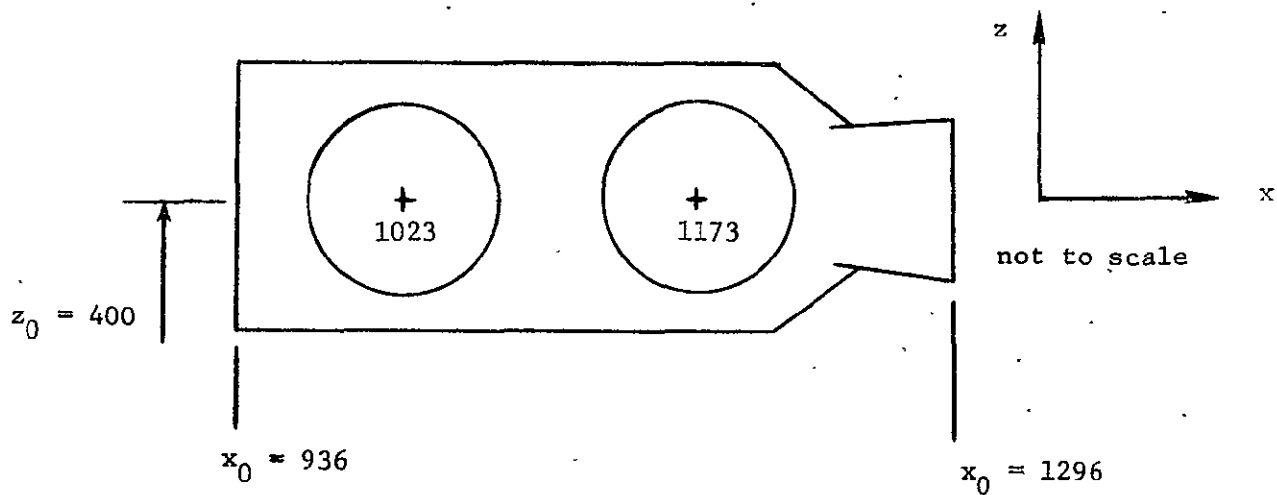


Figure I-4 . Tug Coordinate System for Definition of Inertial Properties

Table I-4 . Tug Inertial Properties

Mass = 178.73 slugs			
Inertia	J_{xx}	J_{yy}	J_{zz}
(slug-ft ²)	5173.5	15939	15191
Center of Gravity	x	y	z
(in.)	1094.3	-0.5	395.8

The inertial and geometric properties of the spacecraft* used in these analyses are shown in Figure I-5 and Table I-5.

* These data taken from SSPD (A-5), March 1973.

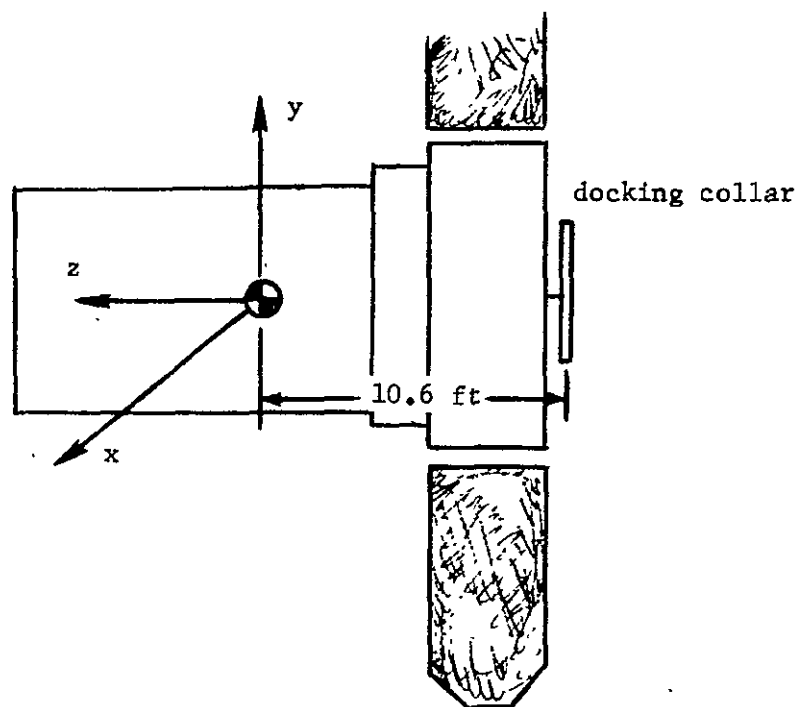


Figure I-5. SEOS Spacecraft Schematic

Table I-5. SEOS Spacecraft Properties

Mass	= 81.86 slugs
J_{xx}	= 3650 slug-ft ²
J_{yy}	= 3660 slug-ft ²
J_{zz}	= 630 slug-ft ²

6. Loads Transformation to Selected Mechanism Points - The simulation monitors constraint forces acting at the several hinge points (eg., some reference point on the impact attenuation mechanism) and this information provides valuable insight into the nature of the interface forces and torques generated as the impacting vehicles move together. However, it is also desirable to ascertain a more complete definition of how these interface forces and torques might be

distributed throughout the attenuation mechanism. With reference to Figure I-6, the forces and torques acting at some reference point on the mechanism can be expressed in terms of those acting at several other mechanism points

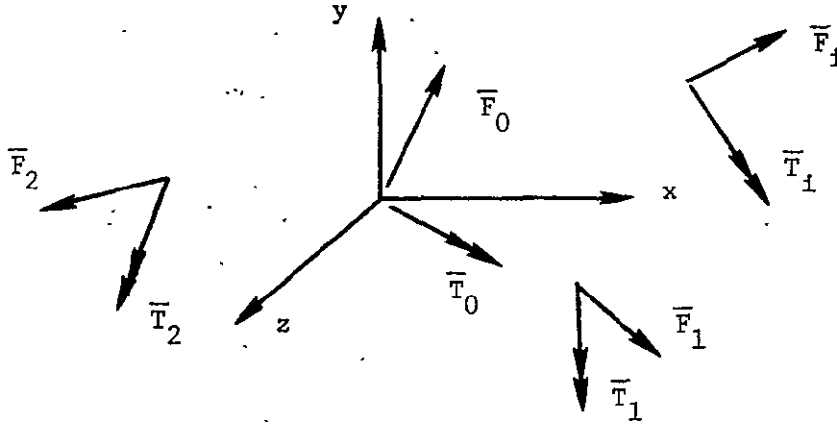


Figure I-6. Mechanism Loads in Terms of Loads at Reference Point

by the expressions

$$\begin{aligned}
 T_{x_0} &= \sum (T_{x_i} + F_{z_i} y_i - F_{y_i} z_i) & F_{x_0} &= \sum F_{x_i} \\
 T_{y_0} &= \sum (T_{y_i} + F_{x_i} z_i - F_{z_i} x_i) & F_{y_0} &= \sum F_{y_i} \\
 T_{z_0} &= \sum (T_{z_i} + F_{y_i} x_i - F_{x_i} y_i) & F_{z_0} &= \sum F_{z_i}
 \end{aligned} \tag{I.B-28}$$

so that we have 6 equations and 6N unknowns of the form

$$\begin{bmatrix} T_{x_0} & T_{y_0} & T_{z_0} & F_{x_0} & F_{y_0} & F_{z_0} \end{bmatrix} = \begin{bmatrix} \dots & T_{x_i} & T_{y_i} & T_{z_i} & F_{x_i} & F_{y_i} & F_{z_i} & \dots \end{bmatrix} \begin{bmatrix} \vdots \\ \hline 1 & & & & & & \\ & 1 & & & & & \\ & & 1 & & & & \\ & & & z_i & -y_i & & 1 \\ -z_i & & & & x_i & & \\ & & & & & 1 & \\ y_i & -x_i & & & & & 1 \\ \hline \vdots \end{bmatrix}$$

or, in condensed form

$$B^T = X^T A^T \quad (I.B-29)$$

which is equivalent to $AX = B$.

Now, given the equations $AX = B$ with more unknowns than available equations, it can be shown that a solution (not necessarily unique) is

$$X = A^T (AA^T)^{-1} B \quad (I.B-30)$$

and this establishes a transformation $(A^T (AA^T)^{-1})$ that establishes the forces and torques at selected points in terms of those at the interface reference point.

7. Power Series Representation of Docking Trajectory - The impact maneuver simulation is structured such that supplied values of initial and final conditions describing relative positions, rates and accelerations of one vehicle

with respect to the other are satisfied through prescription of rheonomically applied constraint conditions. In general, there are six relative degrees of freedom between the spacecraft and Tug (three translation and three rotation) and each of the six are described as a power series function of time as (eg., the longitudinal displacement)

$$x = a_0 + a_1 t + a_2 t^2 + a_3 t^3 + a_4 t^4 + a_5 t^5 \quad (I.B-31)$$

$$\dot{x} = a_1 + 2a_2 t + 3a_3 t^2 + 4a_4 t^3 + 5a_5 t^4$$

$$\ddot{x} = 2a_2 + 6a_3 t + 12a_4 t^2 + 20a_5 t^3$$

where the coefficients are satisfied by the initial and final conditions. Thus, if we prescribe for $t=0$ (initiation of maneuver) that

$$x_0 = A \quad \dot{x}_0 = B \quad \ddot{x}_0 = C$$

and for $t = t_f$ (termination of maneuver) that

$$x_f = D \quad \dot{x}_f = E \quad \ddot{x}_f = F$$

we have

$$a_0 = A \quad a_1 = B \quad a_2 = C/2$$

and

$$\begin{bmatrix} t_f^3 & t_f^4 & t_f^5 \\ 3t_f^2 & 4t_f^3 & 5t_f^4 \\ 6t_f & 12t_f^2 & 20t_f^3 \end{bmatrix} \begin{Bmatrix} a_3 \\ a_4 \\ a_5 \end{Bmatrix} = \begin{Bmatrix} D-A-Bt_f-Ct_f^2/2 \\ E-B-Ct_f \\ F-C \end{Bmatrix}$$

which can be solved for a_3 , a_4 and a_5 . Knowledge of the series coefficients now allows a step-by-step evaluation for acceleration, velocity and displacement

for each of the six relative coordinates as indicated in Figure I-7 .

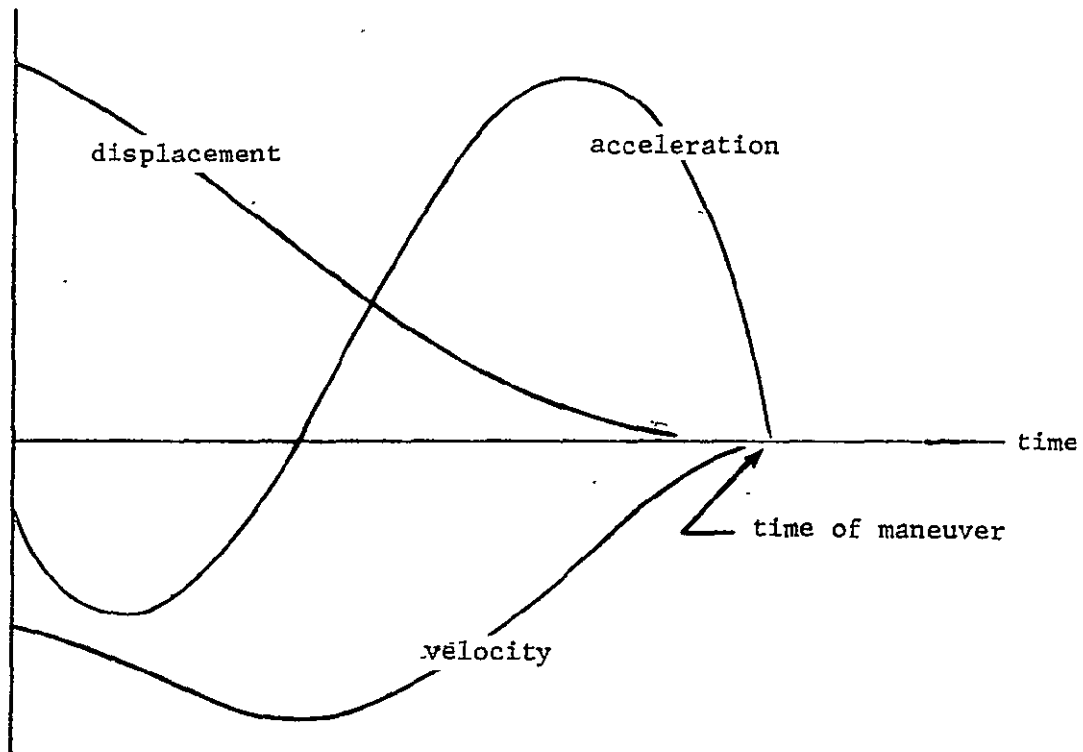


Figure I-7. Typical Docking Trajectory

This technique has been implemented in the digital code although any other prescription of the docking trajectory could be accommodated with only minor changes.

8. Digital Code and Sample Program Data - The digital code presented herein is derived from a more general approach to solutions of systems of interconnected flexible spacecraft systems that was originally developed for Marshall

Space Flight Center under contract NAS8-30761.

The required program input formats are completely described in Volume II of the previously cited reference MCR-75-18 with the exception of two additional input arrays. The first array specifies the initial and final values of displacement, velocity and acceleration across the docking interface hinge in the form

$$\text{DOCDAT} = \begin{bmatrix} \theta_{10} & \dot{\theta}_{10} & \ddot{\theta}_{10} & \theta_{1f} & \dot{\theta}_{1f} & \ddot{\theta}_{1f} \\ \theta_{20} & . & . & . & . & . \\ \theta_{30} & . & . & . & . & . \\ x_0 & . & . & . & . & . \\ y_0 & . & . & . & . & . \\ z_0 & \dot{z}_0 & \ddot{z}_0 & z_f & \dot{z}_f & \ddot{z}_f \end{bmatrix}$$

and the second specifies the coordinate locations of points on the Tug mechanism where forces and torques are desired, viz

$$\text{XYZ} = \begin{bmatrix} x_1 & . & . & . & x_n \\ y_1 & . & . & . & y_n \\ z_1 & . & . & . & z_n \end{bmatrix}$$

II. PROGRAM DOCK DESCRIPTION

This program is a 3-D simulation of the terminal docking of a tug with a spacecraft. Closed loop attitude and translation control utilizes sensors measuring relative range, line-of-sight and target attitude to direct the firing of multiple tug attitude control rockets to maneuver to a docking with the spacecraft. This initial version of the program directs the tug to approach the spacecraft along the docking axis to an impact docking at a prescribed approach velocity. A simple phase plane autopilot controls tug attitude, and translation velocity commands are followed within prescribed dead band tolerances.

A. MATHEMATICAL FORMULATION

The general requirements that resulted in the formulation of this program are discussed in Volume II, Section II.D.2, and are not reiterated here. Rather, this section simply describes how these requirements were met. The geometrical representation is of pitch plane motion of the Space Tug relative to a target spacecraft moving in a circular orbit about the earth. The Tug is controlled by 24 rocket engines (not all of them used in pitch plane motion) which can be pulsed for some minimum duration, or left on as long as desired. These engines are oriented as defined in the MSFC Tug Baseline Descriptions Document (Vol. II, Ref. 7). Pitch attitude control is effected using the phase plane logic described in this same baseline document. The axes are defined differently, being related to the line of sight between Tug and Spacecraft, rather than to inertial attitude. Control laws are used which operate on sensed data (line-of-sight, target attitude and range - reflecting the availability of these data) to direct closure between the vehicles.

In an effort to save computer time, this program does not operate at the shortest airborne computer (minor) cycle at all times. Rather, it preferentially operates at a long 'coast' cycle that will not be a part of Tug airborne computer logic. It then performs a sequence of tests to determine if any shorter computer interval activities were passed over in the simulation. If this is the case, the simulation shortens its

computational interval as required to achieve a true representation of Tug motion. This logic is somewhat involved, as shown in this section, but it results in excellent computer time savings.

Finally, this program generates the summary of output data required to interpret system performance. The principal mathematical formulations required to implement these functions follows:

1. Definition of Geometry

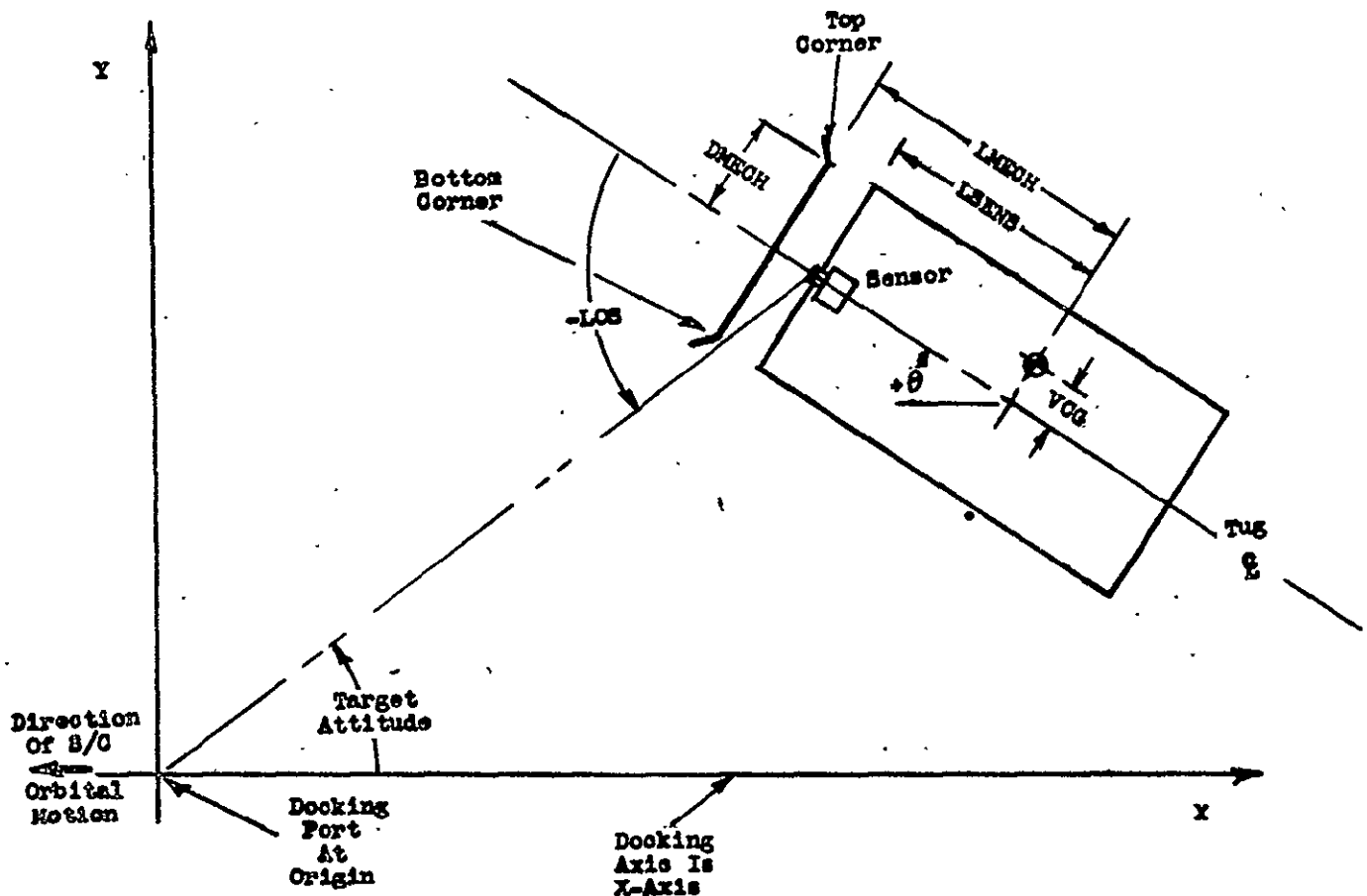
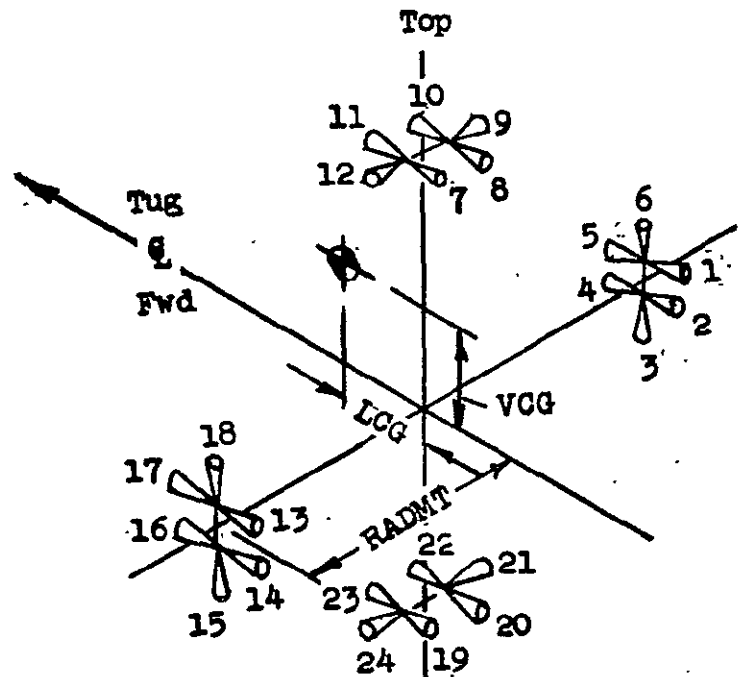


Figure II-1. Program Dock Geometry

The sign conventions and general geometry used in this simulation is shown in Figure II-1. This array permits representation of the physical geometry of the tug, including an offset center of gravity, location of the docking sensors and docking mechanism towards the forward end of the

Tug, and the use of a peripheral type of docking mechanism. The origin of the X-Y axes is at the centerline of the target spacecraft, with the Y-axis along the Earth radius and the X-axis opposite to the direction of spacecraft circular orbital motion. The docking axis, in this formulation, is assumed to be along the X-axis.

The arrangement of RCS engines is as described in the Baseline Tug Description. The numbering of these nozzles is illustrated in Figure II-2. This also shows the C.G. offset with respect to the engine location. Not all of these engines are involved in the pitch plane motion simulated in this program.



PYCANTD--Cant Angle Of Pitch & Yaw Nozzles
 RCANTD--Cant Angle Of Roll Nozzles (Deg)
 (Positive outward From Axes Of Symmetry)

Figure II-2. RCS Engine Geometry

2. RCS Engine Forces & Moments -- The forces and moments created by each of the RCS engines is summarized in Table II-1. The program logic for turning these engines on is as follows. In the sequence, translation commands are honored first, then attitude commands are superimposed. A forward translation command results in engines, 1, 2, 7, 8, 13, 14, 19 and 20 being turned on. An aft translation command results in engines 4, 5, 10, 11, 16, 17, 22 and 23 being turned on. In the superposition for attitude control, a pitch-up command results in engines 7, 8, 22 and 23 being turned on, engines 10, 11, 19 and 20 being turned off if they are on. A pitch down command results in the reverse operation. Thrust forces and propellant utilization are given in terms of an input value of thrust (THR), and a flow rate derived from specific impulse

$$(g_m = \frac{THR}{ISP}, \text{ where } g = 9.81 \text{ m/sec}^2 \text{ (32.174 ft/sec}^2\text{)})$$

3. Coast Integration -- The coast flight motion uses the Clobessy-Willshire formulation for the relative motion between two vehicles, where the origin of a rotating rectangular coordinate system is centered in one of the vehicles as illustrated in Figure V-1. The acceleration of a vehicle coasting in this coordinate frame, assuming a linearization of the acceleration forces, is given by:

$$\ddot{X} = G1 \dot{y}_0$$

$$\ddot{Y} = G2 y_0 - G1 \dot{X}_0$$

where

$$G1 = 2 \left(\frac{\mu}{R^3} \right)^{\frac{1}{2}}$$

$$G2 = \frac{3\mu}{R^3}$$

μ = Earth's gravitational constant

R = Radius of reference circular orbit

$()_0$ = Represents initial condition

Table II-1 RCS Engine Forces and Moments

Engine	Horizontal Translation Force	Vertical Translation Force	Pitch Torque	Use
1 & 2	$2*THR*\cos(PYCANT)$	0	$2*THR*\cos(PYCANT)*VCG$	Move Fwd
3	0	$THR*\cos(RCANT)$	$-THR*\cos(RCANT)*LCG$	Move Up
4 & 5	$-2*THR*\cos(PYCANT)$	0	$-2*THR*\cos(PYCANT)*VCG$	Move Aft
6	0	$-THR*\cos(RCANT)$	$THR*\cos(RCANT)*LCG$	Move Down
7 & 8	$2*THR*\cos(PYCANT)$	$-2*THR*\sin(PYCANT)$	$-2*THR*\cos(PYCANT)*(MTRAD-VCG-LCG*\sin(PYCANT))$	Pitch Down Move Fwd
10 & 11	$-2*THR*\cos(PYCANT)$	$-2*THR*\sin(PYCANT)$	$2*THR*\cos(PYCANT)*(MTRAD-VCG+LCG*\sin(PYCANT))$	Pitch Up Move Aft
13 & 14	$2*THR*\cos(PYCANT)$	0	$2*THR*\cos(PYCANT)*VCG$	Move Fwd
15	0	$THR*\cos(RCANT)$	$-THR*\cos(RCANT)*LCG$	Move Up
16 & 17	$-2*THR*\cos(PYCANT)$	0	$-2*THR*\cos(PYCANT)*VCG$	Move Aft
18	0	$-THR*\cos(RCANT)$	$THR*\cos(RCANT)*LCG$	Move Down
19 & 20	$2*THR*\cos(PYCANT)$	$2*THR*\sin(PYCANT)$	$2*THR*\cos(PYCANT)*(MTRAD+VCG-LCG*\sin(PYCANT))$	Move Fwd Pitch Up
22 & 23	$-2*THR*\cos(PYCANT)$	$2*THR*\sin(PYCANT)$	$-2*THR*\cos(PYCANT)*(MTRAD+VCG+LCG*\sin(PYCANT))$	Move Aft Pitch Down

Sign Convention: Forward, Up Forces And
Nose Up Moment Positive

ORIGINAL PAGE IS
OF POOR QUALITY

An evaluation of the complexity of integration required to achieve adequate accuracy was made for anticipated docking simulation distances and times. It was found that the simplest approach was adequate. Therefore, the following coast integration was employed.

$$\begin{aligned}\dot{\tilde{X}}_1 &= \dot{\tilde{X}}_0 + \ddot{\tilde{X}} \text{ DTC} \\ X_1 &= X_0 + \dot{\tilde{X}}_0 \text{ DTC} + \frac{1}{2} \ddot{\tilde{X}} (\text{DTC})^2 \\ \dot{\tilde{Y}}_1 &= \dot{\tilde{Y}}_0 + \ddot{\tilde{Y}} \text{ DTC} \\ Y_1 &= Y_0 + \dot{\tilde{Y}}_0 \text{ DTC} + \frac{1}{2} \ddot{\tilde{Y}} (\text{DTC})^2\end{aligned}$$

where DTC = Coast integration interval.

Also, in coast flight, there are no forces changing the vehicle pitch rate. Therefore:

$$\dot{\tilde{\theta}}_1 = \dot{\tilde{\theta}}_0 + \ddot{\tilde{\theta}} \text{ DTC}$$

4. Powered Flight Integration -- The powered flight integration is identical in principal. The difference is that the contribution of the thrust of each engine that is turned on to horizontal and vertical components of force and to torque is summed up and set equal to HTHR, VTHR and TORQUE, respectively. Then,

$$\begin{aligned}\theta_1 &= \theta_0 + \dot{\theta}_0 \text{ DTP} + \frac{\text{TORQUE}}{2 I_{YY}} (\text{DTP})^2 \\ \dot{\theta}_1 &= \dot{\theta}_0 + \frac{\text{TORQUE}}{I_{YY}} \text{ DTP} \\ \theta_{\text{AVG}} &= \frac{\theta_0 + \theta_1}{2}\end{aligned}$$

where

DTP = Powered flight integration interval

I_{YY} = Vehicle pitch moment of inertia

$$\begin{aligned}X &= (G1) Y_0 - \frac{\text{HTHR} \cos \theta_{\text{AVG}}}{m} + \frac{\text{VTHR} \sin \theta_{\text{AVG}}}{m} \\ \ddot{Y} &= (G2) Y_0 - (G1) \dot{X}_0 + \frac{\text{HTHR} \sin \theta_{\text{AVG}}}{m} + \frac{\text{VTHR} \cos \theta_{\text{AVG}}}{m}\end{aligned}$$

The integration technique used here is identical to that used in coast flight. Current weight is obtained by integrating propellant flow rate. Moment of inertia is assumed constant.

5. Command Generation -- The commands used to drive the tug to final docking are based upon measurements of range, line of sight and target attitude made by the sensors (See Figure II-1). Measurements are generated by calculating the true location of the sensor, and adding measurement errors:

$$XI = X - LSENS \cos (\text{THETA})$$

$$YI = Y + LSENS \sin (\text{THETA})$$

where

XI, YI are true instrument location

X, Y are true Tug CG location

THETA is Tug pitch angle

LSENS is shown on Figure II-1

Then:

$$RANGS = (XI^2 + YI^2)^{\frac{1}{2}} + RGER$$

$$TAS = \arctan (YI/XI) + TAER$$

$$LOSS = -(\arctan (YI/XI) + \text{THETA} + LOSER)$$

where

RANGS is sensed range

RGER is its measurement error

TAS is sensed target attitude

TAER is its measurement error

LOSS is sensed line of sight

LOSER is its measurement error

NOTE: Error inputs are in degrees

These measurements are then used to generate the components of sensed tug position and velocity.

$$\begin{aligned}
XS &= X - LSENS * \cos (THETA) \\
YS &= Y + LSENS * \sin (THETA) \\
XSD &= XD + LSENS * \sin (THETA) * THD + VHER \\
YSD &= YD + LSENS * \cos (THETA) * THD + VVER
\end{aligned}$$

where

XD, YD are velocities at the Tug C.G.

THD is true Tug pitch rate

VHER, VVER are input components of velocity measurement error

This program deals with the loss of measurements by updating position information in a simulated Tug IMU to agree with sensed position information at the time the measurement is lost, and using these data to generate dummy sensed data. The dummy sensed position data (XIU, YIU) is generated and used after either sensed range data (range less than MRRNG) or target attitude data (range less than MRTA) is lost. Then, at ranges less than MRRNG:

$$RANGS = (XIU^2 + YIU^2)^{\frac{1}{2}}$$

At ranges less than MRTA,

$$TAS = \arctan (YIU/XIU)$$

At ranges less than MRLOS,

$$LOSS = -(\arctan (YIU/XIU) + THETA)$$

The steering, or command, control laws implemented in this simulation are very simple, but have performed adequately:

$$THCOM = LOSS + THETA$$

$$XDCOM = KVAPR$$

$$YDCOM = KVAPR * KSTEER * (YS/XS)$$

where

THCOM is pitch command

XDCOM is X-velocity command (input as KVAPR)

YDCOM is lateral velocity command

KSTEER is steering gain

These calculations are made at the start of each major (powered flight) cycle and held constant throughout that period. Attitude error signals are generated (equivalent to) each minor cycle using the difference between the current pitch attitude and the command.

$$THER = THETA - THCOM$$

Attitude commands are established as described in the next subsection. Translation engine settings are updated once each major cycle by forming translation velocity errors and comparing them with the acceptable dead bond. If the velocity error ($XSD - XDCOM$ or $YSD - YDCOM$) is greater or less than the velocity dead band ($VDBX/2$ or $VDBY/2$), the appropriate translation engine settings are made (Section II.A.2).

6. Attitude Phase Plane Definition

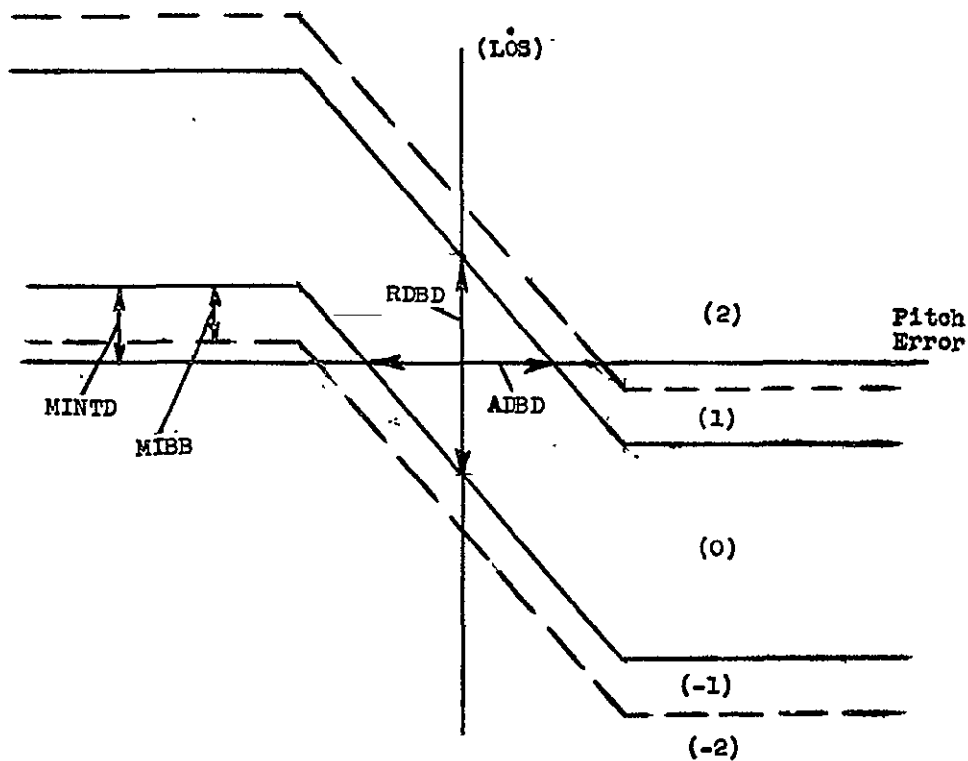


Figure II-3. Phase Plane Representation

The attitude phase plane representation implemented in this program is illustrated in Figure II-3. Program input parameters are illustrated -- it is set up to accept these parameters in degrees and convert them to radians internally. Program logic turns the pitch down engines full on in the (2) region illustrated, on for one minor cycle interval in the (1) region. In the (0) region, no pitch engines are called for. The (-2) and (-1) regions are pitch up regions.

The pitch error entry to the phase-plane control is generated as the current pitch attitude minus the pitch command. Pitch command generation was discussed in subsection II.B.5. The line of sight rate entry is composed of the inertial pitch rate plus a geometric line of sight rate generated from $\frac{\bar{R} \times \bar{V}}{R^2}$, where R and V are the relative range and velocity measured by the rendezvous sensors. Specifically:

$$LSR = THD + \frac{XS * YSD - YS * XSD}{XS^2 + YS^2}$$

where

LSR is the line of sight rate

XS, YS are sensed position

XSD, YSD are sensed velocity

THD is pitch rate

7. Compute Interval Control -- A simplified overall logic flow for PROGRAM DOCK is shown in Figure II-4. This illustrates the main aspects of how the computational interval is controlled.

At the start of each interval, attitude and translation commands are checked. If neither is required, and coast (power off) flight is commanded, a long coast compute interval is initiated (DTCS is the input name for the standard coast interval). If power-off flight is still commanded at the end of the interval, integration at the coast interval is continued. If not, a calculation routine is entered to establish the end of the first major cycle where translation commands were not satisfied, or the end of first minor cycle where attitude commands were not satisfied (whichever came first). The major cycle interpretation is made simply by backing

8. Printout Summary -- The standard printout block is shown in the sample run shown in Table II-4. Several auxiliary calculations are required to show the motion of the docking mechanism with respect to the spacecraft docking port. An approach path, and position and rates of the docking mechanism top corner, bottom corner and centerline are generated. The geometry associated with these parameters is shown in Figure II-1. The resulting equations are given by:

$$\begin{aligned}
 XCL &= X - LMECH * \cos (THETA) \\
 YCL &= Y + LMECH * \sin (THETA) - VCG * \cos (THETA) \\
 XDCL &= XD + LMECH * \sin (THETA) * THD \\
 YDCL &= YD + LMECH * \cos (THETA) * THD - VCG * \sin (THETA) * THD \\
 PATH &= \text{Aton } (YDCL/XDCL) \\
 XTC &= X - LMECH * \cos (THETA) + DMECH * \sin (THETA) \\
 YTC &= Y + LMECH * \sin (THETA) - (VCG - DMECH) * \cos (THETA) \\
 XDTC &= XD + LMECH * \sin (THETA) * THD + DMECH * \cos (THETA) * THD \\
 YDTC &= YD + LMECH * \cos (THETA) * THD - (VCG - DMECH) * \sin (THETA) * THD \\
 XBC &= X - LMECH * \cos (THETA) - DMECH * \sin (THETA) \\
 YBC &= Y + LMECH * \sin (THETA) - (DMECH + VCG) * \cos (THETA) \\
 XDBC &= XD + LMECH * \sin (THETA) * THD - DMECH * \cos (THETA) * THD \\
 YDBC &= YD + LMECH * \cos (THETA) * THD - (DMECH + VCG) * \sin (THETA) * THD
 \end{aligned}$$

where

XCL, YCL is mechanism centerline position
 XDCL, YDCL is mechanism centerline velocity
 PATH is centerline approach path angle
 XTC, YTC is mechanism top corner position
 XDTC, YDTC is mechanism top corner velocity
 XBC, YBC is mechanism bottom corner position
 XDBC, YDBC is mechanism bottom corner velocity
 THETA is Tug pitch angle
 THD is Tug pitch rate
 LMECH is C.G. to Mechanism distance (Figure II-1)
 DMECH is mechanism diameter (Figure II-1)
 VCG is vertical displacement of Tug C.G. (Figure II-1)

B. PROGRAM DOCK DESCRIPTION

1. USERS INSTRUCTIONS

This program utilizes standard FORTRAN namelist input. The arrangement of the run deck is as follows:

- 1) Control Cards (System Dependent)
- 2) Program Deck
- 3) Input Deck

```
P$ INPT
      NAME = X.XX,
      :
      $
P$ INPT
      NAME = X.XX,
      :
      $
```

- 4) EOF

Any number of runs can be sequenced. The input namelist with definitions is:

REFR	Orbital Radius of Target Spacecraft (ft)
LSENS	Distance Fwd of C.G. of Sensor Package (ft)
RGER	Range Measurement Error -- Adds to Measurement (ft)
TAERD	Target Attitude Measurement Error -- Additive (deg)
LOSERD	Line-of-Sight Measurement Error -- Additive (deg)
VHER	Horizontal Velocity Measurement Accuracy (ft/sec)
VVER	Vertical Velocity Measurement Accuracy (ft/sec)
MRRNG	Minimum Range at Which Range can be Measured (ft).
MRTA	Min Range at Which Target Attitude can be Measured (ft)
MRLOS	Min Range at Which Line-of-Sight can be Measured (ft)
KVAPR	Desired Docking Approach Velocity (ft/sec)
KSTEER	Lateral Velocity Steering Gain (Nondimensional)
ADBD	Total Attitude Dead Band (deg)
MNTDD	Minimum THETA Dot at Large THETA for Control Off (deg/sec)

RDBD	Total Rate Dead Band (deg/sec)
MIBBD	Min Impulse Band Width (deg/sec)
PROX	Proximity - Range at Which Compute Interval, Output Change (ft)
DTPR	Powered Flight Compute Interval at Remote Range (sec)
DTPN	Powered Flight Compute Interval at Close Range (sec)
DTAS	Attitude Control Minimum Impulse Compute Interval (sec)
VDBX	Total X-Velocity Dead Band (ft/sec)
VDBY	Total Y-Velocity Dead Band (ft/sec)
VIYY	Vehicle Moment of Inertia (slug ft ** 2)
WTO	Initial Vehicle Weight (lb)
THR	ACS Rocket Thrust (lb)
AISP	ACS Rocket ISP (sec)
PYCANTD	Pitch/Yaw ACS Rocket Cant Angle (deg)
RCANTD	Roll ACS Rocket Nozzle Cant Angle (deg)
VCG	Vertical C.G. Offset (ft)
CGL	Longitudinal Distance of C.G. Ahead of Nozzles (ft)
RADMT	Mount Radius of ACS Engine Modules (ft)
LMECH	Longitudinal Distance from C.G. To Docking Mechanism (ft)
DMECH	Diameter of Docking Mechanism (ft)
YO	Initial X-Position (ft)
YO	Initial Y-Position (ft)
YDO	Initial X-Velocity (ft/sec)
YDO	Initial Y-Velocity (ft/sec)
THO	Initial Pitch Attitude (deg)
THDO	Initial Pitch Rate (deg/sec)
XEND	Final X-Position at Docking
DTGS	Coast Compute Interval

2. PROGRAM DETAILS

The complete flow of program Dock is given in Figure II-5. A listing is shown in Table II-2, sample input in Table II-3 and sample output in Table II-3.

Procedure _____ Drawn By BETTY DICKMAN

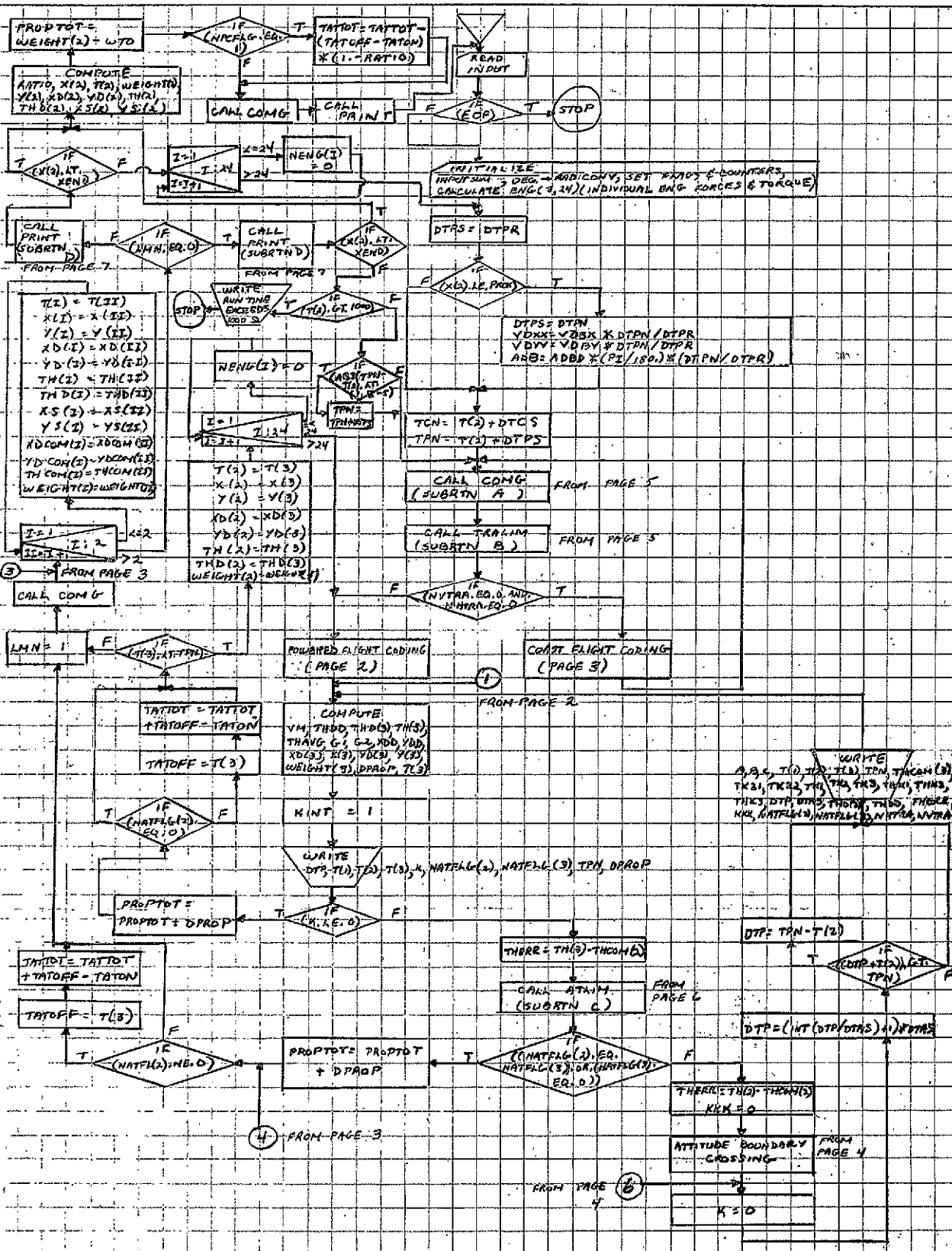


FIG 11-5(a) **DBPAM DOCK Flow Diagram**

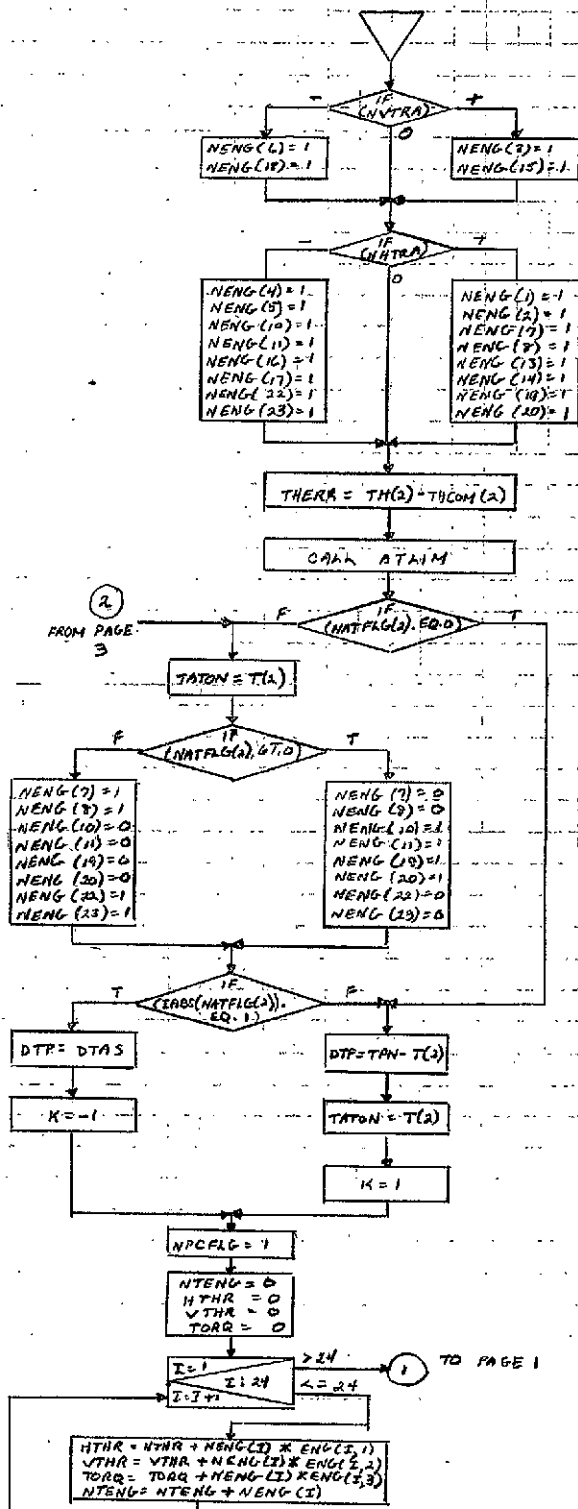
FLOW CHART & BLOCK DIAGRAM

FORM DEN 1103-01 (4-64)

Application _____ Date DECEMBER 1, 1975 Page 2 of 8
 Procedure _____ Drawn By BETTY DICKMAN

POWERED FLIGHT CODING

ORIGINAL PAGE IS
OF POOR QUALITY



Fold

Fold to enter line

Procedure _____ Drawn By BETTY DICKMAN

ORIGINAL PAGE IS
OF POOR QUALITY

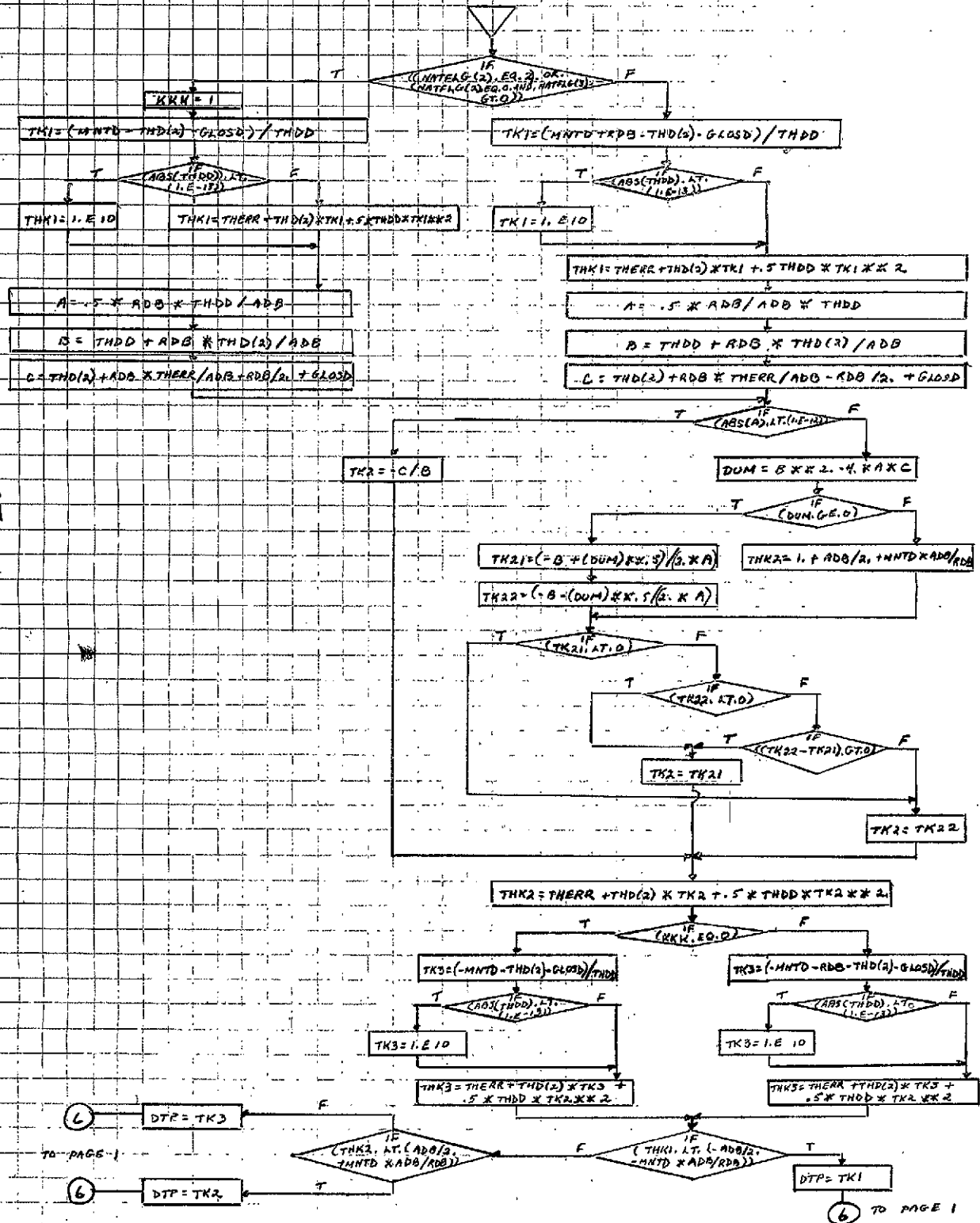


FLOW CHART & BLOCK DIAGRAM

FORM DEN 1103-01 (4-64)

Application _____ Date DECEMBER 1, 1975 Page 4 of 8
 Procedure _____ Drawn By BETTY DICKMAN

ATTITUDE BOUNDARY CROSSING



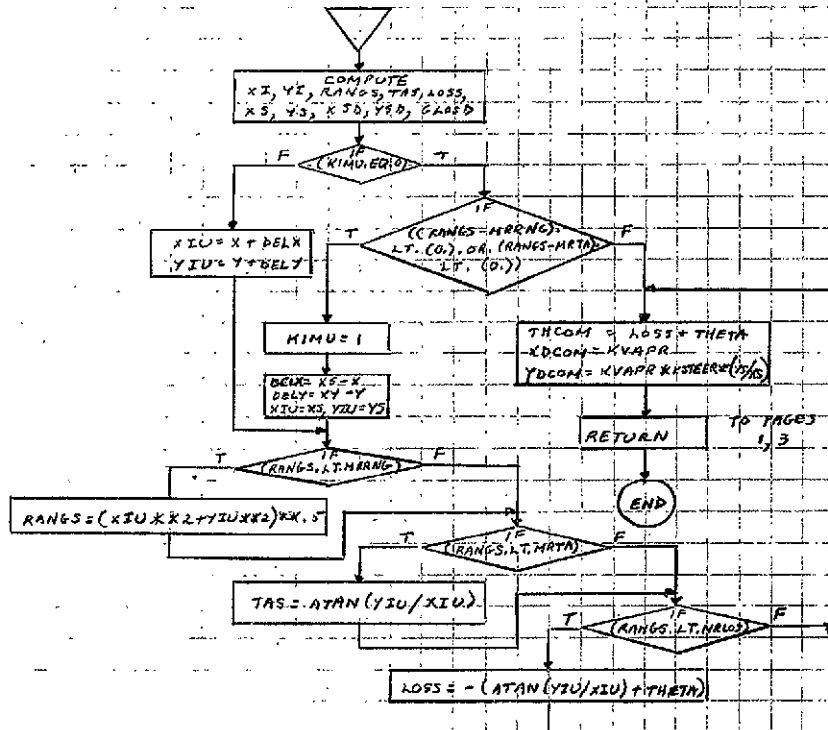
TO PAGE 1

TO PAGE 1

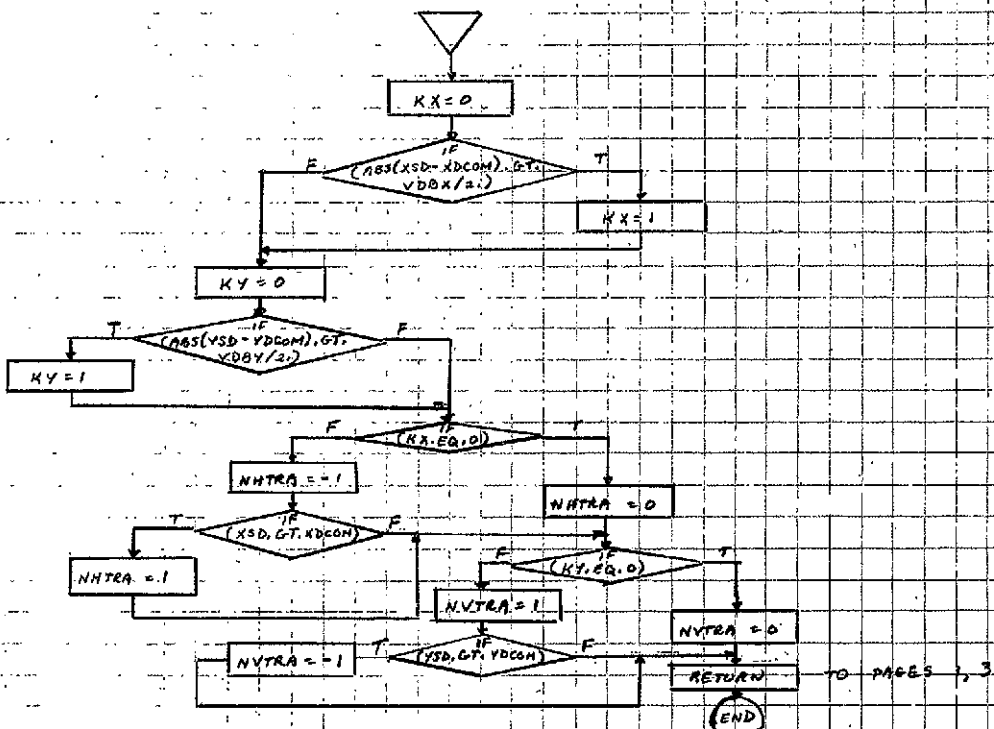
11-20
 FOLDOUT FRAME 1
 ORIGINAL PAGE IS
 OF POOR QUALITY
 Fold
 Fold to enter line FOLDOUT FRAME 2

Procedure _____ Drawn By BETTY DICKMAN

ORIGINAL PAGE IS
OF POOR QUALITY



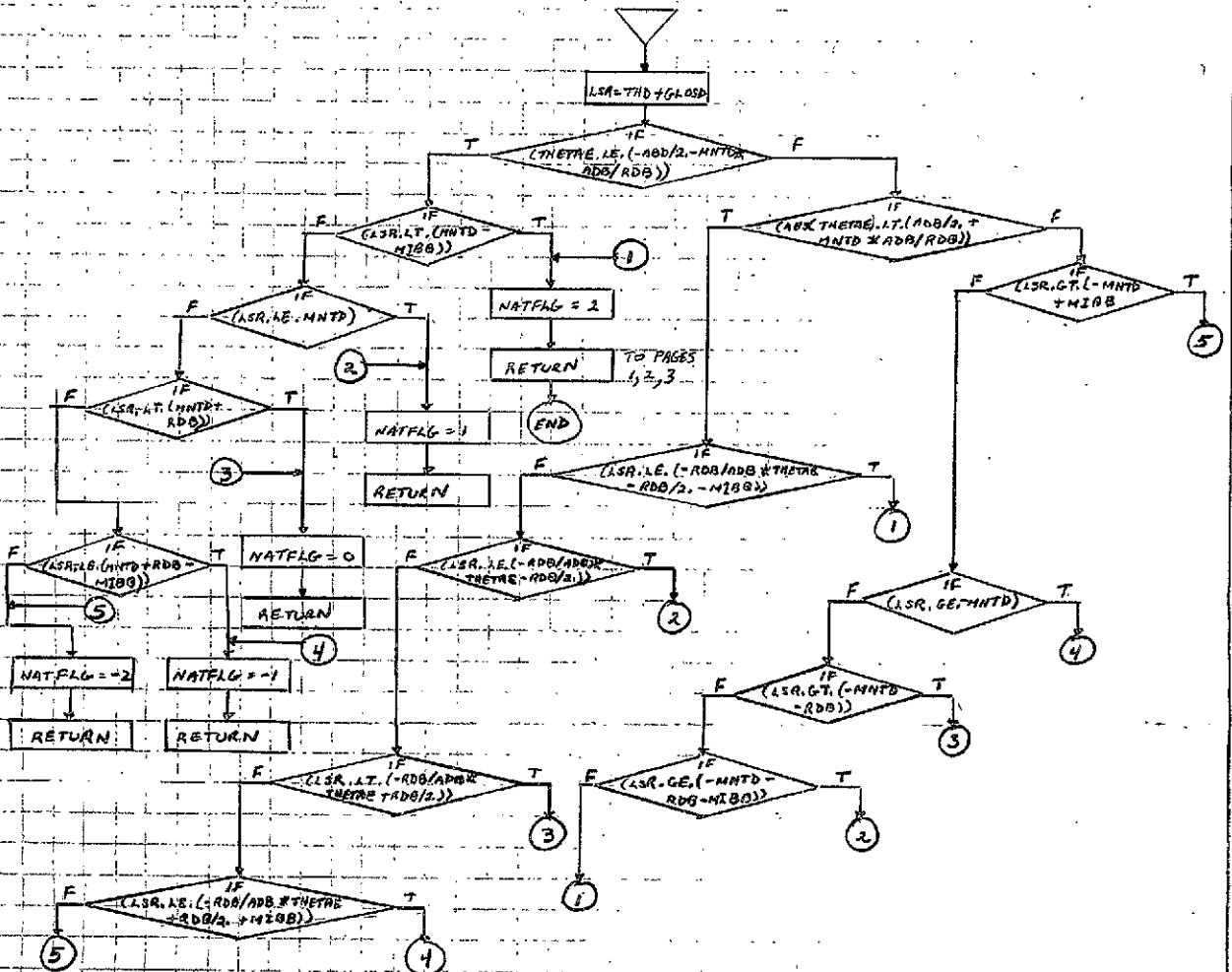
SUBROUTINE TRAINT(B)



FORM DEN 1103-01 (4-64)

Procedure _____ Drawn By BETTY DICKMAN

SUBROUTINE ATIM (C)



WORLD OF

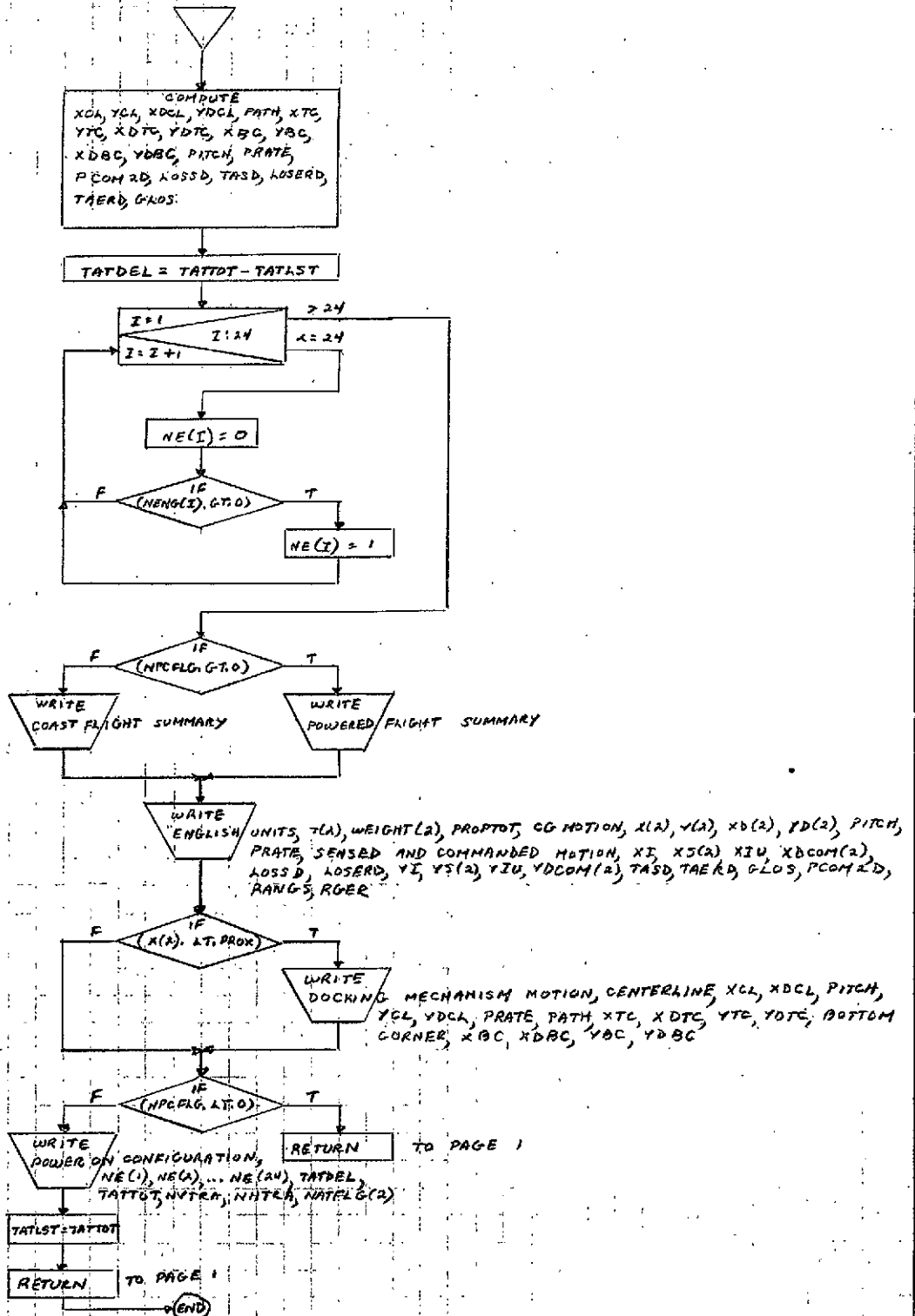
FLOW CHART & BLOCK DIAGRAM

FORM DEN 1105-01 (4-64)

Application _____ Date DECEMBER 1, 1975 Page 7 of 8

Procedure _____ Drawn By BETTY DICKMAN

SUBROUTINE PRINT (D)



FOR YOUR FRAME /

ORIGINAL PAGE IS
OF POOR QUALITY

FOR YOUR FRAME /
FIG 11-5(9)
11-59

FLOW CHART & BLOCK DIAGRAM

FORM DEN 1103-01 (4-64)

Application _____ Date DECEMBER 1, 1975 Page 8 of 8
 Procedure _____ Drawn By BETTY DICKMAN

SUBROUTINE COINT (E)

```

G1 = 2, *(RMU/REFR**3.)*X.5
G2 = 3, *RMU/REFR**3.
XDD = G1 * YOD
YDD = G2 * YD - G1 * XOD
XID = XOD + XDD * DTC
XI = XO + XOD * DTC + .5 * XDD * (DTC) ** 2.
YID = YOD + YDD * DTC
YI = YO + YOD * DTC + .5 * YDD * (DTC) ** 2.
THETA1 = THETA0 + THETAD * DTC
    
```

WRITE
DTC

RETURN TO PAGE 3

END

II-24

Fig II-5(h)

ORIGINAL PAGE IS
OF POOR QUALITY

Table II-2(a) PROGRAM DOCK Listing

```

PROGRAM DOCK (INPUT,OUTPUT,TAPE5=INPUT,TAPE6=OUTPUT)
  DIMENSION K2(2), ENG(24,3)
  COMMON / SENSOR / LSENS,RGER,TAER,LOSER,MRRNG,MRTA,MRLOS,
2RANGS,TAS,LOSS,KVAPR,KSTEER,KIMU,XI,YI,XIU,YIU,VHER,VVER,GLOSD
  COMMON / PRNT / T(3),X(3),Y(3),XD(2),YD(3),TH(3),THD(3),XS(3),
2YS(3),XDCOM(3),YDCOM(3),NPCFLG,TATTOT,NENG(24),LMECH,VCG,PI,DMECH,
3WEIGHT(3),PROPTOT,THCOM(3),NVTRA,NHTRA,NATFLG(3),PROX
  COMMON / ATCON / ADB,RDB,MNTD,MIBB
  REAL LSENS,LOSER,LOSERD,MRRNG,MRTA,MRLOS,KVAPR,KSTEER,MNTD,MNTDD,
2 MIBB,MIBBD,LMECH
  NAMELIST / INPT / REFR,LSENS,RGER,TAERD,LOSERD,MRRNG,MRTA,MRLOS,
2 KVAPR,KSTEER,ADBD,MNTDD,RDBD,MIBBD,PROX,DTPR,DTPN,DTAS,VDBX,
3 VIYY,WTO,THR,AISP,PYCANTD,RCANTD,VCG,CGL,RADMT,LMECH,DMECH,
4 XO,YO,XDO,YDO,THO,THDO,XEND,DTCS,VHER,VVER,VDBY
  DATA PI,RMU,G / 3.141592654,1.4076452 E16,32.174/
1000 WRITE (6,1001)
1001 FORMAT (1H1)
  READ (5,INPT)
  IF (EOF,5) 2000,1005
1003 FORMAT (// 2X,***** PROGRAM DOCK *****
2 / 2X,***** INPUT SUMMARY *****
3 // 2X,*REFR *E15.8* LSENS *E15.8* RGER *E15.8* TAERD *
4 E15.8* LOSERD*E15.8* MRRNG *E15.8
5 / 2X,*MRTA *E15.8* MRLOS *E15.8* KVAPR *E15.8* KSTEER*
6 E15.8* ADBD *E15.8* MNTDD *E15.8
7 / 2X,*RDBD *E15.8* MIBBD *E15.8* PROX *E15.8* DTPR *
8 E15.8* DTPN *E15.8* DTAS *E15.8 )
1004 FORMAT ( 2X,*DTCS *E15.8* VIYY *E15.8* WTO *E15.8* THR *
1 E15.8* AISP *E15.8* PYCANT*E15.8
2 / 2X,*RCANTD*E15.8* VCG *E15.8* CGL *E15.8* RADMT *
3 E15.8* LMECH *E15.8* DMECH *E15.8
4 / 2X,*XO *E15.8* YO *E15.8* XDO *E15.8* YDO *
5 E15.8* THO *E15.8* THDO *E15.8
6 / 2X,*XEND *E15.8* VHER *E15.8* VVER *E15.8* VDBX *
7 E15.8* VDBY *E15.8)
1005 WRITE (6,1003) REFR,LSENS,RGER,TAERD,LOSERD,MRRNG,MRTA,MRLOS,
2KVAPR,KSTEER,ADBD,MNTDD,RDBD,MIBBD,PROX,DTPR,DTPN,DTAS
  WRITE (6,1004)DTCS,VIYY,WTO,THR,AISP,PYCANTD,RCANTD,VCG,CGL,RADMT,
2LMECH,DMECH,XO,YO,XDO,YDO,THO,THDO,XEND,VHER,VVER,VDBX,VDBY
  KIMU=0
  TH(2)=THO*PI/180.
  THD(2)=THDO*PI/180.
  X(2)=XO
  Y(2)=YO
  DO 1010 I=1,24
1010 NENG(I)=0
  XD(2)=XDO
  YD(2)=YDO
  WEIGHT(2)=WTO
  DUM=DTPN
  IF ((XO-PROX).GT.0.) DUM=DTPR
  XS(1)=XO-XDO*DUM
  YS(1)=YO-YDO*DUM
  TAER=TAERD*PI/180.
  LOSER=LOSERD*PI/180.

```

ORIGINAL PAGE IS
OF POOR QUALITY

Table II-2(b)

```

ADB=ADBD*PI/180.
MNTD=MNTDD*PI/180.
RDB=RDBD*PI/180.
MIBB=MIBBD*PI/180.
PYCANT=PYCANTD*PI/180.
RCANT=RCANTD*PI/180.
T(1)=-DUM
T(2)=0.
K1=0.
PROPTOT=0.
TATTOT=0.
TATLST=0.
TTOUT=1.E6
TACUT=1.E6
VDBX=VDBX
VDYY=VDYY
ENG(1,1)=THR*COS(PYCANT)
ENG(1,2)=0.
ENG(1,3)=ENG(1,1)*VCG
ENG(2,1)=ENG(1,1)
ENG(2,2)=0.
ENG(2,3)=ENG(1,3)
ENG(3,1)=0.
ENG(3,2)=THR*COS(RCANT)
ENG(3,3)=-ENG(3,2)*CGL
ENG(4,1)=-ENG(1,1)
ENG(4,2)=0.
ENG(4,3)=-ENG(1,3)
ENG(5,1)=ENG(4,1)
ENG(5,2)=0.
ENG(5,3)=ENG(4,3)
ENG(6,1)=0.
ENG(6,2)=-ENG(3,2)
ENG(6,3)=-ENG(3,3)
ENG(7,1)=ENG(1,1)
ENG(7,2)= -THR*SIN(PYCANT)
ENG(7,3)= -THR*COS(PYCANT)*(RADMT -VCG-CGL*SIN(PYCANT))
ENG(8,1)=ENG(7,1)
ENG(8,2)=ENG(7,2)
ENG(8,3)=ENG(7,3)
ENG(9,1)=0.
ENG(9,2)=0.
ENG(9,3)=0.
ENG(10,1)=ENG(4,1)
ENG(10,2)=ENG(7,2)
ENG(10,3)= THR*COS(PYCANT)*(RADMT-VCG+CGL*SIN(PYCANT))
ENG(11,1)=ENG(10,1)
ENG(11,2)=ENG(10,2)
ENG(11,3)=ENG(10,3)
ENG(12,1)=0.
ENG(12,2)=0.
ENG(12,3)=0.
ENG(13,1)=ENG(1,1)
ENG(13,2)=0.
ENG(13,3)=ENG(1,3)

```

Table II-2(c)

```

ENG(14,1)=ENG(13,1)
ENG(14,2)=ENG(13,2)
ENG(14,3)=ENG(13,3)
ENG(15,1)=0.
ENG(15,2)=ENG(3,2)
ENG(15,3)=ENG(3,3)
ENG(16,1)=ENG(4,1)
ENG(16,2)=0.
ENG(16,3)=ENG(4,3)
ENG(17,1)=ENG(4,1)
ENG(17,2)=0.
ENG(17,3)=ENG(4,3)
ENG(18,1)=0.
ENG(18,2)=ENG(6,2)
ENG(18,3)=ENG(6,3)
ENG(19,1)=ENG(7,1)
ENG(19,2)=-ENG(7,2)
ENG(19,3)=THR*CO$(PYCANT)*(RADMT+VCG-CGL*SIN(PYCANT))
ENG(20,1)=ENG(19,1)
ENG(20,2)=ENG(19,2)
ENG(20,3)=ENG(19,3)
ENG(21,1)=0.
ENG(21,2)=0.
ENG(21,3)=0.
ENG(22,1)=ENG(4,1)
ENG(22,2)=ENG(19,2)
ENG(22,3)=-THR*CO$(PYCANT)*(RADMT+VCG+CGL*SIN(PYCANT))
ENG(23,1)=ENG(22,1)
ENG(23,2)=ENG(22,2)
ENG(23,3)=ENG(22,3)
ENG(24,1)=0.
ENG(24,2)=0.
ENG(24,3)=0.
CALL PRINT
5 DTPS=DTPR
  IF (X(2).LE.PROX) DTPS=DTPN
  IF (X(2).LE.PPROX) VDXX=VDRX*DTPN/DTPR
  IF (X(2).LE.PROX) VDYY=VDBY*DTPN/DTPR
  IF (X(2).LE.PROX) ADB=ADB*(PI/180.)*(DTPN/DTPR)
  TCN=T(2)+DTCS
  TPN=T(2)+DTPS
6 CONTINUE
  CALL COMG (X(2),Y(2),TH(2),THCOM(2),XDCOM(2),YDCOM(2),XS(2),YS(2),
    2XD(2),YD(2),THD(2),XSD,YSD)
  CALL TRALIM (VDXX,VDYY,XSD,YSD,XDCOM(2),YDCOM(2),NVTRA,NHTRA)
  IF (NVTRA.EQ.0.AND.NHTRA.EQ.0) GO TO 270
8 IF (NVTRA)10,30,20
10 NENG(6)=1
  NENG(18)=1
  GO TO 30
20 NENG(3)=1
  NENG(15)=1
30 IF (NHTRA)40,60,50
40 NENG(4)=1
  NENG(5)=1

```

Table II-2(d)

```

      NENG(10)=1
      NENG(11)=1
      NENG(16)=1
      NENG(17)=1
      NENG(22)=1
      NENG(23)=1
      GO TO 60
50  NENG(1)=1
      NENG(2)=1
      NENG(7)=1
      NENG(8)=1
      NENG(13)=1
      NENG(14)=1
      NENG(19)=1
      NENG(20)=1
60  THERR=TH(2)-THCOM(2)
      CALL ATLM (THERR,THD(2),NATFLG(2))
      IF (NATFLG(2).EQ.0) GO TO 85
65  TATON=T(2)
      IF (NATFLG(2).GT.0) GO TO 70
      NENG(7)=1
      NENG(8)=1
      NENG(10)=0
      NENG(11)=0
      NENG(19)=0
      NENG(20)=0
      NENG(22)=1
      NENG(23)=1
      GO TO 80
70  NENG(7)=0
      NENG(8)=0
      NENG(10)=1
      NENG(11)=1
      NENG(19)=1
      NENG(20)=1
      NENG(22)=0
      NENG(23)=0
80  IF (IABS(NATFLG(2)).EQ.1) GO TO 90
85  DTP=TPN-T(2)
      TATON=T(2)
      K=1
      GO TO 100
90  DTP=DTAS
      K=-1
100  NPCFLG=1
      NTENG=0
      HTHR=0
      VTHR=0
      TORQ=0
      DO 110 I=1,24
      HTHR=HTHR+NENG(I)*ENG(I,1)
      VTHR=VTHR+NENG(I)*ENG(I,2)
      TORQ=TORQ+NENG(I)*ENG(I,3)
      NTENG=NTENG+NENG(I)
110 CONTINUE

```

Table II-2(e)

```

111 VM=WEIGHT(2)/G
    THDD=TORQ/VIYY
    THD(3)=THD(2)+THDD*DTP
    TH(3)=TH(2)+THD(2)*DTP+0.5*THDD*DTP**2
    THAVG=(TH(2)+TH(3))/2
    G1=2.*(RMU/REFR**3)**.5
    G2=3.*RMU/REFR**3
    XDD=G1*YD(2)-HTHR*COS(THAVG)/VM+VTHR*SIN(THAVG)/VM
    YDD=G2*Y(2)-G1*XD(2)+HTHR*SIN(THAVG)/VM+VTHR*COS(THAVG)/VM
    XD(3)=XD(2)+XDD*DTP
    X(3)=X(2)+XD(2)*DTP+.5*XDD*DTP**2
    YD(3)=YD(2)+YDD*DTP
    Y(3)=Y(2)+YD(2)*DTP+.5*YDD*DTP**2
    WEIGHT(3)=WEIGHT(2)-NTENG*THR*DTP/AISP
    DPROP=WEIGHT(3)-WEIGHT(2)
    T(3)=T(2)+DTP
    KINT=1
C2500 FORMAT ( /2X,* DTP=*E15.8* T(1)=*E15.8* T(2)=*E15.8* T(3)=*
C      2      E15.8* K=*I3* NATFLG2=*I3* NATFLG3=*I3
C      3 / 2X,* TPN=*E15.8* DPROP=*E15.8)
C      WRITE (6,2500) DTP,T(1),T(2),T(3),K,NATFLG(2),NATFLG(3),TPN,DPROP
      IF(K.LE.0) GO TO 210
      THERR=TH(3)-THCOM(2)
      CALL ATLIM (THERR,THD(3),NATFLG(3))
      IF ((NATFLG(2).EQ.NATFLG(3)).OR.(NATFLG(3).EQ.0)) GO TO 249
      THERR=TH(2)-THCOM(2)
      KKK=0
      IF ((NATFLG(2).EQ. 2).OR.(NATFLG(2).EQ.0.AND.NATFLG(3).GT.0))
1      GO TO 180
      TK1=(MNTD+RDB-THD(2)-GLOSD)/THDD
      IF (ABS(THDD).LT.(1.E-13)) TK1=1.E10
      THK1=THERR+THD(2)*TK1+.5*THDD*TK1**2
      A=.5*RDB/ADB*THDD
      B=THDD+RDB*THD(2)/ADB
      C=THD(2)+RDB*THERR/ADB-RDB/2.+GLOSD
114 IF (ABS(A).LT.(1.E-12)) GO TO 135
      DUM=B**2-4.*A*C
      IF (DUM.GE.0.) GO TO 115
      THK2=1.+ADB/2.+ MNTD*ADB/RDB
      GO TO 120
115 TK21=(-B+(DUM)**.5)/(2.*A)
      TK22=(-B-(DUM)**.5)/(2.*A)
120 IF(TK21.LT.0.) GO TO 140
      IF(TK22.LT.0.) GO TO 130
      IF((TK22-TK21).GT.0.) 130,140
130 TK2=TK21
      GO TO 150
135 TK2=-C/B
      GO TO 150
140 TK2=TK22
150 THK2=THERR+THD(2)*TK2+.5*THDD*TK2**2
      IF (KKK.EQ.0) GO TO 190
      TK3=(-MNTD-RDB-THD(2)-GLOSD)/THDD
      IF (ABS(THDD).LT.(1.E-13)) TK3=1.E10
      THK3=THERR+THD(2)*TK3+.5*THDD*TK3**2

```

ORIGINAL PAGE IS
OF POOR QUALITY

Table II-2(f)

```

155 IF (THK1.LT.(-ADB/2.-MNTD*ADB/RDB)) GO TO 160
    IF (THK2.LT.(ADB/2.+MNTD*ADB/RDB)) GO TO 170
    DTP=TK3
    GO TO 200
160 DTP=TK1
    GO TO 200
170 DTP=TK2
    GO TO 200
180 KKK=1
    TK1=(MNTD-THD(2)-GLOSD)/THDD
    IF (ABS(THDD).LT.(1.E-13)) GO TO 182
    THK1=THERR+THD(2)*TK1+.5*THDD*TK1**2
181 A=.5*RDB*THDD/ADB
    B=THDD+RDB*THD(2)/ADB
    C=THD(2)+RDB*THERR/ADB+RDB/2.+GLOSD
    GO TO 114
182 THK1=1.E10
    GO TO 181
190 TK3=(-MNTD-THD(2)-GLOSD)/THDD
    IF (ABS(THDD).LT.(1.E-13)) TK3=1.E10
    THK3=THERR+THD(2)*TK3+.5*THDD*TK2**2
    GO TO 155
200 K=0
    DTP=(INT(DTP/DTAS)+1)*DTAS
    IF ((DTP+T(2)).GT.TPN) DTP=TPN-T(2)
C2700 FORMAT (2X,*A=*E15.8* B=*E15.8* C=*E15.8* T(1)=*E15.8* T(2)=*E15.8*
C 2* T(3)=*E15.8/2X,*TPN=*E15.8* THCOM3=*E15.8* TK21=*E15.8* TK22=*
C 3 E15.8* TK1=*E15.8* TK2=*E15.8/2X,*TK3=*E15.8* THK1=*E15.8* TH
C 4K2=*E15.8* THK3=*E15.8* DTP=*E15.8* DTAS=*E15.8/2X,*THD2=*E15.8* T
C 5HDD=*E15.8* THER=*E15.8* KKK=*I3* NATFLG2=*I3* NATFLG3=*I3* NHTRA=*I
63* NVTRA=*I3)
    WRITE (6,2700) A,B,C,T(1),T(2),T(3),TPN,THCOM(3),TK21,TK22,TK1,
    2TK2,TK3,THK1,THK2,THK3,DTP,DTAS,THD(2),THDD,THERR,KKK,NATFLG(2),
    3NATFLG(3),NHTRA,NVTRA
    GO TO 111
210 PROPTOT=PROPTOT+DPROP
    IF (NATFLG(2).EQ.0) GO TO 217
    TATOFF=T(3)
    TATTOT=TATTOT+TATOFF-TATON
217 IF (T(3).LT.TPN) 218,220
218 T(2)=T(3)
    X(2)=X(3)
    Y(2)=Y(3)
    XD(2)=XD(3)
    YD(2)=YD(3)
    TH(2)=TH(3)
    THD(2)=THD(3)
    WEIGHT(2)=WEIGHT(3)
    DO 219 I=1,24
219 NENG(I)=0
    GO TO 8
220 LMN=1
    CALL COMG TX(3),Y(3),TH(3),THCOM(3),XDCOM(3),YDCOM(3),XS(2),YS(3),
    2XD(3),YD(3),THD(3),XSD,YSD)
225 CONTINUE

```


Table II-2(g)

```

DO 226 I=1,2
II=I+1
T(I)=T(II)
X(I)=X(II)
Y(I)=Y(II)
XD(I)=XD(II)
YD(I)=YD(II)
TH(I)=TH(II)
THD(I)=THD(II)
XS(I)=XS(II)
YS(I)=YS(II)
XDCOM(I)=XDCOM(II)
YDCOM(I)=YDCOM(II)
THCOM(I)=THCOM(II)
226 WEIGHT(I)=WEIGHT(II)
IF(LMN.EQ.0) GO TO 290
IF (X(2).LT.XEND) GO TO 240
CALL PRINT
DO 230 I=1,24
NENG(I)=0
230 CONTINUE
GO TO 5
240 RATIO=(XEND-X(1))/(X(2)-X(1))
X(2)=XEND
T(2)=T(1)+(T(2)-T(1))*RATIO
WEIGHT(2)=WEIGHT(1)+(WEIGHT(2)-WEIGHT(1))*RATIO
Y(2)=Y(1)+(Y(2)-Y(1))*RATIO
XD(2)=XD(1)+(XD(2)-XD(1))*RATIO
YD(2)=YD(1)+(YD(2)-YD(1))*RATIO
TH(2)=TH(1)+(TH(2)-TH(1))*RATIO
THD(2)=THD(1)+(THD(2)-THD(1))*RATIO
XS(2)=XS(1)+(XS(2)-XS(1))*RATIO
YS(2)=YS(1)+(YS(2)-YS(1))*RATIO
CALL COMG (X(2),Y(2),TH(2),THCOM(2),XDCOM(2),YDCOM(2),XS(2),YS(2),
2XD(2),YD(2),THD(2),XSD,YSD)
CALL PRINT
GO TO 1000
249 PROPTOT=PROPTOT+DPROP
250 IF(NATFLG(2).NE.0) GO TO 260
GO TO 220
260 TATOFF=T(3)
TATTOT=TATTOT+TATOFF-TATON
GO TO 220
270 THERR=TH(2)-THCOM(2)
CALL ATLIM (THERR,THD(2),NATFLG(2))
IF(NATFLG(2).EQ.0) GO TO 280
GO TO 65
280 DTC=TCN-T(2)
285 CALL COINT (REFR,DTC,X(2),Y(2),TH(2),X(3),Y(3),TH(3),XD(3),YD(3),
2 THD(2),XD(2),YD(2))
T(3)=T(2)+DTC
CALL COMG (X(3),Y(3),TH(3),THCOM(3),XDCOM(3),YDCOM(3),XS(3),YS(3),
2XD(3),YD(3),THD(2),XSD1,YSD1)
THER3=TH(3)-THCOM(3)
CALL ATLIM (THER3,THD(2),NATFLG(3))

```

ORIGINAL PAGE IS
OF POOR QUALITY

Table II-2(h).

```

        IF(K1.EQ.0) GO TO 300
        LMN=0
        THD(3)=THD(2)
        TPN=(INT(T(3)/DTPS)+1)*DTPS
        K1=0
        GO TO 225
290 CALL PRINT
1100 FORMAT ( / 10X, * RUN TIME EXCEEDS 1000 SECONDS*)
        IF (T(2).GT.1000.) GO TO 295
        IF (ABS(TPN-T(2)).LT.(1.E-5)) TPN=TPN+DTPS
        GO TO 6
295 WRITE (6,1100)
        GO TO 2000
300 NPCFLG=-1
        IF(NATFLG(3).EQ.0) GO TO 360
        K2(1)=1
        CTR=1
310 TDUM=TCN-CTR*DTPS
        IF(TDUM.LE.T(2)) GO TO 320
        DTC=TDUM-T(2)
        CALL COINT (REFR,DTC,X(2),Y(2),TH(2),XDUM,YDUM,THDUM,XDDUM,
2      YDDUM,THD(2),XD(2),YD(2))
        CALL COMG (XDUM,YDUM,THDUM,THCDUM,DUM,DUM,DUM,DUM,XDDUM,YDDUM,
2THD(2),DUM,DUM)
        THERD=THDUM-THCDUM
        CALL ATLYM (THERD,THD(2),NATDUM)
        IF (NATDUM.EQ.0) GO TO 329
        CTR=CTR+1
        GO TO 310
329 DUM=THERD
        GO TO 330
320 TDUM=T(2)
        DUM=THERR
330 IF(THD(2).LE.0.) GO TO 340
        TOUT=.5*ADB/THD(2)-ADB/RDB- DUM/THD(2)-GLOSD*ADB/(RDB*THD(2))
        GO TO 350
340 TOUT=-.5*ADB/THD(2)-ADB/RDB- DUM/THD(2)-GLOSD*ADB/(RDB*THD(2))
350 IF ((TOUT.LE.0.).OR.(TOUT.GE.DTPS)) TOUT=DTPS-DTAS/2.
        TOUT=TOUT+TDUM
        TAOUT=(INT(TOUT/DTAS)+1)*DTAS
        GO TO 370
360 K2(1)=-1
        TAOUT=1.E6
370 KINT=-1
        CALL TRALIM (VDXX,VDYY,XSD1,YSD1,XDCOM(3),YDCOM(3),NVTRA,NHTRA)
        IF(NVTRA.EQ.0.AND.NHTRA.EQ.0) GO TO 450
        K2(2)=1
        CTR1=1
380 TDUM=TCN-CTR1*DTPS
        IF(TDUM.LE.T(2)) GO TO 400
        DTC=TDUM-T(2)
        CALL COINT (REFR,DTC,X(2),Y(2),TH(2),XDUM,YDUM,THDUM,XDDUM,
2      YDDUM,THD(2),XD(2),YD(2))
        CALL COMG (XDUM,YDUM,THDUM,THCDUM,XDCDUM,YDCDUM,XSDUM,YSDUM,
2XDDUM,YDDUM,THDDUM,XSDDUM,YSDDUM)

```

Table II-2(1)

```

CALL TRALIM (VDXX,VDYY,XSODUM,YSODUM,XDCDUM,YDCDUM,NVTRA,NHTRA)
IF(NVTRA.EQ.0.AND.NHTRA.EQ.0) GO TO 400
CTR1=CTR1+1
GO TO 380
400 TTOUT=TDUM+DTPS
IF(K2(1).NE.1.AND.K2(2).NE.1) GO TO 420
IF(TAOUT.LE.TTOUT) GO TO 430
420 DTC=TTOUT-T(2)
GO TO 440
430 DTC=TAOUT-T(2)
440 K1=1
C 2600 FORMAT (2X,*TAOUT=*E15.8* TTOUT=*E15.8* TDUM=*E15.8* T(2)=*
C      2 E15.8* K2(1)=*I3* K2(2)=*I2)
C      WRITE (6,2600) TAOUT,TTOUT,TDUM,T(2),K2(1),K2(2)
GO TO 285
450 K2(2)=-1
TTOUT=1.E6
IF(K2(1).EQ.-1.AND.K2(2).EQ.-1) GO TO 250
GO TO 430
2000 STOP
END

```

```

SUBROUTINE COINT (REFR,DTC,X0,Y0,THETA0,X1,Y1,THETA1,
IX1D,Y1D,THETAD,X0D,Y0D)

```

```

DATA RMU /1.4076452E16/
G1=2.*(RMU/REFR**3.)**.5
G2=3.*RMU/REFR**3.
XDD=G1*Y0D
YDD=G2*Y0-G1*X0D
X1D=X0D+XDD*DTC
X1=X0+X0D*DTC+.5*XDD*(DTC)**2.
Y1D=Y0D+YDD*DTC
Y1=Y0+Y0D*DTC+.5*YDD*(DTC)**2.
THETA1=THETA0+THETAD*DTC

```

```

C 1 FORMAT (2X,*COAST INTEGRATION DTC=*E15.8)
C WRITE (6,1) DTC
RETURN
END

```

ORIGINAL PAGE IS
OF POOR QUALITY

Table II-2(j).

```

SUBROUTINE COMG (X,Y,THETA,THCOM,XDCOM,YDCOM,XS,YS,
2XD,YD,THD,XSD,YSD)
REAL LSENS,LOSER,MRRNG,MRTA,MRLOS,LOSS,KVAPR,KSTEER
COMMON /SENSOR/ LSENS,RGER,TAER,LOSER,MRRNG,MRTA,MRLOS,
2RANGS,TAS,LOSS,KVAPR,KSTEER,KIMU,XI,YI,XIU,YIU,VHER,VVER,GLOSD
XI=X-LENS*cos(THETA)
YI=Y+LENS*sin(THETA)
RANGS=(XI**2+YI**2)**.5+RGER
TAS= ATAN(YI/XI)+TAER
LOSS=-(ATAN(YI/XI)+THETA+LOSER)
XS=RANGS*cos(TAS)
YS=RANGS*sin(TAS)
XSD=XD+LENS*sin(THETA)*THD+VHER
YSD=YD+LENS*cos(THETA)*THD+VVER
GLOSD=(XS*YSD-YS*XSD)/(XS**2+YS**2)
IF (KIMU.EQ.0) 10,30
10 IF ((RANGS-MRRNG).LT.(0.).OR.(TAS-MRTA).LT.(0.)) 20,50
20 KIMU=1
DELX=XS-X
DELY=YS-Y
XIU=XS
YIU=YS
GO TO 40
30 XIU=X+DELX
YIU=Y+DELY
40 IF (RANGS.LT.MRRNG) RANGS=(XIU**2+YIU**2)**.5
IF (RANGS.LT.MRTA) TAS=ATAN(YIU/XIU)
IF (RANGS.LT.MRLOS) LOSS=-(ATAN(YIU/XIU)+THETA)
50 THCOM=LOSS+THETA
XDCOM=KVAPR
YDCOM=KVAPR*KSTEER*(YS/XS)
RETURN
END

```

Table II-2(k)

```

SUBROUTINE ATLIM (THETA,THD,NATFLG)
REAL MNTD,MIBB,LSR
COMMON /ATCON /ADB,RDB,MNTD,MIBB
COMMON / SENSOR / LSENS,RGER,TAER,LOSER,MRRNG,MRTA,MRLOS,
2RANGS,TAS,LOSS,KVAPR,KSTEER,KIMU,XI,YI,XIU,YIU,VHER,VVER,GLOSD
LSR=THD+GLOSD
IF (THETA.LE.(-ADB/2.-MNTD*ADB/RDB))10,20
10 IF (LSR.LT.(MNTD-MIBB)) GO TO 90
IF (LSR.LE.MNTD) GO TO 80
IF (LSR.LT.(MNTD+RDB)) GO TO 70
IF (LSR.LE.(MNTD+RDB-MIBB)) GO TO 60
GO TO 50
20 IF (ABS(THETA).LT.(ADB/2.+MNTD*ADB/RDB))30,40
30 IF (LSR.LE.(-RDB/ADB*THETA-RDB/2.-MIBB)) GO TO 90
IF (LSR.LE.(-RDB/ADB*THETA-RDB/2.)) GO TO 80
IF (LSR.LT.(-RDB/ADB*THETA+RDB/2.)) GO TO 70
IF (LSR.LE.(-RDB/ADB*THETA+RDB/2.+MIBB)) GO TO 60
GO TO 50
40 IF (LSR.GT.(-MNTD+MIBB)) GO TO 50
IF (LSR.GE.-MNTD) GO TO 60
IF (LSR.GT.(-MNTD-RDB)) GO TO 70
IF (LSR.GE.(-MNTD-RDB-MIBB)) GO TO 80
GO TO 90
50 NATFLG =-2
RETURN
60 NATFLG =-1
RETURN
70 NATFLG =0
RETURN
80 NATFLG =1
RETURN
90 NATFLG =2
RETURN
END

```

```

SUBROUTINE TRALIM (VDBX,VDBY,XSD,YSD,XDCOM,YDCOM,NVTRA,NHTRA)
KX=0
IF (ABS(XSD-XDCOM).GT.VDBX/2.) KX=1
KY=0
IF (ABS(YSD-YDCOM).GT.VDBY/2.) KY=1
IF (KX.EQ.0) GO TO 10
NHTRA=-1
IF (XSD.GT.XDCOM) NHTRA=1
GO TO 20
10 NHTRA=0
20 IF (KY.EQ.0) GO TO 30
NVTRA=1
IF (YSD.GT.YDCOM) NVTRA=-1
GO TO 40
30 NVTRA=0
40 RETURN
END

```

Table II-2(1)

```

SUBROUTINE PRINT
  DIMENSION NE(24)
  COMMON / PRNT / T(3),X(3),Y(3),XD(3),YD(3),TH(3),THD(3),XS(3),
2YS(3),XDCOM(3),YDCOM(3),NPCFLG,TATTOT,NENG(24),LMECH,VCG,PI,DMECH
3WEIGHT(3),PROPTOT,THCOM(3),NVTRA,NHTRA,NATFLG(3),PROX
  COMMON / SENSOR / LSENS,RGER,TAER,LOSER,MRRNG,MRTA,MRLOS,
2RANGS,TAS,LOSS,KVAPR,KSTEER,KIMU,XI,YI,XIU,YIU,VHER,VVER,GLOSD
  REAL LOSER,LOSERD,LMECH,LSENS,MRRNG,MRTA,MRLOS,LOSS,LOSSD,
2KVAPR,KSTEER
  XCL=X(2)-LMECH*COS(TH(2))
  YCL=Y(2)+LMECH*SIN(TH(2))-VCG*COS(TH(2))
  XDCL=XD(2)+LMECH*SIN(TH(2))*THD(2)
  YDCL=YD(2)+LMECH*COS(TH(2))*THD(2)-VCG*SIN(TH(2))*THD(2)
  PATH=(ATAN(YDCL/XDCL))*180./PI
  XTC=X(2)-LMECH*COS(TH(2))+DMECH*SIN(TH(2))
  YTC=Y(2)+LMECH*SIN(TH(2))-(VCG-DMECH)*COS(TH(2))
  XDTC=XD(2)+LMECH*SIN(TH(2))*THD(2)+DMECH*COS(TH(2))*THD(2)
  YDTC=YD(2)+LMECH*COS(TH(2))*THD(2)-(VCG-DMECH)*COS(TH(2))*THD(2)
  XBC=X(2)-LMECH*COS(TH(2))-DMECH*SIN(TH(2))
  YBC=Y(2)+LMECH*SIN(TH(2))-(+DMECH+VCG)*COS(TH(2))
  XDBC=XD(2)+LMECH*SIN(TH(2))*THD(2)-DMECH*COS(TH(2))*THD(2)
  YDBC=YD(2)+LMECH*COS(TH(2))*THD(2)-(+DMECH+VCG)*COS(TH(2))*THD(2)
  PITCH=TH(2)*180./PI
  PRATE=THD(2)*180./PI
  PCOM2D=THCOM(2)*180./PI
  LOSSD=LOSS*180./PI
  TASD=TAS*180./PI
  LOSERD=LOSER*180./PI
  TAERD=TAER*180./PI
  GLOS=GLOSD*180./PI
1  FORMAT (// 2X, '$$$$$$ COAST FLIGHT SUMMARY $$$$$$')
2  FORMAT (// 2X, '$$$$$$ POWERED FLIGHT SUMMARY $$$$$$')
3  FORMAT ( 2X, '$$$$$$$$$$ ENGLISH UNITS $$$$$$$$$$')
4  FORMAT ( 2X, *TIME *E15.8* WEIGHT*E15.8* PROP *E15.8)
5  FORMAT ( 2X, '$$$$$$ C.G.MOTION $$$$$$')
6  FORMAT ( 2X, *XCG *E15.8* YCG *E15.8* XDCG *E15.8* YDCG *
2E15.8* PITCH *E15.8* P-RATE*E15.8)
7  FORMAT ( 2X, '$$$$$$ SENSED AND COMMANDED MOTION $$$$$$')
8  FORMAT ( 2X, *XINST *E15.8* XSENS *E15.8* XIMU *E15.8* XDCOM *
2E15.8* LOSS *E15.8* LOSERR*E15.8)
9  FORMAT ( 2X, *YINST *E15.8* YSENS *E15.8* YIMU *E15.8* YDCOM *
2E15.8* TAS *E15.8* TAERR *E15.8)
10 FORMAT (46X, *GLOSD *E15.8* THCOM *E15.8* RANGS *
2E15.8* RGERR *E15.8)
11 FORMAT ( 2X, '$$$$$$ DOCKING MECHANISM MOTION $$$$$$')
12 FORMAT ( 8X, *CENTERLINE*)
13 FORMAT ( 2X, *XCL *E15.8* XDCL *E15.8* PITCH *E15.8)
14 FORMAT ( 2X, *YCL *E15.8* YDCL *E15.8* P-RATE*E15.8)
15 FORMAT ( 8X, *TOP CORNER*28X*PATH *E15.8)
16 FORMAT ( 2X, *XTC *E15.8* XDTC *E15.8)
17 FORMAT ( 2X, *YTC *E15.8* YDTC *E15.8)
18 FORMAT ( 8X, *BOTTOM CORNER*)
19 FORMAT ( 2X, *XBC *E15.8* XDBC *E15.8)
20 FORMAT ( 2X, *YBC *E15.8* YDBC *E15.8)
21 FORMAT ( 2X, '$$$$$$ POWER ON CONFIGURATION $$$$$$')

```

Table II-2(m)

```

22 FORMAT ( 2X,*ENGINES ON*28I4)
23 FORMAT ( 2X,*ACS TIME THIS INTERVAL =*E15.8,5X*TOTAL ACS TIME =*
  2E15.8* NVTRA *I3* NHTRA *I3* NATFLG(2) *I3)
  TATDEL=TATTOT-TATLST
  DO 30 I=1,24
  NE(I)=0
  IF (NENG(I).GT.0) NE(I)=1
30 CONTINUE
  IF (NPCFLG.GT.0) 31,32
31 WRITE (6,2)
  GO TO 33
32 WRITE (6,1)
33 WRITE (6,3)
  WRITE (6,4) T(2),WEIGHT(2),PROPTOT
  WRITE (6,5)
  WRITE (6,6) X(2),Y(2),XD(2),YD(2),PITCH,PRATE
  WRITE (6,7)
  WRITE (6,8) XI,XS(2),XIU,XDCOM(2),LOSSD,LOSERD
  WRITE (6,9) YI,YS(2),YIU,YDCOM(2),TASD,TAERD
  WRITE (6,10) GLOS,PCOM2D,RANGS,RGER
  IF(X(2).LT.PROX) 40,50
40 WRITE (6,11)
  WRITE (6,12)
  WRITE (6,13) XCL, XDCL, PITCH
  WRITE (6,14) YCL, YDCL, PRATE
  WRITE (6,15) PATH
  WRITE (6,16) XTC,XDTC
  WRITE (6,17) YTC,YDTC
  WRITE (6,18)
  WRITE (6,19) XBC,XDBC
  WRITE (6,20) YBC,YDBC
50 IF (NPCFLG.LT.0) RETURN
  WRITE (6,21)
  WRITE (6,22) NE(1),NE(2),NE(3),NE(4),NE(5),NE(6),NE(7),NE(8),NE(9)
  2,NE(10),NE(11),NE(12),NE(13),NE(14),NE(15),NE(16),NE(17),NE(18),
  3NE(19),NE(20),NE(21),NE(22),NE(23),NE(24)
  WRITE (6,23) TATDEL,TATTOT,NVTRA,NHTRA,NATFLG(2)
  TATLST=TATTOT
  RETURN
  END

```

ORIGINAL PAGE IS
OF POOR QUALITY

Table II-3 Sample PROGRAM DOCK Input

```

PSTNPT
RFFR      =138168243.,
LSENS     =14.0,
RGER      =0.,
TAERD     =0.,
LOSERD    =0.,
MPRNG     =1.0,
MRTA      =15.0,
MRLOS     =2.0,
KVAPR     =-1.0,
KSTEE     =2.0,
AD9D      =1.0,
MNTDD     =0.35,
PD9D      =0.2,
MT99D     =0.02,
PROX      =26.,
DTPR      =1.3,
DTPN      =0.5,
DTAS      =0.020,
VDBX      =0.25,
VDBY      =0.125,
VIYV      =35000.,
WTO       =32000.,
THR       =25.,
AISP      =230.,
PYCANTD   =10.,
PCANTD    =10.,
VCG       =0.0,
CGL       =1.0,
PADMT     =7.5,
LMECH     =16.0,
DMECH     =3.0,
XO        =200.,
YO        =13.0,
XDD       =-2.0,
YDD       =0.1,
THO       =5.0,
THDD      =0.1,
XEND      =16.0,
DTCS      =4.0,
VHEP      =0.,
VVER      =0.,
$

```


ORIGINAL PAGE IS
OF POOR QUALITY

```

$$$$$ POWERED FLIGHT SUMMARY  $$$$$$
$$$$$$!$$$ ENGLISH UNITS  $$$$$$!$$$$$
TIME 2.90000000E+00 WEIGHT 3.19978261E+04 PROP -2.17391304E+00
$$$$$! C.G.MOTION  $$$$$$
XCG 1.9638879E+02 YCG 1.00719662E+01 XDCG -1.64339709E+00 YDCG -2.97377107E-02 PITCH 4.78350747E+00 P-RATE-1.01519028E-01
$$$$$ SENSED AND COMMANDED MOTION  $$$$$$
XINST 1.82387743E+02 XSENS 1.82387743E+02 XIMU 0. XDCOM -1.00000000E+00 LOSS -8.30982888E+00 LOSERR 0.
YINST 1.12394385E+01 YSENS 1.12394385E+01 YIMU 0. YDCOM -1.23247739E-01 TAS 3.52632841E+00 TAEPR 0.
GL OSD 1.48161543E-02 THCOM -3.52632841E+00 RANGS 1.82733723E+02 PGEPFR 0.

$$$$$ POWER ON CCONFIGURATION  $$$$$$
ENGINE# ON 0 1 0 4 5 6 0 0 0 10 11 0 0 0 0 16 17 18 0 0 0 22 23 0
ACS TIME THIS INTERVAL = 4.00000000E-02 TOTAL ACS TIME = 3.80000000E-01 NVTRA -1 NHTRA -1 NATFLG(2) 0

```

Table II-4(b) Sample PROGRAM DOCK Output (Cont.)

```

$$$$$$ POWERED FLIGHT SUMMARY $$$$$$
$$$$$$$$$ ENGLISH UNITS $$$$$$$$$$
TIME 3.00000000E+00 WEIGHT 3.19967391E+04 PROP -3.26086957E+08
$$$$$$ C.G.MOTION $$$$$$
XCG 1.94790710E+02 YCG 1.00099924E+01 XDCG -1.45407601E+08 YDCG -9.44981452E-02 PITCH 4.70390671E+00 P-RATE-6.92759836E-02
$$$$$$ SENSED AND COMMANDED MOTION $$$$$$
XINST 1.80937865E+02 XSENS 1.80837865E+02 XIMU 0. XDCOM -1.00000000E+00 LOSS -8.23470259E+00 LOSERR 0.
YINST 1.11580829E+01 YSENS 1.11580829E+01 YIMU 0. YDCOM -1.23404276E-01 TAS 3.53079517E+00 TAERR 0.
GLOSD -6.80606530E-03 THCOM -3.53079517E+00 RANGS 1.81161777E+02 RGERR 0.
$$$$$$ POWER ON CONFIGURATION $$$$$$
ENGINES ON 0 0 0 4 5 6 0 0 0 10 11 0 0 0 0 16 17 18 0 0 0 22 23 0
ACS TIME THIS INTERVAL = 4.00000000E-02 TOTAL ACS TIME = 3.40000000E-01 NVTRA -1 NHTRA -1 NATFLG(2) 0

```

```

$$$$$$ POWERED FLIGHT SUMMARY $$$$$$
$$$$$$$$$ ENGLISH UNITS $$$$$$$$$$
TIME 4.00000000E+00 WEIGHT 3.19958696E+04 PROP -4.13043478E+08
$$$$$$ C.G.MOTION $$$$$$
XCG 1.93435325E+02 YCG 9.90753944E+00 XDCG -1.25669440E+08 YDCG -1.10407808E-01 PITCH 4.63463073E+00 P-RATE-6.92759836E-02
$$$$$$ SENSED AND COMMANDED MOTION $$$$$$
XINST 1.79481102E+02 XSENS 1.79481102E+02 XIMU 0. XDCOM -1.00000000E+00 LOSS -8.15410214E+00 LOSERR 0.
YINST 1.10387588E+01 YSENS 1.10387588E+01 YIMU 0. YDCOM -1.23007477E-01 TAS 3.51947141E+00 TAERR 0.
GLOSD -1.58709062E-02 THCOM -3.51947141E+00 RANGS 1.79820244E+02 RGERR 0.
$$$$$$ POWER ON CONFIGURATION $$$$$$
ENGINES ON 0 0 0 4 5 0 0 0 0 10 11 0 0 0 0 16 17 0 0 0 22 23 0
ACS TIME THIS INTERVAL = 0. TOTAL ACS TIME = 3.40000000E-01 NVTRA 0 NHTRA -1 NATFLG(2) 0

```

```

$$$$$$ POWERED FLIGHT SUMMARY $$$$$$
$$$$$$$$$ ENGLISH UNITS $$$$$$$$$$
TIME 5.00000000E+00 WEIGHT 3.19950000E+04 PROP -5.00000000E+08
$$$$$$ C.G.MOTION $$$$$$
XCG 1.92277333E+02 YCG 9.78928150E+00 XDCG -1.05929041E+08 YDCG -1.26108062E-01 PITCH 4.56535475E+00 P-RATE-6.92759836E-02
$$$$$$ SENSED AND COMMANDED MOTION $$$$$$
XINST 1.78321752E+02 XSENS 1.78321752E+02 XIMU 0. XDCOM -1.00000000E+00 LOSS -8.06439522E+00 LOSERR 0.
YINST 1.09036281E+01 YSENS 1.09036281E+01 YIMU 0. YDCOM -1.22291621E-01 TAS 3.49904047E+00 TAERR 0.
GLOSD -2.50094960E-02 THCOM -3.49904047E+00 RANGS 1.78654797E+02
$$$$$$ POWER ON CONFIGURATION $$$$$$
ENGINES ON 0 0 0 4 5 0 0 0 0 10 11 0 0 0 0 16 17 0 0 0
ACS TIME THIS INTERVAL = 0. TOTAL ACS TIME = 3.40000000E-01 NVTRA

```

```

$$$$$$ COAST FLIGHT SUMMARY $$$$$$
$$$$$$$$$ ENGLISH UNITS $$$$$$$$$$
TIME 9.00000000E+00 WEIGHT 3.19950000E+04 PROP
$$$$$$ C.G.MOTION $$$$$$
XCG 1.89040024E+02 YCG
$$$$$$ SENSED AND COMMANDED MOTION $$$$$$
XINST 1.74070000E+02 XSENS
YINST

```

II-41

ORIGINAL PAGE IS
OF POOR QUALITY

```

$$$$$ DOCKING MECHANISM ACTION $$$$$$
CENTERLINE
XCL 4.39496988E-01 XDCL -1.05778733E+00 PITCH 1.64478687E+00
YCL -4.24992481E-03 YDCL 5.63070259E-02 P-RATE 2.58409977E-02
TOP CORNER
XTC 5.25605991E-01 XDTIC -1.05643486E+00 PATH -3.04703306E+00
YTC 2.99451403E+00 YDTIC 5.76594999E-02
BOTTOM CORNER
XBC 3.53387969E-01 XDBC -1.05913981E+00
YBC -3.00301388E+00 YDBC 5.49545519E-02
$$$$$ POWER ON CONFIGURATION $$$$$$
ENGINES ON 0 0 3 0 0 0 0 0 0 0 0 0 0 0 0 0 0 0 0 0
ACS TIME THIS INTERVAL = 6.00000006E-02 TOTAL ACS TIME = 7.40

```

Table II-4(d) Sample PROGRAM DOCK Output (Cont.)

ORIGINAL PAGE IS
OF POOR QUALITY

```

$$$$$ POWERED FLIGHT SUMMARY $$$$$$
$$$$$ ENGLISH UNITS $$$$$$
TIME 1.7150000E+02 WEIGHT 3.19939522E+04 PROP -6.04782609E+00
$$$$$ C.G.MOTION $$$$$$
XCG 1.59039084E+01 YCG -4.38931747E-01 XDCG -1.05799087E+00 YDCG 4.91711165E-02 PITCH 1.50656810E+00 P-RATE-5.78716087E-01
$$$$$ SENSED AND COMMANDED MOTION $$$$$$
XINST 1.90874794E+00 XSNS 1.90874794E+00 XIMU 1.90831596E+00 XDCOM -1.00000000E+00 LOSS 1.12347830E+00 LOSERR 0.
YINST -7.08501339E-02 YSENS -7.08501339E-02 YIMU -8.76589456E-02 YDCOM 7.42372865E-02 TAS -2.63004640E+00 TAEFR 0.
GLOSD -3.94474972E+00 THCOM 2.63004640E+00 RANGS 1.91006242E+00 RGEFR 0.
$$$$$ DOCKING MECHANISM MOTION $$$$$$
CENTERLINE
XCL -9.05606919E-02 XDCL -1.06223980E+00 PITCH 1.50656810E+00
YCL -1.82670464E-02 YOCL -1.12381037E-01 P-RATE-5.78716087E-01
TOP CORNER
PATH 6.03921613E+00
XTC -1.16860606E-02 XOTC -1.09253083E+00
YTC 2.98069591E+00 YOTC -1.42672066E-01
BOTTOM CORNER
XBC -1.69435723E-01 XOBC -1.03194877E+00
YBC -3.01723001E+00 YOBC -5.20900081E-02
$$$$$ POWER ON CONFIGURATION $$$$$$
ENGINES ON 0 0 0 0 0 0 7 8 0 0 0 0 0 0 0 0 0 0 0 0 22 23 0
ACS TIME THIS INTERVAL = 5.0000000E-01 TOTAL ACS TIME = 1.24008000E+00 NVTPA 0 NHTRA 0 NATFLG(2) -2

```

```

$$$$$ POWERED FLIGHT SUMMARY $$$$$$
$$$$$ ENGLISH UNITS $$$$$$
TIME 1.71409176E+02 WEIGHT 3.19939917E+04 PROP -6.00833720E+00
$$$$$ C.G.MOTION $$$$$$
XCG 1.69000000E+01 YCG -4.43394177E-01 XDCG -1.05799152E+00 YDCG 4.91570777E-02 PITCH 1.53167539E+00 P-RATE-4.68898948E-01
$$$$$ SENSED AND COMMANDED MOTION $$$$$$
XINST 2.03500219E+00 XSNS 2.00500219E+00 XIMU 2.00440757E+00 XDCOM -1.00000000E+00 LOSS 4.44452999E-01 LOSERR 0.
YINST -6.91798522E-02 YSENS -6.91798522E-02 YIMU -9.21213759E-02 YDCOM 6.90072584E-02 TAS -2.63142812E+00 TAEFR 0.
GLOSD -2.91092411E+00 THCOM 1.97612839E+00 RANGS 2.00619532E+00 RGEFR 0.
$$$$$ DOCKING MECHANISM MOTION $$$$$$
CENTERLINE
XCL 5.71679114E-03 XDCL -1.06149153E+00 PITCH 1.53167539E+00
YCL -1.57206629E-02 YOCL -8.17374251E-02 P-RATE-4.68898948E-01
TOP CORNER
PATH 4.40322506E+00
XTC 8.59055750E-02 XOTC -1.08603425E+00
YTC 2.98320744E+00 YOTC -1.06280144E-01
BOTTOM CORNER
XBC -7.44719928E-02 XOBC -1.03694881E+00
YBC -3.01464876E+00 YOBC -5.71947058E-02
$$$$$ POWER ON CONFIGURATION $$$$$$
ENGINES ON 0 0 0 0 0 0 7 8 0 0 0 0 0 0 0 0 0 0 0 0 22 23 0
ACS TIME THIS INTERVAL = -9.08244576E-02 TOTAL ACS TIME = 1.14917554E+00 NVTPA 0 NHTRA 0 NATFLG(2) -2

```

III. SENSOR AND DOCKING MECHANISM REQUIREMENTS DERIVATION

The effort expended toward the derivation of sensor and mechanism hardware requirements on this study is logically divided into two separate endeavors. In Part A of this section the general approach is discussed, the specific relationships between sensor and mechanism derived, and finally how and in what form the results and data were obtained that parameterized these relationships.

In Part B each of the identified sensor and mechanism hardware parameters are discussed individually. An expected attainable performance value is selected, a margin factor assigned and the resulting recommended specification defined. Specifications for each configuration, i.e., manual, non-impact, etc., are derived independently. Where applicable, the data and/or curves generated in Part A are used in Part B to illustrate and provide justification for the values selected.

A. SENSOR/DOCKING MECHANISM TRADEOFF DATA

As the study progressed it became clear that many of the unique rendezvous and docking system sensor and mechanism requirements in earlier programs and studies were arrived at without any clear, or at least, documented foundation for the values selected. Rather than select seemingly applicable values from this earlier work that, in fact, may be propagating errors from previous inappropriate or erroneous assumptions, a "bottoms up" derivation of requirements was initiated. This section deals with our selected approach to derive the necessary requirements, in a traceable form, from the best knowledge of expected conditions and error sources.

The key hardware of concern in this analysis is, (1) the sensors that provide knowledge for control during the rendezvous and docking; and, (2) the docking mechanism. These are closely interrelated, one affecting the other. The requirements derivation is really a balancing or budgeting exercise, as shown in Figure III-1.

The figure shows some of the more important properties this analysis will be deriving requirements for. The center block, strategies that reduce variables to residual contact values, is accomplished, in general, by the Tug

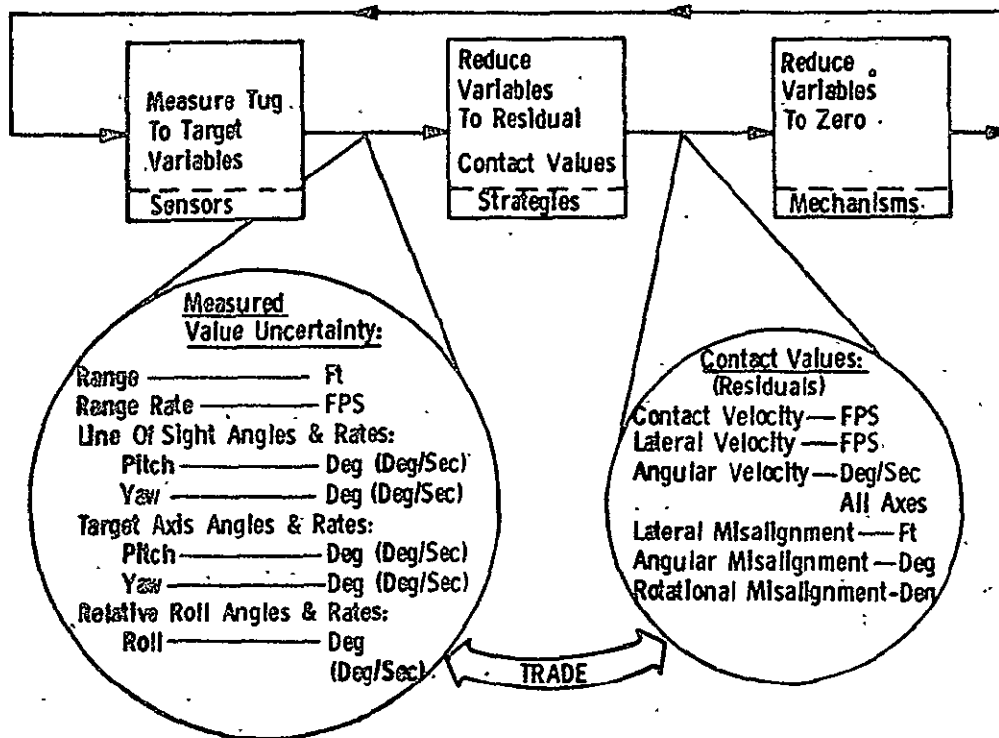


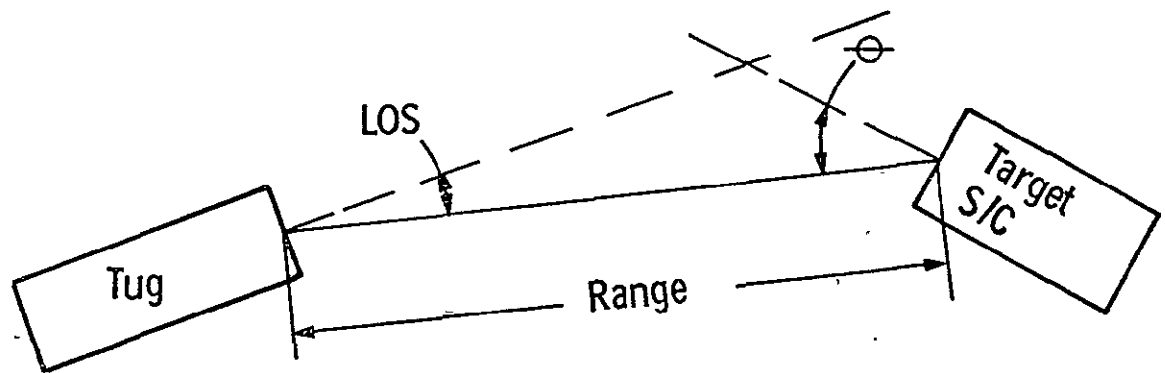
FIGURE III-1 THE DOCKING BUDGET ISSUE

and its subsystem. It will also involve the man for manual configurations. It is not an insignificant factor and requirements for this phase of the docking will be discussed.

The data obtained by sensor that is necessary for vehicle control during the rendezvous and docking are shown in Figure III-2. A key constraint on the availability and accuracy of the data is the range of operation. There are limits on the minimum distances from the target as well as the maximum. Those limiting ranges vary considerably from one type of sensor to another.

On the other end of the budgeting process, some of the docking mechanism design parameters are portrayed in Figure III-3 along with the detail design characteristics that are affected by those parameters.

The center block of Figure III-1, the control system and strategies that bring the two mechanisms together, have certain characteristics that influence success in accomplishing the docking, as mentioned earlier. The more significant are:



Sensors Determine:

Range = Distance from Sensor to Target

LOS = Angle from Tug Q_L to Line-of-Sight (Pitch and Yaw)

\odot = Target Attitude with Respect to LOS (Pitch and Yaw)

Roll = Relative Roll Displacement Between Tug and Target

Figure III-2 Sensors Provide Intelligence

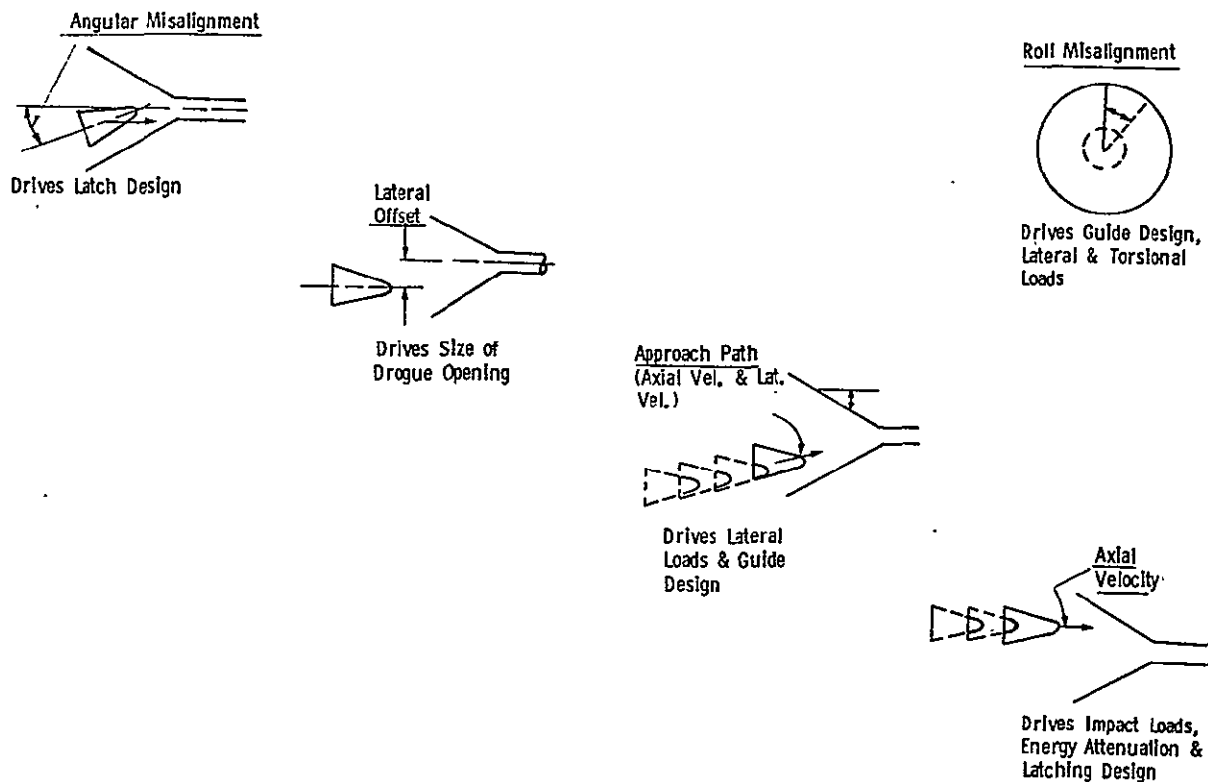


Figure III-3 Mechanisms Complete The Docking

Tug deadband limits and rates,
Spacecraft deadband limits and rates,
Tug ACS jet minimum impulse bit,
Man's visual discernment capability for:
 o S/C position misalignment,
 o Errors in vehicle attitude alignment,
Transmission delays in visual and command data.

All of the above factors are considered in the subsequent analyses.

The relationships between these factors were found to be defined most efficiently by examining, or writing an equation for each docking mechanism in terms of the errors contributed by Tug, man and the sensors.

Nine individual cases were postulated. They are:

- o Angular Misalignment (Impact Docking)
- o Angular Misalignment (Non-Impact Docking)
- o Lateral Displacement (Impact Docking)
- o Lateral Displacement (Non-Impact Docking)
- o Lateral Velocity
- o Contact Velocity
- o Roll Misalignment
- o Steerable Probe Maximum Angle (Non-Impact)
- o Steerable Probe Maximum Rate (Non-Impact)

A detailed description of the geometrical relationship assumed and the resulting equations follow. Note that the non-impact docking requires a differential set of geometrical conditions from the impact cases.

In the discussion that follows, some of the derived equations were complex enough to justify their mechanization in a computer program. Wherever that's the case the program is provided. The programs allow for easy variation and rapid plotting of a multitude of different parameters.

The purpose of these parametric curves is to provide not only quantitative data, but sensitivity information as well for the definition of sensor and mechanism design specifications in Part B.

To avoid an unnecessarily large volume of paper in this report, the many computer generated curves will not be provided. Only applicable curves will be provided and they appear in Part B with the corresponding specification selection they support. Any other data desired could be duplicated by implementing the computer program code supplied and selecting desired values for the input variables.

1. Angular Misalignment, Impact Docking - The geometry assumed to derive the docking mechanism's angular misalignment, referred to as τ , at the time of contact is depicted in Figure III-4.

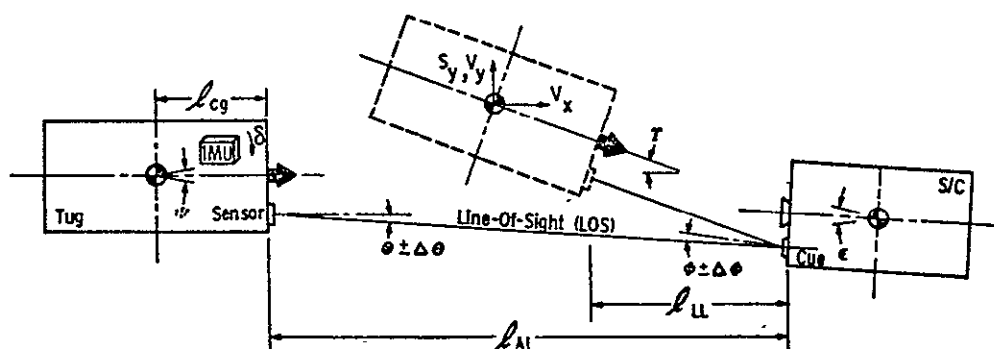


FIGURE III-4 ANGULAR MISALIGNMENT GEOMETRY

The potential error sources are combined as follows:

$$\text{Angular Misalignment} = \sum_{\text{RSS}} \left(\begin{array}{c} \text{lateral position error at loss} \\ \text{of target attitude data} \end{array} \right) + \left(\begin{array}{c} \text{angular uncertainties} \\ \text{at docking} \end{array} \right)$$

$$\text{where lateral position error is} = \sin^{-1} \left[\frac{\text{lateral c.g. offset}}{\text{(Tug c.g. distance to interface at loss of LOS data)}} \right]$$

and angular uncertainties are:

- o Tug deadband
- o Spacecraft deadband
- o LOS determination error
- o Target attitude uncertainty
- o IMU drift after loss of attitude data.

The lateral c.g. offset as defined from Figure III-4 is:

$$\sqrt{\left[\left(\begin{array}{c} \text{distance from Tug to target} \\ \text{at loss of attitude data} \end{array} \right) \times \sin (\text{target attitude uncertainty}) \right]^2 + \left[\text{residual lateral velocity} \times \text{time from last correction} \right]^2}.$$

An RSS combination of errors was utilized after examination showed most errors to be independent of each other.

If τ = angular misalignment
 θ = LOS
 $\Delta\theta$ = LOS determination uncertainty
 ϕ = target uncertainty
 $\Delta\phi$ = target attitude determination uncertainty
 ψ = Tug deadband
 ϵ = spacecraft deadband (or precession)
 δ = IMU drift rate (deg/sec)
 l_{cg} = distance, Tug c.g. to interface
 l_{AL} = distance at loss of spacecraft attitude data
 l_{LL} = distance at loss of LOS data
 V_X = axial velocity
 V_Y = lateral velocity
 δ_Y = lateral position error

Then,

$$\tau = \sqrt{\left[\sin^{-1} \sqrt{\frac{(l_{AL} \sin \Delta\phi)^2 + \left(V_Y \frac{l_{AL}}{V_X} \right)^2}{l_{cg} + l_{LL}}} \right]^2 + \psi^2 + \epsilon^2 + \Delta\theta^2 + \Delta\phi^2 + \frac{l_{AL}}{\delta V_X}}$$

NOTES:

- 1) If IMU drift (δ) is less than .1 deg/hr, the last term is negligible.
- 2) For an earth-pointing spacecraft, the ϵ term becomes $\frac{l_{AL}}{\epsilon V_X}$ where ϵ is earth rate or precession, not spacecraft deadband.

The above equation, being relatively complex, was coded in Fortran for computer solution and plotting. The code is shown below in Figure III-5. Angular

misalignment plots can be seen in Figures III-12, III-14, III-21, and III-22 of Part B.

```

C      PROGRAM ZERNAM(INPUT,OUTPUT,TAPE5=INPUT,TAPE6=OUTPUT,FILMPL)
C
C      NAMELIST /INDATA/ DLCG,DLAL,DLLL,DPHI,DTHE,EPS,PSI,DEL,VX,IFGO
C
C      DIMENSION VY(51),X(51),SAVE(51,3),YNAME(3),PTITLE(4)
C
C      DATA DVY, CON, NIND / 0.005, 57.2957795, 51 /
C
C      CALL RPLT(2HNB,2HLC)
C
C      DO 1 I=1,NIND
1  VY(I) = FLOAT(I-1)*DVY
    KNT = 0
    KPL = 0
999 CALL START
    HEAD (5,5) PTITLE
    5 FORMAT(4A10)
C
C 998 READ (5,INDATA)
    IF(IFGO.EQ. 0) GO TO 999
    CALL PAGEHD
    WRITE(6,INDATA)
    KNT = KNT + 1
C
C      A = PSI**2 + EPS**2 + DTHE**2 + DPHI**2 + (DEL*DLAL/VX)**2
C      H = (DLAL*SIN(DPHI/CON))**2
C      C = DLCG + DLLL
C
C      DO 10 I=1,NIND
C      D = SQRT(8 + (VY(I)*DLAL/VX)**2)/C
C      E = ASIN(U)
10  X(I) = SQRT(A + (E*CON)**2)
C
C      CALL WRITE(X,1,NIND,NAME(2HAM,KNT),1)
C      KPL = KPL + 1
C      DO 20 I=1,NIND
20  SAVE(I,KPL) = X(I)
    YNAME(KPL) = NAME(2HAM,KNT)
    IF(KPL.EQ. 3) CALL PLOT1(VY,SAVE,NIND,KPL,0.0,0.05,
    * 6H1ATVEL,YNAME,PTITLE,1,1,0,51)
    IF(KPL.EQ. 3) KPL = 0
C
C      GO TO 998
C      END

```

FIGURE III-5 ANGULAR MISALIGNMENT PROGRAM

2. Angular Misalignment - Non-Impact Docking - The same physical conditions portrayed in Figure III-4 are applicable; however, for a non-impact docking V_X , or axial velocity, essentially comes to zero at some stationkeeping distance. Also, some means of relative positioning must be present throughout the docking, forcing the range for loss-of-target attitude information and loss of LOS data to be the same. That range will be referred to, for non-impact docking as stationkeeping range (ℓ_{SK}). This is on the order of one to five feet.

For non-impact docking the vehicle is in a translation deadband of a given width (S_Y) and lateral rate (V_Y). Thus, the lateral c.g. offset part of the equation from (1) becomes:

$$\sin^{-1} \frac{S_Y}{\ell_{cg} + \ell_{SK}}$$

This results in an angular misalignment for non-impact docking (τ_{NI}) equal to:

$$\tau_{NI} = \sqrt{\left[\sin^{-1} \left(\frac{S_Y}{\ell_{cg} + \ell_{SK}} \right) \right]^2 + \psi^2 + \epsilon^2 + \Delta\theta^2 + \Delta\phi^2}$$

where:

- τ_{NI} = angular misalignment - non-impact docking
- $\Delta\theta$ = LOS uncertainty
- $\Delta\phi$ = target attitude uncertainty
- ψ = Tug deadband
- ϵ = spacecraft deadband
- ℓ_{cg} = Tug cg to I/F distance
- ℓ_{SK} = stationkeeping standoff distance
- S_Y = stationkeeping translation deadband width

The IMU drift term is not applicable since LOS data is never lost. Figure III-17 in Part B shows typical curves for non-impact angular misalignment.

3. Lateral Displacement (X), Impact Docking - The physical condition of the vehicle is portrayed in Figure III-6.

The lateral displacement error is basically from two sources: angular errors or uncertainties as they are reflected to the docking interface; and translation lateral offsets between the two vehicles that are also reflected to the docking interface.

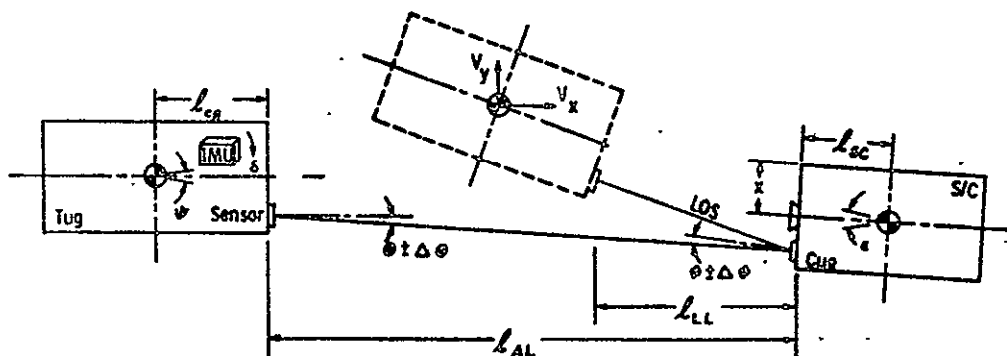


FIGURE III-6 LATERAL DISPLACEMENT GEOMETRY

In the first category are:

- a) lateral offset due to Tug deadband;
- b) lateral offset due to spacecraft deadband;
- c) lateral offset due to LOS uncertainty;
- d) lateral offset due to target attitude uncertainty;
- e) Tug angular error due to IMU drift after loss of LOS data.

In the second category are:

- f) lateral offset due to target attitude determination uncertainty at the time of target attitude data loss;
- g) lateral offset due to residual lateral velocity from the time of attitude data loss to LOS data loss.

Errors f) and g) above can be thought of as being imparted at the Tug c.g. Until loss of LOS data the tug sensors continue to point the tug at the target so the above errors are not translated directly to the docking interface, but rather are considerably less, being scaled down by the factor of $\left(\frac{l_L}{l_{LL} + l_{cg}}\right)$ for the conditions of Figure III-6.

The final lateral error, shown below, is felt at the vehicle c.g., but also is reflected directly across to the docking interface. It is:

- o lateral offset due to residual vehicle velocity from the time of loss of LOS data to docking contact.

The above errors are shown in equation form as follows, with the equations terms in the same order as the errors listed above.

$$x = \sqrt{\left(\ell_{cg} \sin \psi \right)^2 + \left(\ell_{sc} \sin \epsilon \right)^2 + \left(\ell_{LL} \sin \Delta \theta \right)^2 + \left(\ell_{sc} \sin \phi \right)^2 + \left[\ell_{cg} \sin \left(\delta \frac{\ell_{LL}}{V_X} \right) \right]^2} \left\{ \begin{array}{l} \text{angular} \\ \text{errors} \end{array} \right.$$

$$+ \left(\frac{\ell_{LL}}{\ell_{LL} + \ell_{cg}} \right)^2 \left\{ \left[\frac{V_Y (\ell_{AL} - \ell_{LL})}{V_X} \right]^2 + \left[\ell_{AL} \sin \phi \right]^2 \right\} + \frac{V_Y \ell_{LL}}{V_X} \left\{ \begin{array}{l} \text{lateral} \\ \text{offset} \end{array} \right.$$

where:

- x = lateral displacement
- $\Delta \theta$ = LOS uncertainty
- $\Delta \phi$ = target attitude uncertainty
- ψ = Tug deadband
- ϵ = spacecraft deadband
- ℓ_{LL} = range at which LOS data is lost
- ℓ_{AL} = range at which target attitude data is lost
- ℓ_{cg} = Tug cg to I/F distance
- ℓ_{sc} = spacecraft cg to I/F distance
- V_Y = residual lateral vehicle (c.g.) velocity
- V_X = axial velocity

Typical plots of the above relationship over reasonable ranges of some of the parameters is provided in Figure III-13, 15, 23 and 24 of Part B.

The equation above, again a complex one, was coded as shown in Figure III-7.

4. Lateral Displacement Prior to Stem Contact for Non-Impact Docking -

The lateral displacement of an impact docking is based on a continuously closing pair of vehicles and all the displacements they could experience during that closing. In the non-impact docking the vehicles eventually stop at a stand-off distance, allowing time to trim out many of the earlier offsets and angular errors, resulting in an approximate coalignment and stabilized in a translation deadband control condition.

```

C      PROGRAM ZERMLD(INPUT,OUTPUT,TAPES=INPUT,TAPES=OUTPUT,FILMPL)
C
C      NAMELIST /INDATA/ DLG6,DLSC,DLLL,VX,PSI,EPS,DTHE,DEL,PHI,IFGO,DLAL
C
C      DIMENSION VY(51),X(51),SAVE(51,3),INAME(3),PTITLE(4)
C
C      DATA DVY, CON, NIND / 0.01, 57.2957795, 51 /
C
C      CALL BPLT(2HNB,2HLC)
C
C      DO 1 I=1,NIND
1  VY(I) = FLOAT(I-1)*DVY
    KNT = 0
    KPL = 0
999 CALL START
    READ (5,5) PTITLE
    5 FORMAT(4A10)
C
C 998 READ (5,INDATA)
    IF(IFGO.EQ. 0) GO TO 999
    CALL PAGEHD
    WRITE(6,INDATA)
    KNT = KNT + 1
C
C      B = DLLL/(DLLL + DLG6)
    A = (DLG6*SIN(PSI/CON))**2 + (DLSC*SIN(PHI/CON))**2
    *   + (DLLL*SIN(DTHE/CON))**2 + (DLSC*SIN(EPS/CON))**2
    *   + (B*DLAL*SIN(PHI/CON))**2 + (DLG6*SIN(DEL*DLLL/(VX*CON)))**2
C
C      DO 10 I=1,NIND
10 X(I) = SQRT(A + (VY(I)*DLLL/VX)**2 + (B*VY/VX*(DLAL
    *   - DLLL))**2)
C
C      CALL WRITE(X,1,NIND,NAME(2HLD,KNT),1)
C
C      KPL = KPL + 1
    DO 20 I=1,NIND
20 SAVE(I,KPL) = X(I)
    INAME(KPL) = NAME(2HLD,KNT)
    IF(KPL.EQ. 3) CALL PLOT1(VY,SAVE,NIND,KPL,0.0,0.05,
    *   6H1ATVEL,INAME,PTITLE,1,1,0,51)
    IF(KPL.EQ. 3) KPL = 0
C
C      GO TO 998
    END

```

FIGURE III-7 LATERAL DISPLACEMENT PROGRAM

In non-impact docking, then, the area of concern is just how far the extendable probe, or STEM, tip is moving from one TV frame to the next while the ground controller is attempting to insert the STEM into the drogue. The ultimate value really sizes the drogue diameter. It is quite time-dependent, specifically the TV frame update time.

Therefore, the only two dynamic conditions that reflect into lateral displacement for this case are the minimum residual lateral relative velocity between the two vehicles that the man on the ground, or the autonomous translation stationkeeping subsystem, can trim down to, and the two vehicle's deadband rates. In the case of the latter, the vehicle will normally be constrained within a specified deadband, limiting the maximum displacement to .1 ft for the Tug with a .25 deg deadband, and a 23 ft moment arm from Tug c.g. to STEM tip. The spacecraft will be less than this because of the shorter moment arm. On an RSS basis, the above error of an inch or so is negligible compared to the other factor -- residual lateral vehicle velocity. This is especially true for a manual system where that residual is much larger. The equation is:

$$x_{NI} = \sqrt{(V_Y \cdot t)^2 + [(l_{cg} + l_{SK}) \sin \psi]^2 + (l_{sc} \sin \epsilon)^2}$$

where:

- x_{NI} = lateral displacement - non-impact docking
- ψ = Tug deadband
- ϵ = spacecraft deadband
- V_Y = residual lateral vehicle velocity
- t = time from picture to picture, i.e., STEM command to STEM command
- l_{cg} = Tug cg to interface distance
- l_{sc} = spacecraft cg to interface distance
- l_{SK} = stationkeeping distance

A plot of the above relationship is shown as a function of time in Figure III-18 of Part B. This equation was relatively straight forward, consequently no computer aided solution was employed.

5. Lateral Velocity - The relative lateral velocity of the two mechanisms at the docking interface is due to the vehicle rates within their deadband

and the relative lateral velocity of the two vehicles, taken at their c.g.'s. This is depicted in Figure III-8.

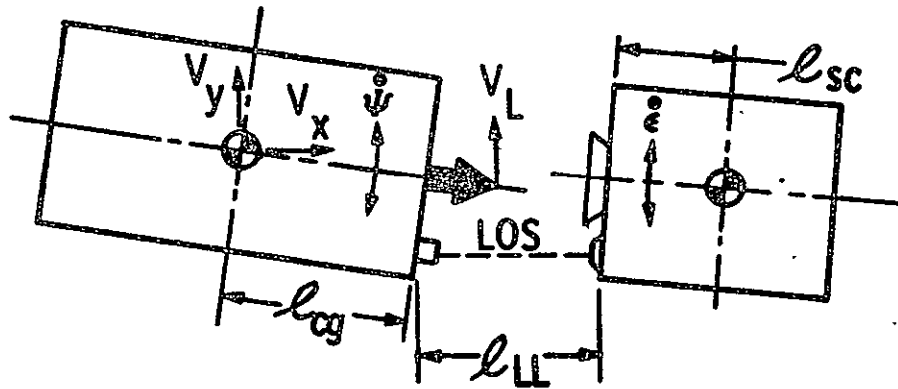


FIGURE III-8 LATERAL VELOCITY GEOMETRY

Algebraically, this can be expressed as follows:

$$V_L = \sqrt{V_Y^2 + (l_{sc} \sin \dot{\epsilon})^2 + (l_{cg} \sin \dot{\psi})^2}$$

where:

- V_L = lateral docking mechanism velocity
- V_Y = lateral vehicle c.g. velocity
- l_{cg} = distance from Tug c.g. to I/F
- l_{sc} = distance from spacecraft c.g. to I/F
- $\dot{\epsilon}$ = spacecraft deadband rate
- $\dot{\psi}$ = Tug deadband rate

Curves plotting the above equation for typical values for the above parameters is shown in Figures III-16 and III-25 of Part B.

The above equation was coded in Fortran for computer solution. The code is provided in Figure III-9.

6. Contact Velocity (V_C) - Axial velocity is straightforward. It is merely the closing velocity plus or minus any uncertainties in accomplishing the closing velocity. That uncertainty is either sensor range rate determination error and/or manual trim capability.

Algebraically,

```

C      PROGRAM ZERMLV(INPUT,OUTPUT,TAPES=INPUT,TAPE6=OUTPUT,FILMPL)
C
C      NAMELIST /INDATA/ DLSC,DLCG,EPSC,PSID,IFGO
C
C      DIMENSION VY(51),X(51),SAVE(51,3),INAME(3),PTITLE(4)
C
C      DATA DVE, CON, NIND / 0.01, 57.2957795, 51 /
C
C      CALL BPLT(2HNB,2NLC)
C
C      DO 1 I=1,NIND
1  VY(I) = FLOAT(I-1)*DVE
   KNT = 0
   KPL = 0
999 CALL START
   READ (5,5) PTITLE
   5 FORMAT(4A10)
C
C 998 READ (5,INDATA)
   IF(IFGO .EQ. 0) GO TO 999
   KNT = KNT + 1
C
C      A = (DLSC*SIN(EPSC/CON))**2 + (DLCG*SIN(PSID/CON))**2
C
C      DO 10 I=1,NIND
10 X(I) = SQRT(VY(I)**2 + A)
C
C      CALL WRITE(X,1,NIND,NAME(2HNV,KNT),1)
   KPL = KPL + 1
   WRITE(6,INDATA)
   DO 20 I=1,NIND
20 SAVE(I,KPL) = X(I)
   INAME(KPL) = NAME(2HNV,KNT)
   IF(KPL .EQ. 3) CALL PLOT1(VY,SAVE,NIND,KPL,0.0,0.05,
* 6H LATEL,INAME,PTITLE,1,1,0.51)
   IF(KPL .EQ. 3) KPL = 0
C
C      GO TO 998
END

```

FIGURE III-9 LATERAL VELOCITY COMPUTER PROGRAM

$$V_C = V_X \pm \Delta V_X$$

where:

V_C = contact velocity

V_X = axial velocity or range rate (\dot{R})

ΔV_X = range rate uncertainty ($\Delta \dot{R}$)

7. Roll Angular Misalignment - τ_R - Roll angular misalignment, as depicted in Figure III-10, is primarily a function of: (a) the ability to determine the misalignment, either manually or by sensor; (b) by the vehicle deadbands, and (c) by IMU drift from the time of last roll attitude correction, which is negligible for all practical purposes. The equation is:

$$\tau_R = \sqrt{\psi_R^2 + \epsilon_R^3 + (\Delta\theta_R) + \left(\delta \frac{l_{AL}}{V_X}\right)^2}$$

where:

τ_R = roll attitude misalignment

ψ_R = tug roll deadband

ϵ_R = spacecraft roll deadband

$\Delta\theta_R$ = roll attitude determination uncertainty

δ = IMU gyro drift

l_{AL} = range at which attitude data is lost

V_X = axial velocity

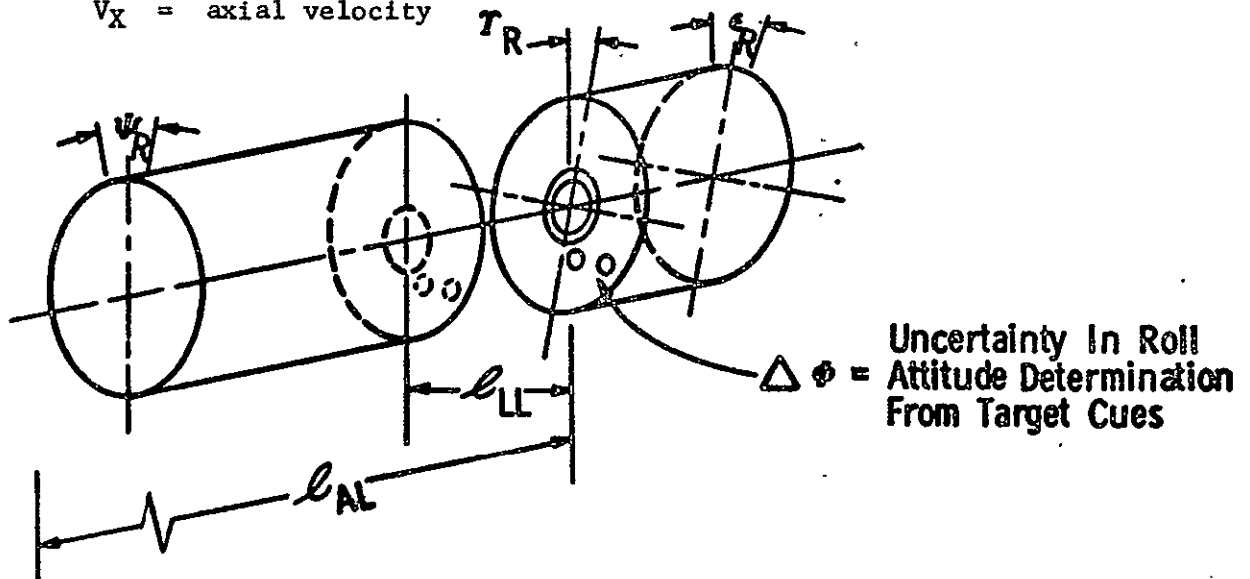


FIGURE III-10 ROLL ANGULAR MISALIGNMENT

8. Stem Maximum Articulation Angle for Non-Impact Docking - The maximum steerable probe (STEM) articulation angle required (see Figure III-11) is determined by:

- a) angular misalignment due to LOS uncertainty during stationkeeping control;
- b) angular misalignment due to target attitude determination uncertainty during stationkeeping;
- c) angular misalignment due to Tug deadband;
- d) angular misalignment due to spacecraft deadband;
- e) STEM angle required to account for the lateral relative translation deadband.

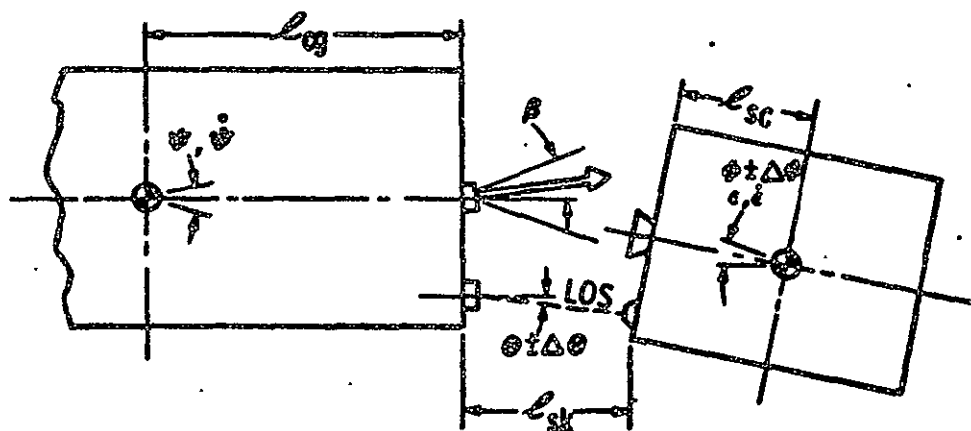
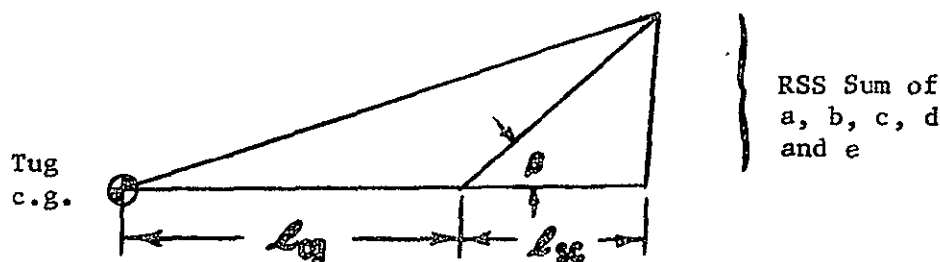


FIGURE III-11 STEM ARTICULATION ANGLE (β)

To relate the above to STEM articulation angle, the angular uncertainties (a through d) are first reduced to lateral offsets at the STEM tip and then are reflected into an angle whose tangent is the RSS sum of those offsets divided by the stationkeeping distance as shown below in a simplified form.



In equation form, this reduces to:

$$\beta = \tan^{-1} \sqrt{\frac{[(l_{cg} + l_{SK}) \sin \Delta\theta]^2 + (l_{sc} \sin \Delta\phi)^2 + [(l_{cg} + l_{SK}) \sin \psi]^2 + (l_{sc} \sin \epsilon)^2 + S_Y^2}{l_{SK}^2}}$$

where:

- β = STEM maximum articulation angle
- $\Delta\theta$ = LOS uncertainty
- $\Delta\phi$ = target attitude uncertainty
- ψ = Tug deadband
- ϵ = spacecraft deadband
- l_{cg} = distance from tug cg to I/F
- l_{sc} = distance from spacecraft c.g. to I/F
- l_{SK} = stationkeeping distance
- S_Y = Tug translation deadband (relative to spacecraft)

A typical plot of the above relationship is provided in Figure III-19 of Part B.

9. STEM Maximum Rate for Non-Impact Docking - The maximum rate the STEM, shown in Figure III-11, must be articulated at is a function of the Tug and spacecraft deadband rates and the translation deadband lateral vehicle rate. These vehicle rates must be reduced to rates the STEM would require with its much shorter moment arm. In equation form, this is:

$$\alpha = \tan^{-1} \sqrt{\frac{[(l_{cg} + l_{SK}) \sin \dot{\psi}]^2 + (l_{sc} \sin \dot{\epsilon})^2 + V_Y^2}{l_{SK}^2}}$$

where:

- α = STEM articulation rate (deg/sec)
- $\dot{\psi}$ = Tug deadband rate
- $\dot{\epsilon}$ = spacecraft deadband rate
- l_{cg} = distance from Tug cg to I/F
- l_{sc} = distance from spacecraft cg to I/F
- l_{SK} = non-impact stationkeeping distance
- V_Y = translation deadband lateral rate

A plot of the above is provided in Figure III-20 of Part B.

B. Hardware Requirements Derivation

A unique set of requirements was derived for each of the following conditions:

- Manual Impact Docking
- Manual Non-Impact Docking
- Autonomous Impact Docking
- Autonomous Non-Impact Docking
- Hybrid Impact Docking

Each of the above is treated separately in this section. For each of the conditions above the requirements have been grouped into five categories. They are:

- Ranging Sensor Requirements
- Video/Lighting Requirements
- Docking Mechanism Requirements
- Target Cue Requirements
- Control System/Man Requirements

The above requirements are compiled in tabular form in this section. Five tables are provided for each of the five different conditions.

1. Manual Impact Docking - The requirements for this type of docking are provided in Tables III-1 through III-5. Curves are provided where applicable to back up the rationale associated with some of the requirements.
2. Manual Non-Impact Docking - The requirements for this type of docking are found in Tables III-6 through III-10.
3. Autonomous Impact Docking - The requirements for autonomous impact docking are presented in Tables III-11 through III-15.
4. Autonomous Non-Impact Docking - The requirements are found in Table III-16 through III-19. The table for TV requirements is not provided since video is not a critical requirement for the autonomous case.
5. Hybrid Impact Docking - Figures III-20 through III-24 summarize the requirements for this case.

TABLE III-1 REQUIREMENTS-RANGING SENSOR

MANUAL IMPACT DOCKING

REQUIREMENTS	SOURCE
a. Attitude Determination Capability - None	All relative attitude corrections are provided manually from TV observation.
b. Acquisition Range= 12.5 n mi Margin $\times 2$ 25.5 n mi	Trajectory error analyses resulted in successful rendezvous from 12.5 n mi with very small ACS penalty over longer range rendezvous, such as 50 n mi.
c. Minimum Range for Range Data - 10 ft	Range data will be necessary on the ground to perform lateral thrusting maneuvers manually. Because of data transmission delays and crew response time no such corrections are probable in the last 10 seconds. At a constant closing rate of 1 fps, the minimum range is 10 feet.
d. Range Accuracy - .5 n mi to 25 n mi- <100 ft 10 ft to .5 n mi - ± 1 ft	<p>Consistent with accuracy of rendezvous algorithm correction capability of <100 feet</p> <p>The time of the last TV picture on which corrections will be based is at least 20 seconds (20 ft) from docking. A one foot error in range would result in an error of 5% in any lateral translation correction that is based on range. This is approximately equal to the error due to the estimated ability of the man to determine the target attitude misalignment (± 1 in.) from which that correction is derived. Specifically, for a nominally lighted offset "T" less than 2 feet across, one inch results in a 4% target attitude misalignment uncertainty.</p> <p>NOTE: The minimum velocity impulse (ACS total minimum impulse bit) is .012 in/sec. At 20 ft (or 20 sec) the <u>minimum</u> offset that could be corrected for is 1/4 inch.</p>

TABLE III-1 REQUIREMENTS-RANGING SENSOR (Cont'd)

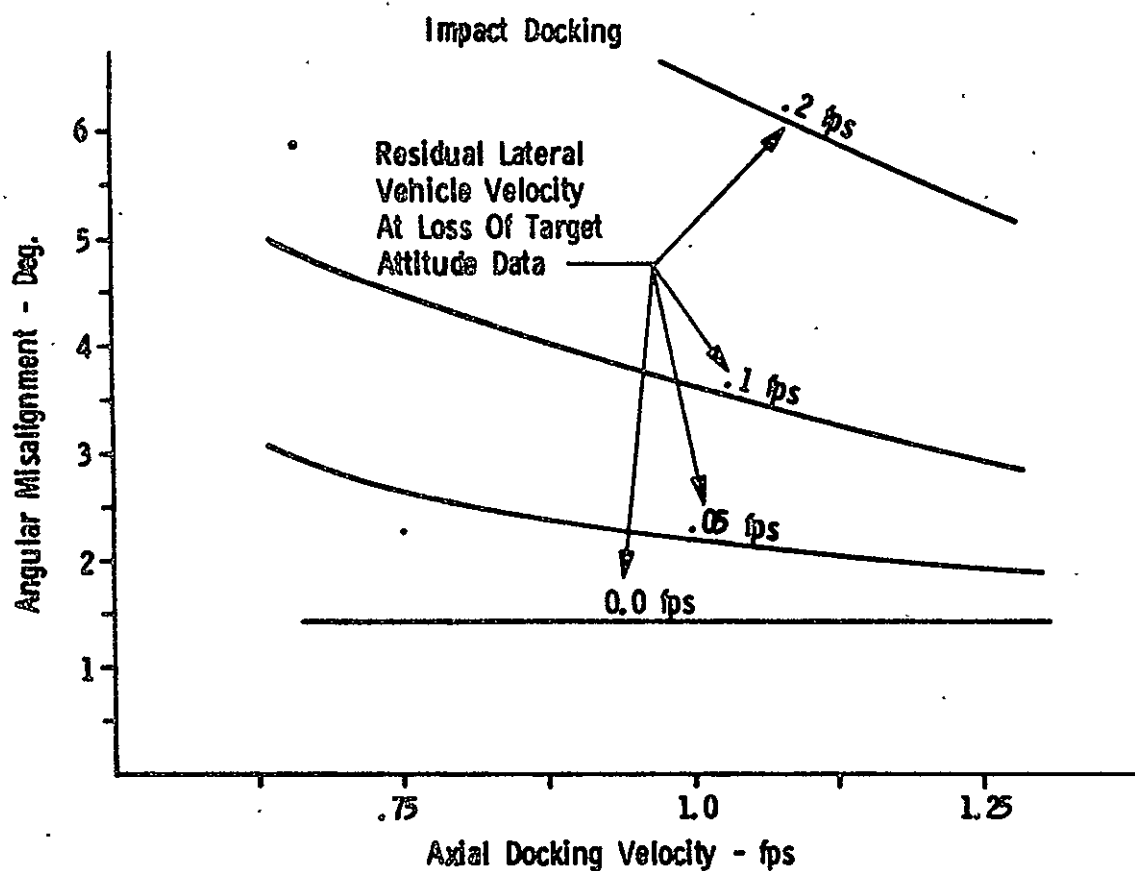
MANUAL IMPACT DOCKING

REQUIREMENTS	SOURCE
<p>e. Range Rate Accuracy Far (.5 n mi to 25 n mi) = TBD fps Near(10 ft to .5 n mi) = $\pm .1$ fps</p> <p>f. Field-of-View ± 15 deg</p>	<p>Rendezvous algorithm requirement.</p> <p>For impact docking a constant range rate of 1.0 fps is desired. Little occurs to perturb this after the last corrections at 10 ft to 20 ft, consequently an accuracy of $\pm .1$ is sufficient to ensure impact well within the structural design margin of the mechanism which is presumed to tolerate at least ± 1.25 fps. Figure III-12 shows a relative insensitivity to Axial Velocity over the range of .75 to 1.25 fps.</p> <p>FOV must be adequate to: (1) find target in FOV at acquisition, (2) track during worst vehicle perturbations, and (3) determine target attitude from a pattern of given diameter up to a specified minimum range. In this case attitude determination by ranging sensor [(2) above] is not required. Previous stored knowledge of the docking port attitude and TV manual attitude coalignment maneuvers are sufficient for docking.</p> <p>Regarding (1), current values of 3 n mi for Tug position error and 1 n mi of spacecraft position result in worst angular LOS error at the minimum acquisition range (12.5 n mi) of</p> $\sin^{-1} \frac{\sqrt{(3^2 + 1^2)}}{12.5} = +15^\circ.$

TABLE III-1 REQUIREMENTS-RANGING SENSOR (Cont'd)

MANUAL IMPACT DOCKING

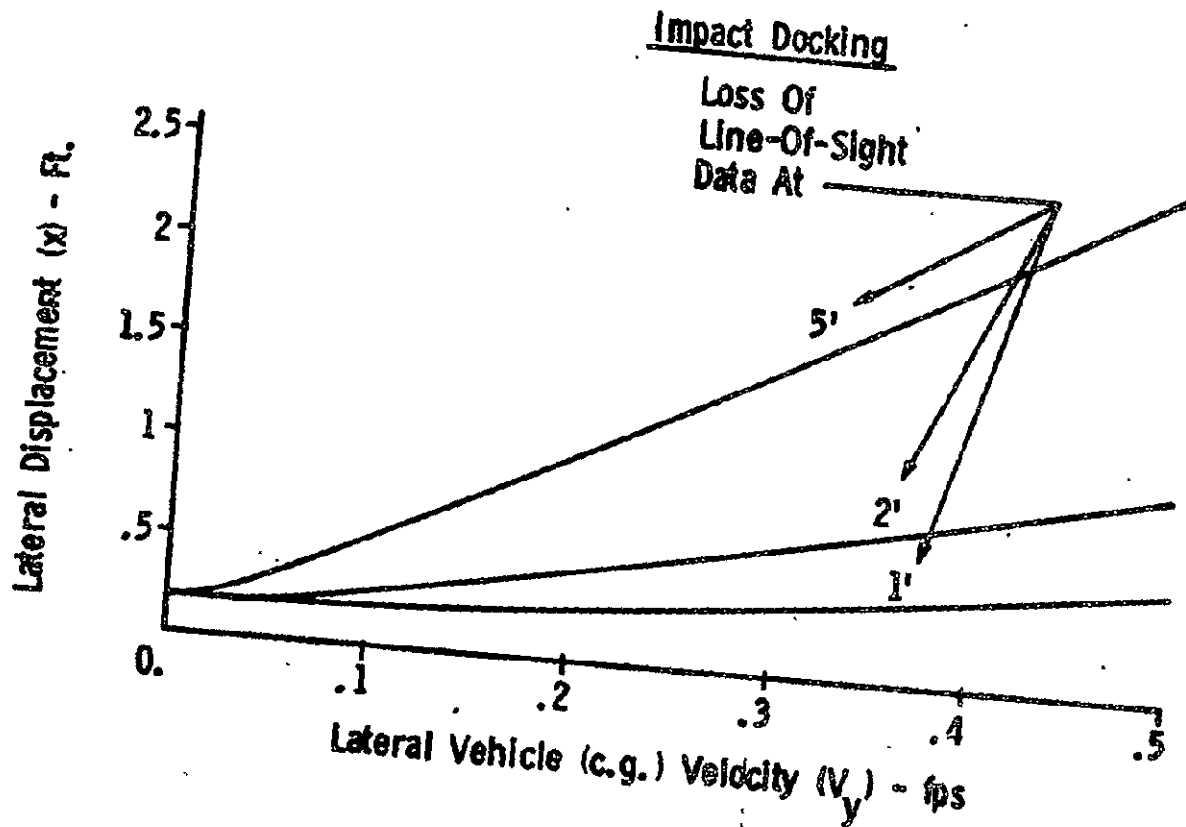
REQUIREMENTS	SOURCE
<p>g. LOS Accuracy - Near - $\pm 1.0^\circ$ Far - TBD</p> <p><u>Preliminary Allocation</u></p> <p>Cue location error = $.5^\circ$ (1 in. at 1 ft)</p> <p>Sensor Alignment on Tug = $\pm .5^\circ$</p> <p>Sensor Accuracy (Bias, Threshold, Quantitization, etc.) = $\pm .75^\circ$</p> <p>Computation Error = <u>Neg</u> RSS 1.0</p>	<p>Docking mechanism design parameters are relatively insensitive to LOS errors less than one degree. A preliminary allocation of errors making up the $\pm 1^\circ$ number is provided. They reflect realistic achievable specifications.</p>
<p>h. Loss of LOS ≈ 1 ft</p>	<p>Lateral offset at the docking mechanism is somewhat sensitive to this. One foot provides sufficient margin and is well within current technology capability. Impact of the loss of LOS data on lateral displacement (the most sensitive docking mechanism parameter) is illustrated in Figure III-13 for the conditions shown.</p>



CONDITIONS

$\Delta\phi = 1^\circ$	S/C Attitude Uncertainty
$\Delta\theta = .5^\circ$	LOS Uncertainty
$\psi = .25^\circ$	Tug Deadband
$\epsilon = .5^\circ$	S/C Deadband
$l_{cg} = 18'$	Tug cg-to-I/F distance
$l_{SC} = 17'$	S/C cg-to-I/F distance
$l_{AL} = 10'$	Range at which Target Attitude Data is Lost
$\delta = .0003^\circ/\text{sec}$	IMU Drift
$l_{LL} = 1'$	Range where LOS Data is Lost

FIGURE III-12 ANGULAR MISALIGNMENT vs AXIAL DOCKING VELOCITY



CONDITIONS

$\Delta\phi = .5^\circ$	LOS Uncertainty
$\Delta\theta = 1.0^\circ$	S/C Attitude Uncertainty
$\psi = .25^\circ$	Tug Deadband
$\epsilon = .5^\circ$	S/C Deadband
$l_{cg} = 18'$	Tug cg to I/F Distance
$l_{SC} = 7'$	S/C cg to I/F Distance
$l_{AL} = 20'$	Range where Target Att. Data is Lost
$V_X = 1$ fps	Axial Velocity
$\delta = .0003^\circ/\text{sec}$	IMU Drift

FIGURE III-13 LATERAL DISPLACEMENT vs LATERAL VEHICLE VELOCITY

TABLE III-2, REQUIREMENTS-VIDEO/LIGHTING

MANUAL IMPACT DOCKING

REQUIREMENT	SOURCE
<p>a) Type - Silicon Intensified Target Vidicon</p> <p>b. Resolution - >500 Lines and >400 Pixels</p> <p>c. FOV = 20°</p> <p>d. Scan Rate = 30 Times/sec</p> <p>e. Bandwidth = 4.5 Megahertz</p>	<p>The silicon intensified vidicon is one of the most sensitive types of television camera tube. For this reason it will minimize the amount of illumination the Tug must provide. The resolution required by the Tug application is in the range achievable with this camera tube, and the wide 500:1 to 1000:1 dynamic range inherent in this technology minimizes the mechanical adjustment required for the aperture of the camera lens.</p> <p>525 lines in a 20° field of view specified for the shuttle camera will cover a one-foot wide area at 100 ft with $525 / (200 \tan 10^\circ) = 15$ lines, which is adequate to display details of objects this size, as required for Tug. As the Tug approaches the target, smaller details will be resolved.</p> <p>Since TV is not used for initial acquisition the driving requirement on FOV is to provide sufficient viewing capability of the s/c during inspection and of the docking port during closing.</p> <ul style="list-style-type: none"> Max S/C cross section = 25' at 100' inspection point $FOV = 2 \left(\tan^{-1} \frac{25/2}{100} \right) = 14.25^\circ$ for S/C inspection Docking port diameter of interest = 3 ft. If last picture is 20 sec (20 ft) from contact $FOV = 2 \left(\tan^{-1} \frac{1.5}{20} \right) = 8.5^\circ$ for docking port viewing. <p>Consequently, 20° FOV should provide sufficient margin.</p> <p>The output bandwidth of a camera is a function of the scan rate and number of picture elements specified for the picture. Scan conversion electronic components are required to reduce the bandwidth of the shuttle camera to the allowed transmission bandwidth for Tug. If an image dissector camera tube were used, the scan rate could be lowered directly,</p>

TABLE III-2 REQUIREMENTS-VIDEO/LIGHTING (Continued)

MANUAL IMPACT DOCKING

REQUIREMENT	SOURCE
d. and e. (cont'd)	
f. Camera Survivability - Look into the Sun	<p>but the other advantages of the shuttle camera would be lost. Therefore, the values shown are not necessarily requirements for Tug, however they are consistent with the other TV requirements shown in this table, all of which were selected with a certain camera development program in mind.</p>
g. Maximum Length - .3m (1 ft)	<p>The candidate camera is specified to be capable of looking directly at the sun. This implies that special protective measures, such as a shutter, will be incorporated in the camera to protect the intensified target tube. A silicon vidicon type of camera tube does not necessarily require this special handling.</p>
h. Target Illumination Required - 5 to 10 ft Candles	<p>This is necessary to provide packaging within the Tug forward structure.</p>
i. Lighting - Strobe or Tungsten Flood	<p>This is the shuttle camera anticipated capability. The lighting requirements in (i) and (j) below are based on this.</p>
j. Lighting Power - 600 watts (Max) 16.5 watts (Avg)	<p>The shuttle camera characteristics require that the target be illuminated to a level of 5 to 10 ft candles (5 to 10 lumens per sq. ft). The power required to furnish this illumination can be estimated as follows:</p>
	<p>Assume a Xenon Short-Arc Lamp within a reflecting housing such that 75% of the light produced falls within a 20° diameter circular cone coincident with the field-of-view of the camera. The area on the surface of a sphere of 100 ft radius illuminated by this cone of light is 970 sq. ft. and the lamp must produce $4700/.75 = 13000$ lumens in order to average 10 lumens per sq. ft. over this area. A well-designed reflector can assure that the edge of the cone will receive not less than half as much illumination per unit area as the central area, and the illumination within the cone will everywhere be greater than 5 lumens per sq. ft. The Xenon Short-Arc Lamp has a luminous efficiency of approximately</p>

TABLE III-2 REQUIREMENTS-VIDEO/LIGHTING (Continued)

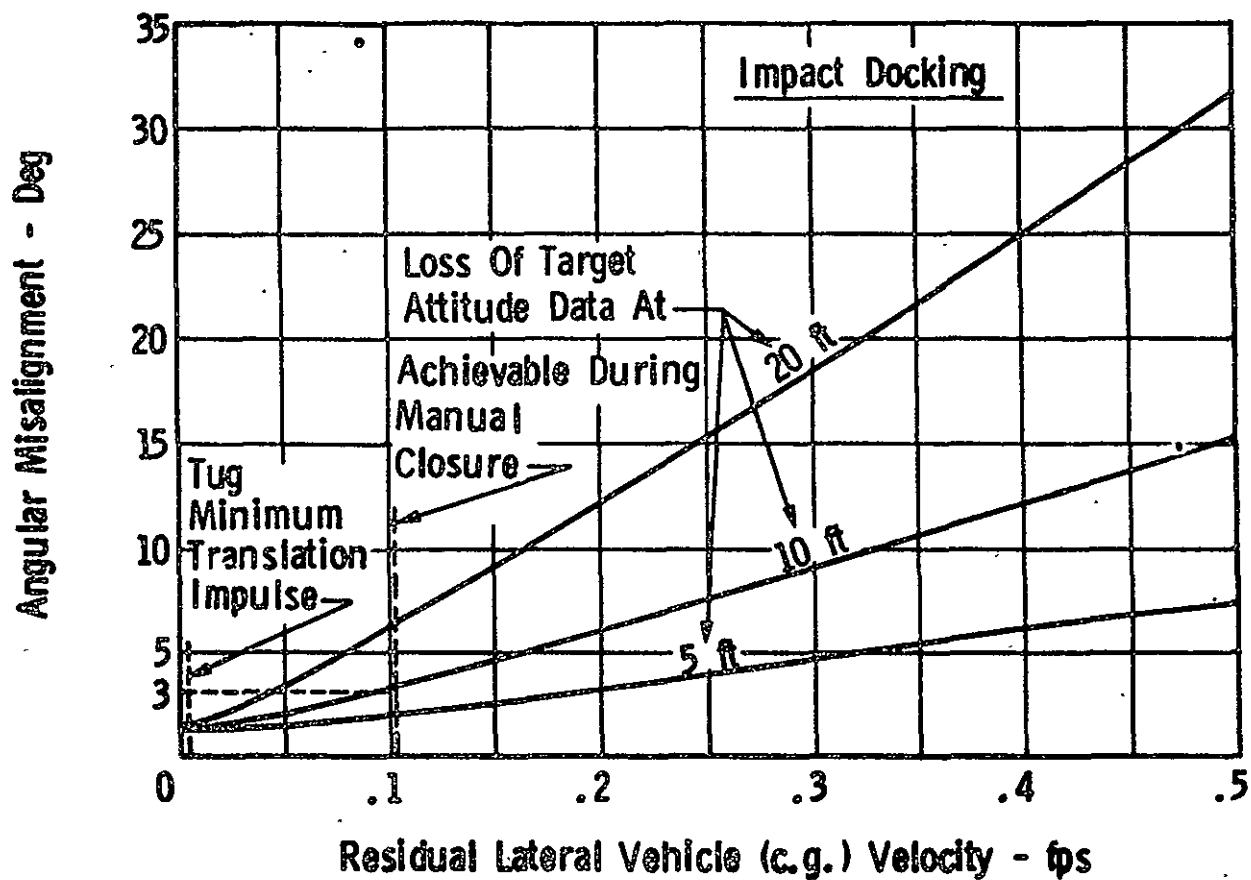
MANUAL IMPACT DOCKING

REQUIREMENT	SOURCE
i. and j. (cont'd)	<p>22 lumens per watt; the lamp power required is about 600 watts, when it is illuminated.</p> <p>The camera scans at 30 frames per sec, and the lamp need be illuminated only a minimum of 2 scan periods for each picture to be transmitted to the operator, a maximum of 1 picture each 3 seconds. The duty cycle of the 1 lamp can therefore be 0.022. Assuming the efficiency of the power supply circuitry to be 0.8, the input power to the overall lamp and its control will average $600 \times 0.022 / 0.8 = 16.5$ watts when the lamp is operating to illuminate the target.</p>

TABLE III-3 REQUIREMENTS-DOCKING MECHANISM.

MANUAL IMPACT DOCKING

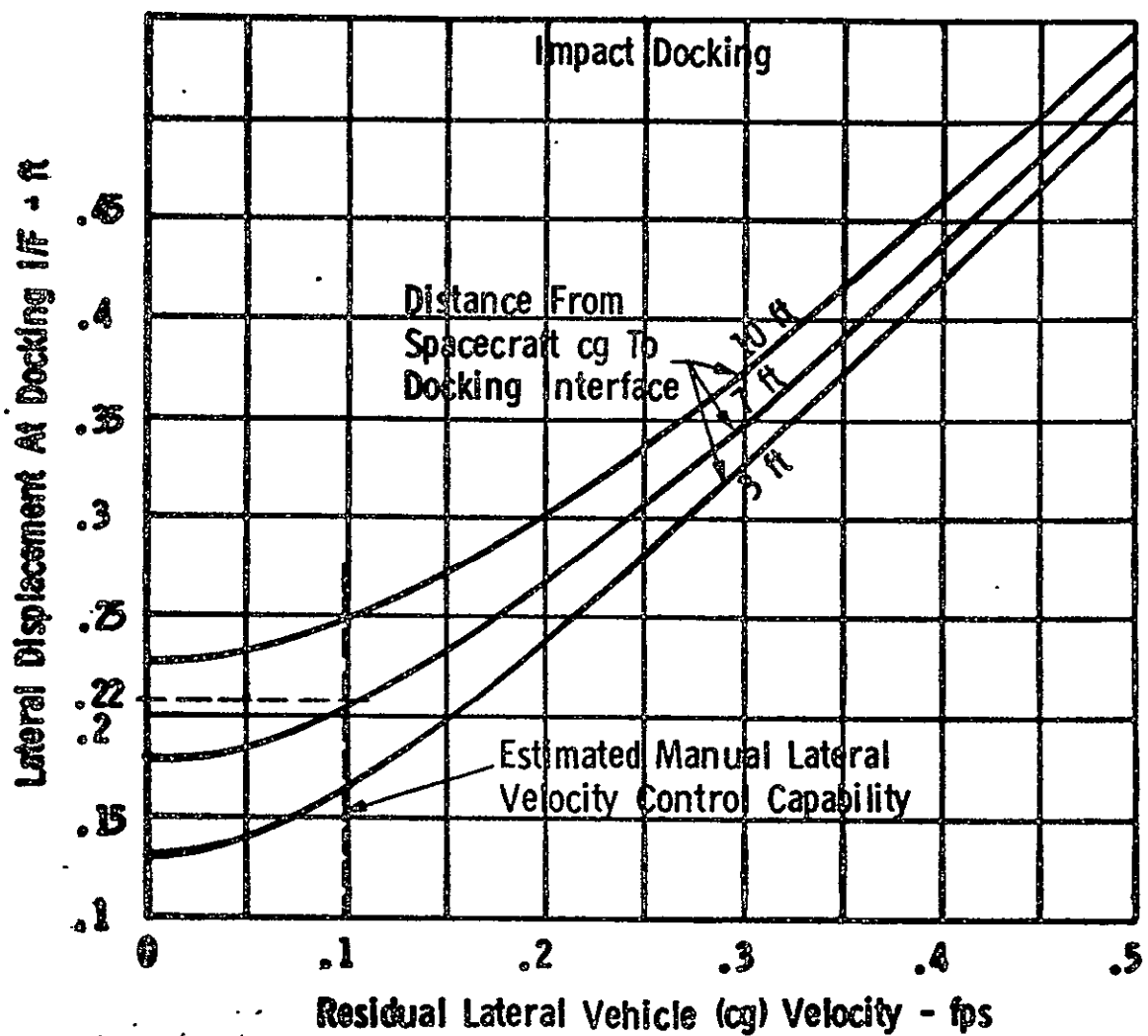
REQUIREMENT	SOURCE
a. Angular Misalignment = 3° Margin + $\frac{1.5^{\circ}}{4.5^{\circ}}$	Figure III-14 portrays angular misalignment vs residual lateral trim velocity error, assuming the uncertainties shown on the plot. In (b) on Table III-5, a trim requirement of .1 ft/sec is established. Based on that, 3 deg is the expected angular misalignment for loss of spacecraft attitude data at 10 ft.
b. Maximum Lateral Displacement = $\pm .21$ ft Margin $\times \frac{2}{\pm .42 \text{ ft} (\pm 5 \text{ in})}$	The value of .21 ft is obtained from Figure III-15, assuming a nominal spacecraft length of ≈ 15 ft (c.g. at 7 ft).
c. Lateral Velocity at Docking Interface = .11 fps Margin $\times \frac{2}{.22 \text{ fps}}$	The lateral velocity at the interface is the lateral vehicle residual velocity error plus deadband rate effects. From Figure III-16 the expected maximum is .11 fps for a lateral vehicle velocity of .1 fps (see (b) in Table III-5). This requirement is relatively insensitive to spacecraft length.
d. Contact Velocity = $1 \pm .1$ fps	This is merely the selected closing velocity plus the range rate uncertainty of the sensor and its axial velocity control loop. Requirement 1h specified the sensor error at $\pm .1$ fps. The control loop error is generally an order of magnitude less than that, so it will be neglected.
e. Roll Misalignment = $\pm 5^{\circ}$	This is a subjective requirement based entirely on man's ability to discern roll misalignment from a target vehicle cue. Five degrees is a reasonable starting value. Man-in-the-loop simulations will be required to verify this selection.



CONDITIONS

$\Delta\theta = .5^\circ$	LOS Uncertainty
$\Delta\phi = 1.0^\circ$	S/C Attitude Uncertainty
$\psi = .25^\circ$	Tug Deadband
$\epsilon = .5^\circ$	S/C Deadband
$l_{cg} = 18'$	Tug cg to I/F Distance
$l_{SC} = 7'$	S/C cg to I/F Distance
$l_{LL} = 1'$	Range at loss of LOS Data
$V_X = 1 \text{ fps}$	Axial Velocity

FIGURE III-14 ANGULAR MISALIGNMENT vs LATERAL VEHICLE VELOCITY



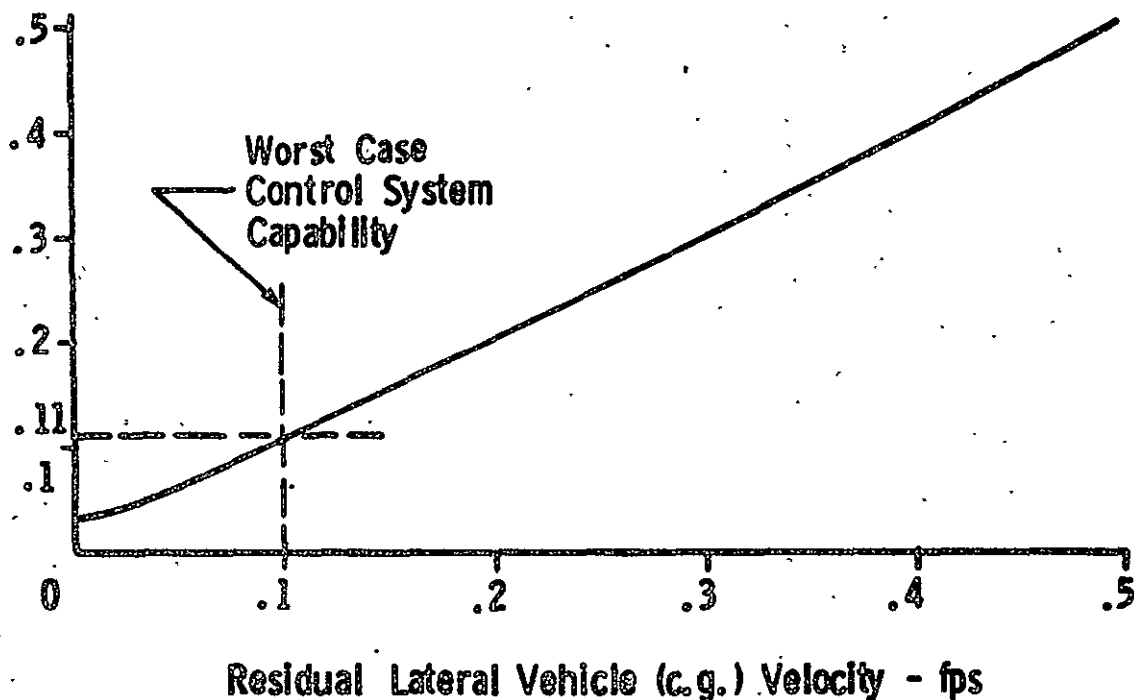
CONDITIONS

$\Delta\theta = .5^\circ$	LOS Uncertainty
$\Delta\phi = 1.0^\circ$	S/C Attitude Uncertainty
$\psi = .25^\circ$	Tug Deadband
$\epsilon = .5^\circ$	S/C Deadband
$l_{cg} = 18'$	Tug cg to I/F Distance
$l_{LL} = 1'$	Range at loss of LOS data
$V_X = 1 \text{ fps}$	Axial Velocity
$\tau = 5^\circ$	Angular Misalignment

FIGURE III-15 LATERAL DISPLACEMENT vs LATERAL VEHICLE VELOCITY

Lateral Velocity At Docking Interface - fps

Impact Docking



CONDITIONS

$\dot{\psi} = .1^{\circ}/\text{sec}$	Tug Deadband Rate
$\dot{\epsilon} = .1^{\circ}/\text{sec}$	S/C Deadband Rate
$l_{cg} = 18'$	Tug c.g.-to-I/F Distance
$l_{sc} = 7'$	S/C c.g.-to-I/F Distance

FIGURE III-16 LATERAL VELOCITY AT DOCKING INTERFACE VS LATERAL VEHICLE VELOCITY

TABLE III-4 REQUIREMENTS-TARGET CUES

MANUAL IMPACT DOCKING

REQUIREMENT	SOURCE
<p>a. A corner reflector is required on the docking axis for the cooperative ranging sensors (RF or laser radar).</p> <p>b. An array of reflectors may be required to ensure ranging data during the rendezvous for the cooperative sensors. The number and location is a function of the preflight knowledge of orbital trajectories. It may be possible to target the approach from the docking port side thereby requiring no more than (a) above. Further analysis is required.</p> <p>c. An offset "T" or similar visual cue is required on the spacecraft for all candidates.</p>	<p>Assumes the docking port attitude is known and the TV will provide sufficient visual data for commit-to-dock.</p>

TABLE III-5 REQUIREMENTS-CONTROL SYSTEM/MAN

MANUAL IMPACT DOCKING

REQUIREMENT	SOURCE
<p>a. Tug ACS Minimum Impulse Bit = 20 ms</p> <p>b. Lateral Translation Trim Capability = .1 fps</p>	<p>Existing Tug baseline. Results in a min. impulse translation of .012 in/sec/pulse with a 1000 slug tug, which is more than adequate, since manual velocity error discernment is at least an order of magnitude greater.</p> <p>For this candidate this is a subjective requirement difficult to demonstrate by analysis. It involves the ability of the man to determine the lateral velocity and position errors by observing a target on a TV, then correcting the errors within the time and picture availability constraints. The value of .1 fps was selected to avoid any unnecessarily tight requirements on mechanism design (as illustrated in Figures III-14, 15 and 16, provided for the three docking mechanism requirements) that result when any lateral velocities over .1 fps must be absorbed by the mechanism. .1 fps does not, at the moment, appear to be an unreasonably tight requirement. It will require demonstration via a man-in-the-loop simulation.</p>

TABLE III-6 REQUIREMENTS - RANGING SENSOR

MANUAL NON-IMPACT DOCKING

REQUIREMENT	SOURCE
Same as Table III-1 with the following exceptions.	
Minimum Range for Ranging - 1 ft.	In a non-impact docking, the vehicle must be accurately maintained in a stationkeeping condition while the STEM is deployed. The range for this operation is 3 - 5 feet, so one foot provides sufficient margin.
Range Accuracy For Near Range (1 ft to .5 n mi) - <u>+ 6 in.</u> - long term, <u>+ 1 in.</u> - short term	The overall accuracy of the range data must be sufficient to avoid the impact of the two vehicles during the 3 - 5 foot stationkeeping range. A .5 ft overall accuracy is sufficient for this. On a short term basis, the minute-to-minute accuracy must be considerably better to avoid damage to the STEM. Less than 1 or 2 in is desirable.

TABLE III-7 REQUIREMENTS-VIDEO/LIGHTING

MANUAL NON-IMPACT DOCKING

REQUIREMENT	SOURCE
Same as Table III-2	

TABLE III-8 REQUIREMENTS-DOCKING MECHANISM

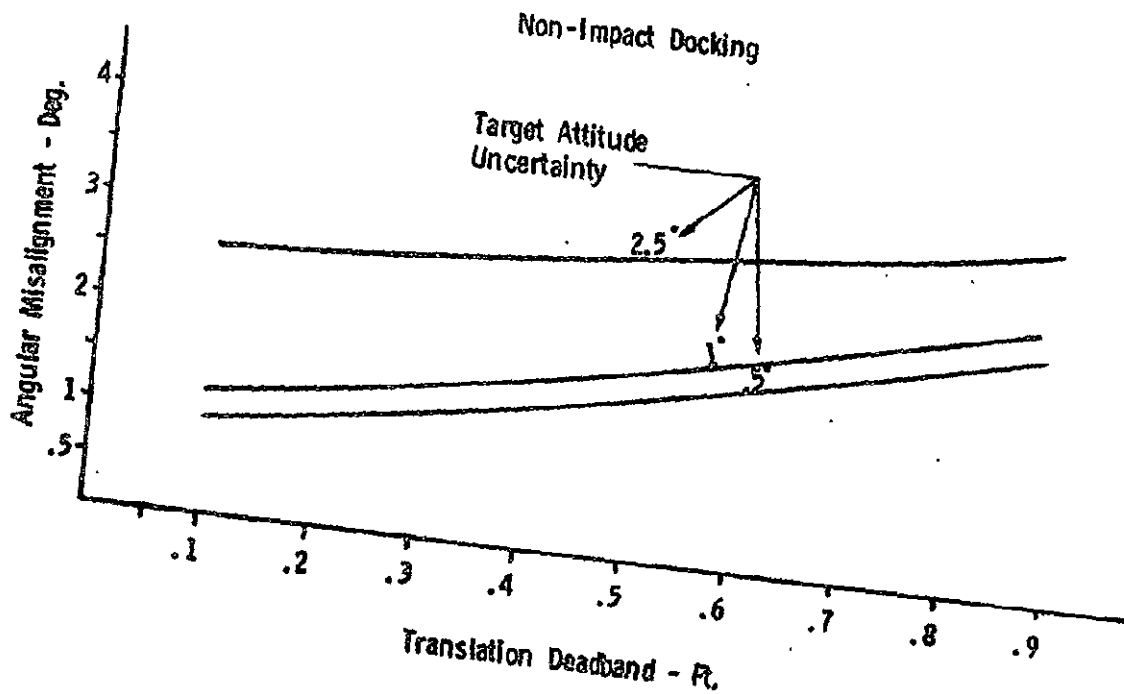
MANUAL NON-IMPACT SYSTEM

REQUIREMENT	SOURCE
<p>a. Angular Misalignment - (prior to STEM contact)</p> <p>SLR 2.6 deg Margin + $\frac{1.5}{4.1}$ deg</p> <p>RF 3.5 deg Margin + $\frac{1.5}{5.0}$ deg</p>	<p>The values of 2.6 deg and 3.5 deg are derived from the attached Figure III-17 where translation deadband, or lateral offset error, is .5 ft or less (SLR), and 1.0 ft (RF)[see (c) on Table III-5], and the target attitude error, which is chiefly a crew discernment problem, is less than 2.5 deg. Again, the latter will require simulation to verify.</p>
<p>b. Maximum Lateral Displacement at I/F (prior to STEM contact)</p> <p> = .2 Margin $\times \frac{2}{1.4 \text{ ft } (\pm 5 \text{ in})}$</p>	<p>This requirement sizes the STEM capture cone diameter. If the STEM were guided manually based on real time TV, this would be negligible. However, there are considerable delays in TV response which will make STEM alignment success subject to vehicle rates and residual lateral velocities from picture to picture. Based on maximum vehicle rate of .1 deg/sec and maximum residual velocity of .002 fps, (see (e) on Table III-10), the maximum lateral displacement is .2 ft if TV response is one picture every 16 seconds (see Figure III-18).</p>
<p>c. Lateral Velocity at Interface</p> <p> N/A</p>	<p>For a non-impact STEM approach, this spec is replaced by 3g, the maximum STEM rate required. With the STEM approach, lateral velocity at docking is essentially reduced to zero.</p>
<p>d. Maximum Contact Velocity</p> <p> .0082 ft/sec Margin $\times \frac{2}{.016 \text{ ft/sec}}$</p>	<p>Contact velocity is derived from the time for reel-in, which should be less than 10 minutes. For a 5 ft arm, $V = 5/600 \text{ sec} = .008 \text{ ft/sec}$ assuming velocity is held relatively constant throughout by continuing to pulse the reel-in motor to overcome friction and avoid compressive loads on the arm.</p>
<p>e. Roll Misalignment = ± 5 deg</p>	<p>Same as (e) on Table III-3.</p>

TABLE III-8 REQUIREMENTS-DOCKING MECHANISM (Continued)

MANUAL NON-IMPACT DOCKING

REQUIREMENT	SOURCE												
f. Angular Misalignment at Contact = 2.6° Margin + $\frac{1.5}{4.1^{\circ}}$	At STEM contact the Tug will go to an attitude hold mode, essentially freezing the misalignments of (a). Consequently, the angular misalignment at vehicle contact should be no greater than at STEM contact.												
g. Maximum Lateral Displacement at I/F at Vehicle Contact = .5 in Margin $\times \frac{2}{1.0 \text{ in}}$	The non-impact STEM approach is specifically implemented to reduce this error to essentially zero, or at least within the manufacturing and assembly hardware misalignments between the two vehicles. This should be less than .5 in.												
h. STEM Maximum Angle <table><tr><td></td><td>SLR</td><td>RF</td></tr><tr><td></td><td>$\pm 6^{\circ}$</td><td>$\pm 12^{\circ}$</td></tr><tr><td>Margin</td><td>$\pm 4^{\circ}$</td><td>$\pm 8^{\circ}$</td></tr><tr><td></td><td>$\pm 10^{\circ}$</td><td>$\pm 20^{\circ}$</td></tr></table>		SLR	RF		$\pm 6^{\circ}$	$\pm 12^{\circ}$	Margin	$\pm 4^{\circ}$	$\pm 8^{\circ}$		$\pm 10^{\circ}$	$\pm 20^{\circ}$	Twelve degrees is selected based on the attached curve (Figure III-19), where the worst case translation limit cycle is 1.0 ft (RF)(see requirement (d) on Table III-10), and the maximum stationkeeping distance is 5 ft.
	SLR	RF											
	$\pm 6^{\circ}$	$\pm 12^{\circ}$											
Margin	$\pm 4^{\circ}$	$\pm 8^{\circ}$											
	$\pm 10^{\circ}$	$\pm 20^{\circ}$											
i. STEM Maximum Rate = $2.3^{\circ}/\text{sec}$ Margin $\times \frac{2}{4.6^{\circ}/\text{sec}}$	This is based on the attached curve, Figure III-20, where the maximum vehicle lateral velocity (deadband rate) is .02 ft/sec (see (e) on Table III-10), and the stationkeeping distance is 3 ft (see (i) on Table III-3).												
j. Maximum STEM Extension = 5 ft	Distances beyond 5 ft are not practical for servicing considerations, nor for STEM boom structural strength design, yet the greatest possible distances are desirable from STEM rate and angle design characteristics, ground control response requirements, safety, etc.												
k. STEM Extension Rate = $.5''/\text{sec}$	Operational considerations would like the probe extended in 2 minutes.												
l. STEM Retract Rate = $.1''/\text{sec}$ maximum	Ground and operational considerations allow 10 minutes for retraction.												



CONDITIONS

$\Delta \theta = .5^\circ$

$\psi = .25^\circ$

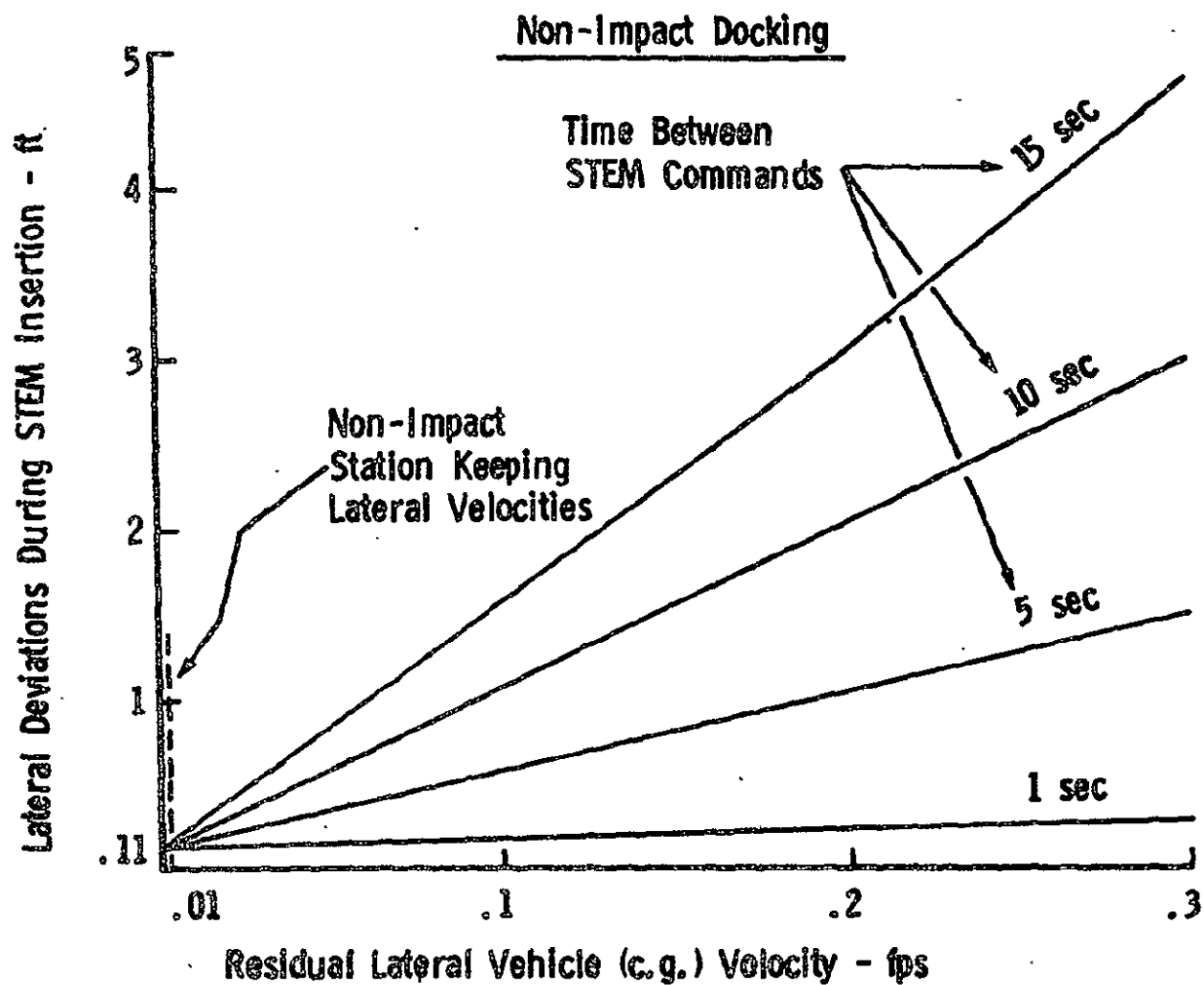
$\epsilon = .5^\circ$

LOS Uncertainty

Tug Deadband

S/C Deadband

FIGURE III-17 ANGULAR MISALIGNMENT VS TRANSLATION DEADBAND

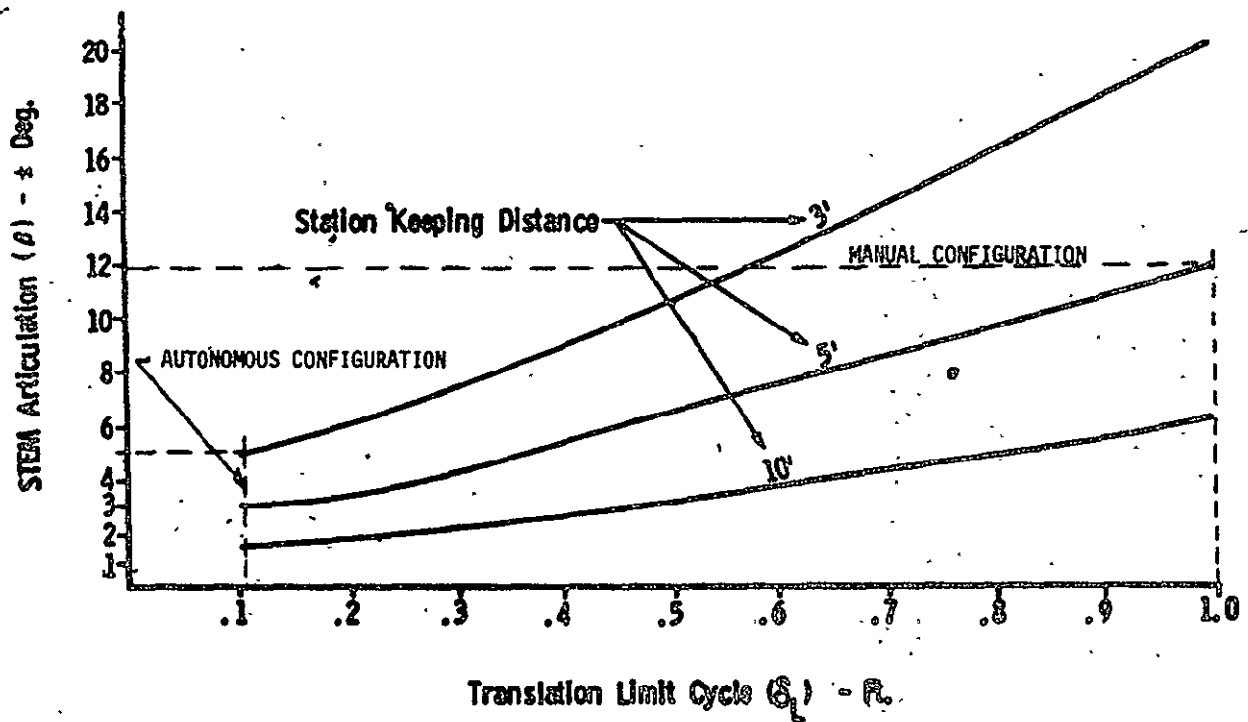


CONDITIONS

$\psi = .25^\circ$	Tug Deadband
$\epsilon = .5^\circ$	S/C Deadband
$l_{cg} = 18'$	Tug c.g.-to-I/F Distance
$l_{sc} = 7'$	S/C c.g.-to-I/F Distance
$l_{sk} = 5'$	Station Keeping Distance

FIGURE III-18 STEM LATERAL DISPLACEMENTS AT INSERTION

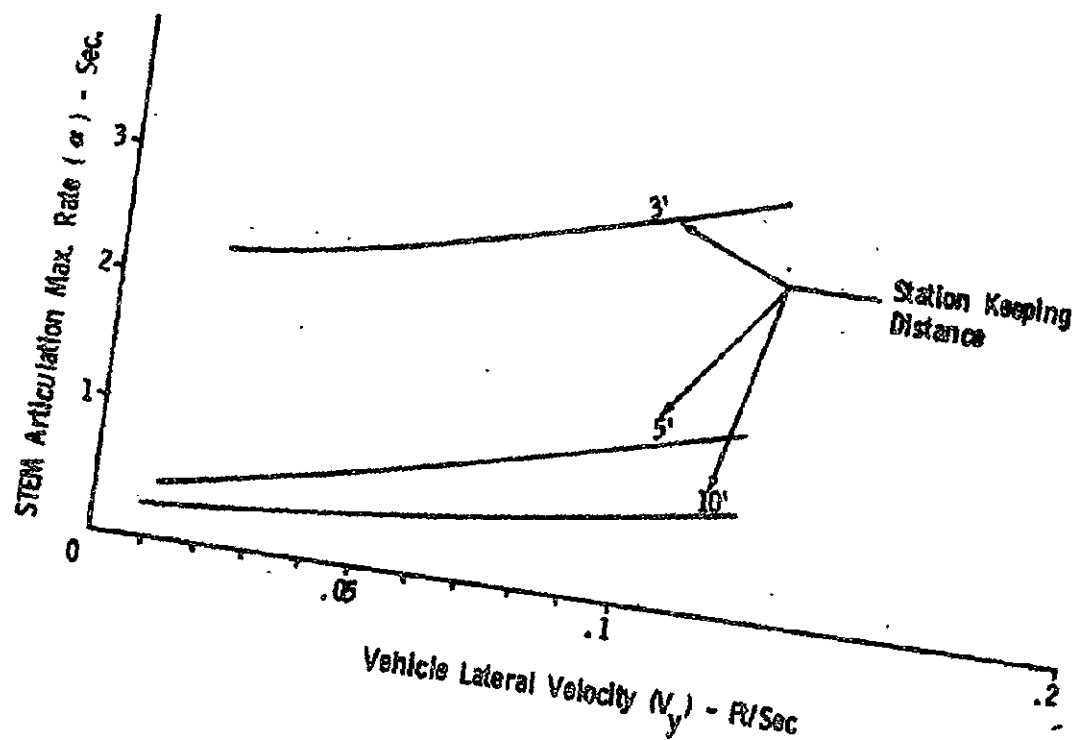
Non-Impact Docking



CONDITIONS

$\Delta \theta = .5^\circ$	LOS Uncertainty
$\Delta \phi = 1.0^\circ$	S/C Attitude Uncertainty
$\psi = .25^\circ$	Tug Deadband
$\epsilon = .5^\circ$	S/C Deadband
$l_{cg} = 18'$	Tug c.g.-to-I/F Distance
$l_{sc} = 7'$	S/C c.g.-to-I/F Distance
$l_{sk} = 5'$	Stationkeeping Distance

FIGURE III-19 STEM ARTICULATION ANGLE VS TRANSLATION LIMIT CYCLE



CONDITIONS

$\dot{\psi} = .1^\circ/\text{sec}$	Tug Deadband Rate
$\dot{\epsilon} = .1^\circ/\text{sec}$	S/C Deadband Rate
$l_{cg} = 18'$	Tug c.g.-to-I/F Distance
$l_{sc} = 7'$	S/C c.g.-to-I/F Distance
$l_{sk} = 5'$	Stationkeeping Distance

FIGURE III-20 STEM ARTICULATION RATE VS LATERAL VEHICLE VELOCITY

TABLE III-9 REQUIREMENTS-SPACECRAFT CUES

MANUAL NON-IMPACT DOCKING

REQUIREMENT	SOURCE
Same as M1 (see Attachment B)	

TABLE III-10 REQUIREMENTS-CONTROL SYSTEM/MAN

MANUAL NON-IMPACT DOCKING

REQUIREMENT	SOURCE
Same as Table III-5 except for addition of the following:	
<p>c. Axial Translation Minimum Trim Capability = .012 in/sec Margin x $\frac{2}{.024 \text{ in/sec}}$</p>	<p>The non-impact docking requires very refined axial translation control. Since the closing rates have been reduced to near zero at the time of STEM extension, the ground controller should be able to detect very small motions in relative errors from picture-to-picture (plus recognition of a change of ≈ 1 in. from ranging sensor data), all of which should allow the stationkeeping rate to be maintained with a single minimum impulse of two axial jets. That capability for a mass of 1000 slugs and a total ACS thrust of 50 lbs is:</p> $V_X = \frac{\text{Impulse}}{\text{Mass}} = \frac{50 \text{ lbs} \times .02 \text{ sec}}{1000}$ $= .001 \text{ ft/sec}^2$ <p>or .012 in./sec.</p> <p>NOTE: Even if TV pictures are 16 sec apart, the motion from picture-to-picture could be as small as .2 in.!</p>
<p>d. Lateral Translation Deadband Capability - Manual - SLR - .5 ft RF - 1.0 ft</p>	<p>This is a man-in-the-loop capability, depending considerably on the man, the cue, the lighting, TV delays, etc; all of them subjective. Simulations will be required to validate the capability. The value selected is relatively large and should encompass a reasonably worst-case situation.</p> <p>Note that an error in reading target attitude error of 1 deg results in a lateral misalignment of only one inch or .08 ft at a stationkeeping distance of 5 ft. Even 5 deg error is less than .5 ft (.43 ft). The RF deadband is twice that of the SLR because of the decreased accuracy in LOS measurement, which affects the deadband size.</p>

TABLE III-10 REQUIREMENTS-CONTROL SYSTEM/MAN (Cont'd)

MANUAL NON-IMPACT DOCKING

REQUIREMENT	SOURCE
e. Minimum lateral translation deadband rate capability - Manual = .012 in./sec Margin x $\frac{2}{}$.024 in./sec (.002 ft/sec)	See c.

TABLE III-11 REQUIREMENTS-RANGING SENSOR

AUTONOMOUS IMPACT DOCKING

REQUIREMENT	SOURCE										
<p>a.1) Autonomous Attitude Determination Capability, Maximum Range = 200 ft Margin + <u>100</u> ft 300 ft</p>	Maximum inspection range of 200 ft is anticipated accounting for smallest TV FOV of 10 deg and largest spacecraft diameter of 35 ft. Attitude determination prior to inspection stationkeeping is not required.										
<p>a.2) Attitude Determination Minimum Range Capability = 10 ft</p>	For impact docking the docking mechanism angular misalignment is affected, more than any other mechanism parameter, by the range at which attitude data is lost. Figure III-21 shows that for residual lateral vehicle velocities of less than .01 ft/sec (see (b) in Table III-15), the angular misalignment is not much different if the range at which data is lost is 5 ft or 10 ft - 1.3 deg vs .4 deg; therefore a minimum range of 10 ft will be used. Docking mechanism angular misalignment capabilities less than 5 deg have little effect on mechanism weight, complexity, or cost.										
<p>a.3) Attitude Determination Accuracy - <u>± 1</u> deg</p>	Figure III-22 shows the sensitivity of angular misalignment to target attitude uncertainty for different ranges at which attitude data are lost and two different values of residual vehicle velocity. It shows little sensitivity to target attitude uncertainty over the range of .1 deg to 1 deg. Beyond 1 deg and as it approaches the angular misalignment itself (≈ 2 deg) it becomes a dominant error source. One degree was chosen as it avoids this dominant range yet minimizes unnecessarily complex sensor and target cue designs. This number does, of course, include the target cue orientation and alignment accuracy as well as the sensor alignment and internal accuracy. An approximate allocation is provided, based on realistic achievable numbers.										
<p><u>Preliminary Allocation:</u></p> <table> <tr> <td>Cue Alignment/Orientation (w/r to s/c axes)</td><td>$\pm 0.5^\circ$</td></tr> <tr> <td>Sensor Alignment on Tug</td><td>$\pm 0.5^\circ$</td></tr> <tr> <td>Sensor Accuracy (bias Threshold, Quantitization, Beam Width, etc.)</td><td>$\pm 0.75^\circ$</td></tr> <tr> <td>Computation Error</td><td>$\pm 0.05^\circ$</td></tr> <tr> <td>RSS</td><td><u>1.03°</u></td></tr> </table>	Cue Alignment/Orientation (w/r to s/c axes)	$\pm 0.5^\circ$	Sensor Alignment on Tug	$\pm 0.5^\circ$	Sensor Accuracy (bias Threshold, Quantitization, Beam Width, etc.)	$\pm 0.75^\circ$	Computation Error	$\pm 0.05^\circ$	RSS	<u>1.03°</u>	
Cue Alignment/Orientation (w/r to s/c axes)	$\pm 0.5^\circ$										
Sensor Alignment on Tug	$\pm 0.5^\circ$										
Sensor Accuracy (bias Threshold, Quantitization, Beam Width, etc.)	$\pm 0.75^\circ$										
Computation Error	$\pm 0.05^\circ$										
RSS	<u>1.03°</u>										

TABLE III-11 REQUIREMENTS-RANGING SENSOR (Continued)

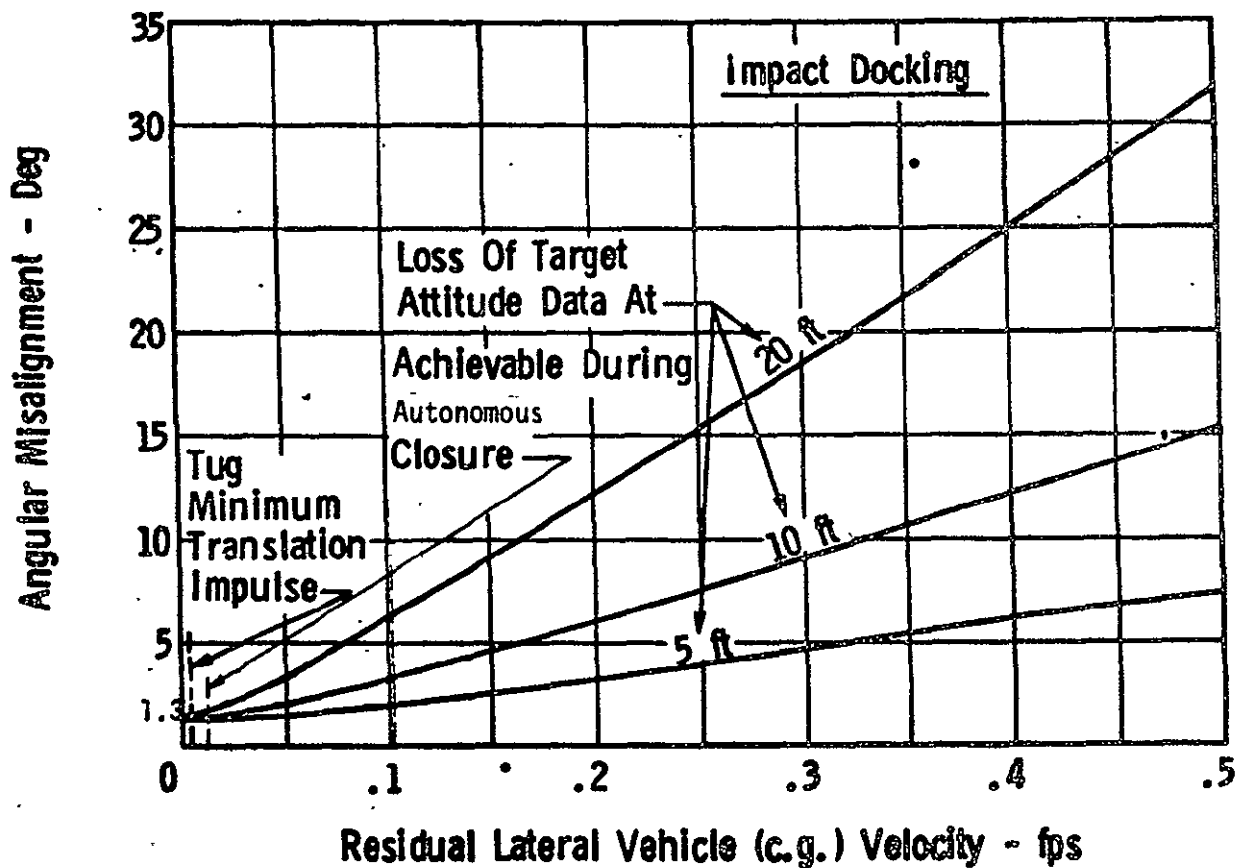
AUTONOMOUS IMPACT DOCKING

REQUIREMENT	SOURCE
b) Maximum Ranging Range (Acquisition) = 12.5 n mi Margin $\times \frac{2}{25.0 \text{ n mi}}$	Trajectory error analysis has shown that with the baseline Tug insertion uncertainty of ± 3 n mi and spacecraft knowledge uncertainty of ± 1 n mi, a terminal phase rendezvous can be accomplished from 12.5 n mi with only negligible increases in ACS propellant over longer ranges. Therefore, in the interest of conserving time and the power/weight impact of longer range sensors, the minimum reasonable range (12.5 n mi) is selected.
c) Minimum Ranging Range = 10 ft	Range data beyond the point where target attitude is determined for the lost time is not required for a non-impact system. See a.2) above.
d) Range Accuracy - .5 n mi to 25 n mi - ± 100 ft 10 ft to .5 n mi - ± 1 ft	Consistent with accuracy of rendezvous algorithm correction capability. For non-impact docking, range is not a critical parameter once the closing velocity is established at 100 ft. It is not the primary parameters on which target attitude is computed. Ten percent of the minimum ranging range of 10 ft seems a reasonable and achievable value.
e) Range Accuracy - .5 n mi to 25 n mi - \pm TBD 10 ft to .5 n mi - $\pm .1$ fps	Rendezvous algorithm requirement. Range rate accuracy determines the tolerance on the axial velocity to be expected at docking. Figure III-13 shows the sensitivity of angular misalignment to axial velocity. It can be seen that for low lateral velocities ($< .05$ ft/sec for the autonomous case) it has little effect anywhere between .75 and 1.25 fps. Since little will occur to perturb the closing velocity when the last corrections are made at the 10 ft minimum range point, a range rate tolerance of $\pm .1$ fps provides more than sufficient margin.
f) Field-of-View = $\pm 15^\circ$	FOV must be adequate to: (1) find the target in FOV at acquisition, (2) track during worst vehicle perturbations, and (3) determine

TABLE III-11 REQUIREMENTS-RANGING SENSOR (Continued)

AUTONOMOUS IMPACT DOCKING

REQUIREMENT	SOURCE
f) Field-of-View (Concluded)	<p>target attitude from a pattern of given diameter up to a specified minimum range. Current values for 3 n mi for Tug position error and 1 n mi of spacecraft position result in worst angular LOS error at the minimum acquisition range (12.5 n mi) of $\sin^{-1} \frac{\sqrt{(3^2 + 1^2)}}{12.5} = 15^\circ$.</p> <p>For a 30 deg FOV and a minimum range of attitude determination of 10 ft (a.2), the maximum target diameter is $2 \times 10 \text{ ft} \sin 15 \text{ deg} = 5.1 \text{ ft}$; more than adequate for a target pattern size.</p>
g) LOS Accuracy - $\pm 1.0^\circ$	<p>Target attitude determination utilizes LOS data, therefore should be compatible with requirement (a.3). The target attitude computation involves more cues and more measurements, but the computation error is small. Meanwhile, the LOS data must be available at a closer range - $\approx 1 \text{ ft}$, making the cue's location accuracy at least as critical an item as alignment of the four cues for target attitude determination was at a 10-ft range for requirement (a.3). The same breakdown of errors as was proposed in (a.3) above, is assumed here.</p>
<u>Preliminary Allocation</u> Cue Location Error = $\pm .5^\circ$ (1 in at 1 ft) Sensor Alignment on Tug = $\pm .5^\circ$ Sensor Accuracy (Bias, Threshold, Quantization, etc.) = $\pm .75^\circ$ Computation Error = <u>neg.</u> RSS $\pm 1.0^\circ$	
h) Loss of LOS Data = 1 ft	<p>Figure III-23 illustrates the sensitivity of lateral displacement (which is affected the most by this parameter) to loss of LOS data. One foot is necessary to minimize the effect of this error source, yet is an achievable number.</p>

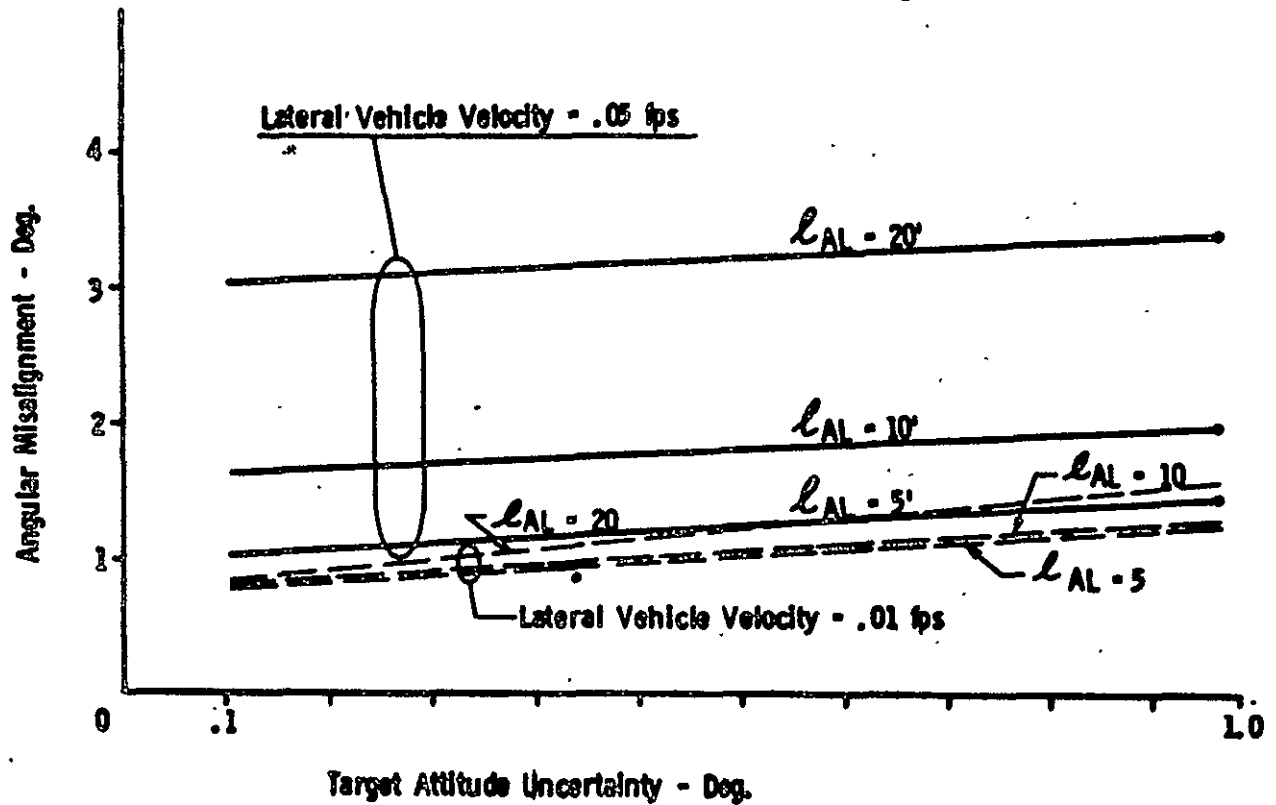


CONDITIONS

$\Delta \theta = .5^\circ$	LOS Uncertainty
$\Delta \phi = 1.0^\circ$	S/C Attitude Uncertainty
$\psi = .25^\circ$	Tug Deadband
$\epsilon = .5^\circ$	S/C Deadband
$l_{cg} = 18'$	Tug c.g.-to-I/F Distance
$l_{sc} = 7'$	S/C c.g.-to-I/F Distance
$l_{LL} = 1'$	Range at loss of LOS data
$V_x = 1 \text{ fps}$	Axial Velocity

FIGURE III-21 ANGULAR MISALIGNMENT VS LATERAL VEHICLE VELOCITY

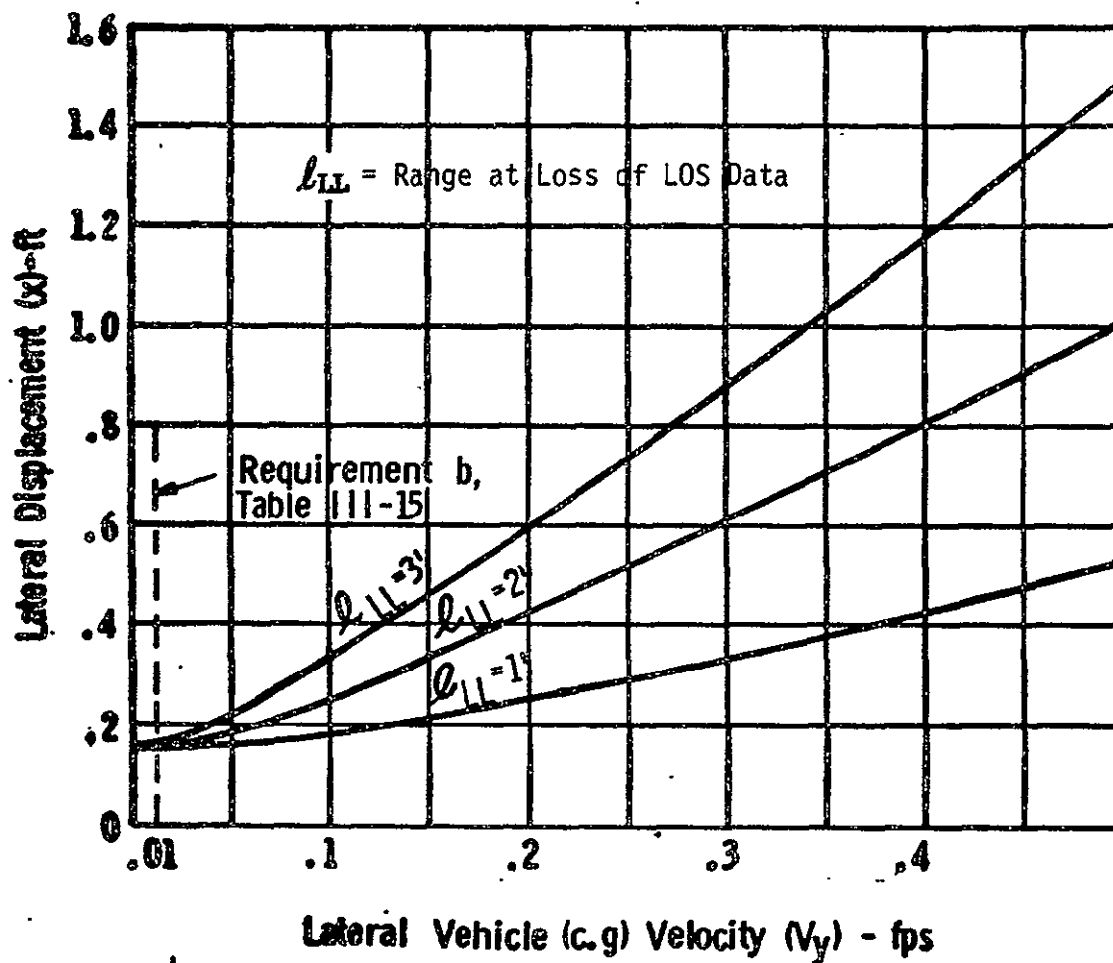
l_{AL} = Range At Which
Target Attitude
Information Is Lost



CONDITIONS

$\Delta \theta = .5^\circ$	LOS Uncertainty
$\Psi = .25^\circ$	Tug Deadband
$\epsilon = .5^\circ$	S/C Deadband
$l_{cg} = 18'$	Tug c.g.-to-I/F Distance
$l_{sc} = 7'$	S/C c.g.-to-I/F Distance
$l_{LL} = 1'$	Range at loss of LOS data
$V_x = 1 \text{ fps}$	Axial Velocity

FIGURE III-22 ANGULAR MISALIGNMENT VS TARGET ATTITUDE UNCERTAINTY



CONDITIONS

$\Delta \theta = .5^\circ$	LOS Uncertainty
$\Delta \phi = 1.0^\circ$	S/C Attitude Uncertainty
$\psi = .25^\circ$	Tug Deadband
$\epsilon = .5^\circ$	S/C Deadband
$l_{cg} = 18'$	Tug c.g-to-I/F Distance
$l_{sc} = 7'$	S/C c.g-to-I/F Distance
$V_x = 1$ fps	Axial Velocity
$l_{AL} = 10'$	Range at loss of Attitude Data

FIGURE III-23 LATERAL DISPLACEMENT VS LATERAL VEHICLE VELOCITY

TABLE III-12 REQUIREMENTS-VIDEO/LIGHTING

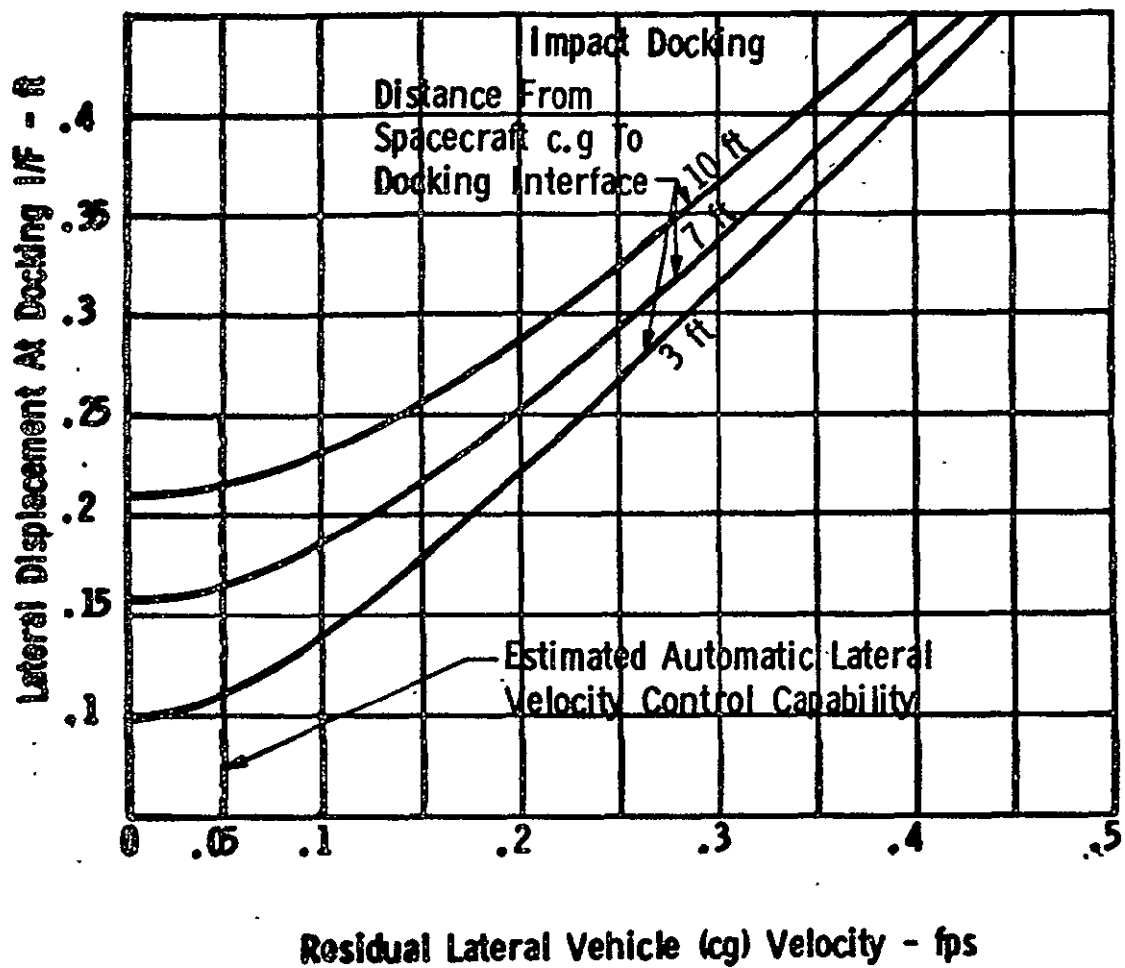
AUTONOMOUS IMPACT DOCKING

REQUIREMENT	SOURCE
<p>The TV is not a critical element in the autonomous candidates, if present at all. Its requirements are quite flexible with many off-the-shelf designs feasibly accommodating the anticipated requirements.</p>	

TABLE III-13 REQUIREMENTS-DOCKING MECHANISM

AUTONOMOUS IMPACT DOCKING

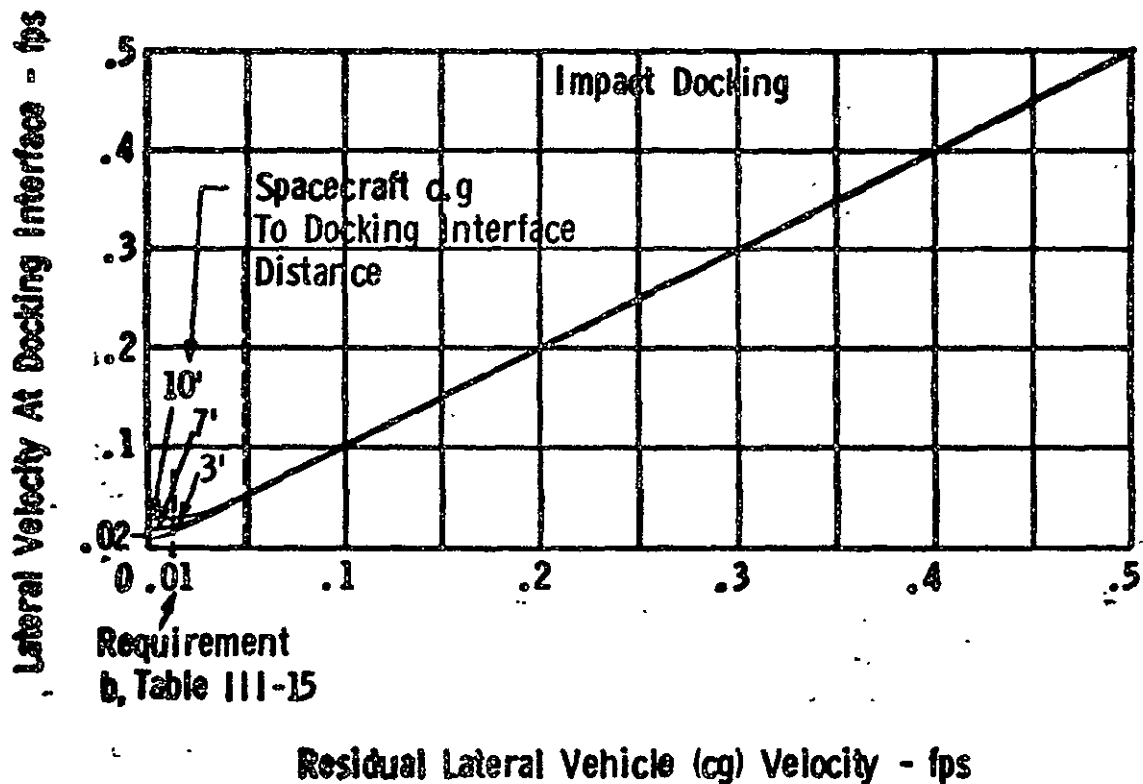
REQUIREMENTS	SOURCE
a) Angular Misalignment = $\pm 1.4^\circ$ Margin $\times \frac{2}{\pm 2.8^\circ}$	Figure III-21 earlier showed the relationship between lateral vehicle velocity and angular misalignment. From (b) in Table III-15, the lateral velocity it is anticipated an autonomous system can achieve is less than .01 fps. That results in a maximum angular misalignment of 1.4 deg for a loss of spacecraft attitude data at 10 ft, assuming an axial velocity of 1 fps and a target attitude uncertainty of 1 degree.
b) Maximum Lateral Displacement = $\pm .16$ Margin $\times \frac{2}{\pm .32(\pm 4.0 \text{ in})}$	A value of $\pm .16$ feet (or ± 2 inches) was selected based on the curve of Figure III-24, a nominal spacecraft length of 15 feet (c.g. at 7 ft), and an achievable maximum lateral velocity residual of .01 fps (see (b) in Table III-15).
c) Lateral Velocity at Docking Interface = .02 Margin $\times \frac{5}{.1 \text{ fps}}$	The value of .02 fps is selected from Figure III-25. The lateral velocity at the docking interface is approximately the vehicle c.g. lateral velocity; which, from requirement (b) in Table III-15 is less than .01 fps for very low velocities where the deadband rates (maximum of .1 deg/sec) become limiting conditions.
d) Contact Velocity = $1 \pm .1 \text{ fps}$	Requirement (g) in Table III-11 specified the range rate accuracy of the ranging sensor at $\pm .1 \text{ fps}$. This essentially establishes the contact velocity tolerance. The control system errors are negligible in an autonomous configuration. The value of 1 fps was selected from the data of Figure III-13 to minimize its effect on angular misalignment.
e) Roll Misalignment = $\pm 5^\circ$	This requirement is limited by the ability of the sensor to determine target attitude. The value of 5 deg is a somewhat arbitrary value selected on the basis of the known capability of most sensors to derive target attitude autonomously and the feasible roll misalignment a mechanism can accommodate.



CONDITIONS

$\Delta \theta = .5^\circ$	LOS Uncertainty
$\Delta \phi = 1.0^\circ$	S/C Attitude Uncertainty
$\psi = .25^\circ$	Tug Deadband
$\epsilon = .5^\circ$	S/C Deadband
$l_{cg} = 18'$	Tug c.g.-to-I/F Distance
$\gamma = 1^\circ$	Angular Misalignment
$l_{LL} = 1'$	Range at loss of LOS data
$V_x = 1 \text{ fps}$	Axial Velocity

FIGURE III-24 LATERAL DISPLACEMENT VS LATERAL VEHICLE VELOCITY



CONDITIONS

$\dot{\psi} = .02^\circ/\text{sec}$ Tug Deadband Rate
 $\dot{\epsilon} = .1^\circ/\text{sec}$ S/C Deadband Rate
 $l_{cg} = 18'$ Tug c.g.-to-I/F Distance

FIGURE III-25 LATERAL VELOCITY AT DOCKING INTERFACE VS LATERAL VEHICLE VELOCITY

TABLE III-14 REQUIREMENTS-SPACECRAFT CUES

AUTONOMOUS IMPACT DOCKING

REQUIREMENT	SOURCE
a) An array of reflectors will be required on the docking axis for attitude determination. The maximum diameter of the array can be 5 feet.	The attitude determination reflector array diameter is based on a sensor FOV of 30 deg [requirement (h) in Table III-11], and a minimum range of 10 ft for attitude determination (requirement (c) in the same Table).
b) The relative alignment/orientation of the reflectors in a) shall all be within .5 deg of each other and the spacecraft axes.	See requirement (d) in Table III-11.
c) A 4π steradian coverage of reflectors shall be provided for the cooperative sensors for signal reflection during rendezvous (as a maximum).	If trajectory conditions are such that a predictable predetermined approach path can be established for a spacecraft, of group of spacecraft, the reflectors may be limited to that side only.

TABLE III-15 REQUIREMENT-CONTROL SYSTEM/MAN

AUTONOMOUS IMPACT DOCKING

REQUIREMENT	SOURCE
a) Tug ACS Minimum Impulse Bit -20 ms	<p>This is current Tug baseline design. It results in a minimum impulse translation rate of .012 in./sec for a 1000 slug mass</p> $\left(\frac{25 \text{ lb} \times 2 \times .02 \text{ sec}}{1,000} \right)$ <p>. This is more than adequate when considering the insensitivity of most docking mechanism parameters to lateral translation rates of less than .05 ft/sec. .05 ft/sec is .6 in/sec or 50 times the minimum capability of .012"/sec</p>
b) Lateral translation trim capability = .012 in./sec Margin x 10 .12 in./sec (.01 ft/sec)	<p>For totally quiescent vehicle states with no major attitude corrections and a reasonably accurate noise-free close-in stationkeeping sensor (attitude and translation) the vehicle could theoretically achieve a translation deadband limit cycle rate approaching the minimum impulse bit capability of .012 in./sec. Considering all the above assumptions, a margin of a factor of 10 is not too conservative and yet quite adequate.</p>

TABLE III-16 REQUIREMENTS-RANGING SENSOR

AUTONOMOUS NON-IMPACT DOCKING

REQUIREMENT	SOURCE
Requirements are the same as the impact docking, Table III-11, except for the following:	
a.2) Attitude Determination Minimum Range Capability = 3 ft	This is the minimum range at which the STEM target retrieval activity will be conducted. Vehicle range and coalignment, utilizing target attitude in the computations, must be maintained during this phase.
c) Minimum Ranging Range = 3 ft	See (a.2) above.
d) Range Accuracy - Same as Impact Plus the following: 3 ft to 10 ft = $\pm .5$ ft (day-to-day) $\pm .1$ ft (short term)	A relatively stringent range accuracy is required during STEM activity so that a tight Tug deadband for the s/c range control loop can be implemented, thereby minimizing the transients and perturbations on the STEM loop. .1 ft accuracy should permit a control loop accuracy of $\pm .2$ ft, or 2.5 inches, which should be below the threshold of range control of the STEM.
e) Range Accuracy - Same as Impact Docking Plus the following: 3 ft to 10 ft = .01 fps (either from a sensor or derived from range data)	For non-impact docking the stationkeeping stability and accuracy is of concern more than tolerance on impact velocity. The requirement is obviously a much more stringent one since range rate must be driven to virtually zero and, at that point, still a key parameter in the stationkeeping control laws.

TABLE III-17 REQUIREMENTS-DOCKING MECHANISM

AUTONOMOUS NON-IMPACT DOCKING

REQUIREMENT	SOURCE
The docking mechanism requirements are the same as for the impact docking, Table III-12, in certain cases. Those that are different are shown below:	
a) Angular Misalignment = $\pm 1.2^\circ$ Margin $\times 2$ $\pm 2.4^\circ$	Angular Misalignment in the non-impact case is determined more by the magnitude of the translation deadband than it is by lateral velocity. LOS and attitude data are never really lost. Figure III-17 shows the relationship between the translation deadband and angular misalignment for several accuracies of target attitude knowledge. Autonomous deadbands of .005 feet are achievable but from (c) in Table III-20, a value of .1 ft is a more realistic maximum for now. This results in 1.2 deg angular misalignment for target attitude data uncertainty of ~ 1 degree.
b) Maximum Lateral Displacement at STEM Insertion - $\pm .1$ ft Margin $\times 2$ $\pm .2$ ft (± 2.5 in)	This requirement sizes the STEM drogue diameter and is principally a function of sampling, or command update, interval of the STEM control loop. In Figure III-18 the sensitivity to this interval is shown for several values -- 1 sec through 15 sec -- where 15 sec relates to a manual ground controlled STEM. In an autonomous mode the automatic control loop will be cycled considerably faster than once each second. It can be seen the lateral displacement is negligible -- less than .1 of a foot.
c) Lateral Velocity at Docking Interface -- Negligible	The lateral velocity is inherently very small for this type of non-impact docking; certainly well below the threshold of impacting mechanism structural characteristics.
d) Contact Velocity - .008 ft/sec Margin $\times 2$.016 ft/sec	Contact velocity is derived primarily from the maximum STEM retract rate which is 5 ft (maximum)/10 min or .008 ft/sec.
e) Roll Misalignment = $\pm 5^\circ$	See requirement (e) in Table III-3.

TABLE III-17 REQUIREMENTS-DOCKING MECHANISM (Continued)

AUTONOMOUS NON-IMPACT DOCKING

REQUIREMENT	SOURCE
f) Angular Misalignment at Contact = 1.2° Margin $\times \frac{2}{2.4^{\circ}}$	At STEM contact the Tug will go to an attitude hold mode, essentially freezing the misalignments of requirement (a) on Table III-16. Consequently, the angular misalignment at vehicle contact should be no greater than at STEM contact.
g) Maximum Lateral Displacement at I/F upon Vehicle Contact = .5 in Margin $\times \frac{2}{1.0 \text{ in}}$	The non-impact STEM approach is specifically implemented to reduce this error to essentially zero, or at least within the manufacturing and assembly hardware misalignments between the two vehicles. This should be less than .5 in.
h) STEM Maximum Angle = $\pm 5^{\circ}$ Margin $\times \frac{2}{\pm 10^{\circ}}$	STEM angle is primarily a function of translation limit cycle as shown in Figure III-19. For a deadband of .1 ft (see requirement(c) on Table III-19) and the closest stationkeeping distance of 3 ft, a value of ± 5 degree is derived.
i) Maximum STEM Rate = $2.2^{\circ}/\text{sec}$ Margin $\times \frac{2}{4.4^{\circ}/\text{sec}}$	Maximum STEM rate is driven primarily by the translation deadband lateral rate, shown in Figure III-20, for several stationkeeping distances. For autonomous systems these rates are very low (see (b) on Table III-19) -- less than .01 ft/sec -- resulting in ~ 2.2 deg/sec for a stationkeeping distance of 3 ft.
j) Maximum STEM Extension = 5 ft	Distances beyond 5 ft are not practical for servicing considerations, nor for STEM boom structural strength design, yet the greatest possible distances are desirable from STEM rate and angle design characteristics, ground control response requirements, safety, etc.
k) STEM Extension Rate - .5 in/sec	Based on operational considerations that would like the probe extended in 2 minutes.
l) STEM retraction Rate - .1 in/sec	Based on an operational timeline allowing 10 minutes for retraction.

TABLE III-18 REQUIREMENTS-SPACECRAFT CUES

AUTONOMOUS NON-IMPACT DOCKING

REQUIREMENT	SOURCE
<p>The cue requirements of the impact systems, Table III-14, are all applicable here, together with the following additional requirement:</p> <p>d) A spacecraft cue will be required in conjunction with close-in sensor performance during stationkeeping at 3 ft. to 5 ft. This sensor will have to aid in derivation of target attitude data as well as relative translational error (LOS) in three axes. Total cross section cannot be more than 1.5 ft based on a 30 deg FOV and a station-keeping distance of 3 ft.</p>	

TABLE III-19 REQUIREMENTS-CONTROL SYSTEM/MAN

AUTONOMOUS NON-IMPACT DOCKING

REQUIREMENT	SOURCE
<p>The control system requirements for the impact system, Table III-15, are all applicable, plus addition of the following:</p>	
<p>c. Axial Translation Minimum Trim Capability = .012 in/sec Margin $\frac{\times 2}{.024 \text{ in/sec}}$</p>	<p>The non-impact docking requires very refined axial translation control. The closing rates have been reduced to near zero at the time of STEM extension, allowing the stationkeeping rate to be maintained with a single minimum impulse of two axial jets. That capability for a mass of 1000 slugs and a total ACS thrust of 50 pounds is:</p> $V_X = \frac{\text{Impulse}}{\text{Mass}} = \frac{50 \text{ lbs} \times .02 \text{ sec}}{1000}$ $= .001 \text{ ft/sec}^2 \text{ or } .012 \text{ in/sec.}$
<p>d. Stationkeeping Translation Deadband $\pm .05 \text{ ft}$ Margin $\frac{\times 2}{\pm .1 \text{ ft}}$</p>	<p>If an ACS duty cycle of one firing per 5 sec is assumed (typical for rotational attitude control narrow deadband duty cycle), the rate from (b), Table III-15, of .01 ft/sec results in .01 x 5 = .05 ft of travel between reversing pulses, which is essentially the nominal boundaries of the translation deadband.</p>
<p>e. Lateral Translation Deadband Rate = .012 in/sec Margin $\frac{\times 2}{.024 \text{ in/sec}}$</p>	<p>See (c) above.</p>

TABLE III-20 REQUIREMENTS-RANGING SENSOR

HYBRID IMPACT DOCKING

REQUIREMENT	SOURCE
a) Attitude Determination Capability	
1) Attitude determination, maximum range capability 200 ft Margin $+ \frac{100 \text{ ft}}{300 \text{ ft}}$	Same as autonomous impact system. See Table III-11.
2) Attitude determination, minimum range capability = 10 ft	Same as autonomous impact system. See Table III-11.
3) Attitude determination accuracy = ± 1 degree	Same as autonomous impact system. See Table III-11.
b) Acquisition range = 12.5 n mi Margin $\times \frac{2}{25 \text{ n mi}}$	Same as autonomous impact system. See Table III-11.
c) Minimum Ranging Range = 10 ft	Same as autonomous impact system. See Table III-11.
d) Range Accuracy .5 n mi to 25 n mi - $\pm 100 \text{ ft}$ 10 ft to 5 n mi - $\pm 1 \text{ ft}$	Same as autonomous impact system. See Table III-11.
e) Range Rate Accuracy Far (.5 n mi - 25 n mi) = TBD Near (10 ft - .5 n mi) = $\pm .1 \text{ fps}$	Same as autonomous impact system. See Table III-11.
f) Field of View - ± 15 deg Margin	Same as autonomous impact system. See Table III-11.
g) LOS Accuracy - Near = 1.0 deg Far = TBD deg	Same as autonomous impact system. See Table III-11.
h) Loss of LOS data - 1 foot	Same as autonomous impact system. See Table III-11.

TABLE III-21 REQUIREMENTS-VIDEO/LIGHTING

HYBRID IMPACT DOCKING


REQUIREMENT	SOURCE
<p>a) Type - Silicon Intensified Target Vidicon</p> <p>b) Resolution - 500 Lines and 400 Pixels</p> <p>c) FOV = 20 deg</p> <p>d) Scan Rate = 30 Times/Sec</p> <p>e) Bandwidth = 4.5 Megahertz</p> <p>f) Camera Survivability - Look into the Sun</p> <p>g) Maximum Length - .3 m (1 ft)</p> <p>h) Target Illumination - Required - 5 to 10 ft candles</p> <p>i) Lighting - Strobe of Tungsten Flood</p> <p>j) Lighting Power - 600 watts (Max) 16.5 watts (Avg)</p>	<p>Same as manual impact system (see Table III-2).</p> 

TABLE III-22 REQUIREMENTS-DOCKING MECHANISM

HYBRID IMPACT DOCKING


REQUIREMENT	SOURCE
a) Angular misalignment = 3 deg Margin $+ \frac{1.5 \text{ deg}}{4.5 \text{ deg}}$	Same as manual impact system (see Table III-3) 
b) Maximum lateral displacement = $+ .21 \text{ ft}$ Margin $\times \frac{2}{+ .42 \text{ ft } (+ 5 \text{ in.})}$	
c) Lateral velocity at docking interface = .11 fps Margin $\times \frac{2}{.22 \text{ fps}}$	
d) Contact velocity = $1 \pm .1 \text{ fps}$	
e) Roll misalignment = $\pm 5 \text{ deg}$	

TABLE III-23 REQUIREMENTS-SPACECRAFT CUES

HYBRID IMPACT DOCKING


REQUIREMENT	SOURCE
<p>a) An array of reflectors will be required on the docking axis for attitude determination. The maximum diameter of the array can be 5 feet.</p> <p>b) The relative alignment/orientation of the reflectors in a) shall all be within .5 deg of each other and the spacecraft axes.</p> <p>c) A 4π steradian coverage of reflectors shall be provided for the cooperative sensors for signal reflection during rendezvous (as a maximum).</p> <p>d) An offset "T" or similar cue is required on the spacecraft for manual backup docking activities.</p>	<p>Same as autonomous impact system (see Table III-14)</p>  <p>Same as manual impact system (see Table III-14)</p>

TABLE III-24 REQUIREMENTS-CONTROL/MAN

HYBRID IMPACT DOCKING

REQUIREMENT	SOURCE
a) Tug minimum impulse bit = 20 ms	Same for all configurations.
b) Lateral Translation Trim Capability = .1 fps	Same as manual impact system (see Table III-5). Although the autonomous control capability can perform much better than this, the docking mechanism, which is affected significantly by this characteristic, must be designed for the worst situation which is the manual backup control mode.

IV. DOCKING MECHANISM EVALUATION

The primary goal of this section is to compare candidate docking mechanisms for the Space Tug that are optimal combinations of hardware to support the design goals specified for the Space Tug. It is significant that we emphasize the requirements and goals of the Tug because up until this point the requirements for docking systems have been very similar. The Tug represents a departure. For previous programs the primary goal was the structural joining of two spacecraft for the specific purpose of providing a pressurized passageway between them. The requirements are different than those for previous systems, therefore, we anticipate that the eventual design solution will be different.

A. DOCKING SYSTEM REQUIREMENTS AND GUIDELINES

Listed below is a summary of the system level requirements identified for the docking system to be applied to the Tug. It was essential to carefully review the requirements established for previous programs to determine their applicability to the Tug. In the past, the goal of the docking system was to structurally attach the two vehicles, providing a pressurized passageway between them. The final phases of the rendezvous was provided by the man-in-the-loop, the astronaut, "flying" the two vehicles together. Now the goals have changed as well as the conditions, thus the system requirements and design guidelines should reflect these changes.

The structural requirements in some ways are more complex than before. Now we must accommodate up to three spacecraft for delivery, and return another. In addition, the one to be returned may be of a different diameter than the one delivered. The interface is further complicated by the requirement to accept spinning payloads.

In other areas, the requirements are found to be analogous. With respect to the budgeting of impact to the design of the Tug or to the payload, the situation is similar to that of the CSM and the LM. Just as it was important to minimize the impact of the docking system on the LM to minimize weight to be taken to the surface of the moon and back, so it is important to minimize the impact of our system on the payloads. The principal mechanism design requirements are:

- Cantilever payload off front of Tug with load carrying capability defined by Tug and orbiter operations;
- Eliminate final misalignment between vehicles to align the docking interface;
- Provide capability to deliver up to three payloads and return one;
- Retrieval interface must be able to accommodate delivery of one diameter payload and return another;

- Deploy payloads with desired low tip-off rate ($.0083^{\circ}/\text{sec}$ minimum, but generally $1^{\circ}/\text{sec}$);
- Deploy or retrieve spinning satellites with rates up to 100 RPM;
- Capable of redocking immediately after deploy (infant mortality);
- Have minimum design impact on payload;
- Minimize weight carried by Tug to maximize payload capability.

The major issues that affect docking mechanism selection are illustrated in Figure IV-1. Compatibility with multiple payload mounting techniques, and the ability to cope (in flight) with different payload diameters are constraining requirements. The issue of whether to support retrieved spacecraft in the Shuttle bay with the docking mechanism or with separate support structure has a significant design impact. Whether to burden the docking mechanism or the sensors with the final spacecraft mounting alignment task is equally significant. The servicing compatibility issue is also significant. These considerations, coupled with the question of the degree to which past-developments can be used to reduce acquisition cost, form the basis for the design and selection of candidate docking mechanisms.

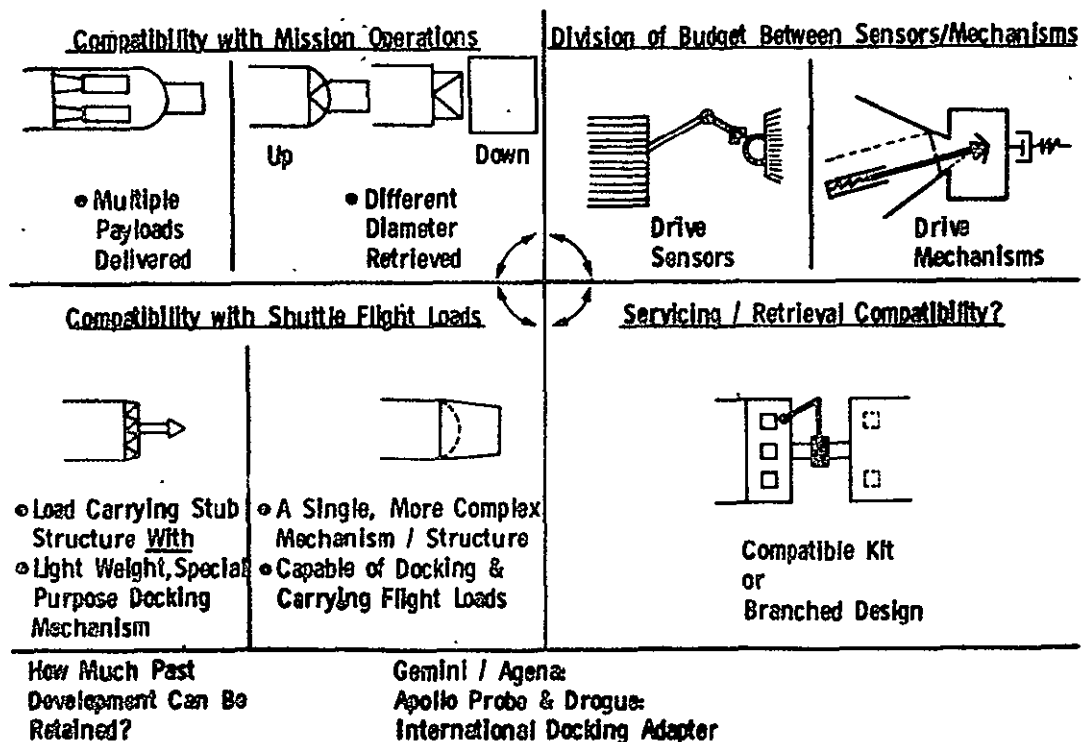


Figure IV-1. Key Docking Mechanism Selection Issues

B. HISTORICAL DOCKING MECHANISM DEVELOPMENT

The following is an overview of the evolution of mechanisms used to structurally join two vehicles in orbit. It presents the concepts developed for the Gemini, Apollo and ASTP programs as well as some of the concepts that were proposed but later eliminated. In addition, it presents a brief analysis of some of the advantages and disadvantages of basic classes of systems.

The U.S. space program's experience with the joining of two vehicles in orbit began with the Gemini Program. The Gemini system employed a large truncated cone, or frustum, mounted to the target vehicle. This cone, essentially what was to become the docking drogue of the Apollo Program, was sized to accept the forward end of the Gemini vehicle. The cone had a larger included angle than the docking portion of the Gemini vehicle to allow lateral displacements, and a slot that accepted a guide bar on the Gemini to provide the desired rotational alignment. Energy dissipation of both rotational and translational energy was provided by three groups of dampers located around the base of the cone on the target vehicle.

The operation of the system involved the rendezvous of the Gemini with the target vehicle, then the maneuvering required to insert the forward end of the Gemini into the cone. Spring loaded latches on the Gemini then engaged receptacles in the cone effecting capture. The spacecraft was then retracted until it contacted structural pads on the target vehicle, thus any subsequent loads were not reacted through the damper assemblies.

In July 1962, NASA announced that they would accomplish lunar landing by the use of the lunar orbit rendezvous technique, thus they had a requirement for an Apollo docking mechanism. The CSM contractor initiated a study that was to result in the selection of the probe and drogue concept in December 1963. To arrive at this decision required an analysis of the systems identified at that time in light of the requirements of the Apollo Program.

The systems were identified as either impact or non-impact in nature. The impact systems required that the active vehicle initiate a closure rate within a specific bandwidth such that this energy could be employed to effect a capture. The non-impact systems, on the other hand, required the active

vehicle to station keep near the target vehicle such that a tether could be extended to capture the target vehicle, allowing it to be retracted back to the active vehicle. The following description and analysis of the seven concepts evaluated for the Apollo Program is from "The Apollo Experience Report, The Docking System" by Robert D. Langley of MSC.

The impact systems evaluated were the probe and drogue, the ring and cone, and the (at that time) yet to be proven Gemini system.

Probe and drogue - The probe and drogue docking system consists of a probe mounted on the CM and a drogue installed in the LM (Fig. IV-2). The probe consists of a probe head, a single center piston for impact energy attenuation, three pitch arms with bungees for lateral loads and vehicle alignment, and an electrical reel mechanism to effect retraction after initial capture. The drogue is a funnel-shaped structure that guides the probe head to the initial capture position, where drogue-mounted latches engage the probe head. For crew transfer after hard docking, both the probe and the drogue have to be removed to provide a clear passageway.

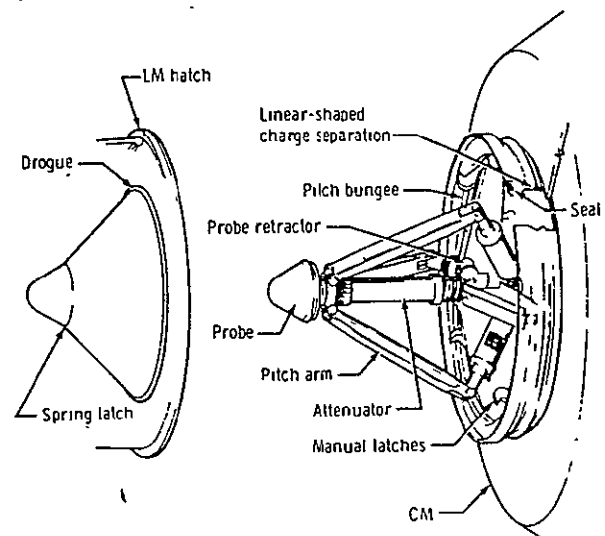


Figure IV-2 - Probe and Drogue Docking System

Ring and cone - The ring and cone docking system was developed by MSC and consists of a ring mounted on the CM and a cone mounted on the LM (Fig. IV-3). The tubular ring is supported by six identical impact attenuators that attach to the CM egress tunnel. After initial capture latching, the two vehicles are pulled together to the hard-dock position by three electrical reel-in mechanisms. The cone consists of four structural elements and capture latches to engage the ring. The cone serves as the guide for the ring from contact to capture latch engagement and is removable, after hard docking, to provide for crew transfer.

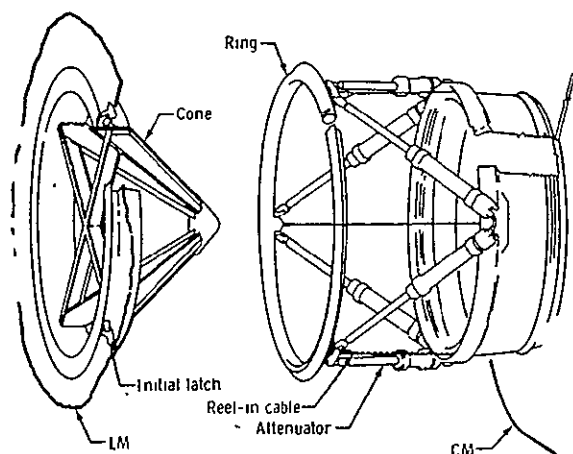


Figure IV-3 - Cone and Ring Docking System

Gemini docking system - The Gemini docking system consists of a structural ring on the CM and a cone on the LM (Fig. IV-4). This system is a reversal of the ring and cone system in that the cone is reversed (similar to drogue) and is supported by the impact attenuators. This system, although used successfully in the Gemini Program, was never seriously considered for the Apollo Program because of the severe weight penalty that would be imposed on the LM.

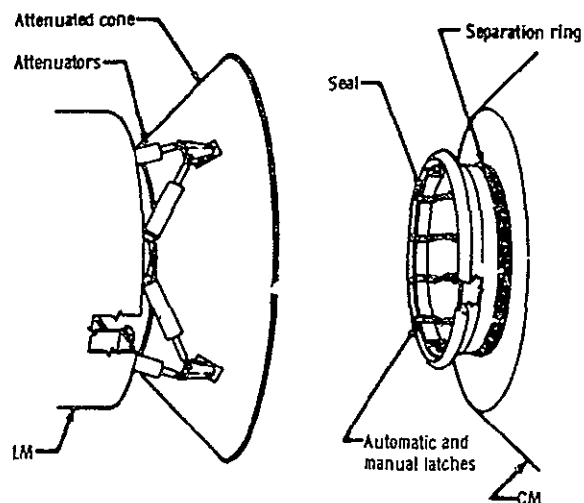


Figure IV-4 - Gemini Docking System

Nonimpact Docking Systems

The nonimpact docking systems include those systems that achieve initial capture of the passive vehicle by extending a member from the active, stationkeeping vehicle. The four nonimpact systems evaluated were the inflatable probe, the stem, the stem and cable, and the inflatable tunnel.

Inflatable probe - The inflatable probe system uses an extendible inflatable tube and support structure mounted on the CM and a conical drogue mounted on the LM (Fig. IV-5). The 4-inch diameter tube is housed on a reel mechanism located at the base of the support structure. The tube is extended to 20 feet and made rigid by gas inflation. The capture latch mechanism is mounted on the forward end of the tube for engagement of the latches in the LM drogue. After capture, the tube is reeled in to achieve hard docking.

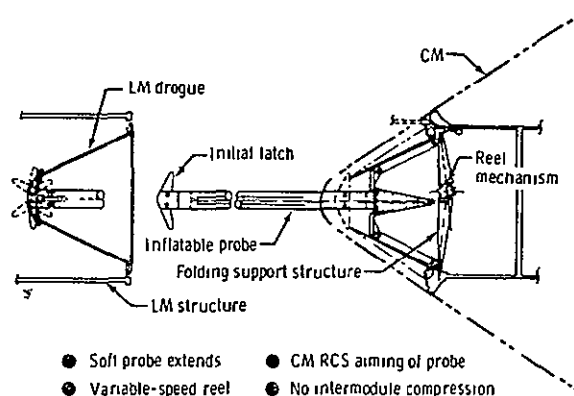
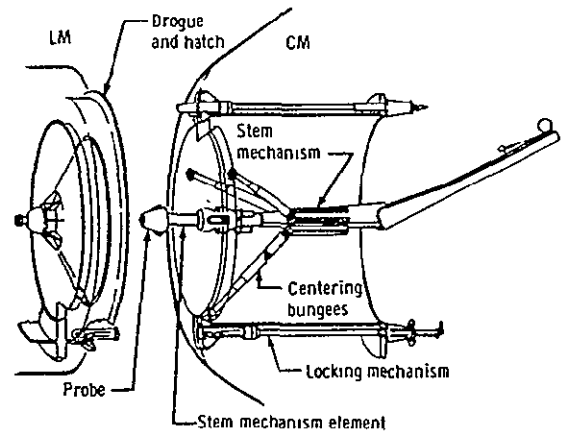


Figure IV-5 - Inflatable Probe Docking System

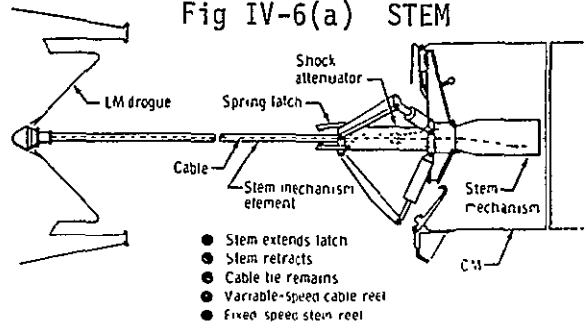
Stem - The stem docking system (Fig. IV-6(a)) consists of a CM-mounted stem device and a combined drogue and hatch installed in the LM. The stem device is constructed of sheet metal that is heat treated in the rolled position so that a metal tube is formed upon extension of the sheet from the spool of the reel mechanism. Once the tube is extended, the crew manually guides the stem probe head into the drogue to effect capture latch engagement. Retraction is provided by the reel mechanism.



- Ball-ended stem extends
- Probe manually aimed
- Variable-speed reel
- No intermodule compression

Fig IV-6(a) STEM

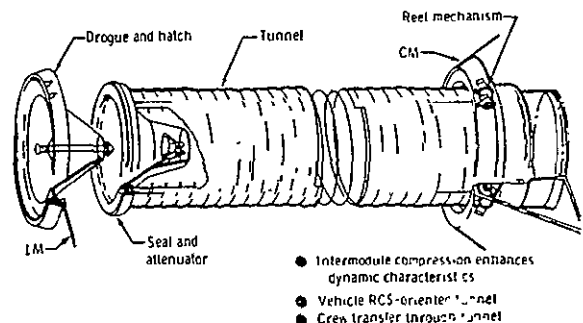
Stem and cable - The stem and cable system (Fig. IV-6(b)) is almost identical to the stem system, except that the stem cannot be manually directed, and the probe head is permanently attached to a cable rather than to the stem. After capture latch engagement, the stem retracts and leaves the vehicles attached by a single cable tether. A variable-speed cable-reel device then effects a closure rate to the hard-dock position.



- Stem extends latch
- Stem retracts
- Cable tie remains
- Variable-speed cable reel
- Fixed speed stem reel

Fig IV-6(b) STEM & Cable

Inflatable tunnel - The inflatable tunnel (Fig. IV-6(c)) is a flexible device that is stowed in the CM tunnel and releases and extends by gas pressure. After capture latch engagement with the LM drogue, the tunnel is retracted to achieve a hard-dock configuration.



- Intermodule compression enhances dynamic characteristics
- Vehicle RCS-orienter tunnel
- Crew transfer through tunnel

Fig IV-6(c) Inflatable Tunnel

The selection process employed both analytical and test techniques to provide information for the trade analysis. Both were done in two dimensions and the fidelity of the simulations were rather crude. However, this did provide data that allowed the concepts to be evaluated with respect to each other. The inflatable probe was found to be marginally feasible, and it was felt that the Gemini system resulted in a prohibitive weight increase in the LM. None of the remaining concepts could be demonstrated to be clearly superior, thus judgment was one of the prime factors in selecting the probe and drogue.

An evaluation of any of these systems' application to docking in future space missions dictates an inspection of the requirements that were used to guide these systems evolution. Then, and only then, we can realistically assess the potential for their application.

For the Gemini, the requirements were to demonstrate the feasibility of aligning (both laterally and in rotation) and joining structurally two vehicles in orbit. To accomplish this goal, the designers recognized that one of the primary functions of the mechanism was to be that of compensating for less than ideal initial conditions between the two vehicles. These conditions can be discrepant in either displacements (lateral and angular) between the two halves of the mechanism at contact or variations in the relative velocity between the two bodies.

The solution to the problem of displacements, or misalignments, of the halves of the docking mechanism is one that has been applied exclusively throughout the American Space Program. That is, one half of the mechanism is inserted into a cone, or drogue, which applies the necessary corrective forces to guide the inserted half, generally a probe, to the apex of the cone thus aligning the mechanism. For the Gemini program the cone was mounted on the target vehicle and the forward end of the Gemini capsule acted as a probe. In addition a slot in the cone was provided such that a guide bar on the capsule provided accurate rotational alignment of the vehicles.

Variations in the closing velocity were accommodated by a spring and damping arrangement attached to the drogue on the target vehicle. Again this is the approach that has continued to be employed, with the exception that in the case of Apollo the drogue was totally passive and the probe provided the energy attenuation.

Finally, an investigation of the action of the latching mechanism reveals that the Gemini employed a two step system in which the first step was that of capturing the target vehicle, and the second was that of pulling them together so that additional latches could be used to provide the desired rigid interface.

An inspection of the Apollo system shows that the basic theory or concept of the Gemini system was employed, but modified to better suit the new design goals. As in the Gemini system, a drogue is used to convert the translational kinetic energy of the active vehicle into the desired forces to align the two vehicles. For Apollo however, due to weight restrictions on the Lunar Module (the target vehicle) a smaller drogue was employed, thus a separate probe was required. In addition, again due to weight constraints, the energy attenuation was moved from the drogue to the probe.

If docking concepts are categorized as central and peripheral then it can be observed that all the proposed concepts for Apollo were of the central type. This is because there was no requirement for the docking interface to transmit

large structural loads, one of the prime assets of a peripheral docking system. If the concept is reviewed closely enough, however, there are characteristics of the Apollo system that lend themselves to application as a basically peripheral system. The probe and drogue are obviously centered, but their duties are only in the initial alignment and capture phases of the docking operation. Figure IV-7 illustrates the separate phases of activity associated typically with the docking operation. The first phase is one that has not been used in the past, but certainly is a possibility for future docking operations. If the docking mechanism is within the field of view of a camera then the docking mechanism itself could provide visual cues as to the final alignment, in addition to the docking aids used in the past. Phases 2 through 7 are those that have been accomplished by the probe and drogue throughout the Gemini and Apollo programs. As can be seen there are two basic activities described: first aligning and capturing the payload, typically with a set of light latches; then drawing the two together so that a firm structural connection can be made by a second set of stronger latches. In the case of the Apollo program, the diameter of the ring of structural latches was dictated by the requirement to provide a crew passageway. Thus, the Apollo system was really a combination of central and peripheral systems, but the diameter of the peripheral portion was small enough to characterize it as a purely central system.

The concepts proposed for Apollo were characterized as impact or non-impact. The final selection was impact, but the rationale behind this must be viewed in light of the requirements that were defined. The obviously advantage of the impact type system is that the kinetic energy of the active vehicle can be transformed into forces to provide the alignment of the two halves of the docking interface. The alternative is to provide a control system that can provide the desired level of alignment itself. Providing the alignment through impact is not without drawback. Complications arise in that the remaining kinetic energy must be removed through an energy absorption system, typically springs and dampers, also, the area of contact and post-contact dynamics is less than desirable. For central systems, the problem of jack-knifing is something to be contended with, and the docking mechanism must be made stronger (heavier) to absorb the loads. For Apollo, the docking was to be between two stabilized vehicles, thus if the first impact did not effect capture (eg Apollo 14) the second attempt was not complicated by tumbling of one of the vehicles. Since docking in the Shuttle era will require docking to passive payloads, this may become a very significant factor in favor of non-impact systems.

Since the Apollo program there have been two major programs that have required on-orbit docking. Skylab continued to use the Apollo probe and drogue, while the Apollo-Salyut/Soyuz program has opted for the development of the International Docking Mechanism (IDM). Figure IV-8 illustrates the major components of this system. Again this is an impact type system. Depending upon the size of the mechanism selected (based upon the loads to be handled)

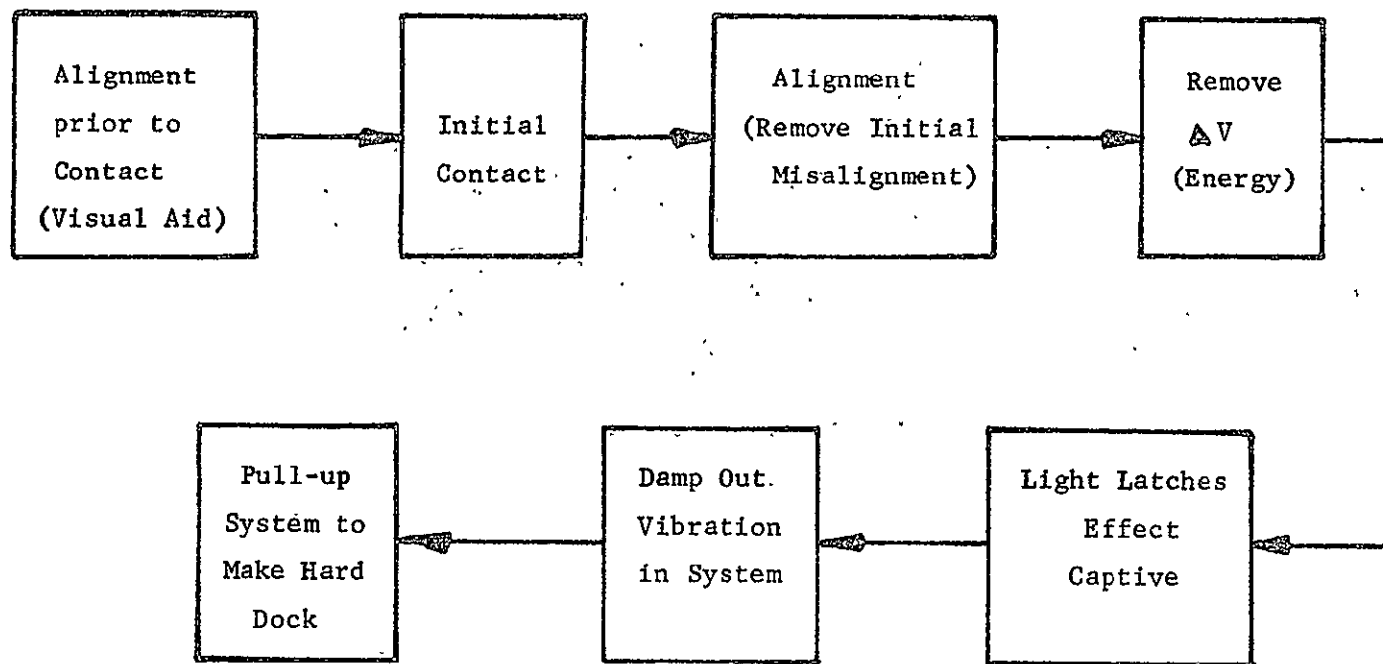


Figure IV-7 - Typical Phases of Docking

it can be considered for either enteral or peripheral applications. The unique feature of this mechanism is that it is androgynous. That is, any two halves can be mated. It is a two step operation of impacting the mechanism with sufficient velocity to allow the guides to align the mechanism, and to deflect the guide ring enough to compensate for angular misalignments so that the capture latches may effect capture. Then retraction cables pull the interface seal surfaces together such that the structured ring latches can make a rigid structural connection between the two vehicles.

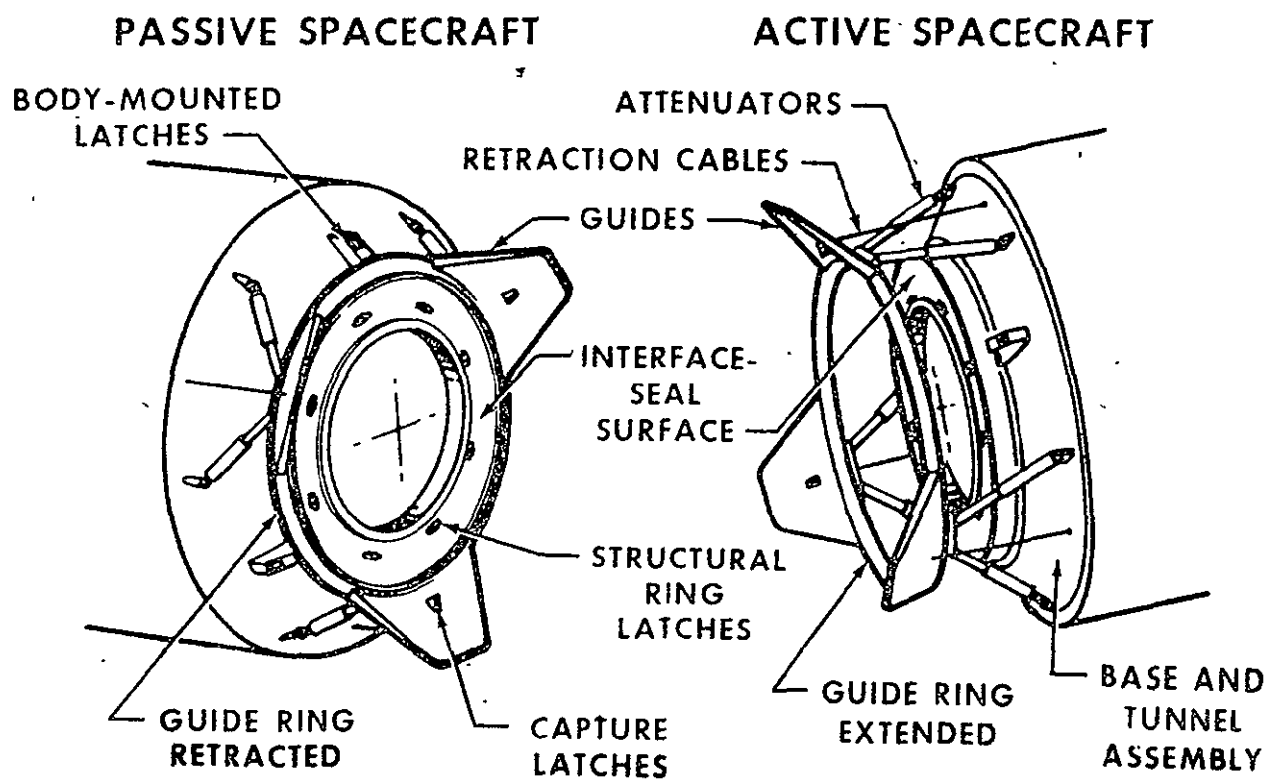
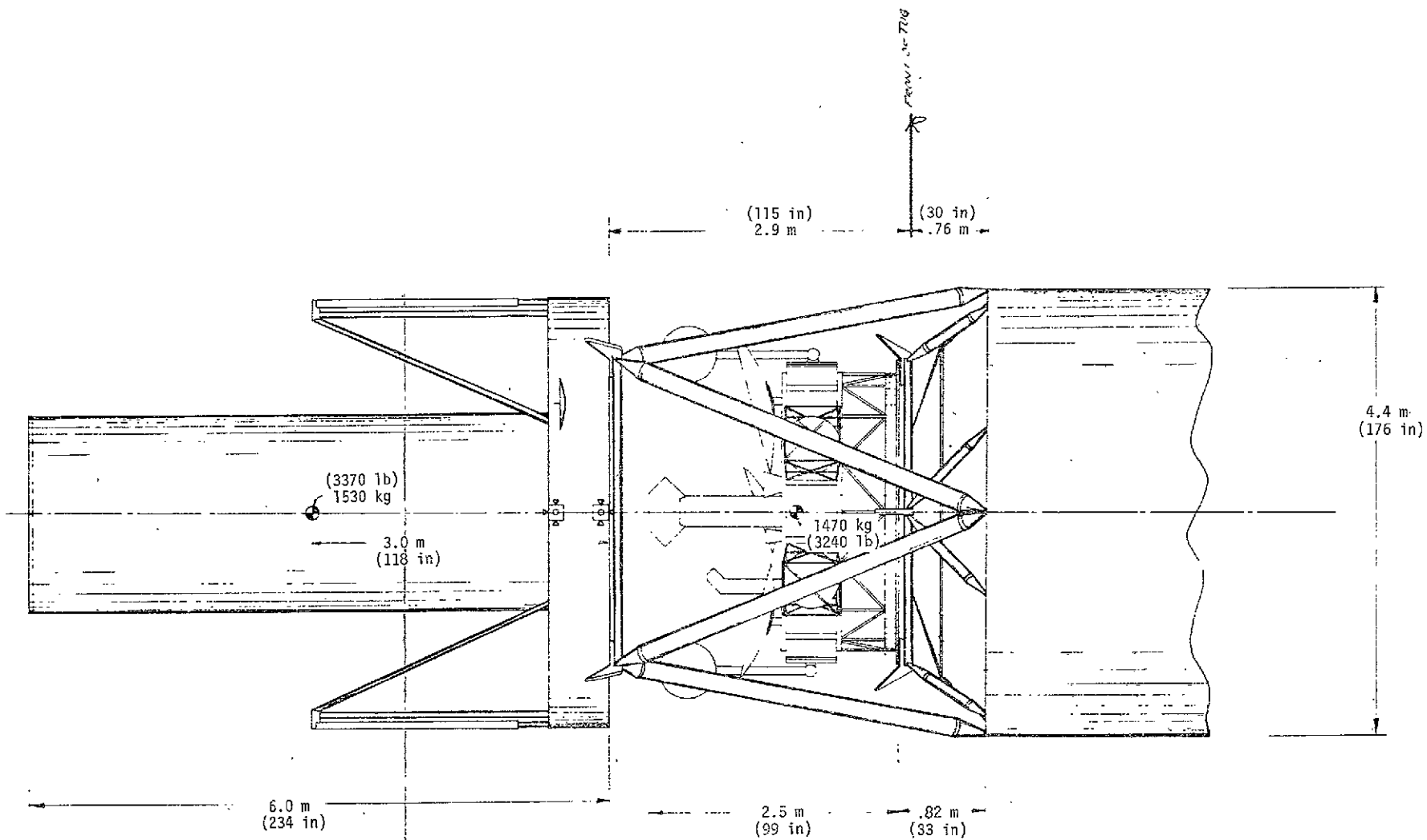


Figure IV-8 - ASTP Docking Mechanism



Multiple Payloads - CN-51 (Aft)
EO-59 (Fwd)

Figure IV-9 NDAC Docking System

C. CANDIDATE DOCKING SYSTEM MECHANIZATIONS

During the course of the study, three types of docking mechanism have proven to be most amenable to Space Tug docking requirements. These are the MDAC square frame system, the MMSE adaptation of the Apollo probe/drogue, and a new hybrid soft dock system that applies the STEM as a contact and closure mechanism. These systems are described in the following subsections.

1. MDAC Square Frame Mechanism - The square frame was the docking mechanism concept recommended by MDAC in their IUS/Tug Payload Requirements Compatibility Study (NAS8-31013). This approach has many virtues, and has been recognized as a suitable candidate in this study. Figure IV-9 illustrates the major elements of the square frame payload support and docking concept. It meets the myriad docking and payload support requirements with a structurally efficient new design featuring a variety of moderately complex mechanisms.

The basic structural component is the A-frame. A family of A-frames are capable of stacking spacecraft as illustrated. Each A-frame member is universally jointed to permit the overall structure to be opened up to support spacecraft of various sizes, and to permit installation of a shock absorbing device in each strut to absorb impact docking loads. An inflight adjustable square frame joints the tips of a set of four A-frames based on the Tug structure. This adjustment capability makes it possible for this design to deliver one spacecraft diameter and retrieve another. Figure IV-10 shows the payload attachment mechanism. This device secures delivered spacecraft prior to deployment, secures retrieved spacecraft, and provides a friction level suitable for despin of spinning spacecraft provided with a despin ring mount. A set of drive motors/idler wheels (not shown) provides a spin-up capability for deployed spacecraft requiring this service.

The servicing potential of this configuration is somewhat limited, or at least interrupted, by the peripheral design of the payload support structure. Separate mechanisms would be required to service components on the base of the spacecraft, inside the square frame, or on the outside of the spacecraft. Conceptual designs for achieving both types of servicing exist.

This concept is basically a new development. MDAC has done a considerable amount of design work, but the hardware is not yet flight qualified. Design virtues such as flexibility and lightweight make this concept a leading contender for Space Tug docking.

2. MMSE Apollo Probe/Drogue Application - The MMC Multi-Use Mission Support Equipment (MMSE) study evolved an interesting application of the flight proven Apollo probe/drogue to Space Tug docking requirements. This approach makes maximum use of the flight proven probe/drogue design, and limits new development to a set of static structure capable of meeting multiple payload support requirements. Figure IV-11 shows how the same spacecraft shown in Figure IV-9 would be supported using the MMSE concept.

This approach meets the same array of requirements as the square frame concept using the flight-proven Apollo Probe/Drogue in combination with an

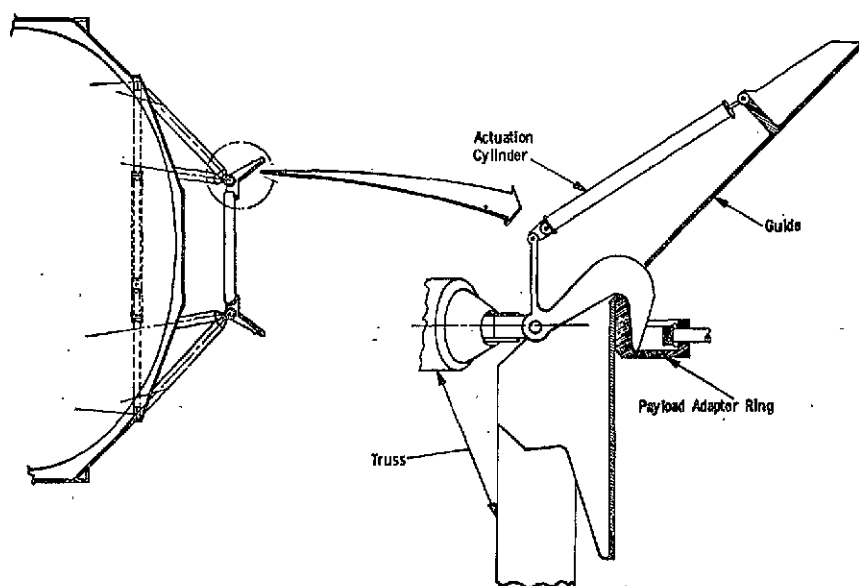
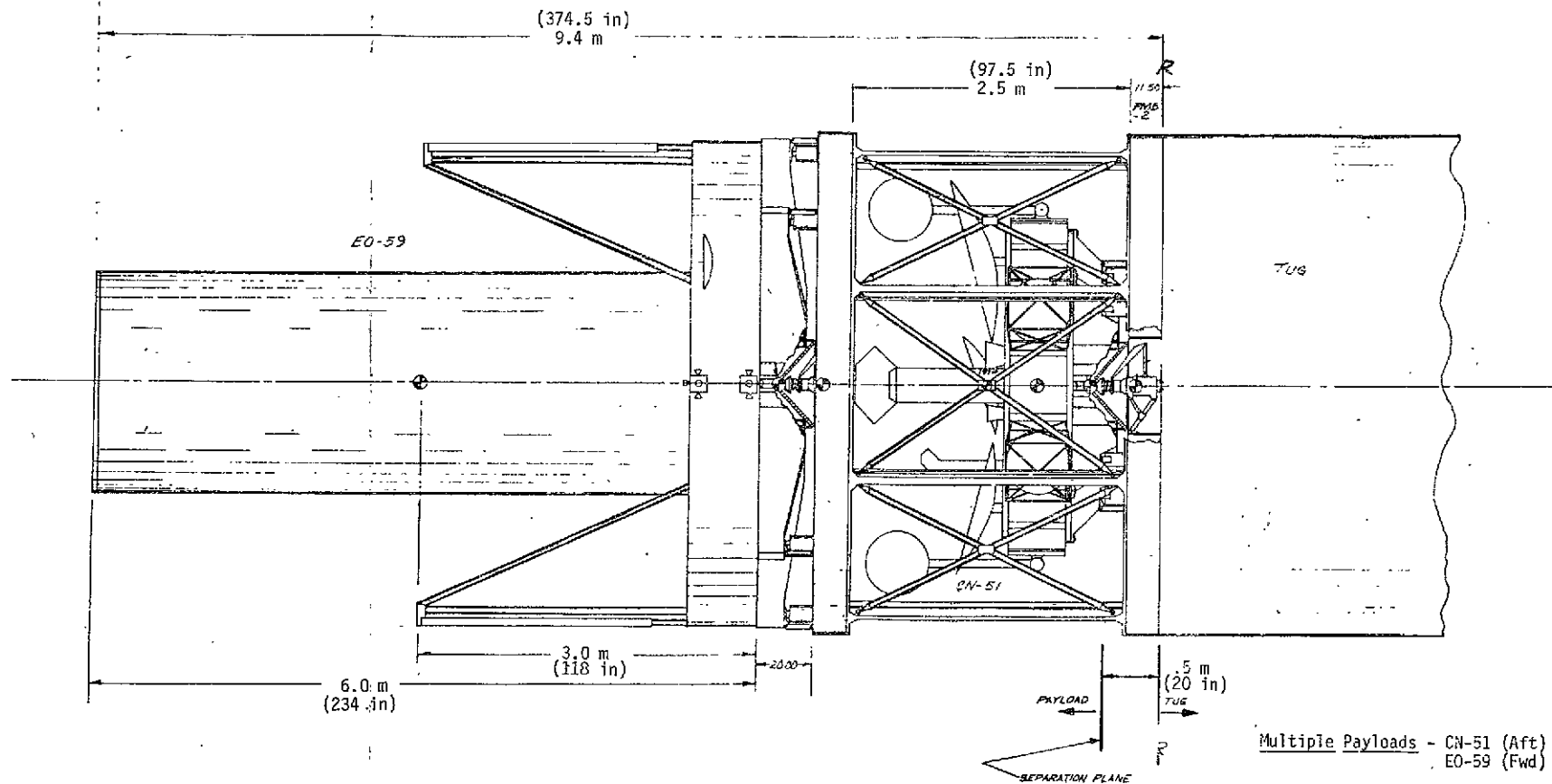


Figure IV-10 Square Frame Payload Attachment Mechanism



Multiple Payloads - CN-51 (Aft)
EO-59 (Fwd)

Figure IV-11 MMSE Docking System

array of static structure. In addition, this approach was conceived to meet IUS and Shuttle automated payload requirements. As a consequence, the design has been standardized for a broader application spectrum than is required specifically for Tug applications. It supplies eight hard mounting points for spacecraft of various diameters using a family of spider beams. Structurally, this approach appears heavier than the square frame approach, but it is simpler, uses more existing hardware, and should be less costly to develop. Provision of spin-up capability in the Apollo probe design will be a significant development problem--the spin-up requirement should be carefully assessed before this capability is implemented.

A more detailed illustration of the MMSE concept support structure is shown in Figure IV-12. A spider beam capable of providing 8-hard point mounts for a spacecraft, and adapting to the basic Tug structure is illustrated. The standardized set of payload interface adapters is also shown. This set of adapters meets the four standard sets of mounting points in the spider beam. These adapters would be unnecessary if the spacecraft hardpoints were standardized to meet the available selection of spider beam mounting points.

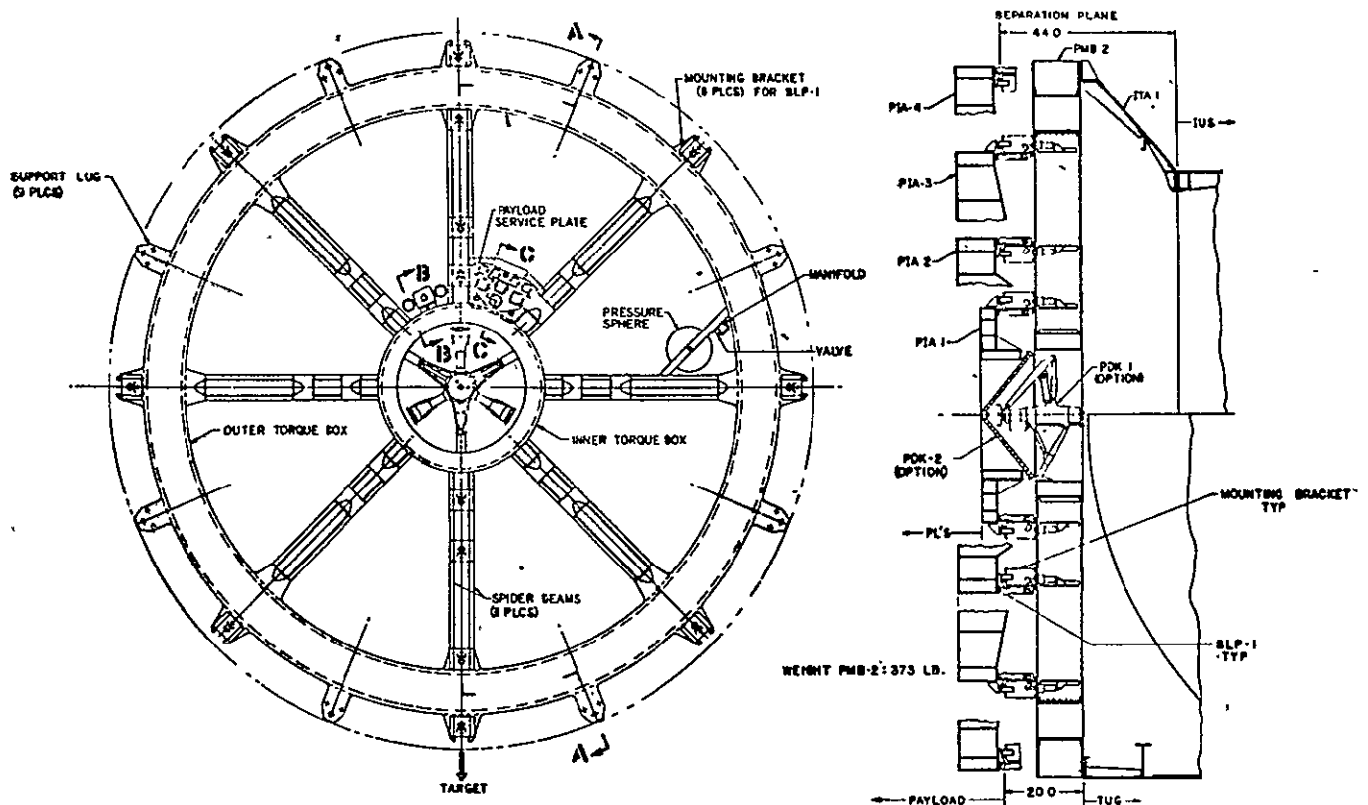


Figure IV-12 - MMSE Structural Detail

The virtue of the MMSE approach is limiting the development of new equipment to static structure, rather than complex mechanisms. The disadvantage is an anticipated higher weight.

3. Hybrid Soft Dock Concept - The hybrid soft docking concept, illustrated in Figure IV-13, incorporates several desirable features. It achieves soft docking through the use of a steerable, extendable STEM-mounted probe. This probe could be controlled in a closed loop fashion by a special sensing device, or could be manually inserted using video concepts. The STEM is then used to draw the spacecraft back for a soft attachment to an open A-frame structure that is in flight adjustable, possibly using an adjustable square frame. Since the A-frame structure need not have the variable geometry associated with hard-dock dynamics, it is singly hinged instead of being U-jointed. This approach should be slightly lighter than the MDAC approach, and overall, somewhat simpler and less costly to develop.

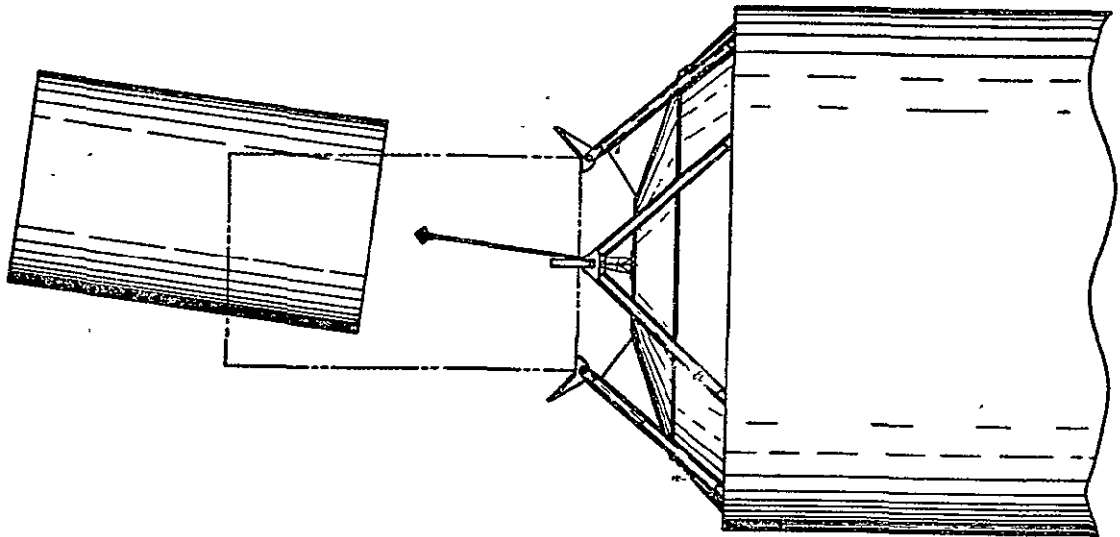


Figure IV-13 Hybrid Soft Dock System

The hybrid soft dock concept has a good potential for minimizing spacecraft design impacts through eliminating contact shock loads, and lightening the specialized docking structure requires on the spacecraft. The steerable boom portion of this design, however, is a new development. The potential advantages do not come free. Since the concept is new, thorough evaluation of concepts and a preliminary design activity was conducted. The results of this activity are reported in the following paragraphs.

a. Candidate Extendable Boom Concepts - A variety of extendable boom concepts is illustrated in Figure IV-14. Extendable tubular booms are elements made of thin metal strips which are wound flat on a spool when stowed and form a circular tube with overlapped or interlocked edges when extended. Two of the most prominent manufacturers of this type extendable boom are Astro Research Corporation of Santa Barbara, California, and Fairchild Industries of Germantown, Maryland. These units have been widely used in space for such applications as antennae and deployment of experiment packages, sensors and cameras.

Extendable contoured booms are also made of metal strips which are spool-stowed, generally have larger package envelopes and offer greater structural strength. They have lenticular (quasi-biconvex) or twin lobe shapes with welded, interlocked or overlapped edges. The Viking Surface Sampler boom, made by Celeco, is a welded lenticular shaped boom. Astro Research Corporation and Boeing Company have also made this type boom while the interlocked edge type is made by Sanders Associates, Inc. of Nashua, New Hampshire, and the twin lobe type by Fairchild. These booms have been used where heavier tip loads are anticipated. The twin-lobe boom, for example, was used on Skylab to transfer film cassettes between the ATM and the airlock.

Telescoping cylindrical booms have not been used extensively in space but were considered for this application due to their simplicity. Commercial units are built by Sanders and Tri-Ex Tower Corporation of Visalia, California. They consist of a series of close-fitting concentric metal cylinders which telescope for stowage and are extended by screw jack or cable with sufficient overlap remaining between sections to maintain structural strength. Package size for the tubes and deployment mechanisms is a major problem for the soft docking extendable boom application.

Expandable linkage booms consist of lazy tong linkages connected to frames at the linkage pivot points. Extension and retraction are accomplished by moving the first frame relative to the base while working against a tensioned centrally-located cable. A version of this boom, developed by the Martin Marietta Corporation, was successfully flown on Skylab to deploy the optical head of the T-027 experiment.

Prestressed element booms consist of cylindrical segments with centrally located axial holes through which a tensioned cable is run. Cable tension is maintained by springs which permit the segments to be stowed on a spool. As the segments are extended, they form a rigid tubular structure by being compressed by the tensioned cable. A working model of this boom has been built at Martin Marietta Corporation. The General Electric Company and the Illinois

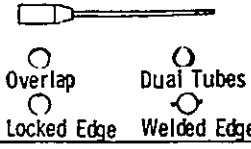
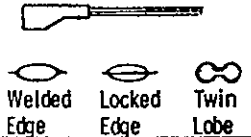
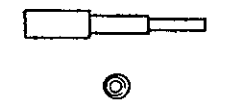
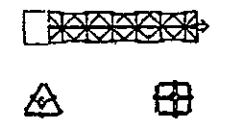

Description	Illustration	Advantages	Disadvantages
Extendible Tubular Booms		<ul style="list-style-type: none"> • Fully Developed And Tested • Flight Experience • Light Weight • Stowed Length Acceptable 	<ul style="list-style-type: none"> • Weak In Torsion And Buckling • Tip Deflection Limited • Single Deployment Speed • Axial Load Capability Not Predictable
Extendible Contoured Booms		<ul style="list-style-type: none"> • Good Binding & Torsional Strength • Reliable For Light Column Loads • Positive Control Of Deployment • Flight Experience 	<ul style="list-style-type: none"> • Buckles In Transition Region • Heavier Than Tubular Booms • Deployment Cycles Limited • Stowed Length Exceeds 1 Ft.
Telescoping Cylinder Booms		<ul style="list-style-type: none"> • Simple Parts, Structural Shapes • Reliable Deployment • Large Column Load Capability • Conventional Proven Design 	<ul style="list-style-type: none"> • Susceptible To Buckling • Binding Possible When Loaded • Considerable Overlap Required • Stowage Length Unacceptable
Expandable Linkage Booms		<ul style="list-style-type: none"> • High Expansion Rates • Can Carry Service Lines • Good Stiffness and Bending Strength • Light Weight 	<ul style="list-style-type: none"> • Large Number Of Parts • Compressible Axial Load Limited • Stowage Length Exceeds 1 Ft. • Requires Extension For Probe
Prestressed Element Booms		<ul style="list-style-type: none"> • Strong in Bending, Shear, Torsion • Very Simple, Reliable Design • Light Weight • Not Degraded By Use 	<ul style="list-style-type: none"> • More Development Work Needed • No Flight Experience • Relatively Large No. Of Parts • Guides Req'd For Torsional Strength

Figure IV-14. Extendable Boom Concepts

Institute of Technology have also prepared working models using this concept. Its simplicity and superior load capability make it attractive for soft docking application. Additional development work appears to be warranted.

b. Capture Latch Concepts - The three types of capture latch mechanisms shown in Figure IV-15 have distinct operational characteristics which influence their use. The pivoting probe latch allows angular motion between the Tug and spacecraft to take place without restraint since the probe is permitted to pivot within the latch fingers. This feature eliminates end moments on the extendable boom but may increase axial loading if axial play cannot be removed. This capture latch concept is much simpler than the clamping type, however, and could more easily incorporate a free rotating probe for capture of spin-stabilized spacecraft.

The clamped probe type capture latch offers maximum control of the spacecraft and eliminates end play between probe and latch. While a somewhat more complex mechanism than the pivoting type latch, operational features are superior. When a sensor has determined that the probe on the end of the steered boom has been captured by the drogue, a spring-actuated clamp is released which engages the conical end of the probe and forces it against the inner surface of the drogue, continuing the probe and hinging the longitudinal axis of the boom

perpendicular to the X-Y plane of the spacecraft. Engagement speed of the clamp is controlled by an integral damping device. Release of the clamp is accomplished by activating a solenoid which retracts and latches the clamp.

The probe may be a passive, rotating or fixed cone or may have an active latching capability. The concept for a latch type probe shown in Figure IV-15 employs spring-loaded pivoted fingers which will swing inward under light load to permit the probe to enter a hole in the drogue and expand when the probe is inside the hole to effect capture. This type latching probe places control of latching and release on the Tug side of the interface which minimizes spacecraft impact.

While three separate concepts have been shown, features of each may be combined. We have recommended a clamping type latch with the latch in the probe as the most versatile system.



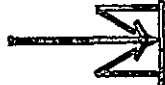
Description	Illustration	Advantages	Disadvantages
Pivoting Probe Latch		<ul style="list-style-type: none"> • Simple Design • Adaptable For Spin Stabilized S/C • No End Moment On Boom 	<ul style="list-style-type: none"> • Release Difficult • Impact Due To Probe Movement • Centered By Latch Fingers
Clamped Probe Latch		<ul style="list-style-type: none"> • Controls Attitude Of S/C • Eliminates Longitudinal Impact • Sensor Activated Snubbed Probe Clamp 	<ul style="list-style-type: none"> • Larger Boom Bore Torques • Stiffer Boom Required • Release Difficult
Latch In Probe		<ul style="list-style-type: none"> • Releasable From Tug • Self Centering • Simplifies S/C Design 	<ul style="list-style-type: none"> • Larger Diameter Drogue Required • Adds Tip Moment To Boom • Extends Storage Envelope

Figure IV-15. Capture Latch Concepts

c. Steering Mechanism Concepts - Steering mechanism concepts considered for extendable boom pointing were of two general types (Figure IV-16)--those having bearing-supported pivot points with integral motor/tachometer assemblies in the pivots, and those having flexure pivot points with separate motor drives.

The AMT star tracker gimbal system is the integral type. This developed hardware has very high performance characteristics such as pointing accuracy of 1 arc sec., weight capability of 500 kg, and a gimbal range of ± 90 degrees in one direction and ± 50 degrees in the other direction. This capability is greater than that required for extendable boom pointing for a nonimpact docking system. Even if simplified to the greatest extent possible, this system would be more costly than a flexure gimbal system due to the use of many more special parts, and more complex electronic controls. Also, this system would require redesign to meet envelope requirements and to interface properly with the extendable boom housing and Space Tug structure.

A system using flexural pivots to provide gimbal capability which uses a minimum number of simple parts has been designed by the Martin Marietta Corporation. Type 800 flexural pivots developed by Bendix provides the required deflection angle and radial load capability along with selectable torsional spring rates. Gear motor/encoder units in the size and capability required for boom pointing have been developed and qualified for other space programs and should, therefore, be available at reasonable cost. The use of tandem-mounted sets of pivots at each pivot location allowing the boom to be steerable while permitting controlled boom movement due to side loads on the boom tip is a unique feature of the flexural pivot type of boom steering system.

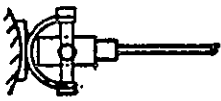
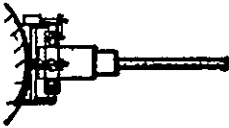
Description	Illustration	Advantages	Disadvantages
Gimbal Steering Mechanism		<ul style="list-style-type: none"> • Flight Experience • Torquers In Pivots • Integral Position Encoders 	<ul style="list-style-type: none"> • More Complex And Costly • Larger Envelope And Weight • Req'd Size Not Available
Flexure Steering Mechanism		<ul style="list-style-type: none"> • Simple Conventional Design • Limits Maximum Boom Moment • Minimum Weight, Size, Complexity 	<ul style="list-style-type: none"> • More Development Required • Limited Articulation Angle • More Power Req'd For Drive

Figure IV-16. Steering Mechanism Concepts

d. Selected System Design - Figure IV-17 depicts a design evolved from the preceding concept trades--for the boom selection, the articulation mechanism, and the latch on the spacecraft. The selected system (Figure IV-18) employs a SPAR-type of extendable tubular boom, a flexure type of articulation, and a clamped probe latch on the spacecraft. The requirements and ground rules utilized in arriving at this design are as follows:

- retracted length of boom assembly = .3 meter (1 ft) maximum;
- extendable boom steerable $\pm .35$ rad (20°), two directions;
- time to retract boom = 10 minutes $\pm .25$ minute;
- time to extend boom = 2 minutes $\pm .25$ minute;
- compatibility with servicing concept desirable;
- low impact capture latch for boom probe;
- centering and gripping mechanism for probe;
- free rotating probe for spin-stabilized spacecraft;
- provide undock and capture release capability;
- maximum boom loads after capture--bending moment, 552 newton (124 lbs), shear, 9.3 newton (2.1 lbs), axial load, 53 newton (12 lbs);
- Tug attitude control system active during retraction;
- Final misalignment removed by guide arms;
- mechanically operated latches make docking connection to spacecraft;
- closing velocity = .38 m/s (1.25 fps) maximum.

The resulting nonimpact docking system design (Figure IV-18) consists of a steerable extendable tubular boom with tip probe gimbal ring mounted on the Space Tug and a drogue and clamping latch on the spacecraft.

The extendable boom housing, which must rotate $\pm .35$ radians in two directions, is attached to the square gimbal ring through two sets of tandem-mounted flexural pivots. In one set, one pivot is motor driven through a gear set to provide the $\pm .35$ radian rotation while the other flexural pivot permits controlled rotation due to side loads on the boom tip. The other set may be similar, to provide redundant drive capability, or both pivots in the set may be free to flex. To provide rotation on the perpendicular directions, two flexural pivot sets are located between square gimbal ring and support brackets which attach to the Space Tug structure. Thus, the extendable boom may be

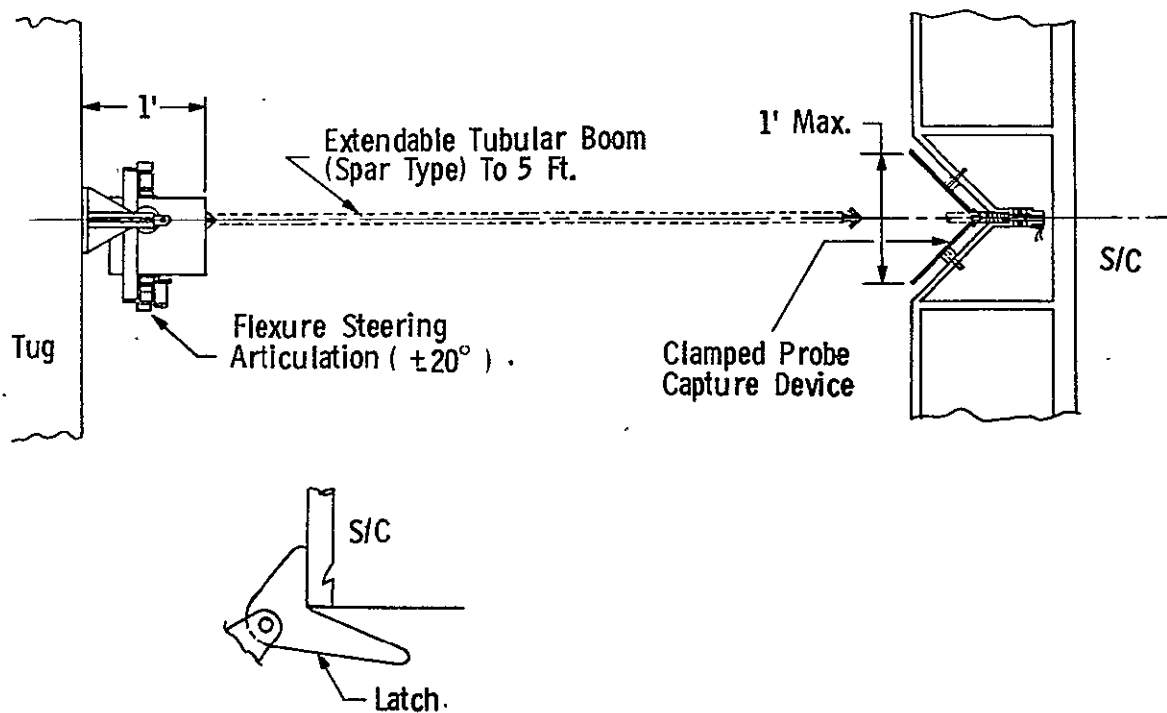


Figure IV-17. Selected Nonimpact Design Concept

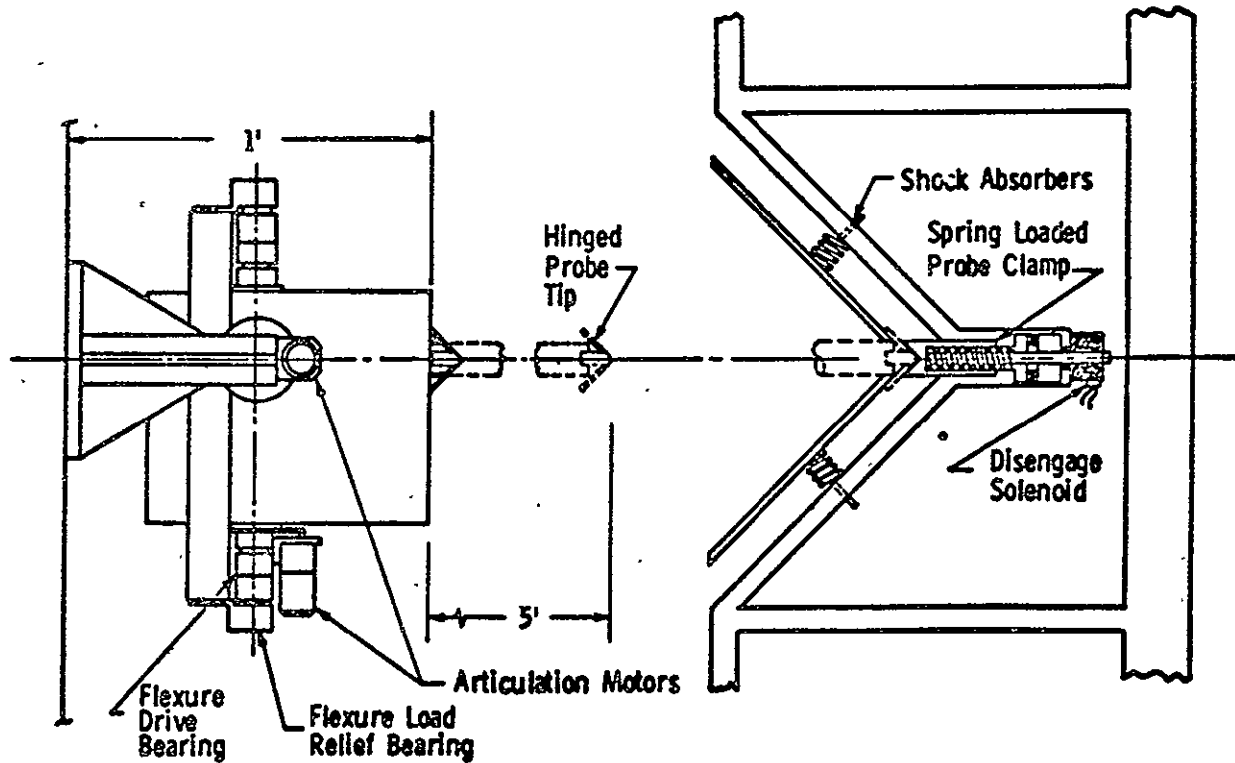


Figure IV-18. Nonimpact System Design Detail

steered as required while being protected from excessive side loading by flexural pivots having torque values compatible with the boom tube ultimate bending moment of 24 newton-meters (210 in lb). Since the flexural pivots seek a null position, they will tend to center the boom.

The probe on the tip of the extendable boom contains spring loaded pivoted arms which retract under light load as the probe passes through a hole in the drogue and expands inside to effect capture. The drogue is mounted on flexible supports to minimize impact loads at capture. Once captured, the probe is clamped against the inside of the drogue by a damped, spring-loaded clamp which centers the probe in the drogue and holds the spacecraft face perpendicular to the boom centerline. Clamping action is initiated by sensors which are activated when the probe is fully within the drogue. Emergency release is accomplished by retracting the clamp and probe arms by solenoid actuation.

Once captured, the spacecraft is slowly drawn to low impact docking with the Tug with the docking frame guide arms providing final alignment. The boom is extended approximately 1.5 meters (5 ft) in two minutes by its tension mechanism while lower speed retraction, taking approximately 10 minutes, is provided to minimize axial loads on the boom and minimize impact loads at mating. A free-rotating probe may be provided for capture of spin-stabilized spacecraft with despin capability provided at the docking interface.

D. SUMMARY COMPARISONS AND RECOMMENDATIONS

Table IV-1 presents the major comparison evolved during the docking mechanism support analyses. These comparisons are given for the three subsystems that were selected as candidates to be used in system synthesis and ranking. No attempt is made to select between these subsystems at the subsystem level. Rather, these criteria evaluations were made an input to the system selection process described in Vol. II, Section III.

The evaluations of system complexity, spacecraft impacts, multiple delivery/retrieval compatibility and spinning spacecraft compatibility are self explanatory and are supported in earlier portions of this section. The weight estimates given reflect an evaluation of the weights required to support the worst spacecraft combination identified in MDAC's Payload Utilization of Tug-Follow on (NAS8-29743), rather than a methodical evaluation of all reasonable combinations. These spacecraft are the CN-51 and EO-59 illustrated in Figure IV-9 and IV-11. Under these ground rules, the 'Standard' weight given for the MMSE approach may be too severely penalized. This weight is the direct output of the MMSE study, which reflects a broad standardization process. The weight of the MMSE approach tailored for the PUT combination is the lighter 323 kg (710 lb) shown in the table. The cost data shown is supported in Volume V of this series.

When these candidates were combined into the system selection process--the square frame candidate was included in all the top ranking systems. The nonimpact system was a close contender in the manual system designs (it was felt to be a risky approach for an autonomous system). The MMSE approach did not rank as well, because of the apparent weight penalty.

Table IV-1. Docking Mechanism Concept Comparison

Criterion Mechanism	System Complexity	Spacecraft Impact	Servicing Compatibility	Multiple Compatibility	Spinning Compatibility	Weight	DDT&E Cost
Square Frame	Requires relatively complex structural support mechanisms integral with docking mechanism	Peripheral docking mechanism has potential for docking/structural support compatibility	Somewhat limits spacecraft accessible region	Achieved with adjustable mechanisms	Can be designed into concept	253 kg (556 lb)	\$3.6 M
Probe Drogue	Uses developed docking mechanism, requires new design only for static structure	Central probe & peripheral structural support for delivery/retrieval must be separate	Provides good access to spacecraft for servicing	Achieved with standard array of interface equipment	Requires some development of Apollo Probe/Drogue	441 kg (970 lb) (Standard) 323 kg (710 lb) (Tailored)	\$1.5 M
Soft Dock	Simple structural support mechanism, but complex soft-dock mechanism	Eliminates docking shock loads without interfering with deliver/retrieval structural support	Can use servicing mechanism as soft-dock steerable probe	Achieved with simpler adjustable mechanisms	Can be designed into concept	241 kg (531 lb)	\$7.2 M

V. OPERATIONS ANALYSES

Identification and classification of mission operational characteristics and constraints which are applicable to rendezvous and docking was performed.

Operational characteristics/constraints are derived from Shuttle, Tug and Spacecraft operations documentation and orbital variations. A typical deliver/retrieve mission profile is illustrated in Figure V-1 with a summary of the operational considerations and constraints.

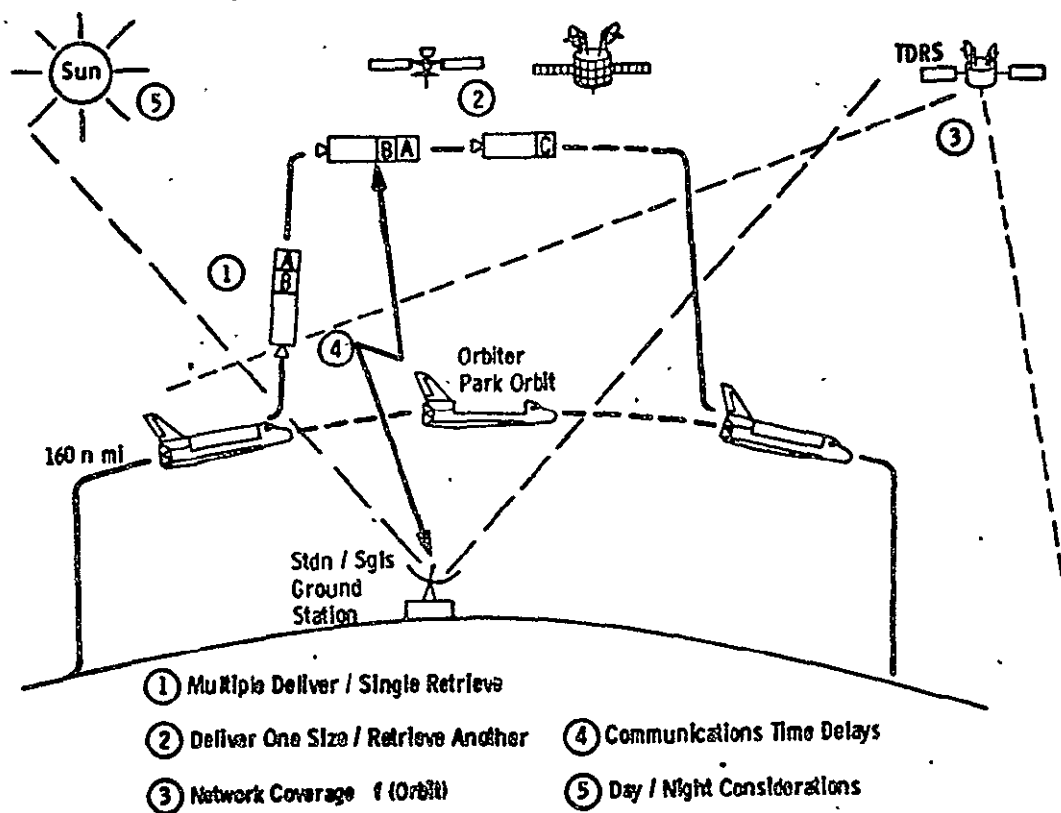


Figure V-1: Mission and Orbital Variations Impact System Design

Operations sequences were delineated to establish the functions which must be performed in order to accomplish mission objectives. The primary operations differences in autonomous, manual and hybrid systems is in the allocation of these functions for performance onboard (automated) or manually (ground

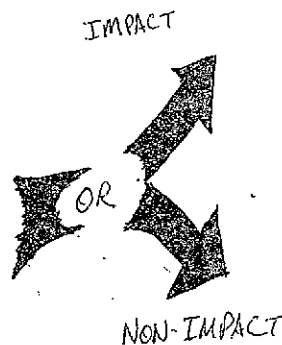
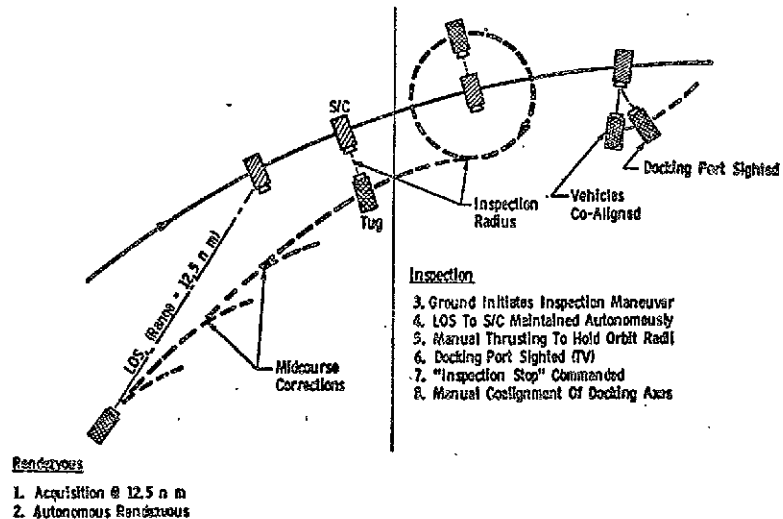
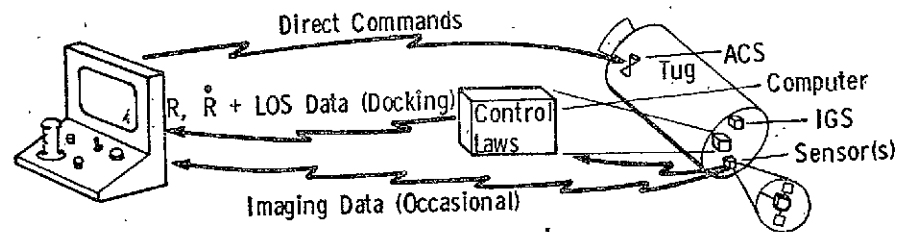
based control). The "best mix" hybrid system optimizes interaction between onboard and ground to make use of the best features of each.

Those operational steps associated with manual system are shown in Figure V-2 for impact and non-impact docking systems. This scenario illustrates that the rendezvous and inspection phases are identical for both impact and non-impact systems. Another noteworthy feature of the operations sequences is that some functions (e.g., Steps 1 and 4) are best performed autonomously, even in a manual system. Operational complexity is seen to increase for non-impact docking and potentially requires two console operators. One to maintain "station-keeping" attitude, while another console operator extends the STEM to capture the spacecraft. The combination of the operations sequences and the interrelationship of the Tug control system with the man-in-the-loop constitutes a definition of the manual system operations concepts used for this study.

A corresponding operations scenario and pictorial definition of the autonomous system is illustrated in Figure V-3. For the autonomous candidate the role of the mission control center was purposely reduced to monitoring only. This was done to define a total autonomy capability in case future requirements should dictate the need for such a system. Both impact and non-impact sequences are shown as is the pictorial definition of the limited degree of interaction for the autonomous system.

The hybrid system mission sequences are presented in Figure V-4 for an impact docking system only. This illustrates the optimum interaction between onboard and ground systems, which makes use of the inherent advantages of each system.

Specifically, the functions allocated to onboard systems are the rapid reaction functions, such as closing the control loop around the sensed data. The functions allocated to the ground include difficult to automate functions such as decision making which require excessive preprogramming of potential problem sets and recognition cues for each potential failure.



Closure

9. Manual Closure Initiated (1 fps)
10. LOS Maintained Automatically to 1 PL
11. Manual Lateral Thrusting To Maintain Coalignment Until R=20'

Closure

9. .5 fps Closure Rate Commanded
10. R Decreased As R Decreases
11. R=0 At R= 3 To 5'
12. LOS Maintained Autonomously
13. Manual Coalignment Of Vehicles

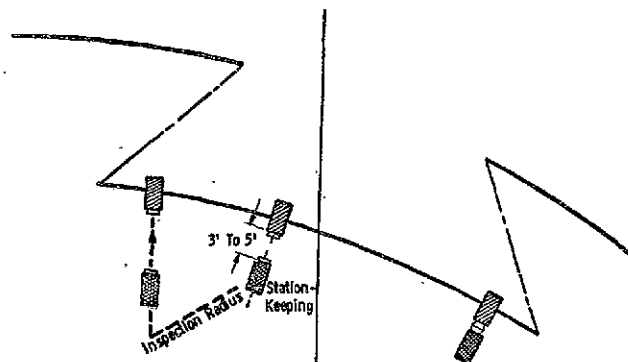
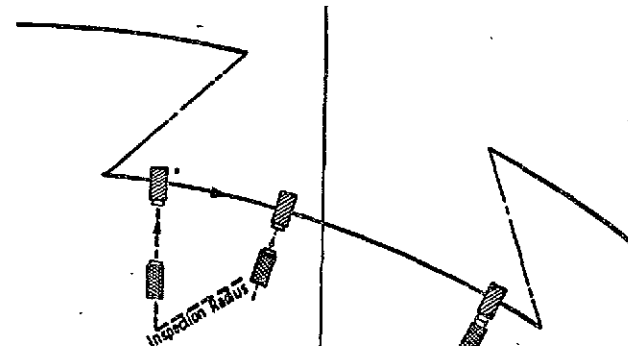
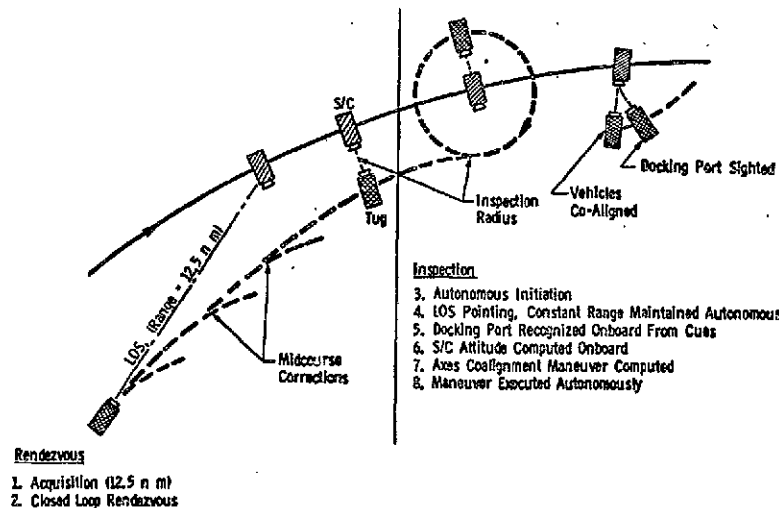
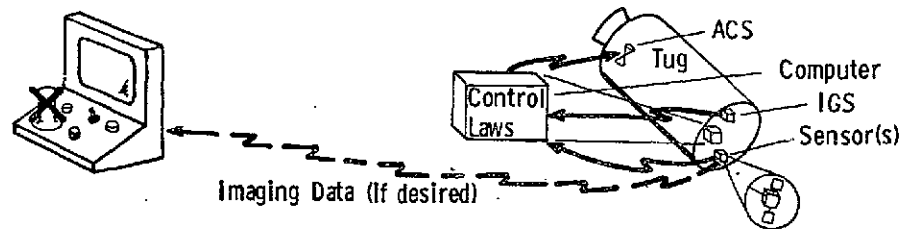
Docking

12. Docking Occurs, S/C Deactivated
13. Mechanism Contact Monitored
14. Hard Latch Commanded

Docking

14. STEM Extended Manually
15. STEM Inserted In Drogue Manually
16. STEM Is Retracted Manually
17. Soft Contact Monitored, S/C Deactivated
18. Hard Latch Commanded

Figure V-2: Manual System Operations Scenario



V-4

OLDOUT FRAME

Figure V-3: Autonomous System Operations Scenario

OLDOUT FRAME 2
C.3

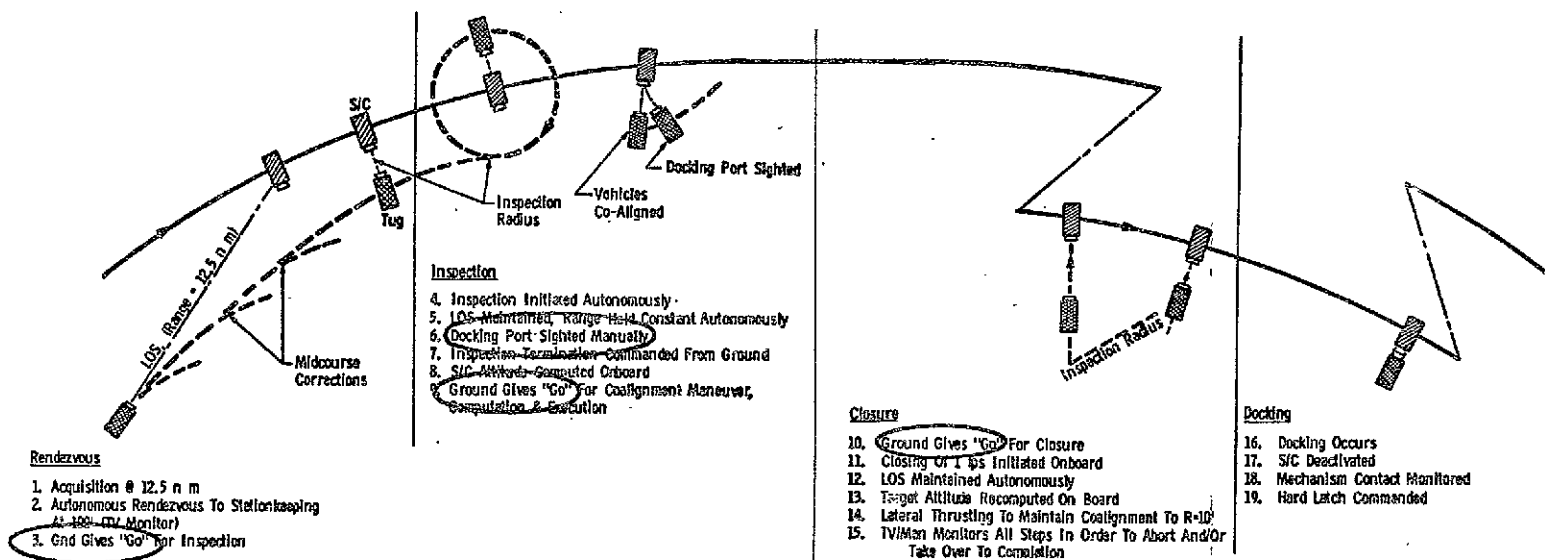
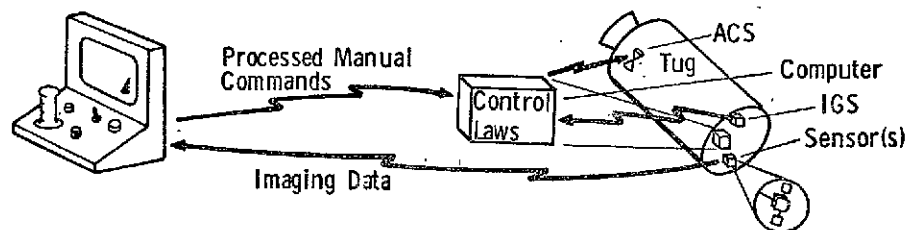


Figure V-4: Hybrid System Operations Scenario

A. MISSION OPERATIONS FUNCTIONAL INTERFACES

Mission model variations and economic factors dictate multiple spacecraft delivery and single retrieval on a single STS flight. Also, for schedule reasons, it is necessary to deliver one size spacecraft and retrieve another. These requirements increase the operations complexity and mission planning required. Complex trajectories are involved and operational interfaces must be established between the Tug control center and control centers for all spacecraft involved. The resultant communications network provides for spacecraft statusing before deployment, infant mortality retrieval, if required, and verification that the spacecraft is safe and ready for retrieval or servicing.

Operations interfaces for a manual rendezvous/docking system are illustrated in Figure V-5, since this system has the most mission operations involvement.

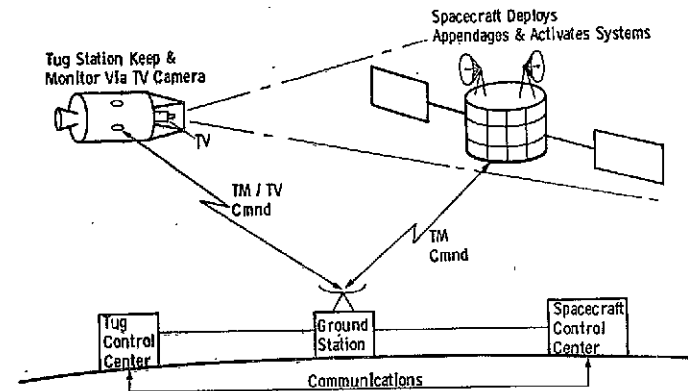


Figure V-5. Manual Docking System Maximizes Mission Operations Interfaces

For a manual rendezvous and docking system the TV image downlink data transmission for real-time support presents a data loading problem. Since the space tug has limited capability for data downlink, the image data is competing with other systems data on the downlink. Also, the network must handle orbiter, tug and other payloads data.

Several alternatives exist to solve this problem. Some onboard software data compression schemes are possible. Narrowing the scan field to eliminate useless background data, image data compression or processing of the image data and transmitting digitized range, range rate, line-of-sight and target attitude angle data and their rates for reconstruction on the ground, are options.

B. CONTROL HANDOVER CONSIDERATIONS

The NASA Space Tracking Data Network (STDN) or DoD Space Ground Link System (SGLS) station coverage is very good at high altitudes. However, the lower altitude coverage is minimal with the reduced number of stations planned. It is anticipated that the Tracking Data Relay Satellite System (TDRSS) will be operational and eliminate coverage voids in the time frame considered. Time delay variations in data transmission and loss of data when switching over from a ground station to the TDRSS must be accounted for and planned around. Control handovers during critical operations should be minimized and analyses were performed to determine methods of minimizing these handovers.

The reference spacecraft selected involve three distinct orbits which cover the range of orbital altitudes from 1667 km (900 n mi) to geostationary altitude and inclinations from 0° through 103° . The analyses included the percent of coverage (communication opportunity) by STDN/SGLS vs TDRSS and the RF transmission time delays for the reference spacecraft orbits. The results are summarized in Figure V-6.

The conclusions reached were that handovers may be minimized by using TDRSS for low earth orbits and using STDN/SGLS stations for medium and high earth orbits.

Another operational consideration included the lighting variations resulting from orbital parameters. This analyses was necessary from two aspects.

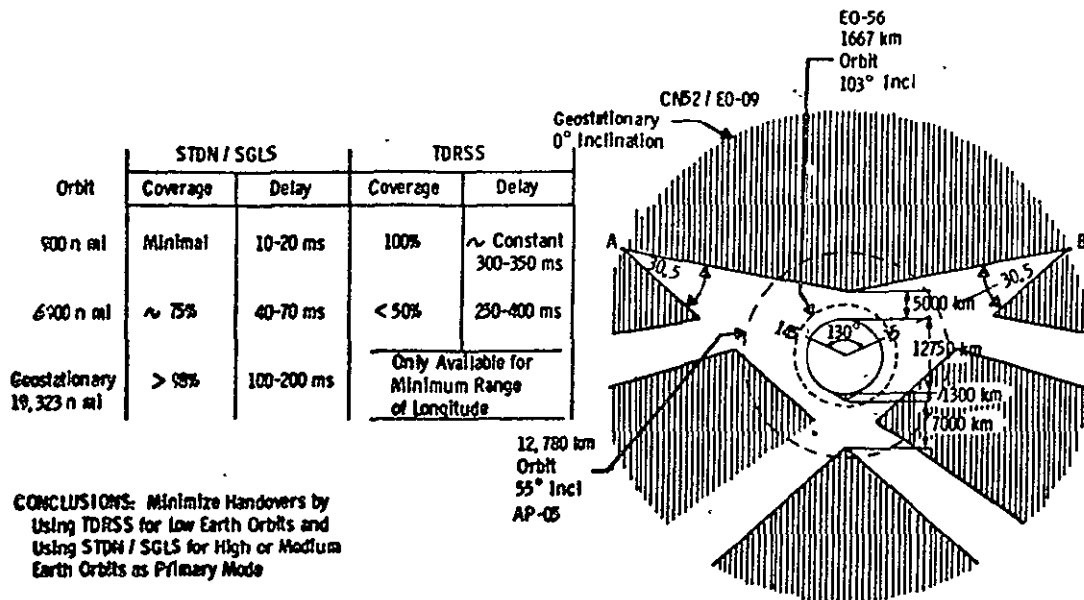


Figure V-6. Mission Control Handover Considerations

Since TV cameras and Scanning Laser Radar (SLR) sensors are being considered for the system, the pointing constraints must be considered. It is well known that some TV cameras cannot be pointed directly at the sun. The SLR operates on a reflected laser beam from the spacecraft being approached and the effects of pointing this sensor at the sun are unknown. Distinguishment of the target spacecraft from celestial bodies may be impacted in certain lighting situations. Each individual spacecraft will present a different operational planning problem based on time of launch and orbital variations. The simulation/demonstration tests for those candidate systems having TV sensors require high fidelity celestial scene simulation to determine the criticality of these effects.

An operational analysis was conducted to determine the variations in orbital day/night cycles for the reference spacecraft selected. The parametric data developed is presented as a family of curves which show percent of orbit in shade as a function of Beta angle and circular altitude. These results are shown in Figure V-7.

Since Beta is the angle between the sun line and the orbital plane, it varies seasonally with orbital precision and is a function of orbital inclination. The time in shadow is maximum for a given orbit when the Beta angle is zero.

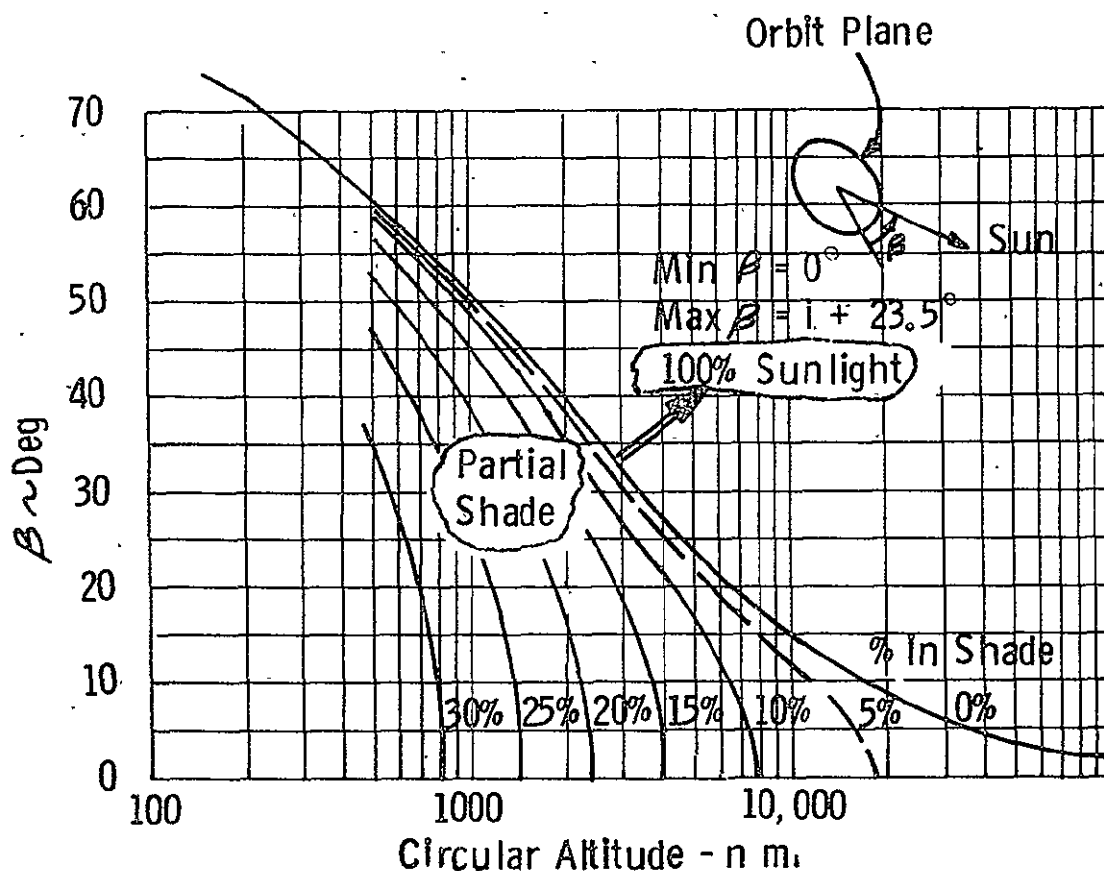


Figure V-7. Time in Darkness is a Function of Orbital Parameters

The maximum time in shadow for the selected reference spacecraft is tabulated in Table V-1 in the form of percent of orbital period and time (minutes)

The results of this operations analysis indicates that, although undesirable, the rendezvous and docking could be planned around these periods of darkness. However, the effect of shadowing the docking port by the spacecraft dictates a light should be provided on the tug to illuminate the docking port and any alignment aids provided by the spacecraft. As an operational constraint, the TV camera must not be pointed within $\pm \text{TBD}$ degrees of the sun line during the mission.

Table V-1: Reference Spacecraft are Shadowed less than 28% of orbital period

Spacecraft	Orbit Altitude	Maximum Time in Shadow
EO 56 - Environmental Monitoring Satellite	900 n mi	28% or 33.5 minutes
AP 05 - Environmental Perturbation Satellite	6,900 n mi	11% or 48.3 minutes
CN 52/EO 09 - Domsat/Synchronous Earth Observation Satellite	Geostationary 19,323 n mi	5% or 16.1 minutes

VI. SUPPLEMENTAL SENSOR ANALYSIS

A. RADAR SYSTEMS ANALYSIS

In compiling the data base of sensor hardware candidates, one area to which little emphasis was placed in recent Tug rendezvous and docking studies was the conventional RF radar as a ranging sensor. Consequently, not because of any bias toward this sensor but rather to treat all potential candidates fairly and with equal detail, a significant effort was made to configure feasible RF radar sensor candidates during this study. Requirements and performance definition had already been done for the other prime ranging systems - the laser radars - all of which was available and much of it applicable to this study. Specifically the most pertinent documentation is Reference 3 and 4 in Volume II. The remainder of this section will be to develop similar requirements and characteristics for RF radars performing a rendezvous and docking function at geosynchronous altitudes.

The first part of the effort was to canvas all available RF radar designs to determine applicability to a rendezvous and docking role. It was found that the RF radars and their functions were best examined in two roles; first, the rendezvous phase or from acquisition at ~ 12.5 nm to down to a range of ~ 100 feet; and secondly, the phase from ~ 100 ft. on to the minimum range at docking of $\sim 3'$ to $10'$. During the first phase, range, range rate and line-of-sight information was desired. For the second phase, data for target attitude derivation was also required, at least for some configurations.

An obvious and the only real candidate defined for accomplishing the first phase was a derivative of the Apollo LM rendezvous radar, which, even with modifications for a passive target and different range requirements, provided a benefit from previous development programs and related flight experience. In addition, the Shuttle Orbiter is proceeding toward procurement of a system with similar requirements to that for Tug. Its developments will undoubtedly benefit the Tug program.

The selection of candidates for the second phase, or close-in docking, was not as easy. No real development of a system fitting the Tug requirement has been done to date. Several designs have been proposed. Those considered as potential candidates for this study were:

- o FM (Coherent Wave radar (Ref. X)
- o Microwave Interferometer pulse radar
- o X-Band Coherent pulsed doppler radar

All of the above are new designs. From these candidates the X-band coherent pulsed doppler design was selected as most straight forward for the Tug rendezvous and docking application. It represented the least complexity, yet met the established requirements..

Four different types of rendezvous and docking systems were considered, each possessing a different configuration and/or set of requirements for the ranging sensor. Some of the candidates required a ranging sensor that performed only rendezvous, the docking being controlled by TV. Others required ranging sensor data on down to 3 to 5 feet. Also, candidates were configured that depended on a cooperative ranging sensor (passive retroreflectors on the target) and others specified non-cooperative (skin track) ranging sensors. The non-cooperative VS cooperative trade was pertinent only to the rendezvous, not the docking, phase requirements. A non-cooperative ranging system for close-in data gathering, specifically attitude determination, is not feasible.

In the following four sections, then a detailed derivation and discussion of requirements for the following RF radar candidate system is provided:

- Rendezvous radar (passive non-cooperative target)
- Rendezvous radar (passive cooperative target)
- Dual mode radar (passive non-cooperative target)
- Dual mode radar (passive cooperative target)

The dual mode radar, as it will be referred to hereafter, is a combination of two systems into a single unit, the conventional rendezvous radar discussed first, and the close-in X-band coherent pulsed doppler radar selected earlier. The non-cooperative VS cooperative for the dual mode refers only to the rendezvous part of the radar.

There is no requirement for a close-in radar by itself for the system candidates configured in Volume II.

1. Noncooperative Pulsed Doppler Rendezvous Radar - The basic Apollo/LM rendezvous radar was developed for NASA by RCA/Burlington and operated in the cooperative active mode with a transponder located on the target vehicle. This technology can be utilized in the design of a rendezvous radar for the Space Tug by employing a pulsed doppler radar with frequency diversity in the noncooperative mode. The radar operates at X-Band and provides precision angle tracking via an amplitude comparison monopulse system. Angle rate is obtained from a rate gyro mounted on the antenna. Range rate information is obtained directly by measuring the two way doppler frequency. An ICW radar design is employed with pulse modulation where the duty cycle is 40%. The advantages of such a design are that much of the circuitry used in the Apollo/LM radar can be employed and this reduces the cost of the rendezvous sensor. Further, accurate range rate information is obtained more efficiently than with either an SLR or a simple microwave pulsed radar. Due to the relatively small target uncertainty and search volume ($10^0 \times 10^0$) the radar can be operated unambiguously in a low PRF mode. Hence a constant PRF is employed during angle search with a correspondingly small eclipsing loss in the search mode, which can be ignored. The employment of frequency diversity increases the target radar cross-section in the noncooperative mode and reduces the radar power requirements. At X-Band, five r.f. frequencies 50 MHz apart can be employed without causing any problems due to excessive r.f. bandwidth, and this will increase the radar cross-section of the target vehicle to 10 meter².

The following parameters during target acquisition apply:

Search time: "ts" - 6 seconds

Angular Search Area: $A_\theta = 10^0 \times 10^0 = 100$

Initial Acquisition Range: $R_m = 50$ n miles

False Alarm Time: $T_{fa} = 1$ hr.

Required probability of detection: $P_d = 0.99$

Spacecraft radar cross-section: 10m²

Range rate ≤ 200 ft/sec

The PRF is 1.6 KHz yielding an unambiguous maximum range of 50 n miles. The antenna diameter is 3 ft., which at X-band yields a half-power beam width of 2.3^0 .

The dwell time of the radar beam on the target is then

$$t_d = \frac{\theta_b^2}{A_\theta} \quad t_s = \frac{(2.3)^2(6)}{(100)} \cdot (10^3) = 317 \text{ m-sec}$$

The number of pulses integrated during the dwell time is:

$$N = (\text{PRF}) t_d = (1.6)(10^3)(317)(10^{-3}) = 507$$

The probability of false alarm is then given by:

$$P_{fa} = \frac{N}{T_{fa} B} = \frac{507}{(3600)(10^3)} = 1.4 \times 10^{-4}$$

This assumes an acquisition bandwidth of $B = 1.0 \text{ KHz}$ for this ICW system.

For a radar system design with a probability of detection of $P_d = 0.99$, the signal to noise requirement for a Swerling Case 1 target with Rayleigh statistics is given by:

$$\frac{S}{N} = \left[D_0(1) + L_i - 10 \log_{10} N + \frac{h_f}{N_e} \right]$$

where:

$$D_0(1) = 14.5 \text{ db}$$

$$L_i = \text{integration loss} = 8 \text{ db}$$

$$L_f = \text{fluctuation loss} = 14 \text{ db}$$

Assuming a frequency diversity system with 5 equally spaced frequencies, we then get $h_f = 14/5 = 2.8 \text{ db}$. Since $N_e = 5$, the transmitter will transmit 101 pulses at each frequency for a period of 63 m-sec.

The signal to noise requirements are, then, given by:

$$\frac{S}{N} = (14.5 + 8 - 27 + 2.8) = 1.7 \text{ db}$$

The transmitter power requirements, i.e. the average transmitter power, is, then, given by:

$$P_{AV} = \frac{(S/N)(4\pi)^3 R_{\max}^4 F (KTB) L d_R}{G^2 \lambda^2 \sigma_T d_T}$$

where d_R, d_T = receiver duty cycle & duty cycle

L = system losses

The power balance is, then, given by:

Parameter	+db	-db
$(4\pi)^3$	33.0	
(S/N)		1.7
R_{\max}^4 (R = 50 .m.)	219.0	
KTb (B = 5.6 KHz)		174.-
F	6.0	
L	6.0	
G^2		74.0
λ^2 ($\lambda = 0.1$ ft)	20.0	
σ_T ($10 \text{ m}^2 = 108 \text{ ft}^2$)		20.0
d_R/d_T	1.6	
Totals	285.6	269.7

The average transmitter power requirements are then 15.9 dbw or 39 watts, which appears reasonable and allows a high-reliability transmitter design.

Range data in this ICW system are obtained by comparing the phase of the dimodulated tones from the received signals with the transmitted phase. From an information point of view, phase detection processing and early/late gate tracking should provide the same accuracy in the measurement of range. A quantitative assessment of the "random" range error of this ICW radar system can be obtained by utilizing the following expressions:

$$\sigma_{\phi} = \frac{1}{\sqrt{2} (S/N)} \quad \text{and} \quad \frac{\sigma_R}{R} = \frac{1}{\left(\frac{S}{N}\right)^{1/2} \frac{2B}{b} \eta}$$

where S/N = I.F. signal to noise ratio

B = I.F. bandwidth

η = duty cycle

b = servo bandwidth

In order to reduce prime power requirements and to maintain a reasonable dynamic range in the radar receiver, the transmitter power levels can be reduced for the terminal rendezvous phase. A 20 db reduction in power is assumed for this phase, and the receiver bandwidth is increased to 100 KHz. The resulting radar signal to noise ratio, σ_{ϕ} , and $\sigma_{R/R}$ at close range are listed in Table VI-1 below ($\eta = 0.4$, $B = 100$ KHz, and $b = 5$ Hz).

Table VI-1 Close-in Signal-to-Noise Ratio

Range (R)	(S/N)	$\sigma \phi$ - radians	$\sigma_{R/R}$
1000 ft	64.8 db	4.1×10^{-4}	2.6×10^{-9}
500 ft	76.8 db	1.0×10^{-4}	1.7×10^{-10}
300 ft	85.8 db	3.8×10^{-5}	2.1×10^{-11}
200 ft	92.8 db	1.6×10^{-5}	4.2×10^{-12}
100 ft	104.8 db	4.1×10^{-6}	2.6×10^{-13}

The results shown in Table VI-1 indicate that the "random" range error at close ranges is negligible. Hence, the range measurement accuracy will be determined solely by the bias error. The bias error has been plotted as a function of range in Figure VI-1. This error is determined by the highest tone frequency so that to achieve lower bias errors in the range measurement at close ranges would require a higher tone frequency. This change can be easily accomplished by adding an additional modulation tone at 820 kHz which will reduce the bias error to 10 ft. at a range of 100 ft. Without this modification, the range measurement accuracy at close ranges will be as shown in Figure VI-1. The range rate measurement accuracy is determined by the two way doppler measurement accuracy and will be 0.1 ft/sec at the close ranges considered here ($R \leq 1000$ ft). The angular accuracy is determined by the amplitude monopulse system and is again made up of "random" and "bias" component errors. Due to the high signal to noise ratios at close ranges the random error will again be negligible and the angular accuracy of the system will be determined by the bias error. This error is 8 mrad. per axis. A summary of the system characteristics for the modified Apollo/LM rendezvous radar is given in Table VI-2. A block diagram of the system is shown in Figure VI-2. The four modifications indicated in this block diagram are for the conversion of the current cooperative active Apollo/LM system to a high PRF non-cooperative rendezvous radar for the Shuttle orbiter. This modified system required a multiple PRF, pulsed doppler radar implementation because of the larger angular search volume, which will not be required in the Space Tug rendezvous radar. RCA/Burlington has built such a modified rendezvous radar for NASA/JSC under contract NAS9-13-576 ("Tracking Techniques for Space Shuttle Rendezvous").

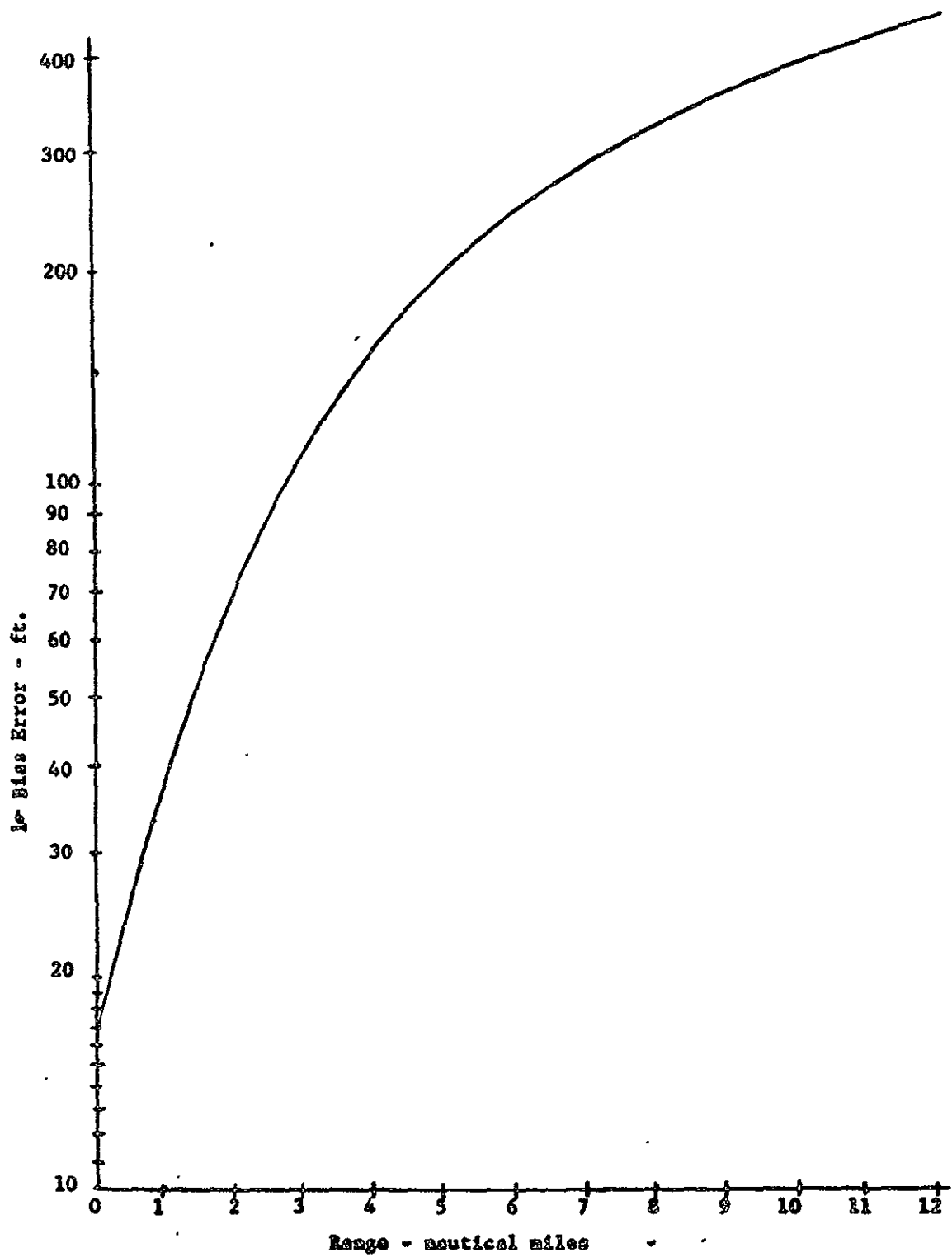


Figure VI-1: Modified Apollo/LM Rendezvous Radar-Range
"Bias" Error vs Range

Table VI-2. Radar Characteristics Summary - Modified Apollo/LM Radar

Type: Non-Coherent Pulsed Doppler
Frequency: X-Band ($\lambda = 3.2$ cms)
Modulation: ICW
PRF: 1.6 KHz
Duty Cycle: 40/60
Transmitter Average Power: 39 watts
Maximum Range: 50 n miles
Minimum Range: 100 ft.
Frequency Diversity: 5 frequencies 50 MHz apart
Target Radar Cross Section: 10 meter² (diversity)
Radar System Losses: 6 db
Radar Antenna: 3 ft. dia. dish (Cassegrain)
Antenna Beam Width: 2.3°
Angular Coverage: 10° x 10°
Acquisition Time: 6 seconds
Range Accuracy: See Figure VI-1
Range Rate Accuracy: 0.1 ft/sec
Angular Accuracy: 8 mrad (per axis)
Weight: Antenna 51 lbs
 Transmitter - 12 lbs Total weight - 85 lbs
 Electronics - 22 lbs
Input Power: 200 W(max)
MTBF: 2000 hrs

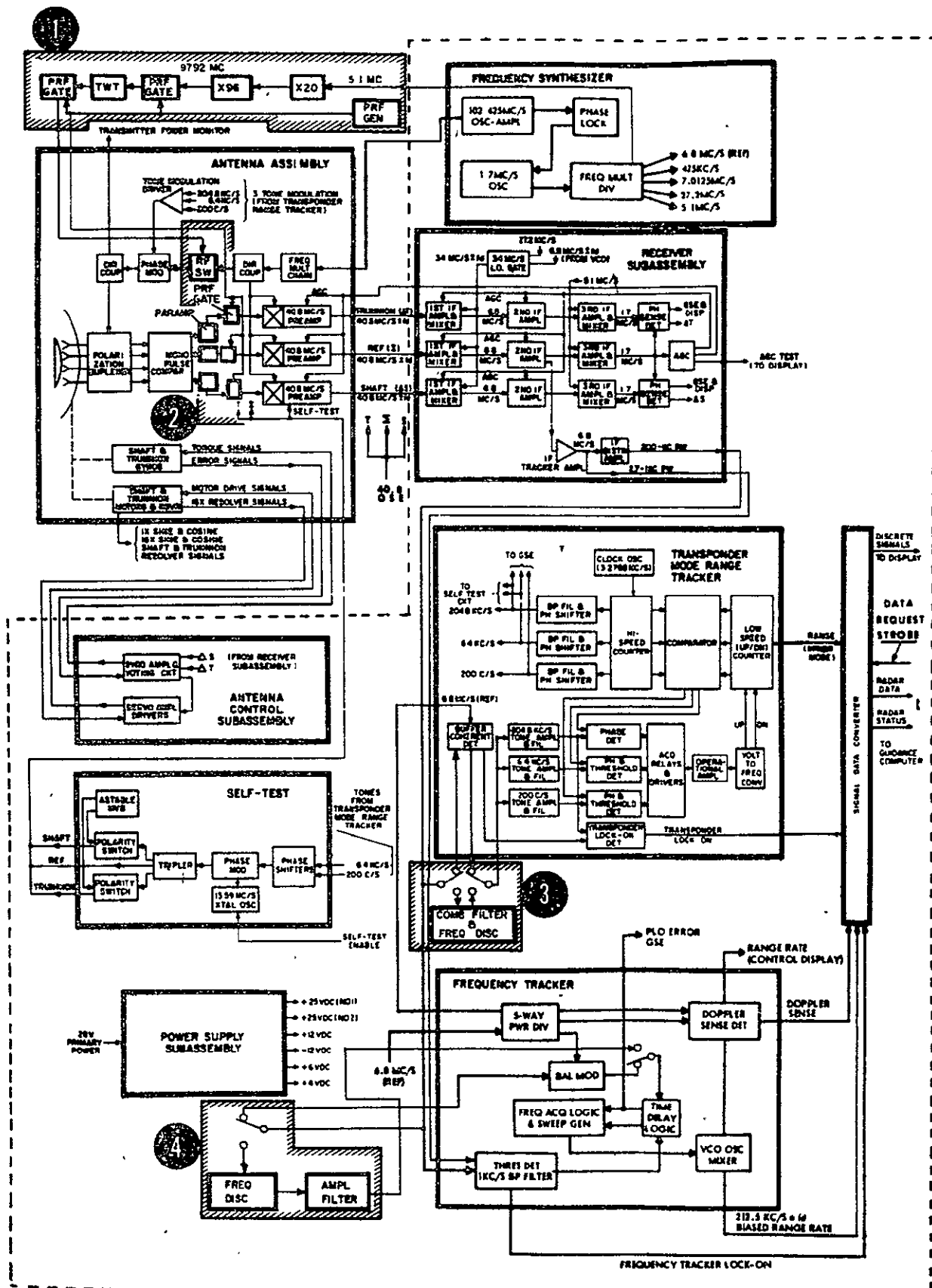


Figure VI-2 Rendezvous Radar Block Diagram

ORIGINAL PAGE IS
OF POOR QUALITY

This system employed 5 r.f. frequencies at X-Band and 5 PRF's and demonstrated excellent performance down to a minimum range of 100 ft. Thus, there is every reason to believe that a modified Apollo/LM radar can be built for the Space Tug that will operate satisfactorily down to 100 ft.

Another interesting tradeoff that was investigated involved a change in the diameter of the radar antenna. The 3 ft. diameter Cassegrain dish antenna employed in the Apollo/LM radar may conceivably cause some mechanical installation problems in the Space Tug docking adaptor. Thus, the effects of a smaller antenna diameter on the radar system performance were investigated and traded off against other radar parameters. In particular, a reduction of the antenna diameter to 2 ft. appeared to be interesting and a preliminary design was performed. The details of this tradeoff analysis are given below:

Antenna Diameter - 2 ft. Half Power Beam width = 3.45°

$$t_d = \frac{(3.45)^2}{100} 6 (10^3) = 714 \text{ m sec}$$

$$N = (1.6)(10^3)(714)(10^{-3}) = 1142$$

$$P_{fa} = \frac{1142}{(3600)(5.6)(10^3)} = 5.6 \times 10^{-5}$$

The increased antenna beam width and associated lower antenna gain can be traded off against a lower detection probability. For a radar system design with a probability of detection of 0.9 instead of 0.99 we get $D_0(1) = 12.5 \text{ db}$.

The new signal to noise requirements at 50 n miles are, then, given by:

$$S/N = (12.5 + 9.1 - 30.6 + 1.6) = -7.4 \text{ db}$$

The antenna gain for a 3 ft. diameter dish was 37 db at X-band. For a 2 ft. diameter dish, the antenna gain is:

$$G = \frac{E \pi^2 D^2}{\lambda^2} = 33.8 \text{ db and } G^2 = 67.5 \text{ db}$$

The new transmitter average power requirements can now be obtained by again employing the radar range equation, as follows:

$$P_{AV} = \frac{33.0 + 219.0 + 6.0 + 6.0 + 20.0 + 1.6}{7.4 + 174.0 + 67.5 + 20} = \frac{285.6}{268.9} = 16.7 \text{ dbw}$$

The average transmitter power requirements have now been increased to 16.7 dbw or 47 watts which is only slightly larger than the previous transmitter design. Hence, a similar transmitter can be employed and no substantial change in the transmitter weight is expected. However, there will be a reduction in the antenna weight due to the smaller dish so that an overall weight of 75 lbs. for the pulsed doppler rendezvous radar is now a realistic estimate. The system power requirements have been slightly increased to 200 watts.

A major change in the specifications of the acquisition parameters necessitated a revision of the acquisition strategy. The new specifications as determined at a meeting at NASA/Huntsville on 11/5/1975 are given below:

Search Time: "ts" = 1 minute

Target 3 σ uncertainty angle (per axis): $\pm 30^\circ$

Angular Search Area: $A_\theta = 60^\circ \times 60^\circ = 3600$

Initial Acquisition Range: $R_m = 25$ n miles

False Alarm Time: $T_{fa} = 1$ hr.

Required Probability of Detection: $P_d = 0.90$

Spacecraft Radar Cross Section: 10 m^2 (diversity)

Range Rate 200 ft/sec

In contrast to the situation where the angular search area is relatively small, the requirement of a larger search area of $60^\circ \times 60^\circ$ results in a substantially larger eclipsing loss that has to be accounted for in the power balance. To minimize this loss, a multiple PRF approach during search will be employed. This concept is similar to the modified Apollo/LM radar for the Shuttle Orbiter application. For the 2 ft. diameter antenna, the dwell time of the radar beam on the target is, then:

$$t_d = \frac{(3.45)^2 (60)}{3600} (10^3) \sim 200 \text{ m-sec}$$

The doppler uncertainty is 4 kHz for a relative velocity of 200 ft/sec. The radar acquisition bandwidth will be maintained at 1 KHz, so that the dwell time of the signal in this bandwidth, when the radar is simultaneously searching in doppler, is 50 m-sec. During this interval five different PRF's are employed at the following frequencies:

$$\begin{aligned}
\text{PRF}_1 &= 85 \text{ KHz} \\
\text{PRF}_2 &= 85.75 \text{ KHz} \\
\text{PRF}_3 &= 86.5 \text{ KHz} \\
\text{PRF}_4 &= 87 \text{ KHz} \\
\text{PRF}_5 &= 89.4 \text{ KHz}
\end{aligned}$$

Hence, each PRF is turned on for a period of 10 m-sec. Similarly, to take advantage of the frequency diversity system, five different carrier frequencies are again employed during this 50 m sec time interval. Hence, each r.f. carrier frequency is turned on for a period of 10 m-sec. The bandwidth-integration time product is, then:

$$n = B \frac{t_d}{4} = (10^3)(50)(10^{-3}) = 50$$

The probability of false arm, is, then:

$$P_{fa} = \frac{50}{(3600)(10^3)} = 1.39 \times 10^{-5}$$

This is slightly better than the P_{fa} for the single PRF system and assumes an acquisition bandwidth of 1 KHz for this ICW system implementation.

The signal to noise requirements for this system and a detection probability of $P_d = 0.90$ is, then, given by:

$$\frac{S}{N} = (12.5 + 4.5 - 17 + 1.6) = +1.6 \text{ db}$$

The new power balance for $P_d = 0.9$, $G^2 = 67.5 \text{ db}$ (2 ft. diameter antenna), and $R_m = 25 \text{ n miles}$ is shown below:

Parameter	+ db	- db
$(4 \pi \frac{R_m^2}{\lambda^2})^3$	33.0	
R_{max} ($R_m = 25 \text{ nm}$)	207.0	
(S/N)	1.6	
KTb ($B = 1 \text{ KHz}$)		174.0
F	6.0	
L	11.0	
G^2		67.5
λ^2 ($\lambda = 0.1 \text{ ft}$)	20.0	
σ_T ($10 \text{ m}^2 = 108 \text{ ft}^2$)		20.0
d_R/d_T	1.6	
Totals	280.2	261.5

Here, the system losses "L", are the total system losses including the eclipsing loss. The average transmitter power requirements are 18.7 dbw or 74 watts, which again appears reasonable and allows a high reliability transmitter design. A summary of the system characteristics for this system is given in Table VI-3. The system modifications in Figure VI-2 for the modified Apollo/LM radar, now, would apply to the Space Tug Radar as well.

Table VI-3 Radar Characteristics Summary - Modified Apollo/LM Radar

Type: Non-Coherent, Pulsed Doppler
Frequency: X-Band (λ = 3.2 cms)
Modulation: ICW
PRF: 85 KHz, 85.75 KHz, 86.5 KHz, 87 KHz, 89.4 KHz
Duty Cycle: 40/60
Transmitter Average Power: 74 watts
Maximum Range: 25 n. miles
Minimum Range: 100 ft.
Frequency Diversity: 5 r.f. carrier frequencies 50 MHz apart
Target Radar Cross-section: 10 meter² (diversity)
Radar System Losses: 11 db (inc. eclipsing loss)
Radar Antenna: 2 ft. diam. dish (Cassegrain)
Antenna Beam width: 3.5°
Angular Coverage: 60° x 60°
Range Accuracy: See Figure VI-1
Range Rate Accuracy: 0.1 ft/sec
Angular Accuracy: 8 mrad (per axis)
Weight: Antenna - 41 lbs
 Transmitter - 12 lbs Total - 75 lbs.
 Electronics - 22 lbs.
Input Power: 275 watts (max.)
MTBF: 2000 hrs.

2. Rendezvous Radar for Passive Cooperative Rendezvous - A detailed description of the pulsed doppler rendezvous radar was given in Part I. It describes a radar which utilizes a "non-cooperative" rendezvous radar for acquisition and tracking from a maximum range of 25 n miles down to a minimum range of 100 ft. This system employs frequency diversity and, therefore, requires no target aids or corner reflectors. A similar system can be employed in the cooperative passive mode with some savings in power and weight if a corner reflector is used on the target vehicle.

Employment of a single trihedral corner reflector at the docking port of the spacecraft will reduce power requirements and acquisition time in the case where the attitude of the spacecraft with respect to the Tug is known apriori to within $\pm 40^\circ$ of the radar boresight axis. If the attitude of the spacecraft is not known apriori then an array of corner reflectors would have to be employed to obtain 360° solid angle coverage. An alternative target aid configuration is a Luneberg lens which is insensitive to target aspect angle and will provide an almost constant radar cross-section as a function of the spacecraft attitude. This type of target aid can also be mechanized in terms of two hemispherical lenses each of which would cover a 180° solid angle. Unfortunately these devices are somewhat bulky and do not lend themselves to a simple mechanical installation on the spacecraft. However, they should be considered in spacecraft applications where volume restrictions are not of paramount importance. The radar cross-section of a Luneberg lens "Ecco" Reflector is given by:

$$\sigma = \frac{4\pi^3 r^4}{\lambda^2} \quad \text{where; } r = \text{radius of spherical lens used}$$

$\lambda = \text{wavelength}$

Measured values of these lenses are close to the predicted radar cross-section (see Figure VI-3). Ecco reflectors are available in almost any specified size in the range of 3" to 48" nominal diameter. At X-Band the Emerson & Comming Inc. Type 140 lens gives a return over a full 140° solid angle with the 3 db points at $\pm 65^\circ$. A 12 in. diameter lens will have a maximum radar cross-section of 65 meter² and will guarantee a 30 meter² cross-section over a 130° solid angle. This design appears attractive for certain installations and would allow a 4.8 db reduction in radar transmitter power with some reduction in sensor weight. The weight of this target aid is 11 lbs. Omni-azimuth Luneberg lens Ecco reflectors are also

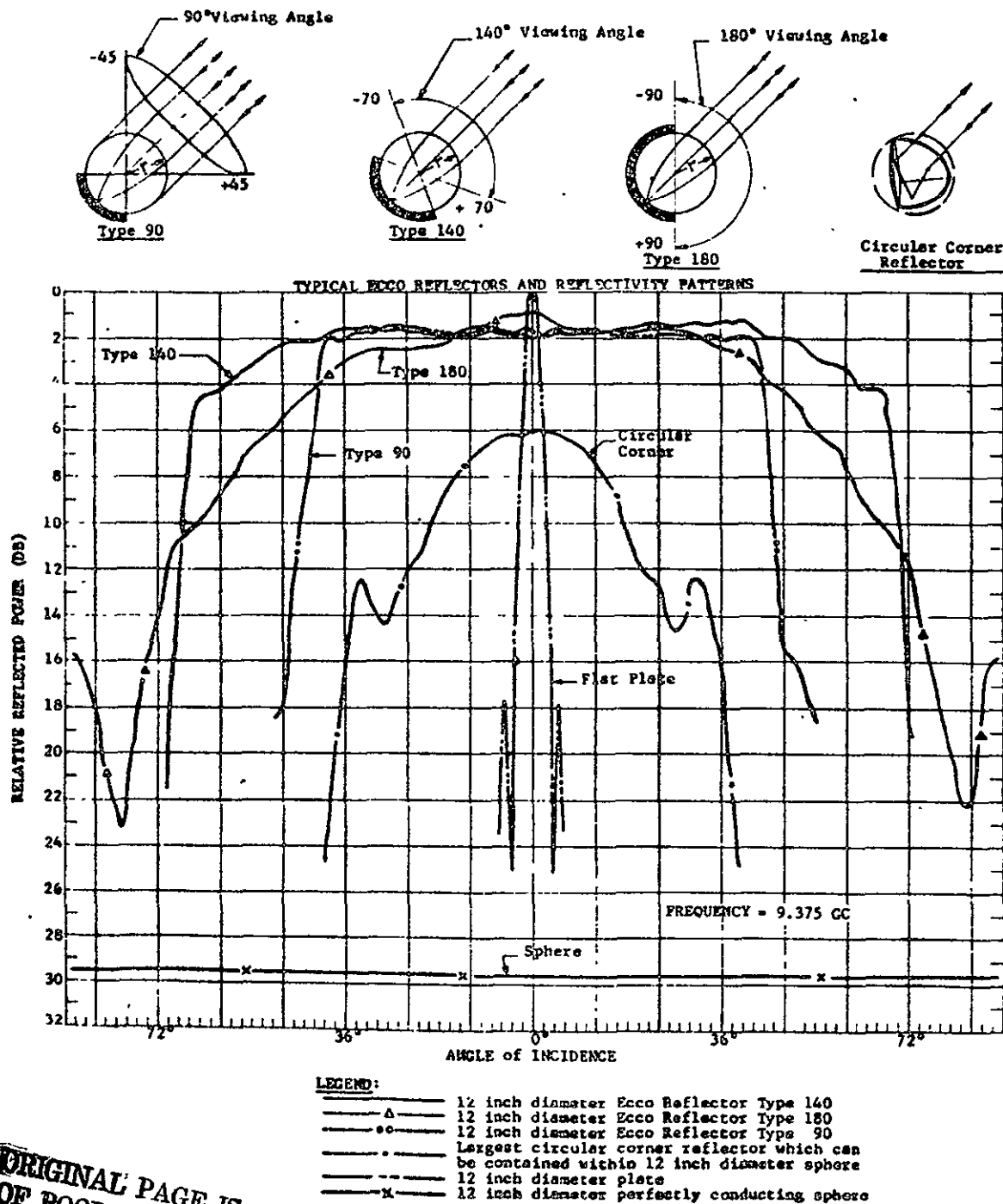


Figure VI-3 ECCO Reflector Experimental Data

available with a uniform value of radar cross-section for all values of azimuth angles and for elevation angles within the range of approximately $\pm 15^\circ$. In this case, clusters of reflectors would not be required for complete azimuth coverage, but the penalty for this feature is a greatly reduced effective target radar cross-section. Thus, a 12 inch diameter omni-azimuth lens will have a radar cross-section of 13 meter² at X-band and will weigh approximately 13 lbs. Omni-Directional Luneberg lens reflectors which provide full 360° solid angle coverage are also available but are not recommended because of their still lower radar cross-section.

Another target aid configuration is a two-dimensional Van-Atta array which is a phased array antenna designed to irradiate the radar signal in the direction of the incident wave. This device can be implemented as a flat microstrip array and will provide effective coverage over a $\pm 60^\circ$ angle. Thus, again, multiple devices would be required to cover the full range of aspect angles if the spacecraft attitude is not known. This device could be incorporated into solar arrays and panels with a minimum amount of interference thus providing angular coverage over a region which is normally inaccessible for other target aids. Still, the most popular radar target aid for the rendezvous mission is the corner reflector. If the orientation of the spacecraft is not known apriori a minimum of 6 corner reflectors would be required, and the size and installation considerations for these target aids becomes important.

If a trihedral, triangular course reflector is employed, the radar cross-section of such a target aid is given by:

$$= \frac{4\pi a^4}{3\lambda^2} \quad \text{where: } a = \text{side of course reflector}$$

$$\lambda = \text{wavelength}$$

To provide an apparent target radar cross-section of 15 meter² then would require a corner reflector having a 0.8 ft length on each side at X-Band. This size appears reasonable for a cooperative passive rendezvous system. In the absence of a target aid (non-cooperative mode) a target radar cross-section of 10 meter² can be achieved regardless of the spacecraft orientation if a frequency diversity radar is employed instead of a monofrequency radar. This radar implementation would employ five X-Band frequencies 50 MHz apart for a total bandwidth

of 250 MHz. The apparent target radar cross-section for this mode is 10 meter². This is brought about by the complex scattering pattern of the target vehicle which contains many peaks and nulls which are frequency dependent. Hence, a frequency diversity radar will effectively see the average target radar cross-section which is substantially greater than the mono-frequency radar cross-section. Thus, by employing a frequency diversity system in the cooperative passive mode the radar should never see a target cross-section of less than 10 meter² even if it is not pointed to within $\pm 40^\circ$ of the axis of the corner reflector target aid.

A comparison between a non-cooperative and cooperative passive rendezvous radar was made in the report "Radar Acquisition and Tracking Systems". For a target aid consisting of a 0.8 ft trihedral corner reflector with a 15 meter² radar cross-section, the radar characteristics as well as the estimated size and weight are given below:

Type: Non-Coherent, pulsed doppler system
Frequency: X-Band (3.2 cms)
Peak Power: 10 Kw
Pulse Width: 1 μ sec 0.2 μ sec
PRF: 1.6 KHz 8.0 KHz
Duty Cycle: 1.6%
Average Power: 16 watts
Radar System Losses: 6 db
Diversity Bandwidth: 250 MHz (3.75%)
Radar Antenna: 3 ft. diam. dish (Cassegrain)
Antenna Beamwidth: 2.3°
Angle Tracking: Amplitude Comparison Monopulse
Receiver Bandwidth: 1.4 MHz 7.0 MHz
Angle Tracking Accuracy (1σ):
 Bias - 8 mrad.
 Random - 2 mrad.
Range Accuracy (1σ): 24 ft.
Acquisition Time: 6 sec.
Maximum Range: 25 n miles

Minimum Range: 100 ft.

Estimated MTBF: 2000 hrs.

Weight: 70 lbs

System Power: 120 watts

Search Volume: $60^{\circ} \times 60^{\circ}$

Target Aid:

Trihedral, triangular Corner Reflector - 0.8 ft on side

Target Radar Cross-Section - 15 meter²

Alternate Approach: Passive, Microstrip Van-Atta Array (located
on solar panels) or 12" Luneberg Ecco Reflector
(Type 140)

3. Dual Mode Radar (Passive Non-cooperative) - The dual mode radar is comprised of the rendezvous radar, described earlier in part 1, and a new design close-in radar for ~ 300 ft on in to at least 3 ft from the target. This section will describe only the close-in design, however, a summary of both will be provided at the end of this section. A discussion of the target aids for this close-in design is also presented in this section.

In the docking mode ($R < 328$ ft) the radar utilizes a wide pulse width to allow time sharing of the received pulse from the target vehicle tracking aids. These tracking aids consist of 4 passive antennas and delay lines equally displaced about the docking port. The geometrical layout is illustrated in Figure VI-4 which also gives rough dimensions of the antennas. The 4 antennas are identical, circularly-polarized microstrip antennas with a relatively broad beam width, i.e. a half-power beam width of about $40-60^\circ$. Each antenna is terminated by a delay line and reflecting short circuit. Hence, the target aids are completely passive and require no power from the spacecraft. Each delay line has a different amount of delay so that the reflections from each target aid can be readily separated by the radar. The minimum amount of delay required in each delay line is set by the transmitted pulse width and the target depth in order to avoid arrival of the return pulse while the long transmitted pulse is still on, and to allow receiver gating of all reflections from the spacecraft to avoid problems due to glint and scintillation. This should allow the radar to operate all the way to docking except for field of view limitations. After establishing the minimum delay required for each delay line, the pulse returns are "tagged" by adding additional delay to each target aid which allows separation of the returns on a time shared pulse basis. Range is measured by utilizing the target aid return providing the smallest delay, i.e. by measuring the roundtrip pulse propagation time to the leading edge of the return pulse utilizing a wide bandwidth receiver (100 MHz bandwidth) to provide the necessary range measurement precision. A digital range measurement implementation can be employed to determine target range in increments of 1 nano-second which provides a range accuracy of 6 in.. This is similar to the SLR range measurement technique. Range rate can be obtained by differentiating the range data or by performing doppler measurements. If the relative velocity of the target spacecraft with respect to the Tug is too low it may be

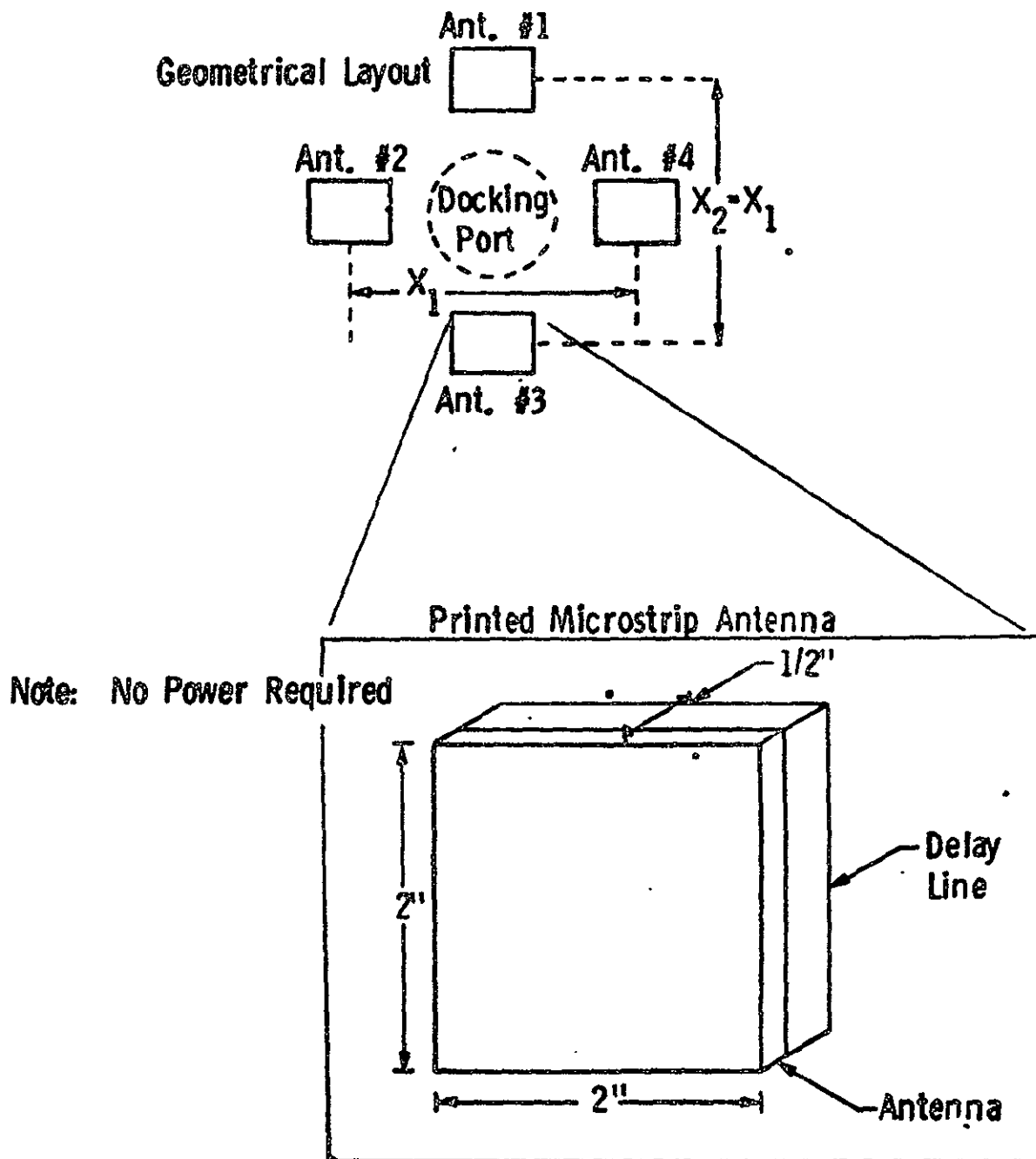


Figure VI-4 Passive RF Tracking Aids (Docking Mode)

desirable to employ the former approach. An alternative method of providing the multiple target measurements is to employ multiple receiver channels, range gated at different times to cover the appropriate interpulse interval. Each channel would, then, contain a filter bank covering all velocities of interest during the docking phase. Angle measurements are performed with the amplitude comparison monopulse system of the rendezvous radar, although for the docking mode measurements a phase comparison monopulse implementation would be preferred. All of the radar measurements may be obtained in either digital or analog form. This provides digital information to the guidance computer and analog data for astronaut monitoring.

The measurements obtained by the radar during the docking phase will, therefore, yield the following parameters:

- (1) Range to the 4 target aids equally displaced around the docking ports
- (2) Angle and angle rates to the 4 target tracking aids
- (3) Roll angle between the 2 vehicles (derived)

By measuring the range and angles to the 4 target aids the relative target attitude and the relative roll angle between the 2 vehicles can be calculated without the use of active equipment on the spacecraft.

The location of the target aids on the spacecraft is determined by the resolution capability of the docking radar. The target aids may be assumed to be point source targets, so that the angular resolution of the radar can be obtained from the following expression:

$$\sigma_{\theta} = \frac{\theta}{K_m \sqrt{S/N \text{ PRF/b}}}$$

In order to allow the radar to operate at short ranges it is desirable to utilize a radar antenna with a wide enough beamwidth to properly illuminate all four target aids. This can be accomplished in a dual-mode radar by removing the subreflector from a Cassegrain antenna system so that the radiation pattern of the radar is simply the illumination pattern of the hyperboloid subreflector. In a monopulse tracking radar a four-horn feed is normally employed to provide this illumination. The illumination beamwidth is typically 30° or greater.

An alternative approach would be to employ a separate antenna cluster at the back side of the subreflector and switch in this monopulse array at the start of the docking phase of the rendezvous mission. We may, then, utilize the following parameters:

$$\begin{aligned}\theta &= 30^\circ & \text{PRF} &= 1 \text{ kHz} \\ K_m &\sim 1.5 & b &= 5 \text{ Hz} \\ \theta &= \frac{30}{1.5 \sqrt{S/N (200)}} \text{ deg.} = \frac{24.7}{S/N} \text{ mrad.}\end{aligned}$$

Hence, to achieve an angular accuracy of 3 mrad or better requires a system signal to noise ratio of at least 20 db. This will directly affect the maximum range of the docking sensor for a given separation of the target aids on the spacecraft. Assuming a maximum range of 500 ft. and a target aid separation of 3 ft, it should, then, be possible to employ a docking sensor with an angular accuracy of 3 mrad.

The radar equation can now be employed to obtain the radar transmitter power requirements for the docking mode. A monopulse feed consisting of a 4 horn cluster with a total aperture of 2.75" x 2.75" will be assumed for the radar antenna. This array has the following characteristics at X-band:

E - Plane Beamwidth: 30°
H - Plane Beamwidth: 29.5°
E - Plane Sidelobe Level: -22.2 db
H - Plane Sidelobe Level: -23.6 db
E - Plane Error Slope Per Sum Beamwidth: 1.42
H - Plane Error Slope Per Sum Beamwidth: 1.50
Gain Factor: 0.59

Antenna Gain:

$$G = 0.59 \left(\frac{4\pi A}{\lambda^2} \right) = 15.5 \text{ db}$$

A circularly polarized, microstrip antenna having an aperture of 2" x 2" will be assumed for the target aid antenna. This antenna has the following characteristics:

Beamwidth: 43.5°
Gain: 14.2 db

System losses are assumed to be 10 db which includes the losses due to the delay line terminating the target aid antenna. A wideband receiver must be employed in the docking mode in order to achieve the required range measurement accuracy. Hence, a receiver bandwidth of 100 MHz is selected for preliminary calculations which should yield an accuracy of about 6 in. in the range measurements to the four target aids. The system power requirements for the docking mode are, then, calculated from the radar range equation:

$$P_T = \frac{(29.94)(10^3) \left(\frac{S}{N}\right) R^4 KTB F_n}{G_T^2 G_R^2 \lambda^4 L}$$

where: $\frac{S}{N}$ = signal to noise ratio
 R = range
 B = receiver bandwidth
 F_n = receiver noise figure
 G_T = radar antenna gain
 G_R = target aid antenna gain
 L = system losses
 λ = radar wavelength

The power balance is given below:

Parameter	+db	-db
$(29.94)(10^3)$	44.0	
S/N	20.0	
R^4 ($R_{max} = 500$ ft)	108.0	
KTB ($B = 100$ MHz)		124.0
F_n	6.0	
G_T^2		31.0
G_R^2		28.4
λ^4 ($\lambda = 0.105$ ft)	39.2	
L (inc. delay line)	10.0	
Totals	227.2	183.4

The peak power requirement for docking mode operation is, then, 43.8 dbw or 24 Kw. The transmitter peak power requirement for the rendezvous mode has previously been calculated at 44 Kw so that, despite the larger receiver bandwidth, sufficient power should be available from the transmitter of the dual-mode radar. The average transmitter power for docking mode operation is given by:

$$P_{AV} = (24)(10^3)(10^3)(9)(10^{-6}) = 216 \text{ watts}$$

This is about a factor of 3 greater than the average transmitter power in the rendezvous mode at maximum range ($R = 25 \text{ n.m.}$). However, it is still feasible to use the same radar transmitter if other parameters in the radar range equation are appropriately modified. A reduction in the radar pulse repetition frequency is probably the simplest way of achieving this goal since the relative velocity between the 2 vehicles during the docking phase is very low. Thus, it is relatively easy to reduce the PRF to about 320 cycles which would yield the same average power as in the rendezvous mode. A reduction in the servo loop noise bandwidth to 3 Hz will then maintain an angular resolution of about 3 mrad.

The minimum range limitation of the sensor is again dictated by antenna field of view limitations since the delay line in the target aid will theoretically allow the radar to operate to contact. For a nominal radar antenna beamwidth of 30° and a target aid spacing of 3 ft., the "pseudo" minimum range of the radar is 5.6 ft. This assumes illumination of the target aid antennas at the half-power point and obviously shorter ranges are possible with reduced range measurement accuracies. Although this would appear adequate, operation at shorter ranges could also be achieved by broadening the radar antenna beamwidth so that minimum ranges of 2 ft. could be readily implemented.

The range measurement accuracy is mainly determined by system bandwidth considerations and a digital pulse ranging system is normally employed in the automatic mode to measure the pulse propagation time delay to the target aid and back. This is determined by a leading edge measurement on the return pulse so that the r.m.s. time error in the pulse delay measurement is a function of the leading edge perturbation by noise. This is given by the following expression:

$$T = \frac{1}{B\sqrt{S/N}}$$

Hence, utilizing a docking radar system with a receiver bandwidth of 100 MHz and a system signal to noise ratio of 20 db (R = 500 ft), we get:

$$T = \frac{1}{(100)(10^6) \sqrt{100}} = 1 \text{ n-sec}$$

This corresponds to a range measurement accuracy of 6 inches at maximum range, which appears more than adequate. As the two vehicles come closer together the system signal to noise ratio will increase, thus improving the range measurement accuracy and providing greater accuracies in the relative target attitude and roll angle determination. This results because the S/N ratio increases as the fourth power of the decrease in range and the angle tracking noise error decreases as the square root of the increase in the S/N ratio (see previous discussion). The above parameters selected for docking mode operation thus appear reasonable for preliminary design purposes and indicate that a dual-mode radar is indeed feasible for rendezvous and docking and will do a satisfactory job in isolating the docking port from the remainder of the spacecraft structure. This can be accomplished without the use of a scanning system so that range and angle data to the 4 target aids is always available.

A summary table of a dual-mode radar which can provide the docking measurements as well as the search acquisition, and track functions required for rendezvous is given below:

Type: Non-Coherent, Pulsed Doppler

Frequency: X-Band (λ 3.2 cms)

Modulation: ICW

PRF: 85 KHz, 85.75 KHz, 86.5 KHz, 87 KHz, 89.4 KHz

Duty Cycle: 40/60

Transmitter Average Power: 74 watts

Maximum Range: 25 n miles

Minimum Range: 100 ft.

Frequency Diversity: 5 r.f. carrier frequencies 50 MHz apart

Target Radar Cross-section: 10 meter² (diversity)

Radar System Losses: 11 db (inc. eclipsing loss)

Radar Antenna: 2 ft. diam. dish (Cassegrain)
Antenna Beamwidth: 3.5°
Angular Coverage: $60^{\circ} \times 60^{\circ}$
Range Accuracy: See Figure 1
Range Rate Accuracy: 0.1 ft/sec
Angular Accuracy: 8 mrad (per axis)
Weight: Antenna - 41 lbs
 Transmitter - 12 lbs Total - 75 lbs.
 Electronics - 22 lbs
Input Power: 275 watts (max)
MTBF: 2000 hrs.

Docking Mode

Peak Power: 24 Kw (reduces as R^4)
Pulse Width: 9 μ sec (time shared received pulse)
PRF: 320 Hz
Average Power: 67 watts
Antenna: Same (subreflector removed) or four-horn cluster on back side of
 subreflector
Antenna Size: 2.75 in. x 2.75 in.
Half-Power Beamwidth: 30°
Receiver Bandwidth: 100 MHz
Maximum Range: 500 ft.
Minimum Range: 2 ft.
Range Measurement Accuracy: 6 in. ($R = 500$ ft)
Angle Measurement Accuracy: 3 mrad
Total Sensor Weight: 80 lbs
Input Power: 275 watts max.
MTBF: 3000 hrs.

Target Aids

Rendezvous Mode: None (Frequency Diversity)
Docking Mode: 4 passive antennas & delay lines in "Diamond" configuration
 around docking port
Antenna: Flat, microstrip antenna (2" x 2" aperture)

Antenna Beamwidth: 43.5°
Antenna Polarization: Circular
Antenna Gain: 14.2 db
Power Requirements: None
Target Aid Weight: 2 lbs
Target Aid Spacing: 3 ft.

The operational docking mission utilizing this sensor is quite similar to missions utilizing the SLR sensor in the cooperative passive mode. The docking phase will include inspection, alignment, closure, and docking and will start from a stationkeeping phase at a range not exceeding 500 ft. The radar sensor is mounted on the Space Tug and the target aids are mounted on the spacecraft surrounding the docking port. A minimum target aid spacing of 3 ft. is desired. The hardware mounting locations and the Space Tug docking trajectory are such as to keep the target aid array within the radar's field of view throughout the final docking phase. During the inspection and alignment phase the Space Tug orientation will be adjusted via the Space Tug guidance system until the target aid array falls within the 30° FOV of the radar and the target aids are required. The guidance system will accept the range, range rate, and angle data and the relative target attitude and roll angle data will be computed. The system will act on this data to decrease the range and eliminate vehicular orientation errors according to the desired docking trajectory. As the range between the 2 vehicles decreases the range and angle measurement accuracies of the radar will improve until the minimum range of 2-5 ft. is reached where the docking parameter errors are negligible. During the docking phase, then, the radar will continuously track the target aids until the LOS, pitch, and yaw errors have been nulled out and the radar is tracking on "boresight", utilizing the sharp pattern null of the monopulse tracking patterns.

The advantages of a dual-mode radar are summarized below:

- (1) High measurement accuracies at close ranges (Docking accuracies comparable to those of the SLR sensor system)
- (2) Low minimum range limitation
- (3) No glint or scintillation errors at short ranges

- (4) Easy location and isolation of docking port
- (5) Automatic handover from rendezvous sensor
- (6) Automatic docking mission operation by closing the loop directly through the guidance system
- (7) State-of-the-art sensor design and previous experience from Apollo/LM rendezvous system development
- (8) Implementation with highly reliable components that are already space qualified.

4. Dual Mode Radar (Passive Cooperative) - The dual mode cooperative radar is merely a combination of the rendezvous system described in Part 2 and the close-in radar discussed in Part 3. Consequently no further detailed discussion is required, however a summary of the characteristics taken from those earlier sections, is provided here for completeness.

Rendezvous Mode

Type: Non-Coherent, pulsed doppler system
Frequency: X-Band (3.2 cms)
Peak Power: 10 Kw
Pulse Width: $1 \mu \text{ sec} \infty 0.2 \mu \text{ sec}$
PRF: 1.6 KHz ∞ 8.0 KHz
Duty Cycle: 1.6%
Average Power: 16 watts
Radar System Losses: 6 db
Diversity Bandwidth: 250 MHz (3.75%)
Radar Antenna: 3 ft. diam. dish (Cassegrain)
Antenna Beamwidth: 2.3°
Angle Tracking: Amplitude Comparison Nonopulse
Receiver Bandwidth: 1.4 MHz ∞ 7.0 MHz
Angle Tracking Accuracy (1σ):
 Bias - 8 mrad.
 Random - 2 mrad.
Range Accuracy (1σ): 24 ft.
Acquisition Time: 6 sec.
Maximum Range: 25 n miles
Minimum Range: 100 ft.
Estimated MTBF: 2000 hrs.
Search Volume: $60^\circ \times 60^\circ$

Rendezvous Target Aid:

Trihedral, triangular Corner Reflector - 0.8 ft. on side
Target Radar Cross-Section - 15 meter^2
Alternate Approach: Passive, Microstrip Van-Atta Array (located on solar panels) or 12" Luneberg Ecco Reflector (Type 140)

Docking Mode

Peak Power: 24 Kw (reduces as R^4)
Pulse Width: 9 μ -sec (time shared received pulse)
PRF: 320 Hz
Average Power: 67 watts
Antenna: Same (subreflector removed) or Four-Horn cluster on back side
of subreflector
Antenna Size: 2.75 in. x 2.75 in.
Half-Power Beamwidth: 30°
Receiver Bandwidth: 100 MHz
Maximum Range: 500 ft.
Minimum Range: 2 ft.
Range Measurement Accuracy: 6 in. (R = 500 ft.)
Angle Measurement Accuracy: 3 mrad.
Target Aids: 4 passive antennas & delay lines in a "diamond" configura-
tion around docking port. See Part 3.
Total Sensor Weight: 75 lbs.
Input Power: 275 watts max.
MTBF: 3000 hrs.

B. VIDEO SENSOR ANALYSIS

The TV camera is an integral and, in fact, the key element in a manual rendezvous and docking system. In space related activities, to date, it has generally performed only the function of gathering an image and transmitting it to a viewer, either onboard or on the ground, leaving him to perform the necessary actions. In the manual configuration this is still basically the role of the camera. It was found, and is proposed, that some of the relatively busy and critical tasks of the ground controller can be relieved by providing an autonomous capability to do some processing of the TV imaging data onboard and use the output to perform some vehicle control functions; e.g., maintaining the Tug line-of-sight on the center of the target.

When considering the TV in an autonomous role, this and considerably more image processing capabilities must be added. These were assumed to be feasible when configuring those autonomous candidates employing a TV. This approach provides considerable potential toward improving system performance via software processing additions. It certainly warrants further studies and implementation concept development.

Image data processing is of special interest to the Tug program. The baseline Tug downlink data rate of 50 Kbs places a finite constraint on the rate of which pictures can be sent to the ground. General Dynamics' Space Tug Avionics Definition Study assumed a new picture on the ground only once each 16 seconds. This makes reliable ground control of the Tug a marginal situation at best. Some onboard image data processing and control command computation is one possible approach to relieving this concern. Another possible alternative, and one that should be pursued in parallel with the image data processing studies, is to incorporate data compression of the imaging data onboard, followed by reconstruction on the ground. Studies by MMC, and others, has shown considerable reduction of data can be accomplished for very minimal loss of picture quality.

The thrust of this section, then, will be threefold; first, detailed discussions of hardware requirements for the TV camera and its lighting aids will be presented in Part 1. Following that, in Part 2, are results and related discussion of some TV image data processing feasibility work done at Martin Marietta.

Recommended additional effort is also provided. Finally, some concepts for image data compression and related discussion is provided in Part 3.

1. TV Camera Requirements - The space tug will use a television camera as an aid in inspection of and docking with a satellite. The satellite will be passive in these procedures, but it may have such features as retroreflectors, visual orientation cues, and other passive (non-powered) facilities.

The docking may be a man-in-the-loop, autonomous, or manually supervised semi-autonomous procedure. The camera will be required to function at a maximum distance of 100 feet from the satellite. At this distance it must allow study of one-foot-diameter surface features in detail in order to permit determination of satellite relative orientation and to allow visual inspection of the satellite before docking is attempted.

Because the satellite may be in the shadow of the earth during this procedure, lighting must be provided by the tug to allow camera operation in the absence of solar illumination.

The data link to the operator will permit approximately one picture of 525 lines by 430 pixels every 10 to 20 seconds, but data compression techniques may be employed to increase this rate substantially.

Several camera types, existing or yet to be developed, may be suitable to meet the technical requirements for space tug, but the ultimate selection criterion is cost, technical performance being adequate. Other factors such as bandwidth, power required, weight, and size become important largely as they impact the cost of the total system.

One way to reduce cost is to use, to the extent possible, technology that has already been developed or is being developed for other programs. The space shuttle camera, shortly to be developed, will be operating in a similar environment with similar requirements and is a case in point. If it should prove to meet tug requirements, using it with minor modifications would save the cost of developing a new camera for the tug. The intended characteristics of the shuttle camera are summarized in Table VI-4. It is possible the shuttle may be able to use a silicon vidicon tube. It is anticipated tug requirements will require an intensified target tube.

TABLE VI-4 SHUTTLE CAMERA CHARACTERISTICS

TYPE	1" Silicon Intensified Target (SIT) Vidicon Tube
FOV.	20°
RESOLUTION	525 Lines by 430 Pixels
CAMERA SURVIVABILITY	Look Directly at Sun
OUTPUT BANDWIDTH	4.5 Megahertz
DYNAMIC RANGE.	Approximately 10,000:1
TARGET ILLUMINATION REQUIRED .	5 to 10 foot Candles
MAXIMUM LENGTH	12"
POWER.	15 Watts at 28 VDC
WEIGHT	15 Pounds
IMAGE SCAN RATE.	30 Times/Second
LIGHTING	Strobe or Tungsten Flood Lamps
DEVELOPMENT STATUS	RFP in Spring 1976; ATP 11/76

The tug camera will be used for autonomous, man-in-the-loop or manually supervised semi-autonomous docking, for satellite inspection, and for close-in range determination. Lighting during these operations may vary from full sun to earth shadow. The camera should have the ability to look directly into the sun without damage, and the tug should have the ability to provide illumination of the satellite. The data link to earth permits direct transmission of one picture every 10 to 20 seconds, but this rate can be increased by the use of data compression, as discussed elsewhere in this report, to the order of one frame every several seconds. Some on-board data processing algorithms have already been developed by Martin Marietta.

Compatibility of Shuttle Camera Specifications with tug requirements is summarized below:

- a. Type - The silicon intensified vidicon is one of the most sensitive types of television camera tube. For this reason it will minimize the amount of illumination the tug must provide. The resolution required by the tug application is in the range achievable with this camera tube, and the wide 500:1 to 1000:1 dynamic range inherent in this technology minimizes the mechanical adjustment required for the aperture of the camera lens.

b. Resolution and Field of View - The 525 lines in a 20° field of view specified for the shuttle camera will cover a one-foot wide area at 100 feet with $525/(200 \tan 10^\circ) = 15$ lines, which is adequate to display details of objects this size, as required for tug. As the tug approaches the target, smaller details will be resolved. Further, the rendezvous system is able to point the tug accurately enough to acquire the satellite within the 20° field of view.

c. Camera Survivability - The candidate camera is specified to be capable of looking directly at the sun. This implies that special protective measures, such as a shutter, will be incorporated in the camera to protect the intensified target tube. A silicon vidicon type of camera tube does not necessarily require this special handling.

d. Output Bandwidth and Scan Rate - The output bandwidth of a camera is a function of the scan rate and number of picture elements specified for the picture. Scan conversion electronic components are required to reduce the bandwidth of the shuttle camera to the allowed transmission bandwidth for tug. If an image dissector camera tube were used, the scan rate could be lowered directly, but the other advantages of the shuttle camera would be lost.

e. Target Illumination and Lighting

The shuttle camera characteristic requires that the target be illuminated to a level of 5 to 10 foot Candles (5 to 10 lumens per square foot). The power required to furnish this illumination can be estimated as follows.

Assume a Xenon Short-Arc Lamp within a reflecting housing such that 75 percent of the light produced falls within a 20-degree-diameter circular cone coincident with the field of view of the camera. The area on the surface of a sphere of 100 ft radius illuminated by this cone of light is 970 square ft, and the lamp must produce $4700/.75 = 13000$ lumens in order to average 10 lumens per square foot over this area. A well-designed reflector can assure that the edge of the cone will receive not less than half as much illumination per unit area as the central area, and the illumination within the cone will everywhere be greater than 5 lumens per square foot. The Xenon Short-Arc

Lamp has a luminous efficiency of approximately 22 lumens per watt; the lamp power required is about 600 watts, when it is illuminated.

The camera scans at 30 frames per second, and the lamp need be illuminated only a minimum of two scan periods for each picture to be transmitted to the operator, a maximum of one picture each 3 seconds. The duty cycle of the lamp can therefore be 0.022. Assuming the efficiency of the power supply circuitry to be 0.8, the input power to the overall lamp and its control will average $600 \times 0.022 / 0.8 = 16.5$ watts when the lamp is operating to illuminate the target.

Another function of the target illuminator is to illuminate the retroreflectors or the visual cues furnished to indicate relative orientation of the target with respect to the tug during docking operations. These retroreflectors will always appear much brighter to the camera than their surrounding background on the target, and should present no unusual problem to the monitoring operator or to the circuitry designed for their detection and data processing. The retroreflectors themselves must be designed to produce return beams large enough to accommodate the geometry of the positions of the illuminators with respect to the camera. Several kinds of retroreflectors are available for this purpose, including optical corner cubes, optical "cat's eyes", beaded screens, and the like.

In summary, then, the SIT vidicon camera, yet to be developed for the Space Shuttle, with the characteristics outlined in Table VI-1, will be suitable for use on Tug, and would probably be a cost-effective implementation. Scan conversion equipment will be required to adapt its essentially conventional TV scan rate to the much lower data rate allowed by the ground communication link for Tug. When the final camera selection is made for Tug, other camera implementations should be subjected to analysis of their possible contributions to the overall system cost effectiveness.

2. TV Image Data Processing - A study by Martin Marietta for NASA Langley Research Center (Contract NAS1-13558) was conducted that focused on the use of the TV for generating data other than just images for visual viewing. The title of the final report is "Video Guidance, Landing, and Imaging Systems for Space Mission" by Roger T. Schappell, Robert L. Knickerbocker, John C. Tietz, Christopher Grant, Robert B. Rice, and Richard D. Moog. The study was concerned with exploring the adaptive potential of video guidance technology for earth orbital and interplanetary missions. The premise is that since a number of imaging systems are available and will undoubtedly be flown on future spacecraft for scientific imaging, inspection or remote control functions, it is logical to explore further utility and capability of these sensors in terms of autonomous real time target acquisition, pointing, and tracking, thereby augmenting the primary guidance, navigation, and attitude control hardware, and enhancing the scientific data gathering ability of the vehicle.

More specifically, the study was concerned with the application of video acquisition, pointing, tracking, and navigation technology to three primary missions--a planetary lander, an earth resources satellite, and spacecraft rendezvous and docking. The emphasis is on making maximum use of available information to enhance the onboard decision-making capabilities of a given spacecraft.

The synopsis of the study results to be discussed in this section relates to the latter application; spacecraft rendezvous and docking. It has been established that most future spacecraft such as Space Tug, Earth Orbital Teleoperator Spacecraft and Free Flying Satellite Experiments will carry a TV camera for manned observation and possibly remote control. Since a camera is available and the potential mission requirements are such that real time autonomous operation would extend the operational capability of the chosen vehicle, consideration must be given to making maximum use of available data such as the video output. A discussion of the feasibility of this technique and experimental results follows.

The primary objective of the study was to develop algorithms for the missions discussed above and to evaluate them in the laboratory using a physical

simulator and scaled surface models. The first phase of the study resulted in a successful feasibility demonstration of the planetary landing site section system.* Subsequent to this, other algorithms were developed and tested for the earth resources and rendezvous and docking missions, respectively.

The approach taken was as follows:

- 1) Establish the reference mission requirements and constraints.
- 2) Perform the necessary analytical and digital simulation studies in order to assist in arriving at representative guidance and navigation requirements.
- 3) Develop video data processing algorithms as a function of target characteristics and observables.
- 4) Breadboard video data processing logic and integrate it with the TV camera, display, and physical simulator.
- 5) Develop software for automating experiments and for providing a permanent record of results.
- 6) Design and build scaled surface models.
- 7) Integrate and checkout 6D simulator, breadboarded algorithms, scan electronics, TV camera, surface model, and PDP-9 scientific computer.
- 8) Run experiments and document results.

The significance of this study, as verified by the analytical and experimental results, is that the output of a scanning sensor system such as a TV camera can be operated on by conventional filtering techniques and simple processing algorithms to arrive at an adaptive and autonomous sensor system capable of making intelligent decisions with regard to the observed area or constituent of interest.

* Schappell, R. T., Knickerbocker, R. L., Tietz, J. C., Grant, C., and Flemming, J. C., Final Report, Video Guidance, Landing, and Imaging System (VGLIS) for Space Missions, NASA CR-132574, February 1975.

In other words, one does not require large computational complexity and hardware to provide a degree of intelligence for the applications of interest in this study. On the other hand, further experimental work is required to provide a more comprehensive definition and selection of the observables, and to optimize the algorithms and data formatting electronics for a particular mission. This future activity is discussed in the summary and recommendations section.

· Theory of Operation - The following discussion outlines an approach to automatically provide steering and stationkeeping on an unmanned vehicle for rendezvous and inspection of other spacecraft. The system comprises a TV camera, specialized scan control, analog pre-processor or dedicated microprocessor and onboard digital computer as shown in Figure VI-5. The system components function in much the same way as the planetary lander video guidance system in that the digital computer provides a supervisory function while data rate computation is performed in the microprocessor hereafter referred to as the video processor (VP). Large data block storage in the spacecraft digital computer and a high-speed A/D converter interface are, therefore, not required. The system is essentially self-contained, thus minimizing processing by the onboard computer.

The several different tasks will be based on a common sequence of processing. The camera is commanded to scan a certain area of given coordinates and size of scan in the field of view. The VP operates on the camera data and issues discrete values to the spacecraft digital computer at the end of a frame. The digital computer then decides what the next camera operation and VP function will be. A wide variety of tasks may be accomplished in this manner depending on the digital computer software. With this scheme, all mundane calculations are performed in the VP leaving the digital computer free for other work and allowing lower data rates on A/D converters. Also, detailed logic and complex calculations are resident in the digital computer which is best suited to this purpose.

As an example of this type of processing, consider the problem of horizon detection. Assume the object is a bright disk on black background. The digital computer would set the camera frame size to be approximately twice the

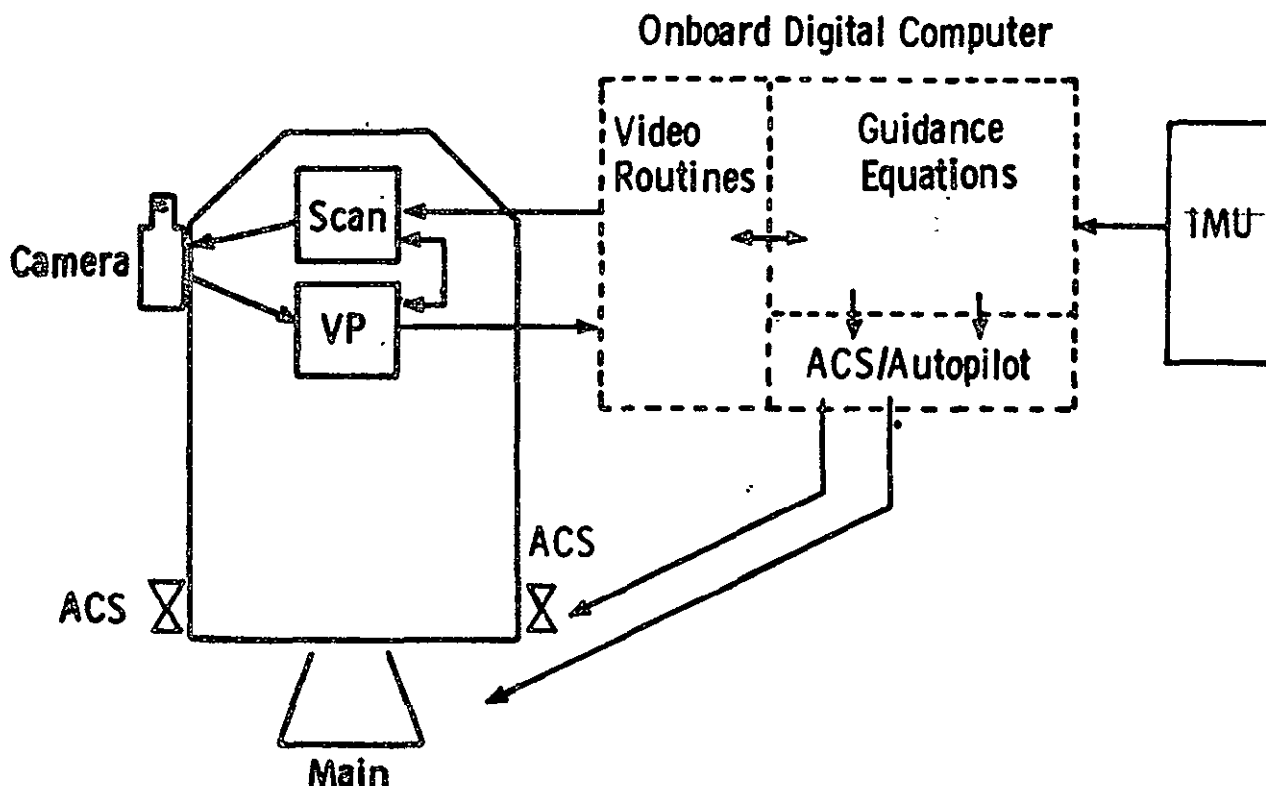


Figure VI-5 Onboard Rendezvous and Docking System Configuration

expected area of the object. A frame would be scanned in which the VP would take the following functions: Integral video (threshold), first X moment, first Y moment. At the end of scan, this information is passed to the digital computer which calculates area, diameter and center in X and Y coordinates. The next step would be to scan four smaller frames which would be positioned to cross the limb in each of four directions for more accurate measurement. The digital computer would command each of these in sequence and retain the results for a precise determination of object relative position. During scans the digital computer is free for other tasks while the VP is collecting data.

The basic functions required in the VP, of course, depend on the particular task, but it would appear the following are adequate for most and are surprisingly easy to accomplish in the analog hardware as well. The following functions are to be calculated over one frame of scan.

Ave - Integral of the video signal
 S_X - First moment of the video signal in the X direction
 S_Y - First moment of the video signal in the Y direction
 I_{XX} - Second moment of the video signal in the X direction
 I_{YY} - Second moment of the video signal in the Y direction
 I_{XY} - Cross moment

Figure VI-6 shows a block diagram of the VP. As shown, some thresholding and filtering of the video is required. The system shown is a small analog version of the processor. It is commanded directly by the digital computer.

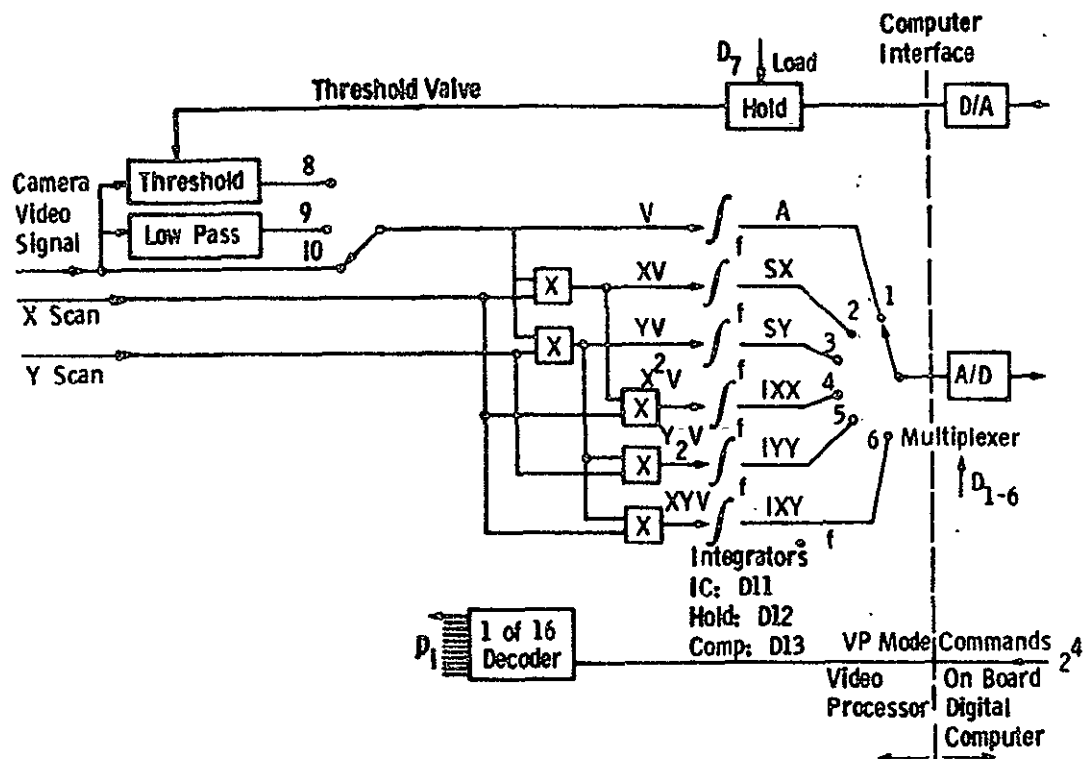


Figure VI-6 Video Processor Block Diagram

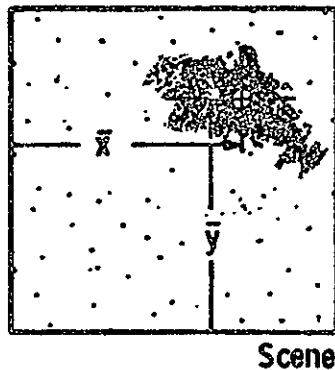
It is also possible to mechanize these functions in a microprocessor.

- 1) Far Steering
- 2) Near Steering

3) Feature Detection and Inspection (Track Intermittently)

- a) Spacecraft sizing
- b) Axis orientation determination
- c) Spin rate determination
- d) Home on predetermined features
- e) Determine whether dock is feasible
- f) Docking maneuver

Figure VI-7 shows a simplified scene and the associated video function required for far steering. The guidance equations determine when the object is within range and field of view. Then a frame is scanned and the VP takes A , S_X , and S_Y . The digital computer then calculates \bar{X} and \bar{Y} in camera coordinates and translates these to steering signals. At the appropriate distance, determined from \underline{A} (proportional to size) or a ranging device, the system changes to near steering logic, as shown in Figure VI-8.



VP Functions/Frame of Scan

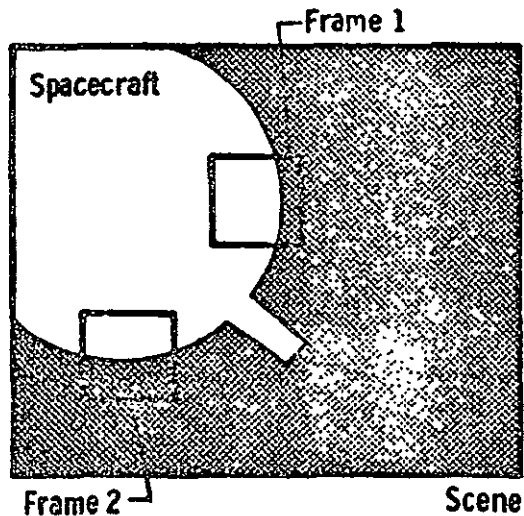
$$\begin{aligned}
 A &= \int_f \text{Video}^* dt \\
 S_X &= \int_f \text{Video} X_S dt \\
 S_Y &= \int_v \text{Video} Y_S dt
 \end{aligned}$$

Then the Object Center is Defined by

$$\begin{aligned}
 \bar{X} &= S_X/A \\
 \bar{Y} &= S_Y/A
 \end{aligned}$$

• It May be Required for Low-Pass Filter to Remove Starfield and Modify the Gray Scale for Contrast Enhancement

Figure VI-7 Far-Steering Video Functions



Given Approximate Data from Previous Scans, Accurate Relative Position Is Obtained by Scanning an Area Covering Object Boundaries in Two or More Places. By Knowing the Commanded Scan Coordinates and the Relative Placement of the Camera, Frame 1 Yields Data on the X Position of the Spacecraft Edge, While Frame 2 Shows What the Y Coordinate Is.

Figure VI-8 Near-Steering and Stationkeeping

Figure VI-8 shows one possible method of near steering and stationkeeping to be performed while doing other tasks. This approach may be used while taking pictures, looking for predetermined features, or performing surveillance maneuvers.

Following are a few of the functions which may be performed with the appropriate software additions and the same basic hardware.

- Geometric area
- Average brightness
- Major and minor axes of an equivalent ellipse
- Angular orientation of major axis
- Search for predetermined feature
- Track feature (i.e., automatic docking)
- Determine spin axis and spin rate (software may be quite complex)

Physical Simulator and Video System Electronics - Figure VI-9, the rendezvous and docking experimental system, involves a camera and electronics mounted on a 3-degree-of-freedom translation servo. A PDP-9 computer commands

the scan position of the camera and samples the video signal at that point in the field of view.

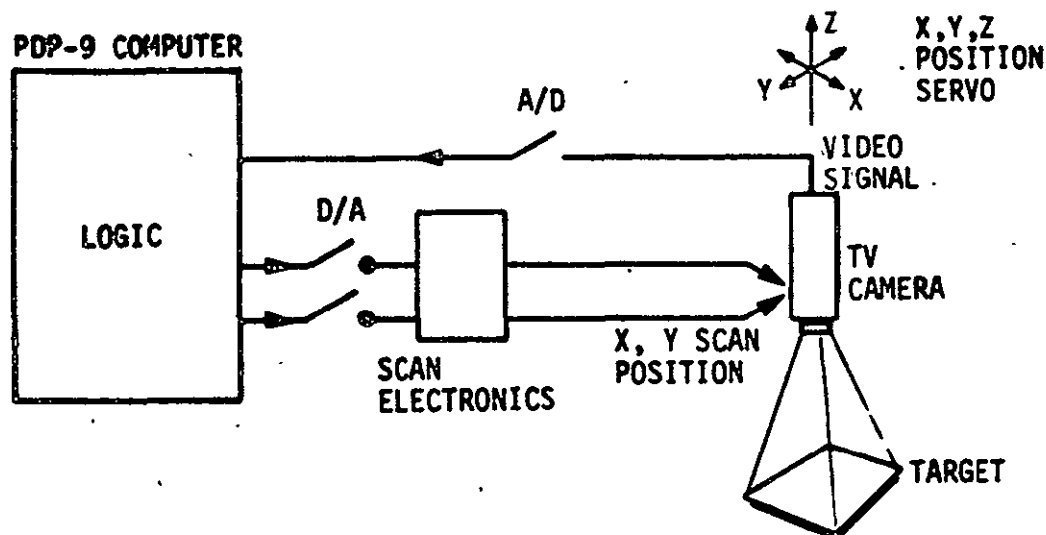


Figure VI-9 Laboratory Setup

The following algorithms were tested in the laboratory with representative scenes: Calculations for area, object center, angular orientation, and ranging. A means of recording the scene scanned by the camera was developed. The actual scene is shown in Figure VI-10. Figure VI-11 is essentially a brightness map with the video signal quantitized on a scale of 0-9. Each number represents a sample point brightness. In this case, the frame is composed of 5000 points, 100 in the X direction and 50 in the Y. The printout is dimensionally distorted due to the fixed printer spacing.

In order to calculate area and centers more accurately, thresholding was used on the video signal. This sharpens edges and excludes background clutter. It is assumed the object of interest is brighter than the background. The logic used is; if the video signal is larger than the threshold, a "one" is assigned to the pixel; if it is less, a "zero" is assigned. Figure VI-12 is a thresholded version of Figure VI-11. In the following, only threshold signals are used.



Figure VI-10 Test Scene

ORIGINAL PAGE IS
OF POOR QUALITY

BRIGHTNESS HISTOGRAM

Figure VI-11 Digitized Brightness Map; 0 = Dark, 9 = Light

Several targets of known areas were placed in front of the camera. Repeated measurements of the 1 sq. in. objects were used for calibration. Table VI-5 shows the system calculations of the object areas. It is felt that the larger errors on the small object are due to the coarseness of sample points. Repeatability was checked with several other objects of varying size. Experimental results are shown in Table VI-6 for a simulated satellite.

Table VI-5 Area Calculations

Shape	Actual Area	System Calculation
Square	.25 in. ²	.313 in. ²
Square	1	.996 in. ²
Rectangle	2	1.918 in. ²
Rectangle	2	1.882 in. ²
Satellite	--	2.837 in. ²

Table VI-6 Area Measurement Repeatability

Shape	Measurements (1.000 = Frame Size)	Mean	Std. Dev.
Dot	.0072, .0070, .0042, .0034, .0054, .0056	.0055	.0015
Ats	.088, .0918, .0928, .091, .0912	.0910	.0018
Oval	.2084, .2088, .2070, .2124	.2092	.0023

It is seen that there is a sizable dispersion on the smaller object measurements in relation to its area calculation.

Geometrical center calculation tests were performed to simulate conditions of small far-off objects and also near objects with discernable shapes. Figure VI-13 illustrates a small bright dot which was moved around the field of view. The equipment-calculated center has been scaled and drawn onto the figure (marked X and Y) to show how well the hardware worked. The area of the dot is approaching the coarseness of the sample points; hence, the area calculations are poor. Nonetheless, the center was calculated correctly. Figure VI-14

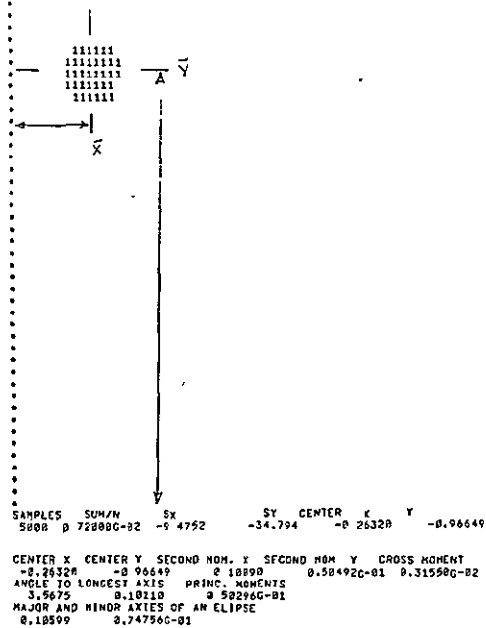


Figure VI-13 Object Center Test A

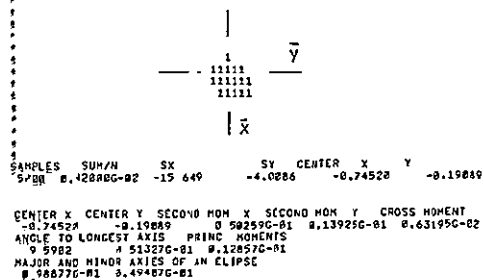


Figure VI-14 Object Center Test B

shows some bias in the Y direction. Figures VI-15 and VI-16 show the images for a representative spacecraft in different orientations. The algorithm appears to have found the same point on the object in each test.

The orientation algorithm was used to calculate the angle from local horizontal to the major axis of an oblong object. Figure VI-17 shows two images produced by these tests. The calculated angles and centers have been drawn on the printouts for reference. The angles range from -90° to 90° since the algorithm does not distinguish one end of the object from the other.

Figure VI-18 and VI-19 illustrate the use of two cameras separated by a distance $2d$, plus center-finding calculations to find range data. To simulate this, the laboratory camera was translated in the X direction for the second picture. Using the formula derived previously:

$$\text{Range} = \frac{2df}{X_L - X_R} = \frac{2 \times 1. \times 5.9}{1.2, 24 - .60546} = 19.4 \text{ feet}$$

Although it is not clear what this range means for a 3-dimensional object, which may have projections toward and away from the viewer, this problem can be circumvented by viewing only a portion of the object of interest and ranging that small area alone. This would involve feature detection prior to ranging.

Basic Algorithms - The integral of the video signal over a frame provides the average brightness of the scene. This signal is useful for automatically setting camera iris. If the video signal is thresholded such that if it is below a certain level, a zero is produced; and if it is above that level a one is produced. The, the integral of this signal over a frame is the sum of the geometric areas of the bright objects in the field of view. The objective is to set the threshold at a value which passes the object of interest and eliminates the background noise. Fortunately, if the object is large enough in the field of view, background noise (stars) will not contribute significantly to the area calculation.

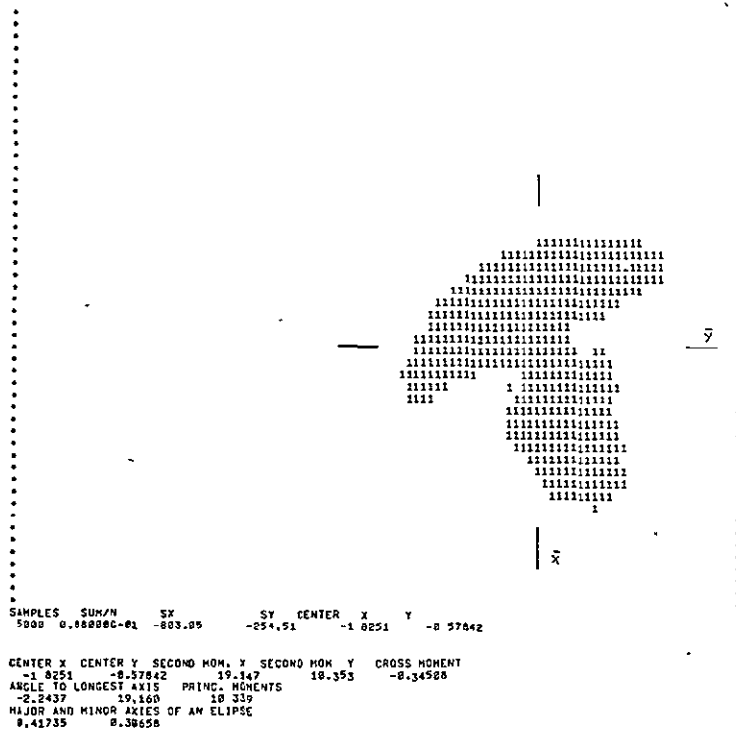


Figure VI-15 Center Test, Simulated Spacecraft 1

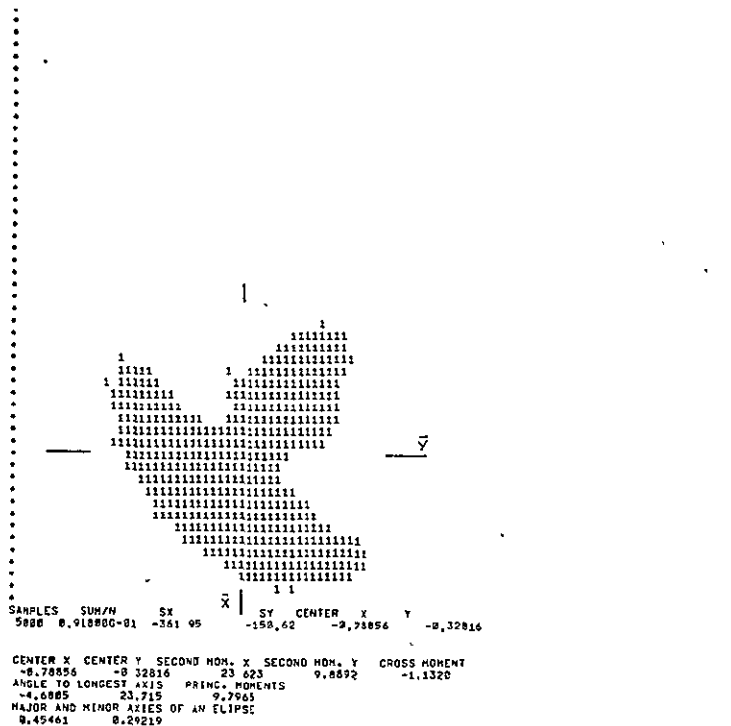


Figure VI-16 Center Test, Simulated Spacecraft 2

ORIGINAL PAGE IS
OF POOR QUALITY

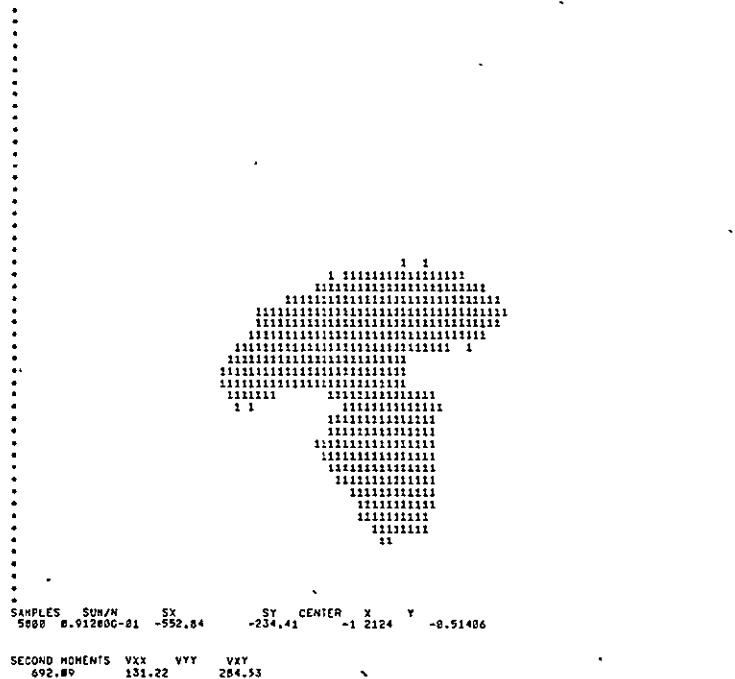


Figure VI-18 Stereo Ranging Test (Left View)

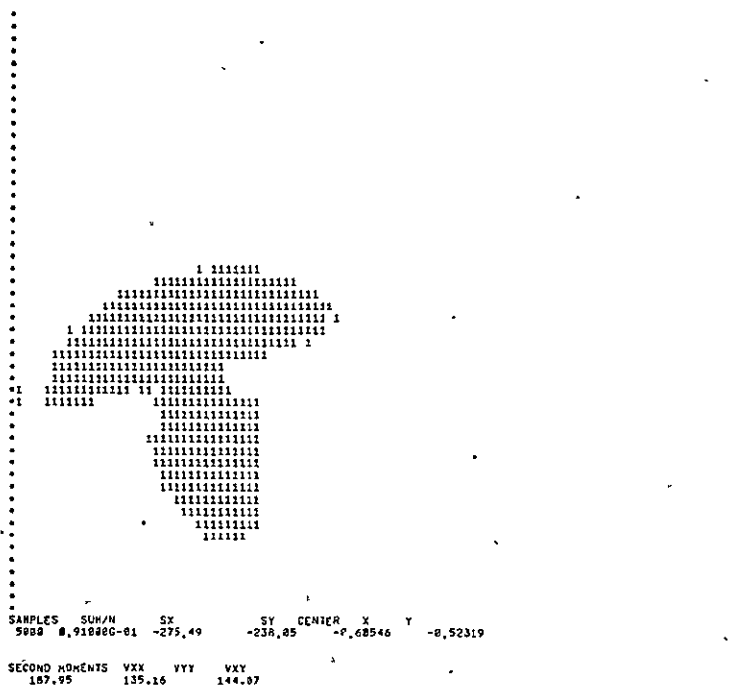


Figure VI-19 Stereo Ranging Test (Right View)

In equation form:

$$\text{AVE} = \int_F V \, dt$$

$$\text{AVE}_T = \int_F V_T \, dt$$

where T denotes a thresholded signal, and V is the video signal.

By calculating the first moment of brightness in both the X and Y directions, the center of brightness may be calculated as follows:

$$SX = \int_F V \cdot X \, dt$$

$$SY = \int_F V \cdot Y \, dt$$

then the centers are,

$$\bar{X}_B = \frac{SX}{\text{AVE}}$$

$$\bar{Y}_B = \frac{SY}{\text{AVE}}$$

where X is the X deflection on the image plane

Y is the Y deflection on the image plane

\bar{X}_B is the X coordinate of center of brightness, and

\bar{Y}_B is the Y coordinate of center of brightness.

To calculate the geometric centroid, a thresholded video signal is used

$$\bar{X} = \frac{\int_F V_T X \, dt}{\int_F V_T \, dt}$$

$$\bar{Y} = \frac{\int_F V_T Y \, dt}{\int_F V_T \, dt}$$

The orientation of an elliptical object may be calculated by using second moments and the cross-product moment; in all cases using a thresholded video signal.

$$I_{XX} = \int_F VX^2 dt$$

$$I_{YY} = \int_V VY^2 dt$$

$$I_{XY} = \int_F VXY dt$$

These values are then changed to object-centered coordinates.

$$I'_{XX} = I_{XX} - AVE_T \bar{X}_T^2$$

$$I'_{YY} = I_{YY} - AVE_T \bar{Y}_T^2$$

$$I'_{XY} = I_{XY} - AVE_T \bar{X}_T \bar{Y}_T$$

The angle to the major axis of the object is then:

$$\sigma = 1/2 \tan^{-1} \frac{2 I'_{XY}}{I'_{XX} - I'_{YY}}$$

Results and Conclusions - As shown in the laboratory results, the basic routines are written and checked out which will accomplish the basic processing for a multitude of tasks. For steering, the centroid routines would be used. Automatic threshold setting will have to be worked out, as will the guidance equations, to translate the camera image plane coordinates to spacecraft or rendezvous coordinates. Automatic ranging with dual cameras or split optics looks feasible with the algorithms as developed. This is attractive since the same system that provides cross-range steering will also yield range and range rate information.

Close-in steering and stationkeeping with this system also appears feasible, but here special problems must be overcome. Since the object is 3-

dimensional, some distinction must now be made as to what point on the object should be tracked and what parts avoided (i.e., solar panels and booms). Computer logic will be required for this in addition to some type of feature detection. The same basic algorithms will probably be used, but will be imbedded in a larger logical procedure for each task.

Recommendations - Short-term future work should be in the area of dimensionally calibrating the system, including target and camera. This will involve a mathematical model of the system such that when a position is commanded by the computer, the scan spot on the target is known. Also, an error model will be required. For this, many frames of the same scene are needed to produce a spread of data and, thus, the error dispersion for the several measurements. The area calculation errors, for example, will be a function of object size in the field of view, sample point resolution, and the focal length. Centroid measurement will also be troubled by lens aberration and angular distance from the optical centerline. These items fall under the category of refinement of the laboratory setup.

Longer term future work should center on the problems of how the system is to be implemented onboard the spacecraft. Here, trades need to be made between using a special analog preprocessor vs a microprocessor dedicated to this task. In each case, the unit should be self-contained and not require a great deal of external processing by the onboard computer. Another major area of investigation will be some type of supervisory software to provide autonomous completion of the required task. This will involve a rudimentary artificial intelligence scheme with enough capacity that it will not be easily fooled by the range of scenes it will encounter. The tradeoff here will be between software complexity vs probability of success.

The following tasks are recommended:

- 1) Performing a stationkeeping and docking phase requirements analysis for space vehicles such as Shuttle Orbiter, Space Tug, Interim Upper Stage, Earth Orbital Teleoperator Spacecraft, Free Flying Satellite Experiments, and the Astronaut Maneuvering

Unit. This will provide the necessary parametric data for establishing a realistic set of design requirements. Consideration should also be given to a multiple spacecraft docking system. Maximum use should be made of past and current study results relating to the various spacecraft.

- 2) Conducting design investigations and feasibility studies on video processing algorithms, hardware alternatives, target definition, and target spacecraft motion effects. This task involves the utilization of work accomplished at MSFC and MMC on the development of stationkeeping and docking algorithms and an evaluation of preliminary experimental results thus far achieved. Camera tradeoffs should also be performed as a function of mission requirements.
- 3) Demonstrating the feasibility of the video system in a computer/hardware six-degree-of-freedom simulator. This will enable the evaluation of various rendezvous and docking algorithms in a dynamic environment with realistic scaled target vehicles.
- 4) Performing a preliminary design for an engineering prototype system for the next phase of development. This will include the definition of weight, power, and cost estimates for the eventual fabrication of a protoflight system.
- 5) Design, develop, and evaluate a prototype video stationkeeping and docking sensor system.

3. TV Image Data Compression Techniques - The use of TV image data downlink became commonplace during Apollo Lunar missions, Skylab and Apollo Soyuz Test Project. However, the data management required a wide band data link capability to be added to the Space Tracking Data Network (STDN). The current study is based on using the baseline Space Tug data and communications system which is a 16k bps PCM telemetry system. General Dynamics Avionics study recommendation avoided the addition of a wide band downlink capability to the Tug by reducing the image data downlink rate. This provided the mission control console operator with an image update at 16-second intervals for "supervisory" control.

However, a more frequent display update would be very desirable, if not mandatory, when the operator is required to respond to an off nominal situation and assume full control of the active vehicle.

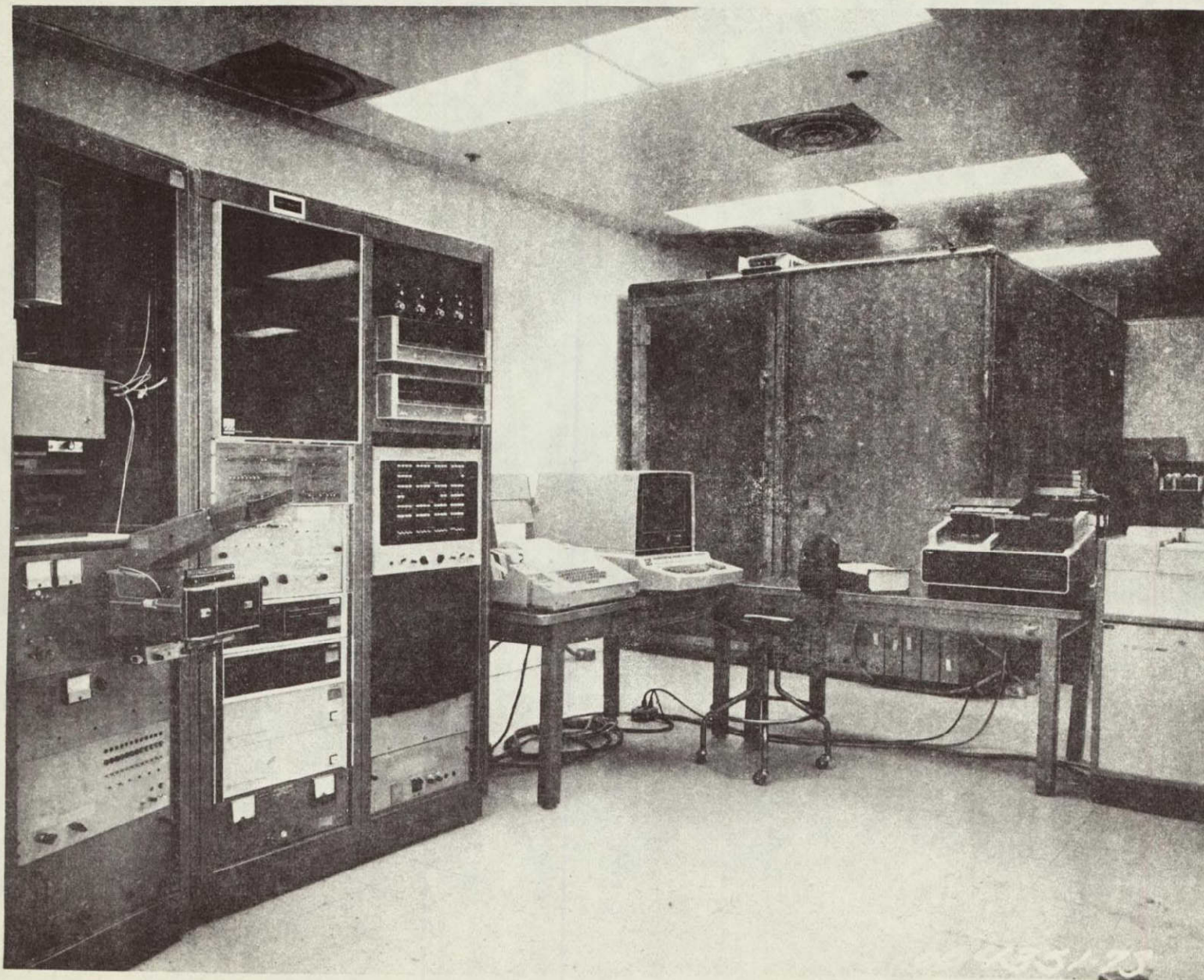
Several alternative methods are considered feasible to provide adequate update rates for manual control. Typically, for previous programs, mission control center display updates have occurred at approximately 2-second intervals and were limited by RF propagation and network processing delays. Uplink capabilities have been such that with sub-bit encoding the uplink command generation and transmission capability was one 35-bit command word, approximately each 300 milliseconds. Therefore, the time delays in the STDN remote site and Mission Control Center, processing are not the constraining factors on the operation.

Martin Marietta has performed image data compression and enhancement analyses during the Skylab program. These techniques were applied to Earth Resources Experiment Program (EREP) image data with very good results. An illustration of the Martin Marietta facility used for image data processing studies is presented in Figure VI-20.

An image monitor software package has been developed with 71 operational commands used to do image operations such as; correlation studies, feature extraction, image screening, two-dimensional Fourier transforms, convolution studies, and digital filtering studies. The large amount of programming work necessary to establish a workable image processing capability has been accomplished, including:

- 1) Monitor subprocedure and conditional sequence control commands.
- 2) Image subblocking and scan conversion routines.
- 3) Random access core to disc data management commands.
- 4) Scanning, digitalization and display of images.
- 5) Dynamic core area allocation and buffer sizing to allow effective use of the core size.
- 6) An extensive library of histogram, graphing, statistical and data study routines.

ORIGINAL PAGE IS
OF POOR QUALITY



VI-59

Figure VI-20 Image Data Laboratory Setup

- 7) A compatible tape writing and reading routine for IBM and CDC formats.
- 8) Parameter table assignment system to allow dynamic exchange of constants and operation data during processing.
- 9) Several point intensity commands such as scaling, biasing, thresholding, logarithmic contrast expansion and compression, and non-linear operations.
- 10) A fast two-dimensional Fourier transform using fixed point arithmetic and batch scaling, including centering, bit reversal, and radial filtering routines. This is important because of the relation of correlation operators to transforms.
- 11) Convolution, correlation, and digital filtering routines which relate to many effective and efficient processing techniques such as feature extraction, noise elimination, template screening, enhancement, and image separation.
- 12) The Walsh-Hadamard transform routine for research in new algorithmic techniques.

Considerable emphasis for the Image Facility has been on small computer and dedicated processors that could perform onboard imagery processing.

Thirteen papers have been authored by Martin Marietta personnel on the subject of data compression (Bibliography 1 through 13). The scope of Martin Marietta's previous imagery data handling and compression studies was broader in nature, but the techniques and approach are applicable to the problem at hand. A functional block diagram flow of the process is illustrated in Figure VI-1 in which the onboard TV camera performs the "Image Sensing" function. The sensed image is digitized and source encoded onboard. Some advantages and disadvantages of data compression schemes investigated for the source encoding function are shown on the diagram. The flow illustrates that channel encoding is performed followed by transmission to the STDN ground station as via TDRSS to the Mission Control Center. The remaining functions are performed on the ground

ORIGINAL PAGE IS
OF POOR QUALITY

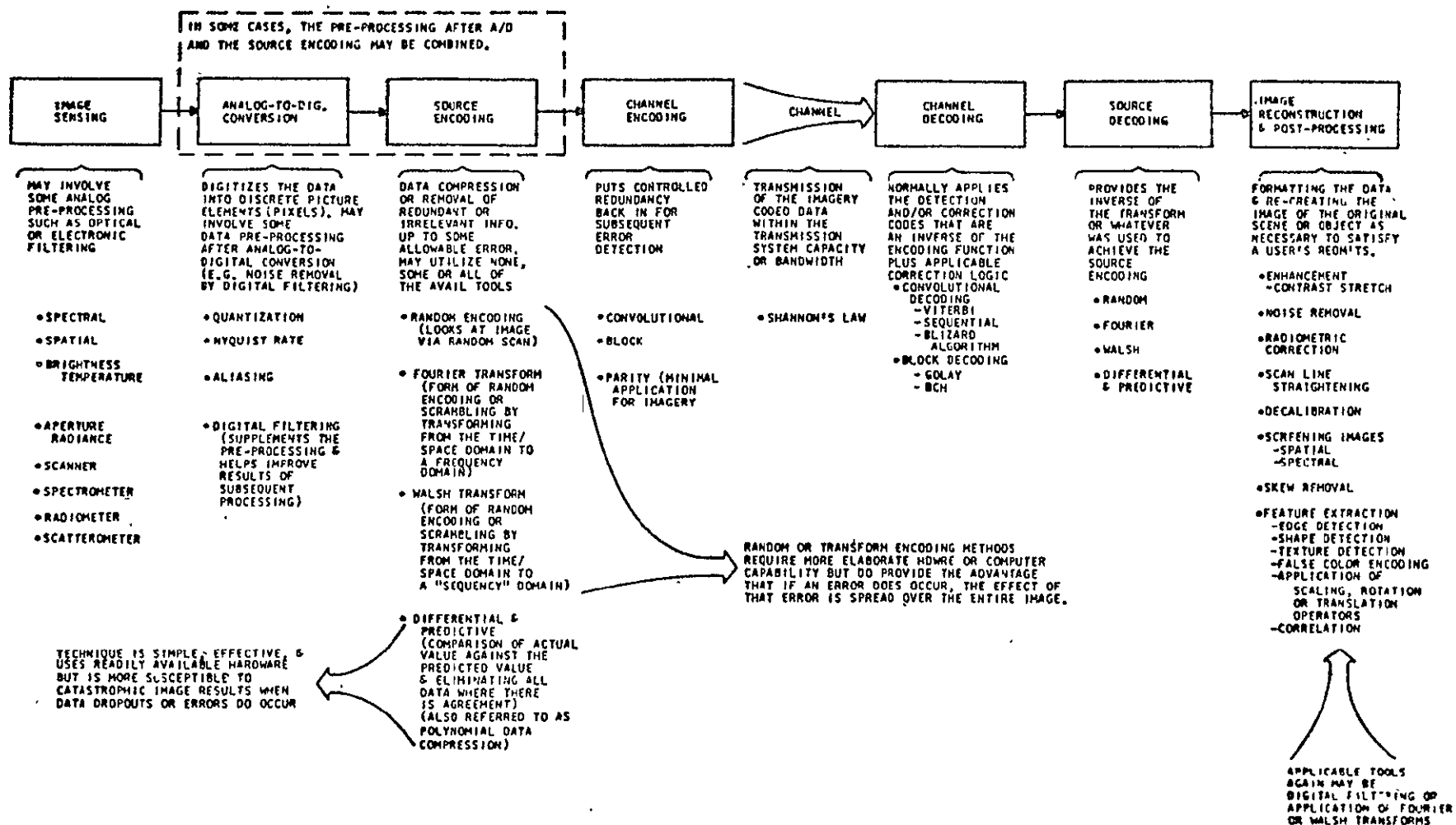


Figure VI-21. Image Data Compression, Transmission and Reconstruction Flow

and reconstruct the image. A data compression and error control program was performed at Martin Marietta under NASA Contract NAS9-9852. The purpose of the study was to evaluate digital data processing and error correcting code techniques and how they could be applied to Apollo VSB communication systems.

Several methods for reconstruction of the data was considered in this study and some examples are shown in Figures VI-22 through VI-25, with the original curve and the reconstruction of the same using the method indicated.

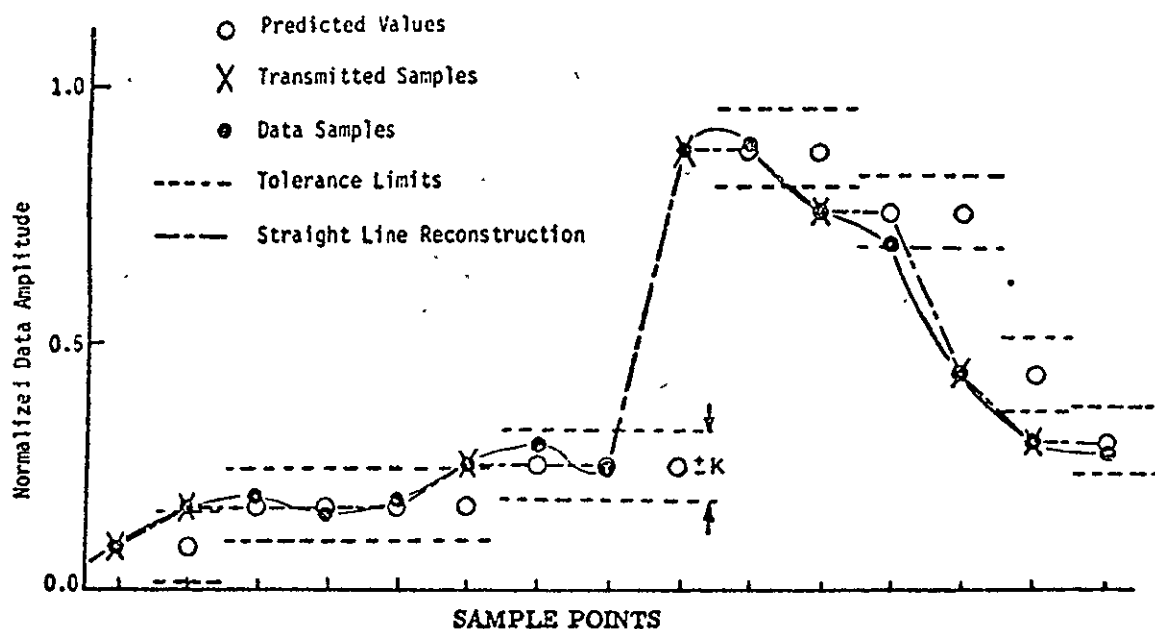


Figure VI-22. Zero Order Predictor, Floating Aperture

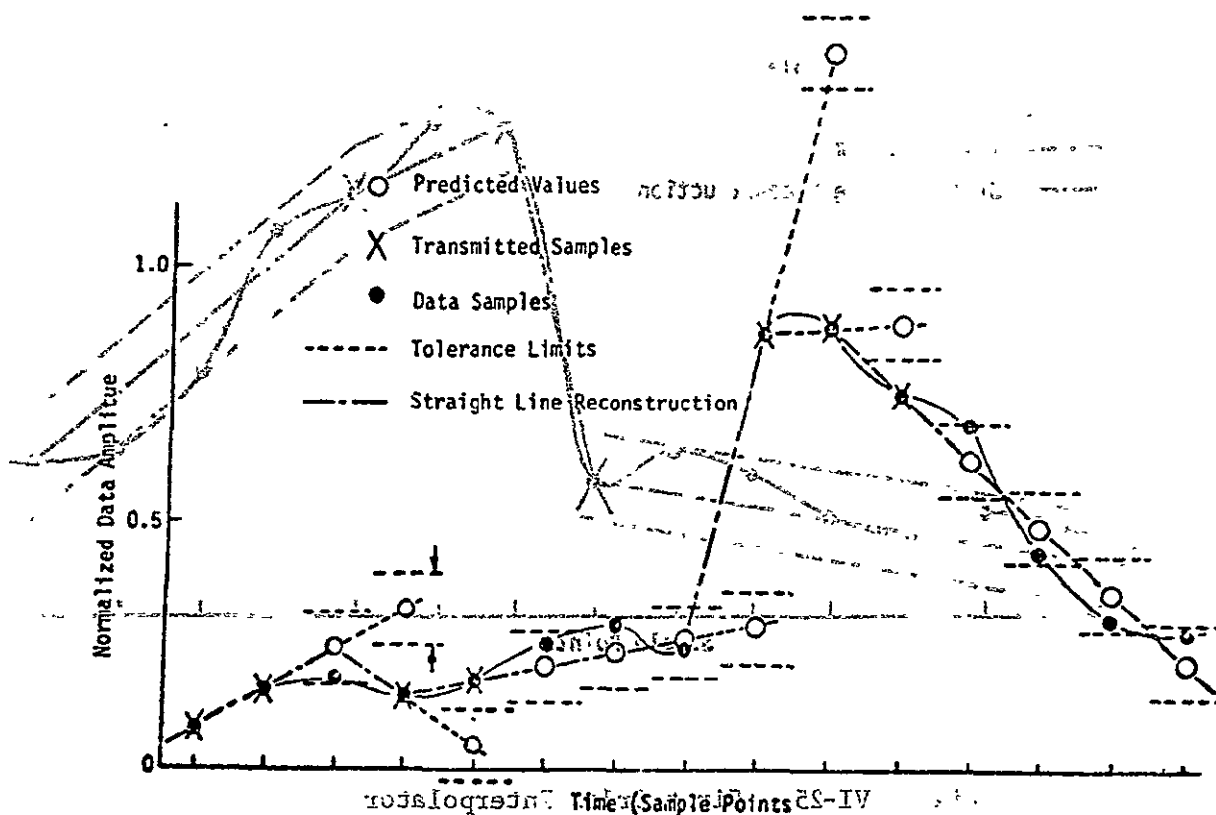


Figure VI-23. First Order Predictor

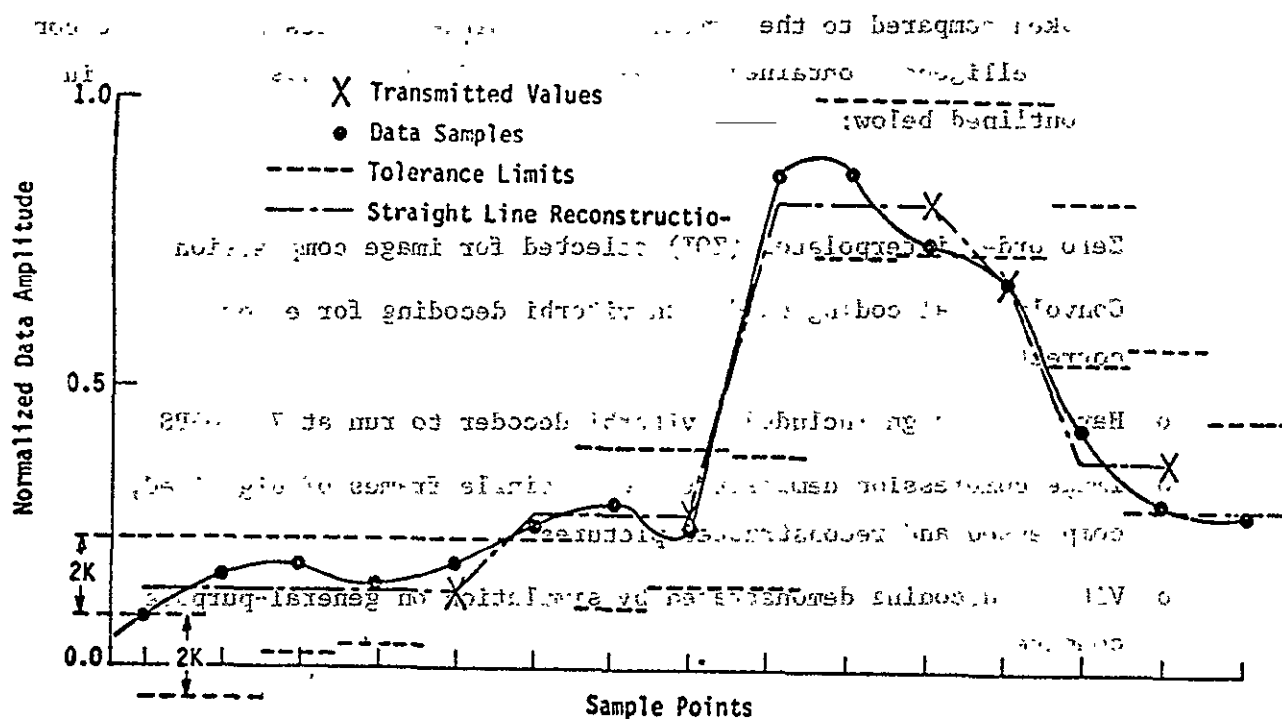


Figure VI-24. Zero Order Interpolator (Peak Error Criteria)

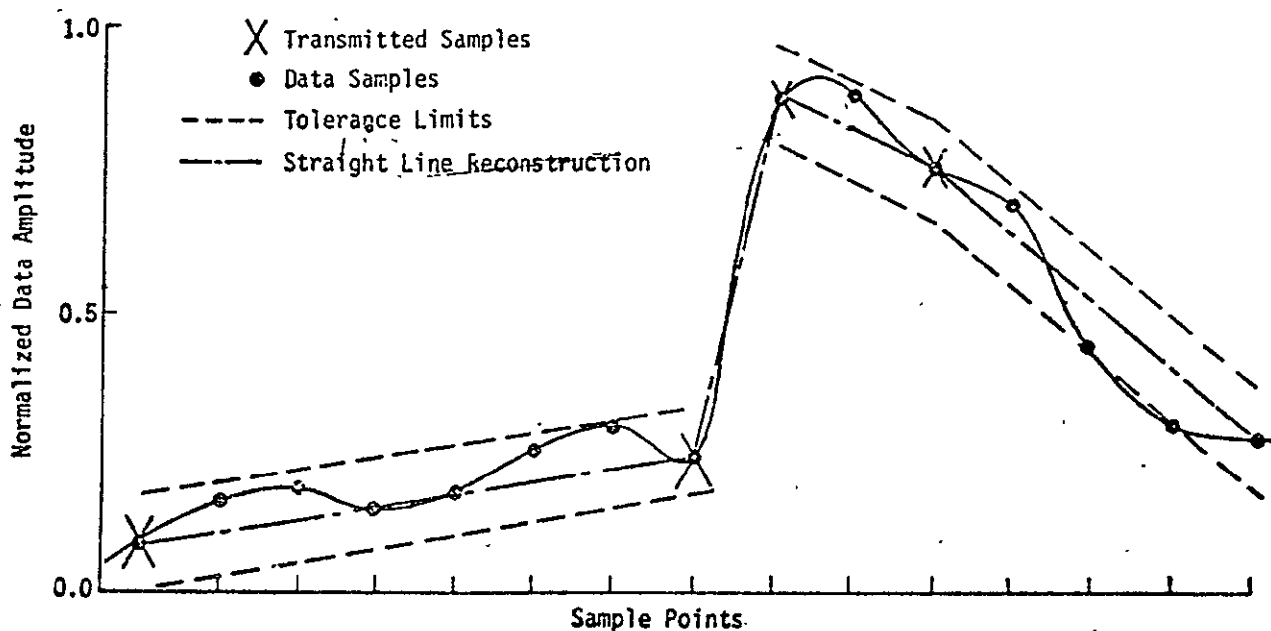


Figure VI-25. First Order Interpolator

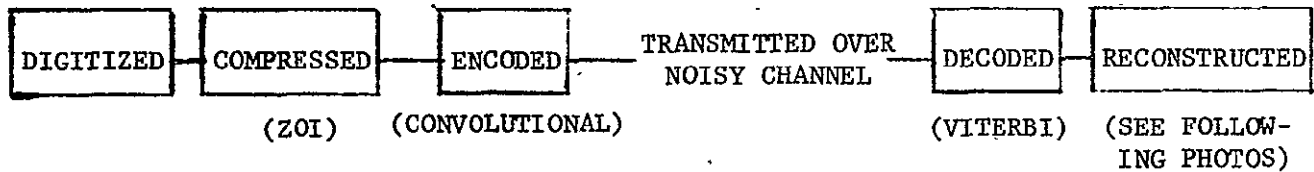
The method which gave the best results, as applied to image data, was the zero order interpolation (ZOI). Data compression ratios are based on the number of data samples taken compared to the number of transmitted samples required to convey the basic intelligence contained in the curve. The study was conducted in two phases as outlined below:

PHASE 1:

- o Zero-order interpolator (ZOI) selected for image compression
- o Convolutional coding used with viterbi decoding for error correction
- o Hardware design included a viterbi decoder to run at 7.5 MBPS
- o Image compression demonstrated with single frames of digitized, compressed and reconstructed pictures
- o Viterbi decoding demonstrated by simulation on general-purpose computer

PHASE 2:

- o Effects demonstrated for combination of compression and channel errors using viterbi decoding (errors tend to come in bursts out of viterbi decoder; a single error can significantly impact compressed data)
- o Complete simulation showed results for a picture that is:



- o ZOP compressor also evaluated
- o Results verified the validity of combining error control with data compression as a means of reducing RF power without sacrificing picture quality
- o During viterbi decoding studies, an iterative process (Blizard) for increasing performance was discovered and developed into an independent decoding algorithm that appears to have good potential for communications

The application of this technology for image data compression for a manual rendezvous and docking system should be studied further, since data loading on the network is expected to become more critical. The major elements of a typical end-to-end data management system application of this technique is illustrated in Figure VI-26.

SPACE TUG OR OTV

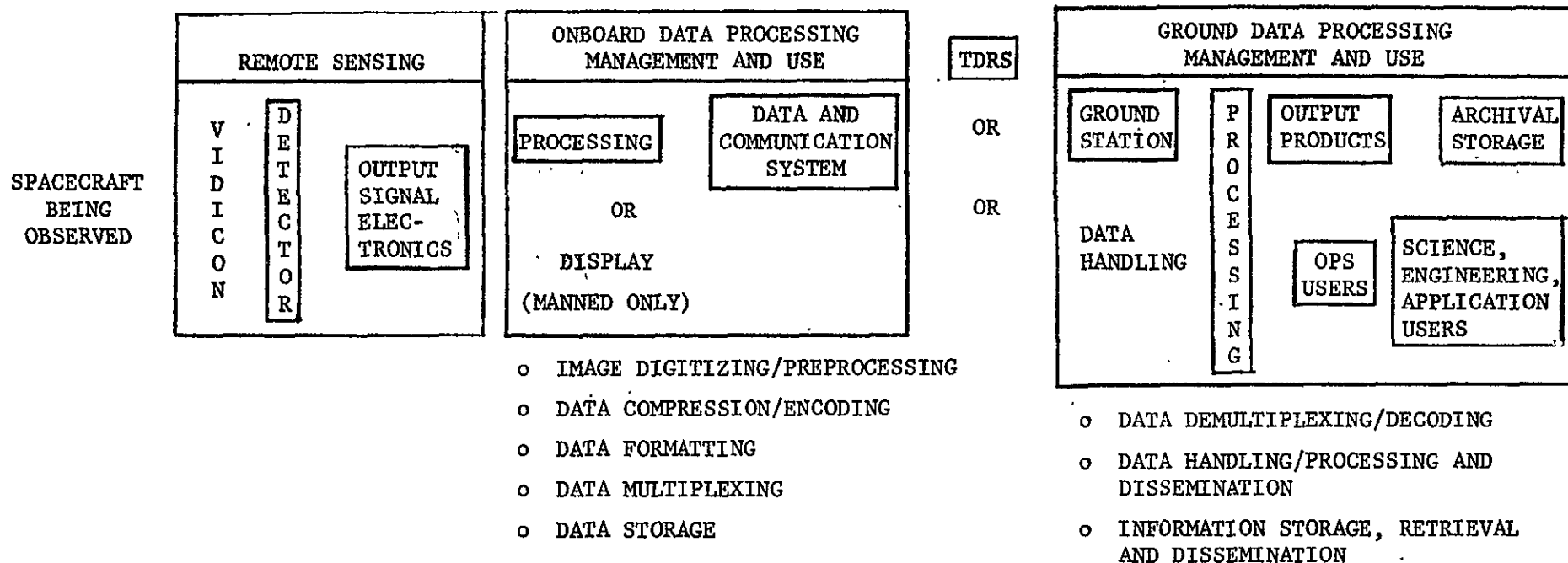


Figure IV-26. System Block Diagram

Bibliography of MMC papers published relative to data compression:

- 1) Clausen, R. H. and L. A. Pownall, "Science Data Management Automation", Proceedings AAS-ORSA Joint National Meeting, Denver, June 1969.
- 2) Hardin, R. H. and L. A. Pownall, "Remote Multiplexing Data Systems for Naval Ships", National Telemetry Conference Record, 1968.
- 3) McCoy, R. W. and W. A. Stenens, "Data Compression Concepts and Philosophies", AAS Proceedings, 1967.
- 4) Pownall, L. A., "A Stored Program Data Compression Developmental System", EASCON Record, 1968.
- 5) Stevens, W. A., and L. A. Pownall, "Digital Data Compression Buffer Queue Control", EASCON Record, 1968.
- 6) Sheldahl, S. A., "Data Compressor Hardware Comparison", National Telemetry Conference Record, 1968.
- 7) Sheldahl, S. A., "Channel Identification Coding for Data Compressors", EASCON Record, 1968.
- 8) Stevens, W. A., "Multichannel Data Compression Simulation", Conference Proceedings, Rocky Mountain Section, American Astronautical Society, July 1968.
- 9) Blizard, R. B., "Data Compression with Sequential Decoding", MMA Research Report No. R-69-1, 1969.
- 10) Blizard, R. B., "Quantizing for Correlation Decoding", IEEE Transactions on Communication Technology, Vol. COM 15-4, August 1964, p. 655-657.
- 11) Blizard, R. B., "A Comparison of Biorthogonal and Bisimplex Codes", IEEE Transactions on Communication Technology, Vol. COM 15-4, August 1967, p. 657-658.

- 12) Blizard, R. B., "Compound Coding for Deep-Space Communication", Supplement to IEEE Transactions on Aerospace and Electronic Systems, Vol. AES-3, November 6, 1967, p. 24-29.
- 13) Dunklee, A. L., "The Use of Walsh Transforms in Image Processing", MMC paper presented at the Symposium for Applications of Walsh Functions, Washington, D.C., April 1973.